



**Università
di Genova**

DEPARTMENT OF EXPERIMENTAL MEDICINE

PhD COURSE IN EXPERIMENTAL MEDICINE

Curriculum of Biochemistry

**NOVEL VX-809 HYBRIDS AS CORRECTORS OF F508del- CYSTIC
FIBROSIS TRANSMEMBRANE CONDUCTANCE REGULATOR (CFTR)
PROTEIN**

Candidate: Alice Parodi

Tutor: Prof. Enrico Millo

PhD Program Coordinator
Prof. Ernesto Fedele

Academic Year 2021-2022

XXXV Cycle

Index

| | |
|---|-----------|
| Abstract | 4 |
| Abbreviations | 6 |
| Chapter 1: Cystic Fibrosis | 8 |
| 1.1 Diagnosis | 8 |
| 1.1.1 Newborn Screening | 8 |
| 1.1.2 Sweat Test..... | 9 |
| 1.1.3 Investigation of the CFTR Gene | 10 |
| 1.1.4 Nasal Potential Difference Measurements and Intestinal Current Measurement..... | 11 |
| 1.2. CFTR Protein | 12 |
| 1.2.1 CFTR Structure..... | 12 |
| 1.2.2 Asymmetry in CFTR | 13 |
| 1.2.3 CFTR as Anion Channel..... | 14 |
| 1.2.4 Function of CFTR under Normal Conditions | 14 |
| 1.2.5 Biogenesis and Trafficking of CFTR..... | 16 |
| 1.2.6 Classes of Mutations..... | 19 |
| 1.3 Cystic Fibrosis Disease | 21 |
| 1.3.1 Lung Disease | 21 |
| 1.3.2 Gastrointestinal Disease..... | 22 |
| 1.4 Therapies | 23 |
| 1.4.1 Symptomatic Therapies | 23 |
| 1.4.2 Therapies Against the Basic Defect | 25 |
| 1.4.3 Potentiators | 26 |
| 1.4.4 Correctors | 27 |
| Chapter 2: Methods and Instrumentations | 31 |
| 2.1 High Performance Liquid Chromatography | 31 |
| 2.1.1 HPLC: instrumentation | 32 |
| 2.1.2 Pumping System | 33 |
| 2.1.3 System for the Introduction of the Sample | 33 |
| 2.1.4 Columns..... | 34 |
| 2.1.5 Detectors | 34 |
| 2.1 Mass Spectrometry | 35 |
| 2.2.1 Mass Spectrometer: instrumentation..... | 35 |
| 2.2.2 Introduction of the Sample | 36 |
| 2.2.3 Ionization Source | 36 |
| 2.2.4 Analyzer | 38 |
| 2.2.5 Detector | 39 |
| 2.2.6 HPLC-MS Coupling | 39 |
| 2.3 Nuclear Magnetic Resonance Spectroscopy | 39 |
| 2.3.1 Energy Absorption..... | 40 |
| 2.3.2 Production of the NMR Signal | 40 |
| 2.3.3 Chemical Shift | 41 |
| 2.3.4 Peak Area..... | 42 |
| 2.3.5 NMR Spectrometer: instrumentation..... | 42 |
| 2.3.6 Magnets | 45 |
| 2.3.7 Systems to Ensure the Stability of the Magnetic Field | 45 |

| | |
|---|------------|
| 2.3.8 Systems to Reduce Noise Overlapping on the NMR Signal | 46 |
| 2.3.9 Processing the Collected Data | 46 |
| 2.3.10 Probes for the Sample | 46 |
| 2.3.11 Digitation | 47 |
| 2.4 Fluorescence Assay to Test CFTR Activity..... | 47 |
| 2.4.1 Basics of YFP Proteins | 47 |
| 2.4.2 Principle of the Test..... | 47 |
| Chapter 3: Experimental Section | 49 |
| 3.1 Background..... | 49 |
| 3.2 Aim of the Thesis | 51 |
| 3.3 Chemistry | 53 |
| 3.4 CFTR assay..... | 60 |
| Chapter 4: Results and Discussion | 61 |
| 4.1 Role of the Portion A and of the Portion B..... | 61 |
| 4.2 Role of the Portion C | 63 |
| 4.3 Discussion | 74 |
| 4.4 Further Biological Assays on the First Library Hybrids..... | 76 |
| 4.5 Further Biological Assays on the Second Library Hybrids | 80 |
| 4.6 Molecular Docking Studies | 84 |
| Conclusion..... | 89 |
| Experimental | 90 |
| Chemistry | 90 |
| Biological evaluations | 140 |
| Cell culture | 140 |
| Fluorescence assay for CFTR activity | 141 |
| Trans epithelial electrical resistance (TEER) evaluation | 141 |
| Biochemical analysis of CFTR expression pattern | 142 |
| Statistics..... | 142 |
| Surface plasmon resonance binding assays | 142 |
| References | 144 |

Abstract

Cystic fibrosis (CF) is an autosomal recessive genetic disease that affects different organs as the lungs, the digestive system and the reproductive tract, also impacting on the growth of subjects. To date, the known CFTR gene mutations are more than 2000, but in particular the most widespread is the deletion of a phenylalanine at position 508 that involves the synthesis of a defective protein, that it is not able to lead the correct folding and is degraded early in the proteasome. When some mutated CFTR proteins reach the plasma membrane (PM), the activity of the channel is impaired.

Today, in addition to symptomatic therapies, molecules have been developed against the basic defect of CFTR, in particular they are small molecules called modulators, including potentiators and correctors. The potentiators act on the gating of CFTR allowing the correct opening, while the correctors save the CFTR protein allowing it to obtain the correct conformation and stabilization at the PM. The first corrector to be approved was VX-809 called Lumacaftor (by Vertex Pharmaceuticals), for homozygous patients for the F508del-CFTR mutation.

The VX-809 was then used in combination with the potentiator VX-770 in the Orkambi (by Vertex Pharmaceuticals) formulation to achieve a better effect. Since VX-809, both alone and in combination with VX-770, shows some defects, it became necessary to search new molecules with similar mechanism of action, but with fewer side effects. In this regard Vertex designed a corrector called VX-661, which acts with similar mechanism of action, but has better pharmacokinetic characteristics. Despite recent advances in drug therapy of CF and the improvement of patients' well-being, there are still many problems that arise; on the one hand, the study of active molecules against more rare mutations is necessary, on the other hand the discovery of more powerful molecules than those commercially available.

In this thesis I report the synthesis, characterization and purification of molecules active as correctors, of which both biological evaluation and molecular docking studies have been carried out. In particular starting from the structure of a molecule previously synthesized by my team, called **2a**, and studying its portion, I found a common backbone to be able to decorate with different functional groups for investigating the effect of each chemical group on the biological activity.

Hence, I got a series of more active compounds, which showed higher potency than both the progenitor **2a** ($EC_{50} = 0,08 \mu\text{M}$) and the commercial VX-809 ($EC_{50} = 2,60 \mu\text{M}$), whose activity was deepened with further biochemical assays and tested in combination with other correctors in order to study synergic or additives effects.

Through a multidisciplinary approach (bioinformatic, chemistry and biochemistry), it was possible to obtain promising molecules as correctors of F508del-CFTR, in particular more potent than the

initial prototype, such as **34** ($EC_{50} = 0,02 \mu\text{M}$), **42** ($EC_{50} = 0,07 \mu\text{M}$), **70** ($EC_{50} = 0,06 \mu\text{M}$), **74** ($EC_{50} = 0,03 \mu\text{M}$) and **81** ($EC_{50} = 0,03 \mu\text{M}$).

Abbreviations

AAT: aminoarylthiazole

ABC: ATP- binding cassette

ACN: acetonitrile

ASL: airway surface liquid

CF: cystic fibrosis

CFTR: cystic fibrosis transmembrane regulator

CI: chemical ionization

CNX: calnexin

DIPEA: N,N- diisopropylethylamine

DMF – DMA: N,N- dimethylformamide dimethyl acetal

EI: electronic impact

ENaC: amiloride- sensitive epithelial Na⁺ channel

ER: endoplasmic reticulum

ERAD: endoplasmic reticulum-associated protein degradation

ESI: electrospray ionization

EtOAc: ethyl acetate

EtOH: ethanol

FEV₁: forced expiratory volume in the first second

FID: free induction decay

FT-NMR: Fourier transform – nuclear magnetic resonance

GFP: green fluorescent protein

HATU: 1 - [Bis (dimethylamino) methylene] - 1*H* -1,2,3-triazolo [4,5-*b*] pyridinium 3-oxid

hexafluorophosphate

HPLC: high performance liquid chromatography

HPLC-MS: high performance liquid chromatography – mass spectrometry

HSP: heat shock proteins

HS- YFP: halide-sensitive yellow fluorescent protein

ICM: intestinal current measurement

ICL: intracellular loop

IRT: immunoreactive trypsinogen

LC: liquid chromatography

MeOH: methanol

NBD: nucleotide binding domain
NBS: newborn screening
NEF: nucleotide exchange factor
NMR: nuclear magnetic resonance spectroscopy
N,N- DMF: N,N- dimethylformamide
NPD: nasal potential difference
PM: plasma membrane
PQC: protein quality control
QSAR: quantitative structure activity relationship
ROS: reactive oxygen species
RT: room temperature
SAR: structure activity relationship
SPR: surface plasmon resonance
TEER/PD: trans epithelial electrical resistance and potential difference measurements
TFA: trifluoroacetic acid
THF: tetrahydrofuran
TMD: transmembrane domain
WB: western blot
WT: wild type
YFP: yellow fluorescence protein

Chapter 1: Cystic Fibrosis

1.1 Diagnosis

Cystic fibrosis (CF) is an autosomal recessive pathology that is transmitted from the parents to the son, when the child inherits a mutated copy of the CFTR gene from both the parents. Subjects who only have a mutated copy of the CFTR gene are healthy carriers and show no symptoms.

In the Western world the frequency of healthy carriers is one in every 25 people. When two healthy carriers conceive a child, there is a one in four chance that the child will be born with CF.

In most cases, CF is diagnosed at birth, through a neonatal test and it is later confirmed by sweat test. When the sweat test provides intermediate or borderline results, CF can be confirmed through other tests such as Nasal Potential Difference (NPD) measurement and Intestinal Current Measurement (ICM). Finally, it is important to identify which mutation is responsible for CF, to direct the patient to the appropriate therapy.

1.1.1 Newborn Screening

In many countries, the CF Newborn Screening (NBS) has been introduced. The screening test must be simple, safe, accurate and validated, so the NBS became concrete after the introduction of a radioimmunological test. The test consists in the measurement of Immunoreactive Trypsinogen (IRT) in the infant's sample blood, drawn from the heel (Castellani et al., 2016).

The IRT is a marker of pancreatic injury. The rational use of the IRT derives from the finding of elevated values of this enzyme in the blood of newborns affected by CF in the first months of life, because the trypsin refluxes towards the blood circulation, probably as a result of an obstruction of the pancreatic ducts.

The test is performed from the third - fifth day of life, but high values of IRT can also be found in non-CF subjects. Then the subjects tested positive at the first test are subjected to a second blood test (retesting) at 20-30 days of life, to confirm the condition of hyper-trypsinemia. In non-CF subjects, in fact, the IRT tends to normalize, while in CF subjects this parameter remains high over time.

Anyway, the diagnosis must be confirmed by a positive sweat test, detecting two CFTR disease-causing mutations or by NPD or ICM measurement.

CF newborn screening is however very important since it paves the way for an early diagnosis; every baby in whom the diagnosis of CF is confirmed must receive immediate follow-up and treatment in a CF reference center.

1.1.2 Sweat Test

The sweat test is the most reliable and widely available diagnostic test in CF, in fact, the infants with a positive NBS test are subjected for the sweat test to confirm the diagnosis of CF (Castellani et al., 2009). It consists in the measurement of chloride concentration in sweat.

The sweat test can be performed from the age of 2 weeks on infants who are normally hydrated and not acutely ill.

Isotonic sweat is produced in the secretory coil, but normally the sweat is hypotonic because in the sweat duct most of the chloride is reabsorbed via the CFTR channel. In CF, reabsorption of chloride doesn't occur and the concentration of chloride is higher in the sweat.

The test is a functional assay, it measures the function of CFTR determining the concentration of chloride in the sweat. In the first part of the test, sweating is induced in a small area of the forearm with a colorless and tasteless substance (Pilocarpine), under the stimulus of a small amount of electric current (pilocarpinic iontophoresis), this phase lasts about 5 minutes. Then the sweat is collected on a filter paper or on a gauze or through a plastic tube wrapped in a spiral, this phase lasts 30 minutes. Then, the collected sweat is sent to the laboratory to measure the concentration of chlorine.

The first condition necessary to consider a suitable sweat sample is the amount of sweat collected which should not be less than 75 mg, if collected on paper/gauze, or 20 microliters, if collected with plastic spirals (Guidelines for the performance of the sweat test for the investigation of cystic fibrosis in the UK 2nd version; 2014).

For the diagnosis of CF, it is recommended to measure the chlorine ion (Cl^-) in sweat (the result is expressed in milliequivalents per liter or per Kg (mEq/L or mEq/Kg of chlorine) or in millimole per liter or Kg (mmol/L or mmol/Kg), (see table 1).

In some laboratories, sodium is also measured in addition to chlorine or alternately NaCl equivalents are measured by conductivity method; the conductivity method measures the electrical conductivity of sweat, linked to the concentration of salt molecules in sweat and their concentration is expressed as mmol/L of NaCl. However, this measure was only validated as a screening test and not as a confirmation test for CF diagnosis (Wayne; 2019).

| | Chlorine (mEq/ L) | Interpretation |
|-------------------------|--------------------------|--------------------------|
| Age < 6 month | ≤ 29 | Normal |
| | 30 - 59 | Intermediate, borderline |
| | ≥ 60 | Elevate |
| Age > 6 month | ≤ 39 | Normal |
| | 40 - 59 | Intermediate, borderline |
| | ≥ 60 | Elevate |

Table 1: Values of chlorine in the sweat, expressed in mEq/L, and their interpretation. Elevated values support the diagnosis of CF.

It is important to know that the sweat test, if repeated over time to the same individual, can give different results, sometimes even in different diagnostic intervals. This phenomenon of up and down characterizes above all those values of chlorine to the first test of the sweat that turn out intermediate called borderline.

In recent years, the intra- as well as inter-subject variability in sweat chlorine value in patients with CF has been better studied (Cirilli et al., 2018). The most of the variability in sweat chlorine (56%) is determined by the specific CFTR genotype. Other causes of variability are: variation over time (14%), environmental factors (13%), residual factors such as test variability (10%) and unique individual factors (7%) (Collaco et al., 2016).

When the sweat test is not straight for the purpose of diagnosing disease, clinicians may require additional diagnostic insights such as the extended genetic investigation of the CFTR gene, the measurement of NPD or ICM (Edelman, 2010).

1.1.3 Investigation of the CFTR Gene

The CFTR gene was discovered more than 30 years ago. Today, we know that more than 2000 mutations can affect the CFTR gene, but only one mutation, F508del, is frequent and occurs in about 70% of CF alleles; by comparison all other mutations are rare. In most countries, only 6–8 mutations have a frequency above 1% so, many patients have mutations that are rare or ultra-rare that means only occurring in a few or even a single individual (ECFSPR annual report 2014). The panel of mutations covers a variable frequency depending on the population. For all these reasons there is currently no ideal genetic test capable of identifying all mutations, but it is very important to identify the mutations responsible for CF in the individual because mutation specific therapies have become available.

The techniques used must meet sensitivity criteria, reproducibility and speed; standard commercial kits are available, related to an increasing degree of complexity and extension of genetic testing. Generally, each laboratory should use a panel of mutations more common in its area that allows a good identification rate (detection rate). The presence of two mutations makes it possible to diagnose the disease, while, in case of identification of a single mutation, the sweat test can discriminate between carriers and patients with only one identifiable mutation.

The first step of genetic analysis, using techniques such as Reverse Dot Blot or Oligonucleotide Ligation Assay, has less coverage, but allows the search for known mutations. Further genetic analysis identifies by scanning all exons and neighboring regions, recognizes sequence variations, and can lead to sequencing of a specific region of the CFTR gene. The most widely used techniques for scanning are Denaturing Gradient Gel Electrophoresis, and Denaturing High Performance Liquid Chromatography.

Currently the scanning of the gene is not integrated in the neonatal screening protocols, both for its technical complexity and because the identification of unknown variants (not necessarily mutations cause of disease) makes their interpretation and correlation with the phenotype difficult.

1.1.4 Nasal Potential Difference Measurements and Intestinal Current Measurement

NPD and ICM are bioassays of CFTR function, as the sweat test.

NPD is an *in vivo* test that measures the transmucosal voltage potential. The measure of the transepithelial potentials of the nasal mucosa consists in evaluating the difference in potential that is established between an electrode placed on the nasal mucosa and one placed on the skin, through an electric potential detector (voltmeter). This difference in nasal potential, which is always negative, is dependent on the movement of ions, chlorine and sodium, that occurs at the level of the nasal epithelium and therefore the degree of functioning of the protein CFTR, which regulates most of the chlorine and sodium movements (Rowe et al., 2011).

Under normal conditions NPD is around -20 millivolts (mV), in CF is mainly between -40 and -60 mV. In addition to the baseline measurement of NPD, other measurements are conducted after perfusing the mucosa with some substances that can modify the starting NPD, depending on the degree of functionality of CFTR: first perfusing with amiloride, that blocks sodium channel, to see how much sodium resorption is corrected; then, with a chlorine-free solution, which in normal conditions stimulates the secretion of chlorine through CFTR; finally, with isoproterenol, a substance that activates the chlorine channel CFTR. The test is usually performed in children of 6 years on, but an abbreviated protocol is available for babies (Sermet-Gaudelus et al., 2010).

The weakness of NPD is the intra-subject variability and that there's no universal values, so every laboratory can use his own cut-off values.

ICM is a useful technique to explore the functionality of the CFTR channel, but unlike NPD, this measurement cannot be made *in vivo*, but is obtained by using a mucosal fragment of the last portion of the rectum that is inserted in a Ussing chamber (*ex vivo* test).

In patients with CF, intestinal chlorine secretion is impaired, while absorptive processes remain normal or are increased. There is thus a clear difference in ICM between CF and healthy. The ICM technique allows the direct registration of CF-induced changes in electrogenic transepithelial ion transport (chlorine, bicarbonate and potassium) in a Cl⁻ secretory epithelium, and on the basis of pharmacological criteria is able to discriminate between CFTR-mediated Cl⁻ secretion and secretion through alternative anion channels.

The principal diagnostic criterion are the direction and magnitude of two substances, carbachol and histamine (De Jonge et al., 2004). The response to carbachol and histamine in intestinal tissue contains two components: a lumen positive current by apical potassium efflux and a lumen negative current by CFTR mediated chloride secretion. In ICM of healthy person, the potassium efflux is masked by the much larger chloride efflux. In people with CF, the current is reversed because only the potassium efflux is present.

Since a fragment of rectal mucosa (about 2-3mm) must be removed by biopsy, although rectal biopsy is a common practice, this type of test still shows limits, as it is not without risks, so it is used more rarely, in case of more difficult diagnoses, especially for confirmation of CF in the absence of two disease-causing CFTR mutations, exclusion of CF despite intermediate sweat test or age groups unsuitable for nasal potential difference measurements (Derichs et al., 2010).

1. 2. CFTR Protein

1.2.1 CFTR Structure

The cystic fibrosis transmembrane conductance regulator CFTR protein is a member of ATP- binding cassette (ABC) transporters, a family of membrane protein that use the energy derives to ATP hydrolysis to pump substrates across cellular membrane. The CFTR protein is the only member of ABC transporter that act as an ion channel. It's located on the apical membrane of epithelial cells where it allows the flow of anions as chloride, bicarbonates and thiocyanate.

CFTR share the common architecture of 2 transmembrane domains TMDs and 2 nucleotide binding domains NBDs that form the unit of transport, as the other ABC transporters (see Figure 1). Unique to CFTR is, instead, a regulatory region as well as long N- and C- terminal extensions about 80 and 30 residues, respectively (Cant et al., 2014).

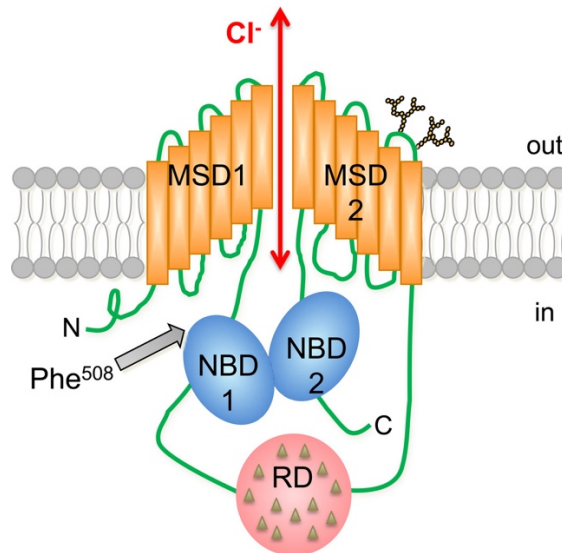


Figure 1. Structure of the cystic fibrosis transmembrane conductance regulator (CFTR) protein (Farinha et al., 2013).

Each TMD of CFTR consist of 6 membrane- spanning alfa- helices (TM1-12) that form a pore through ions can flow. NBDs contain two ATP binding sites, each formed by the Walker A and Walker B sites on the 'head' of an NBD and the ABC specific signature sequence (LSGGQ) located on the tail of the opposite NBD (Vergani et al., 2005).

The unique regulatory domain, located between two TMD–NBD complexes, contains multiple consensus serine/threonine residues for PKA-dependent phosphorylation; phosphorylation of the R domain is essential for the activation of CFTR proteins (Seibert et al., 1999). However, the detailed mechanism of how the R domain regulates the channel remains unclear.

CFTR’s pore and gate reside in its TMDs so, the interfaces between NBDs and TMDs likely play an important role in coupling NBDs motion and gate opening in TMDs.

In the cryo-electron microscopy structures is reported a portion of the R domain density located in proximity to the interface between NBD1 and the intracellular loop (ICL) 4 (connecting TM10 and TM11); it is noted that many disease-associated mutations, including the most common F508del, are clustered in this region. There are also studies suggesting that several mutations located at this interface, as F508del, are associated with slower phosphorylation-dependent activation (Wang et al., 2000; Chin et al., 2017). Further NMR studies provide evidence that the F508del mutation may affect phosphorylation-modulated domain–domain interactions (Kanelis et al., 2010).

1.2.2 Asymmetry in CFTR

The ABC transporters usually have TMD1 and TMD2 structurally similar, so the proteins show a twofold symmetry of the TMDs along the central axis, but CFTR’s TMD2 is quite different from its

TMD1 in that TM8 bears a short segment of loop-like structure, interrupting the continuity of the helix. The distorted segment of TM8 impinges toward the central vertical axis of the pore. The accompanied lateral displacement of TM7 away from the core of the protein arrange for a TM7 located at a different position than its counterpart TM1. This breakdown of twofold symmetry explains why TM7 does not contribute to the pore formation (Wang et al., 2014; Zhang and Hwang, 2015), whereas TM1 is pore-lining (Wang et al., 2011; Gao et al., 2013). This same local impingement of TM8 also enables its contacts with TM9 and TM12, which are not seen between their counterparts TM2, TM3, and TM6 in TMD1. These structural deviations away from twofold symmetry may explain some of the existing data supporting the asymmetry of the pore.

1.2.3 CFTR as Anion Channel

CFTR is an anion channel; some positively charged residues, such as K190 (TM3), R248 (TM4), and R370 (TM6), located at the cytoplasmic entrance of the channel, may attract chlorine from the bulk solution to the interior of the pore (El Hiani and Linsdell, 2015). Some charged residues seen within the internal vestibule, such as K95, R352, and R303 (Zhang and Chen, 2016; Liu et al., 2017), may tune the energetic profile within the internal vestibule to allow the flow of anions from the cytoplasmic entrance to the interior of CFTR. These charged side chains could work as individual “anion binding sites” (Linsdell, 2017), or the role of positively charged residues in the internal vestibule could be to create a favorable electropositive potential for anion (Hwang et al., 2018). In addition, an important role, assumed by the positively charged residues in the pore, is to neutralize the negatively charged side chains that may pose unfavorable local energetic profile for anion permeation. Collectively, an energetically favorable profile for anion movement in the pore requires a balanced and well-tuned cross talk, involving multiple charged residues along the permeation pathway, although different charged residues may play different functional roles in gating, permeation, or even protein folding/maturation.

1.2.4 Function of CFTR under Normal Conditions

CFTR is a transmembrane protein that functions as an anionic channel and has an important role in the secretion and absorption of electrolytes and fluids, regulating the composition of the mucus in secretory epithelia.

In sweat glands CFTR is involved in the secretion of chlorine (primary sweat) and in its absorption (final sweat). In particular, the sweat gland consists of a secretory coil, located in the hypodermis, and an absorptive duct that leads to the skin surface. CFTR is expressed both in the secretory coil and in the epithelial cells, lining the excretory duct. In the secretory coil occurs the formation of the

primary sweat that's isotonic with the blood plasma. Under normal condition, the reabsorption of salts takes place in the excretory duct to avoid a significant loss of salts (Quinton, 2007).

In particular, the excretory duct is covered by epithelial cells that carry CFTR on the apical membrane, which reabsorbs chlorine, and because of a functional interaction, the ENaC channel absorbs sodium in the epithelial cells. In this way the concentration of electrolytes in the final sweat is decreased by 5-6 times compared to that of the primary sweat and to that of the plasma.

At the level of the bronchi, pancreas and intestines the functional need is to properly moisturize the mucus. In these organs, Cl^- flows through CFTR from the inside of the cell outwards (e.g. the bronchial lumen), where it meets the mucus and, together with the sodium ion (Na^+), which follows the destiny of Cl^- (they form the saline aggregation), guides the secretion of water from the inside to the outside of the cell, resulting in a fluidizing effect on mucus (Figure 2).

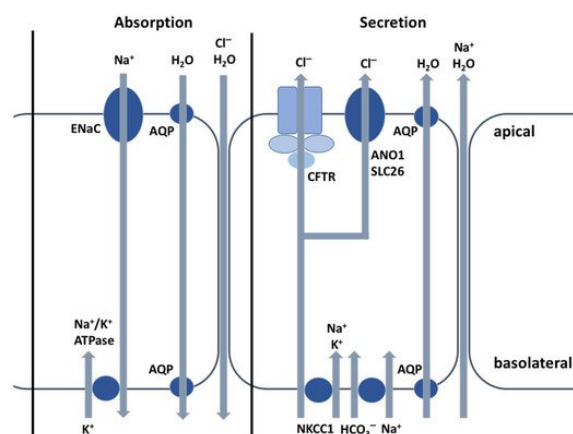


Figure 2. Schematic representations of ion transport in airway epithelia.

Cl^- secretion across the epithelial cell apical membrane depends on the CFTR channel opening and number, and creates the driving force for Na^+ secretion across the epithelial cells through the paracellular pathway, with water following osmotically via aquaporins or the paracellular pathway (ANO1 = anoctamin-1; AQP = aquaporins; NKCC1 = Na-K-Cl cotransporter), (Hanssens et al., 2021).

CFTR secretes bicarbonate in the lungs, pancreas, salivary glands, intestines and reproductive tract, while it reabsorbs bicarbonate in the sweat glands. Bicarbonate controls the pH of the liquid layer at the surface of epithelial cells where the protein is expressed (Zajac et al., 2021). In addition, correlations between CFTR expression levels, bicarbonate secretion and defense against pathogens have also been reported; bicarbonate is an essential component of ASL and it has the role of

maintaining its pH neutral, promoting antimicrobial activity to protect the lungs against infection. Bicarbonate inhibits bacterial growth, lung colonization, and biofilm formation (Dobay et al., 2018).

Beside its role in innate immunity related to ion transport, the CFTR protein is also expressed in macrophages and neutrophils (Yoshimura et al., 1991).

The alveolar macrophages help maintain immunological and physiological homeostasis in the lungs and are the front line of cellular defense against pathogens that were not eliminated by the mechanical defenses of the airways. They also participate to start inflammatory response and to recruit activated neutrophils into the alveolar spaces, through the synthesis and secretion of cytokines and chemokines.

1.2.5 Biogenesis and Trafficking of CFTR

The CFTR gene, located on chromosome 7, encodes a 1480 amino-acids protein. The gene is transcribed in the nucleus, the m-RNA moves to the cytosol and is translated on the ribosomes of the endoplasmic reticulum (ER). The polypeptide is folded and inserted in the ER lipidic bilayer, at the same time. CFTR interacts with different chaperons to achieve the correct folding.

Molecular chaperones are a family of proteins that primarily play their role in determining the proper folding of other proteins. In particular, they ensure the achievement and maintenance of the correct conformational state of newly synthesized polypeptide chains; they direct the assembly of multienzyme complexes; they act on damaged proteins to facilitate their re-folding or degradation.

When CFTR is correctly folded, it can move to the Golgi complex where it gradually assumes the mature form, in particular a molecule of mannose is replaced by a more complex oligosaccharide (Farinha et al., 2016).

The composition of glycan chain is useful to monitor trafficking of CFTR biochemically through western-blot technique, in fact CFTR has two N-glycosylation sites, and the core-glycosylated, immature ER form (B band) is easily distinguishable from the Golgi-processed form (C band) with its heterogeneous glycan chains.

The presence of a protein, called COP II is necessary for CFTR to reach the Golgi; COP II is located at the ER and allows CFTR to maintain the correct folding. Once completed the maturation process, CFTR is transferred to the plasmatic membrane PM of the cells through vesicles.

The half-life of CFTR at the PM is about 12-24 h. The CFTR pool at the membrane is maintained by a balance between anterograde trafficking, endocytosis recycling to the membrane and lysosomal degradation.

CFTR is subjected to multiple protein quality control (PQC). The quality control is made at two levels, at the ER, as CFTR is synthesized, and in post- ER compartments, after its folding and trafficking. The PQC build a pathway that can lead to the degradation or to the folding of proteins, in fact some factors bind to CFTR to promote the folding and the maturation of the protein, but other factors recognize unfolded CFTR and lead these proteins to degradation (Estarbrooks et al., 2020).

The first components that interact with CFTR are the molecular chaperons named HSP90 and HSP70 (Heat shock proteins).

The chaperone HSP70 has ATPase activity; in the ATP-bound state, the monomeric HSP70 cannot bind substrate polypeptide stably, whereas, in the ADP-bound state, the substrate is tightly bound. Two classes of co-chaperones regulate the HSP70 ATPase cycle: DNAJ co-chaperones that stimulate ATP hydrolysis and substrate binding by HSP70 through a conserved J domain; and the nucleotide exchange factors (NEFs) that promote the release of ADP from HSP70, re-binding of ATP and dissociation from substrate.

In a cycle (Figure 3), first, HSP 70 is in the ATP bound state and does not bind substrate polypeptide; then a substrate-binding DNAJ co-chaperone contacts HSP70 to stimulate ATP hydrolysis. In the ADP-bound state HSP 70 binds substrate and the DNAJ dissociates. At the end, NEF co-chaperone promotes the exchange of ADP for ATP and dissociates, so HSP 70 returns in the ATP-bound state. (Palleros et al., 1993; Szabo et al., 1994; Mayer and Bukau, 2005; Kampinga and Craig, 2010; Young, 2010; Hartl et al., 2011).

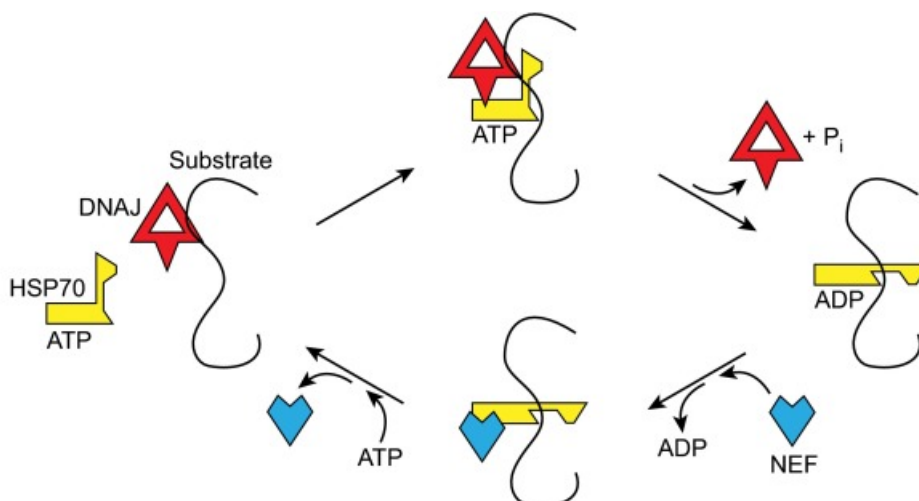


Figure 3. ATPase cycle of HSP70 (Young 2014), see details in the test.

In particular, the co-chaperone DNAJ1 activates the binding of HSP70 to CFTR promoting the correct folding of the protein. Then, the co-chaperone HOP transfers CFTR from HSP 70 to HSP 90 to complete the folding. (Young, 2014).

Another important chaperon is calnexin (CNX); it's located in the ER where affects the folding of CFTR transmembrane domains. While the binding of CNX to CFTR can prevent pro-degradation quality control proteins from binding immaturely folded CFTR, studies also suggest that CNX can obstruct channel maturation. In fact, inhibition of CNX improves trafficking of wildtype-CFTR (WT) from the ER to the PM. However, such inhibition has little effect on F508del-CFTR, perhaps indicating that F508del is targeted for degradation prior to the role of CNX in the quality control pathway.

(Rosser et al., 2008; Farinha et al., 2005).

When CFTR isn't corrected folded, it's tagged with ubiquitin, a 76-amino acid polypeptide that signals the release of CFTR from the ER membrane to the degradation. This process of ubiquitination involves the lysine residues of the proteins. Rather than trafficking to the cell membrane, ubiquitin-tagged CFTR is hydrolyzed by the proteolytic chymotrypsin-like activity of the proteasome (Oberdorf et al., 2001).

The ubiquitin-proteasome endoplasmic reticulum-associated protein degradation (ERAD) pathway process requires 3 enzymes, E1, E2 and E3. The first step begins with the activation of E1 through the ATP hydrolysis. The E1 enzyme catalyzes the C-terminus of ubiquitin and then transfers ubiquitin to an E1 active site cysteine residue (Mulder et al., 2016).

Next, E2 ubiquitin-conjugating enzymes are recruited to E1-ubiquitin complex and catalyze the transfer of ubiquitin to the active site cysteine of E2.

E3 ubiquitin ligases bind both E2 enzymes and substrates while transferring ubiquitin from the E2 to the substrate. E3 ubiquitin ligases often transfer multiple ubiquitin polypeptides to a substrate, creating a polyubiquitin chain. Ubiquitinated proteins are then trafficked to the proteasome for degradation.

To date, several E3 ubiquitin ligases have been shown to ubiquitinate CFTR. For example, RMA1 (sometimes called RNF5) and its homologue RNF185, ubiquitinate misfolded CFTR following NBD1 translation.

Unlike RMA1 and RNF185, the E3 ubiquitin ligase CHIP only acts on fully translated CFTR. As RMA1, RNF185, and CHIP are unable to directly bind to CFTR, these proteins ubiquitinate misfolded CFTR through adaptor proteins. Specifically, RMA1 and RNF185 require Derlin-1, while

CHIP binds HSP70. HSP70 often promote CFTR folding, so CHIP is able to deviate this chaperone to trigger ERAD (Strub and McCray., 2020). The HSP 70-CHIP complex functions at the cell surface quality control, where promotes the degradation of misfolded CFTR, already located at the PM, in the lysosome.

In conclusion, the chaperone HSP 70 is involved both in the folding of CFTR and in its degradation.

1.2.6 Classes of Mutations

To date, more than 2000 mutations of the CFTR gene are reported in the Cystic Fibrosis mutation database (CFTR1 Database) and about 15% of the genetic variants is not associated with a clinical phenotype. Mutations have been divided into 6 classes (Figure 4) correlating their effect on the final protein.

This approach is helpful because it relates to the molecular and cellular processes in gene translation and protein processing and has some useful clinical correlates.

Class I mutations lead to no protein synthesis or translation of truncated forms. They result from splice site abnormalities, frameshifts due to deletions or insertions, or nonsense mutations, which generate premature termination codons (no protein production).

Examples of Class I mutations include R553X and G542X, the second most common CFTR mutation.

Class II mutations lead to a misfolding protein that fails to achieve conformational stability in the endoplasmic reticulum and fails to reach the Golgi apparatus, so, CFTR isn't fully glycosylated and it does not traffic to the PM. The protein is identified as misfolded by ERAD quality control mechanisms and is prematurely degraded by proteasomes (folding and trafficking defect).

Belonging to this class is the F508del; it is the most common mutation to cause CF, affecting about 82% of the CF individuals and it is caused by a three base pair deletion on exon 11 that results in the loss of a phenylalanine at residue 508. This mutation leads to CFTR protein misfolding that is arrested by the ER quality control, precluding its processing and trafficking to the PM, the protein is targeted and prematurely degraded by proteasomes. A small amount of the mutant protein may evade the quality control checkpoints and reach the PM, but it's affected by a defective gating and a reduced protein stability (Okiyoneda et al., 2010).

Class III mutations cause a gating channel defect, although the protein is located at the PM (gating defect).

This type of mutation is usually located in the NBD or in the phosphorylation sites of the regulatory domain of CFTR.

Examples of III class mutations are G551D and S1255P. G551D is the third most common CFTR mutation and produces a protein that, after reaching the cell membrane, has about 100-fold lower open probability than that of wild-type. Dimerization of the NBDs of CFTR forms two ATP binding pockets, termed ABP1 and ABP2. Whereas binding of ATP to ABP1 helps to stabilize the open channel conformation of CFTR, channel opening is dependent on ATP binding of ABP2 (Bompadre et al., 2007). The G551D mutation, is located in ABP2, the second ATP binding pocket of CFTR, and its presence prevents ATP binding, thus inhibiting opening of the CFTR channel. (Bompadre et al., 2008).

The S1255P mutation, found in NBD2, alters the ATP-binding pocket, resulting in gating instability (Zeitlin, 1999).

Class IV mutations cause a defect in channel conductance with a reduction in CFTR-dependent chloride transport (decreased conductance).

Mutations affecting channel pore activity often arise in arginine residues (e.g., R117H, R347P, R334W). Some Class IV mutations, including R117H, also decrease the open probability of CFTR. (Yu et al., 2016).

Class V mutations lead to a reduction in protein abundance of functional CFTR caused by a reduced synthesis or inefficient protein maturation (reduced protein abundance).

The most prevalent examples of Class V mutations include c.3717+12191C>T and c.3140-26A>G.

Class VI mutations cause a reduced stability of CFTR at the PM, which results in increased endocytosis and degradation by lysosomes, and reduced recycling to the PM (unstable protein).

Examples include c.120del123 and F508del when rescued by low temperature or correctors (rPhe508del) (Marson et al., 2016).

Mutations in classes I, II and III are also known as minimal function mutations since they demonstrate a very little CFTR activity, while those in classes IV, V, and VI are known as residual function mutations, since they demonstrate some CFTR function, although it is lower compared to the wild type CFTR. For this reason, mutations in class I, II and III are usually associated with a more severe disease than the last three classes.

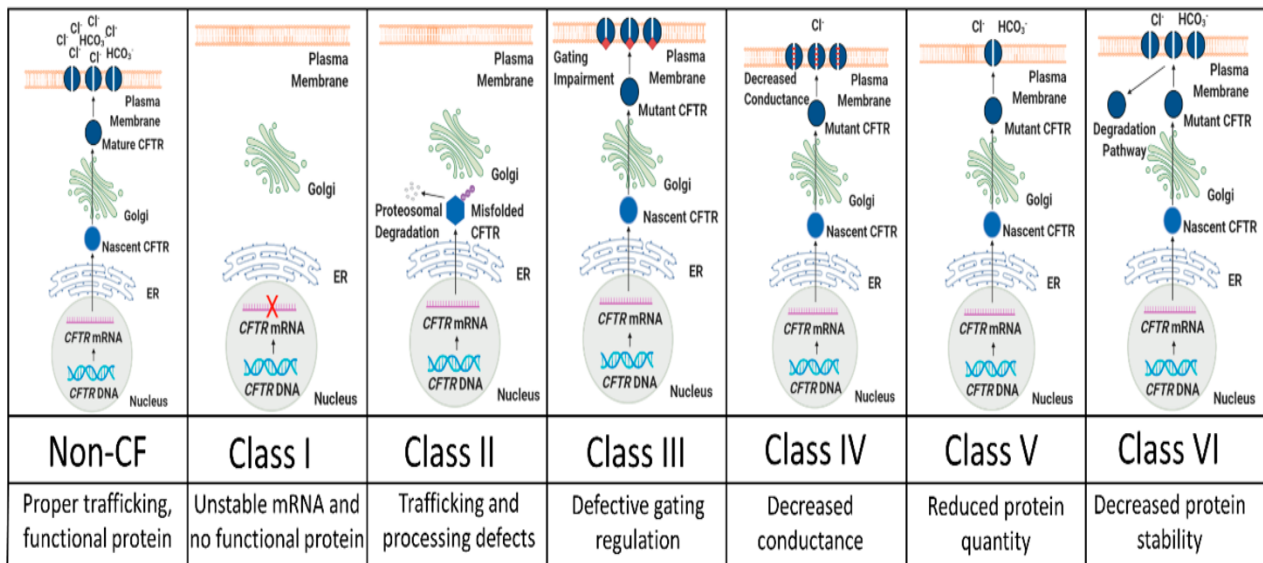


Figure 4. Classes of mutations (Strub and McCray, 2020).

1.3 Cystic Fibrosis Disease

Cystic fibrosis is a multi-organ disease characterized by a wide spectrum of symptoms. Different genotypes correspond to different phenotypes. The classic image of the patient with CF shows a patient suffering from digestion problems, linked to pancreatic insufficiency, and chronic pulmonary obstruction, with recurrent bacterial infections. In addition, the large clinical variability suggests that factors not directly related to CFTR also play an important role in the development of individual clinical history (Drumm et al., 2005).

1.3.1 Lung Disease

The lung is an organ affected very early, inflammatory markers are found in the bronchial fluid and the lung structure damage is highlighted by High Resolution Chest Tomography in asymptomatic children (Tiddens, 2002). In fact, the lack of CFTR or its malfunction leads to a lower water content in the periciliary fluid and to an abnormal dense mucus. The mucus becomes particularly viscous because mutated CFTR down-regulates the ENaC channel, located on the apical membrane of epithelial cells, too, causing an over-absorption of sodium and a consequent reduced hydration of mucus. The viscous secretions at the level of the lungs compromise the ciliary activity and the pulmonary clearance (Tang et al., 2014). The lack or malfunction of CFTR is also related to an increase in the inflammatory response and a reduced activity of the defense mechanisms. The inflammatory response of the lung is characterized by excessive neutrophil infiltration, pro-inflammatory cytokine production, and the presence of free elastases released by neutrophils.

Elastase, along with other enzymes, such as cathepsin S and metalloproteases, cause lung lesions that are worsened by the presence of reactive oxygen species (ROS). CFTR is also involved in the transport of glutathione and thiocyanate, both with an important role as antioxidants in the lungs (Linsdell and Hanrahan; 1998; Conner et al., 2007). Two glutathione molecules react in the presence of the enzyme glutathione peroxidase reducing hydrogen peroxide to water, while the thiocyanate reacts with hydrogen peroxide generating hypothiocyanin, harmless in the lung tissue. As these ROS defense systems fail, the lung suffers high oxidative stress. Bacterial, fungal and viral infections are facilitated in this pro-inflammatory environment.

The bacteria that most commonly cause the development of infections in the CF patient are *Staphylococcus Aureus*, *Haemophilus Influenzae* and *Pseudomonas Aeruginosa*. *Staphylococcus Aureus* is the most commonly identified bacterium in standard cultures and is found in more than 30% of children during the first 6 months of life (Sly et al., 2009).

When these microorganisms are found in the lower respiratory tract of infants and young children, they are associated with lung inflammation, even in the absence of symptoms.

P. aeruginosa is a significant pathogen due to clinical decline and increased mortality (Emerson et al., 2002). Infection with *P. aeruginosa* occurs early in life, with median age of first detection at around 2 years and as early as 3 months of age (Mott et al., 2012). In add, the environment, together with host and bacterial factors, plays a part in acquiring infection with this organism. Detection and eradication of *P. aeruginosa* during the preschool years may prevent the morbidity and mortality associated with chronic *P. aeruginosa* infection, but it doesn't seem enough to prevent the development of structural lung disease (Wainwright et al., 2011) or lower lung function. Structural damage to the lung is the endpoint of the pathophysiological injury incurred through infection and inflammation. Lung function is diminished after diagnosis of CF in infants after newborn screening and is characterized by reduced forced expiratory flows and volumes, elevated functional residual capacity and lung clearance index, suggesting airway obstruction, air trapping, and ventilation inhomogeneity, respectively (Hoo et al., 2012).

Infection with a proinflammatory pathogen in the first 2 years modifies disease progression, resulting in persistent impairments to respiratory function. Early surveillance and interventions need to identify and eradicate infections with respiratory pathogens, not just with *P. aeruginosa*, until modifying agents are available. The infants who remain free of pulmonary infections during infancy could improve lung function and minimize structural lung disease (Ramsey et al., 2014).

1.3.2 Gastrointestinal Disease

The intestine, pancreas and liver are the organs the most affected in the gastrointestinal apparatus.

PANCREAS

CFTR is expressed in ductal epithelial cells in the pancreas where the lack of CFTR function results in reduced water content of the pancreatic secretions and decreased pH. The luminal content has an increased viscosity and the presence of pancreatic enzymes cause obstruction and progressive destruction of the acini, inflammation and fibrosis.

The developing of pancreatic exocrine insufficiency cause fat malabsorption and it is detectable at birth in 60–80 % of affected infants and causes malnutrition and poor growth (Cipolli et al., 2007).

Related to malnutrition and a lower absorption of D vitamin, there is the problem of bone disease like risk of osteopenia, osteoporosis, and vertebral fractures (Sermet-Gaudelus et al., 2011). It's worsed by the severity of lung disease, poor mobility, use of steroids, circulating inflammatory cytokines, and increased bone turnover.

Episodes of pancreatitis are recurrent and, in the long term, there's a total loss of enzyme secretion. In older ages, parenchymal progressive destruction leads to the CF-related diabetes.

CF-related diabetes has distinctive peculiarities that make it different from type 1 and type 2: it originates from reduced secretion of insulin, but is also partially due to insulin resistance, particularly during acute pulmonary exacerbations. Its insurgence is associated with worsening of the respiratory disease, but good control of hyperglycemia reduces the number of respiratory exacerbation and slows down pulmonary disease progression.

INTESTINE

In the intestine CFTR guides bicarbonate secretion and it is essential to buffer gastric acidity and to allow expansion and hydration of the intestine mucus. Meconium ileus affects approximately 20 % of CF neonates and is more frequently associated with severe mutations (Dupuis et al., 2016). Older patients may exhibit constipation and may develop a sub-occlusive or occlusive manifestation called distal intestinal obstructive syndrome.

LIVER

CFTR is expressed in epithelial cells of the biliary duct and regulates bile acid independent bile flow. Viscous bile may cause obstructive liver disease progressing to multilobar biliary cirrhosis and portal hypertension. The prevalence of severe liver disease peaks in adolescence and about 5 % of patients may require liver transplantation (Flass and Narkewicz; 2013).

1.4 Therapies

1.4.1 Symptomatic Therapies

Current therapies treat the symptoms of pathology and include antibiotics, anti-inflammatory agents, mucolytics, hypertonic nebulized saline formulations, use of pancreatic enzymes and lung

transplantation (Ashlock and Olson, 2011; Cuthbert et al., 2011).

The main goals of CF therapy are to promote clearance of secretions, control lung infections, provide adequate nutrition and prevent intestinal obstruction.

- Diet: in children with CF the energy requirement is greater because of lung infections and decreased intestinal absorption, even in the presence of adequate intake of pancreatic enzymes. The diet must be hypercaloric (on average equal to 120-150% of the levels normally recommended for subjects of the same sex and age), the content of lipids and proteins must be augmented. The share of carbohydrates should promote the intake of starches with a percentage of sugars with rapid absorption not exceeding 10%. It is necessary to ensure an adequate intake of mineral salts and in particular sodium, especially in the hot season or during gastroenteritis, fat-soluble vitamins and vitamin B12 in subjects who have had extensive intestinal resections.
- Use of gastro-protected pancreatic enzymes: the patient with pancreatic insufficiency takes digestive enzymes at each meal in a dose appropriate to the absorption of the ingested fats and according to the degree of pancreatic insufficiency of the subject.
- Aerosol therapy: it is carried out with several sessions throughout the day, with the aim of hydrating the airways and conveying different classes of drugs such as bronchodilators and corticosteroids, antibiotics, recombinant human DNAase, Hypertonic saline and other moisturizing agents.
- Respiratory physiotherapy: it aims to keep the lungs free from secretions. The removal of thick and viscous mucus from the airways reduces the possibility of infection; also keeping the respiratory apparatus free of secretions improves breathing, helping the drugs to perform their best action. The techniques used and the time commitment required must be individualized. Respiratory physiotherapy is recommended 1 to 4 times a day. After draining each lung segment, the patient is encouraged to cough, blow, and perform forced exhalations. Voluntary coughing and repeated forced exhalation with positive expiratory pressure (PEP-mask) may also be useful to eliminate mucus.
- Antibiotic therapy: viscous mucus obstructing the respiratory tract promotes the proliferation of bacteria. Antibiotic therapy, preferably aerosol, plays an important role in infection control. This should be prescribed only on the basis of the result of the microbiological analysis of bronchial secretions obtained after coughing or by pharyngeal aspiration. This examination should be repeated every 2 or 3 months. In particular, attention must be paid to the treatment of *Pseudomonas aeruginosa* infection, to prevent it from becoming chronic. The first infection with *Pseudomonas aeruginosa* must be dealt with promptly, to eliminate the germ preventing

its chronicization. In the treatment of chronic infection, however, it would be good to implement a rotation of the prescribed drugs in combination with high doses and in associations, to prevent the occurrence of resistance to the antibiotics themselves.

- Anti-inflammatory therapy: oral corticosteroids are indicated in infants with prolonged forms of bronchiolitis and in those patients with refractory bronchospasm, allergic bronchopulmonary aspergillosis and inflammatory complications. Prolonged use of corticosteroid therapy may slow the deterioration of lung function; due to steroid complications it is not recommended as a routine treatment. Ibuprofen, administered for several years, appears to reduce the rate of deterioration of respiratory function.
- Night Oxygen Therapy and Support with Non-invasive Ventilation: it is necessary for patients with advanced lung disease, who experience nocturnal hypoxemia and hypercapnia, especially during infectious exacerbations of pulmonary disease.

1.4.2 Therapies Against the Basic Defect

Currently the most interesting therapeutic approach is represented by therapies that treat pathogenic mechanisms or that are aimed to correct the defects underlying the loss of function of CFTR. In recent years particular molecules, called modulators, have been introduced in therapy. CFTR modulator drugs enhance or restore the expression, function, and stability of defective CFTR in different ways and in relation to their effect on CFTR mutation, they are classified in five groups: potentiators, correctors, stabilizers, read-through agents and amplifiers.

Potentiators are compounds that restore or enhance the channel open probability of CFTR.

Correctors are molecules that rescue folding, processing and trafficking to the PM of a CFTR mutant. These compounds may act by distinct mechanisms, but they usually enhance protein conformational stability during the ER process.

Read-Through agents are compounds that induce a ribosomal over-reading of a premature terminator codon, enabling the incorporation of a foreign amino acid in that place and the continued translation to the normal end of the transcript (Pranke et al; 2018).

Stabilizers are agents that anchor CFTR at the PM, preventing its removal and degradation by lysosomes (Fukuda and Okiyonedo, 2018).

Amplifiers are compounds that increase the expression of CFTR mRNA and the biosynthesis of the CFTR protein (Giuliano et al; 2018).

1.4.3 Potentiators

About 5% of mutation causing CF are mutations of class III and IV, so they need a potentiator to restore the gating defect. Genistein in figure 5, an isoflavone, was one of the earliest compounds identified as potentiator, it shown to bind and inhibit protein-tyrosine kinase with an increased in the cAMP levels and a potentiation of the activity of CFTR in cells (Illek et al., 1995). However, in clinical application it was not useful.

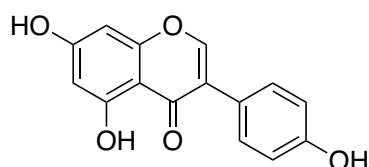


Figure 5. Structure of Genistein.

Some years later, Vertex identified a small molecule, called VX-770 in figure 6, or Ivacaftor, by High Throughput Screening, that partially restored activity of CFTR in cell lines expressing G551D mutation and in primary bronchial epithelial cells (Van Goor et al; 2009).

VX-770 demonstrated to increase the forced expiratory volume in one second (FEV₁), a measure of lung function, by 10% after 2 weeks of treatment in adult patients; to improve the weight (>2.5 kg over 48 weeks) of patients and to reduce the sweat chloride levels.

For these reason, VX-770 passed the clinical studies and in 2012, the Food and Drug Administration and the European Medicinal Agency approved its use (Kalydeco, Vertex Pharmaceuticals) for CF patients older than 6 years and carrying at least one G551D mutation.

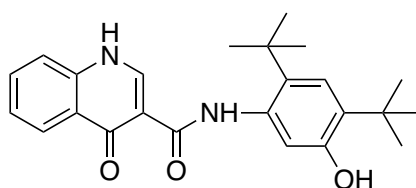


Figure 6. Structure of Ivacaftor (VX-770).

Now, Ivacaftor has been approved for 38 different mutations (Sheppard et al., 2017), including gating, residual function, splicing and conduction mutations, increasing the number of individuals that can find a benefit in this drug. Ivacaftor shows to slow the lung deterioration and reduce pulmonary exacerbation, (McKone et al; 2014); it's linked to a better body mass index and a better quality of life. In add, it improves pancreatic function and muco-ciliary clearance.

Despite the demonstrated benefits, lung function decline at long terms. However, today in clinical trial there are novel candidates with promising effects, as QBW251 (Novartis), CTP-656 (Concert Pharmaceuticals) and GLP1837 (AbbVie/ Galapagos) (Quon et al., 2016). The obstacle to developing such compounds is that there is currently little understanding of existing potentiators' action mechanisms (including Ivacaftor).

1.4.4 Correctors

Correctors are molecules that can act as pharmacological chaperones, so they bind directly to misfolded CFTR, or as proteostasis regulators that modulate the interaction between CFTR and protein homeostasis such as chaperones, cochaperones, kinases, or ubiquitin ligases that affect the synthesis, folding, stability, and trafficking to the plasma membrane of the mutant CFTR. In all the case, these compounds allow the passage of CFTR through the ER quality control checkpoints (Lukacs and Verkman, 2012), increasing the number of mutant CFTR at the PM. In particular, pharmacological chaperones have been classified, based on their molecular targets, in three classes: class I correctors stabilize NBD1 with TMD1 or TMD2 interfaces; class II correctors stabilize NBD2 and its interfaces with other CFTR domains; class III correctors directly stabilize NBD1 (Okiyoneda et al., 2013). This classification is utilized to evaluate combinations of molecules with a possible complementary mechanism of action. In fact, correctors of the same type do not exhibit additive effects and are proposed to share a similar mechanism, while correctors from different classes seem to act through different mechanisms, and some of these can be combined to synergistically promote CFTR folding (Farinha et al., 2013; Pedemonte et al., 2005; Veit et al., 2018, 2020).

The first corrector approved was VX-809 or Lumacaftor (figure 7), discovered by Vertex Pharmaceuticals. It causes a rescue of CFTR on cells with the F508del mutation and in primary bronchial epithelial cells (Van Goor et al; 2011). VX-809 is considered a type 1 corrector (Okiyoneda et al., 2013).

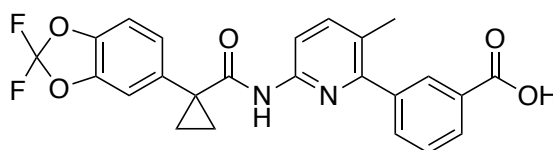


Figure 7. Structure of Lumacaftor (VX-809).

In a 2014 study, Baroni et colleagues (Baroni et al; 2014) observed that VX-809 was homogeneously distributed in the phospholipid bilayer and acted through membrane perturbation; later studies proposed instead that VX-809 acted directly on CFTR; in fact, VX-809 binds to purified CFTR and stabilizes F508del-CFTR after its rescue at the cell surface (Eckford et al., 2014), but the binding site was unknown (Farinha and Canato 2017; Okiyoneda et al. 2013; Ren et al. 2013).

Different functional studies have demonstrated that VX-809 promotes folding of isolated TMD1, stabilizing truncated CFTR fragments that contain complete TMD1 (Loo et al., 2013; Ren et al., 2013).

These functional studies have been recently supported by Fiedorczuk and Cheng (Fiedorczuk and Chen, 2022) that determining the cryo-EM structure of VX-809 related to CFTR in both the NBD-separated conformation and in the NBD-dimerized conformation, demonstrated that VX-809 binds to CFTR in both conformations, pointing out that VX-809 binding site is in TMD1.

Once the N-terminal TMD1 is synthesized, it adopts a tertiary structure that is intrinsically unstable in the ER membrane. Binding of type 1 corrector as VX-809, stabilizes TMD1, making it less susceptible to targeted degradation by protein quality control machinery. By stabilizing TMD1, the overall probability of creating a fully assembled structure increases and thus allosterically rescue many disease-causing mutants residing in other parts of CFTR (Fiedorczuk and Chen, 2022).

In addition to these data on TMD1, NMR spectroscopy, differential scanning calorimetry, and statistical analysis conducted previously, revealed VX-809 binds to NBD1 directly and in addition, allosteric coupling between the binding site and the distant F508 position, at the NBD1:ICL4 interface (Hudson 2017).

In this context, the Rusnati's research group reported surface plasmon resonance (SPR) studies on F508del-NBD1 performed with the corrector VX-809 (Rusnati et al., 2018), molecular docking and dynamics simulations, highlighting a statistically significant correlation between the observed binding capability to F508del-NBD1 and the results of the computational methods, supporting a key role played at the NBD1 level of CFTR by the corrector VX-809.

Moreover, Baatallah and colleagues (Baatallah et al., 2021) explored the potential VX-809 binding sites in both TMD1 and NBD1, by combining blind docking and molecular dynamics simulations with biochemical experiments. They showed that VX-809 can be stably accommodated in an TMD1 groove and described an allosteric coupling linking this site to the F508del region on NBD1, hence, same authors observed that VX-809 has another binding site in NBD1.

Although these promising results *in vitro*, Lumacaftor alone didn't give beneficial effects on patients in clinical, but a significant improvement in lung function was given by the cotreatment with Ivacaftor. In 2015 the FDA and the EMA approved Orkambi, by Vertex Pharmaceutical, a combination of Lumacaftor and Ivacaftor. This novel drug has reported clinical benefits in F508del homozygous patients, older than 12 years, as a reduced number of pulmonary exacerbations, improvement in the body mass index and slower lung deterioration (Konstan et al; 2017). Recently, Orkambi has been approved also for homozygous patients older than 2 years.

Interaction between Lumacaftor and Ivacaftor have a negative impact on the rescue of F508del-CFTR protein. Chronic Ivacaftor exposure ($>1 \mu\text{M}$) reduces Lumacaftor-rescued CFTR in F508del-expressing cells (Cholon et al., 2014; Veit et al., 2014). Lumacaftor also triggers cytochrome P450 3A4 activation, resulting in reduced plasma concentration of Ivacaftor (Schneider, 2018). Such findings underline the importance of better studying the interactions between different drugs. For these reasons other molecules with corrector activity have been developed starting from the structure of Lumacaftor, as Tezacaftor or VX-661(Fig. 8). VX-661 is structurally an analogue of VX-809, it turns out to have the same mechanism of action, so it is classified as corrector type 1, but its pharmacokinetic characteristics are better than those of VX-809, as well as also appears to be reduced the number of side effects.

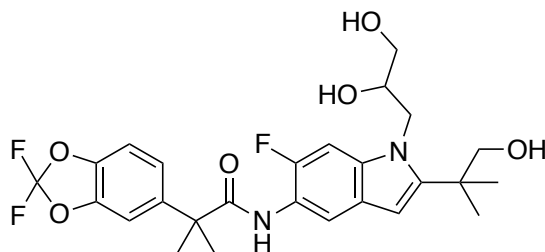


Figure 8. Structure of Tezacaftor (VX-661).

In 2018, cotreatment between VX-661 and VX-770 was approved, marketed as Symdeko, which in clinical trials showed similar effects to Orkambi in homozygous F508del patients, but other heterozygous patients (F508del with G551D or other residual function mutations) are more responsive to Symdeko than Orkambi (Donaldson et al., 2018; Rowe et al., 2017).

Symdeko is the treatment of CF in patients aged 6 years and older who have two copies of the F508del mutation, or who have at least one mutation in the CF gene that is responsive to treatment with this dual therapy.

Symdeko decreases sweat chloride levels, improves lung function (FEV_1) and lowers the risk of having a pulmonary exacerbation.

Since that administration of combination of molecules that act simultaneously in multiple sites of the CFTR pathway has an additive or synergic effect on the rescue of mutated CFTR, a new formulation containing two correctors and a potentiator, in particular Elexacaftor, Tezacaftor, and Ivacaftor (Trikafta, Vertex Pharmaceuticals, Boston, MA) has recently been approved. It is indicated for patients with CF 12 years of age and older who have at least 1 mutation in the F508del gene, regardless of their second mutation type. This increases the eligibility for CFTR modulating therapy to around 90% of patients who have CF (Ren et al., 2018).

Elexacaftor (Fig. 9) is a next generation corrector that exhibits additive or synergistic effects in combination with a type 1 corrector and with the potentiator, leading to markedly increased PM expression of F508del-CFTR (Veit et al., 2020). Although the mechanism of action of Elexacaftor is not fully known, it has been proposed to act as a corrector type 3. Even if, recently data by Laselva (Laselva et al., 2021) showed that Elexacaftor, exhibited dual activity as both corrector and potentiator and suggested that the potentiator activity contributes to its pharmacological activity.

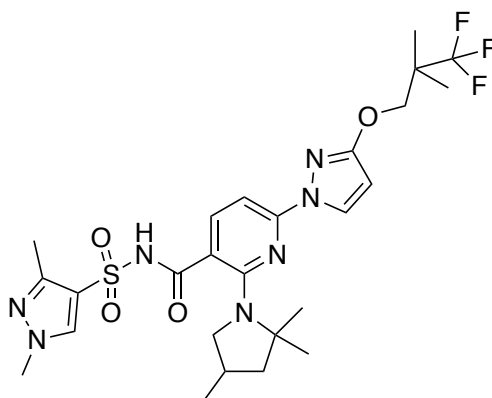


Figure 9. Structure of Elexacaftor (VX-445).

This drug combination provides potential therapy to many patients who had previously been excluded from CFTR modulation therapy due to the nature of their genetic mutations. The efficacy demonstrated in clinical trials exceeds the currently available therapies related to lung function, quality of life, sweat chloride reduction, and reducing exacerbations.

Chapter 2: Methods and Instrumentations

2.1 High Performance Liquid Chromatography

The HPLC, high performance liquid chromatography, is the instrumental version of the column liquid chromatography; in the same manner as all chromatographic techniques, it allows to separate two or more compounds present in a mixture, exploiting the affinity balance between a "stationary phase", placed inside the chromatographic column, and a "mobile phase" that flows through it.

It is considered to be one of the most efficient analytical techniques, both in quantitative and in qualitative analysis. In particular, the greater the affinity of a molecule for the stationary phase, the longer it will take to elute from the column.

The time taken by the analyte to go through the column is referred to as "retention time". HPLC differs from classical chromatography in that separation is carried out at high pressures, up to 400 bar; this allows a much faster and more efficient separation than traditional chromatography, although the cost is much higher.

HPLC techniques can be classified according to phase polarity, in fact chromatography can be in direct phase, if the stationary phase is polar and the mobile phase is apolar, or reverse phase, if the stationary phase is apolar and the mobile phase is polar. Moreover, chromatographic techniques are distinguished according to the physical and chemical principles that influence the distribution between the two phases, in adsorption chromatography, repartition (based on hydrophobicity), dimensional exclusion (based on size), ion exchange (based on charge), affinity (based on ligand specificity). The interactions that occur between the substances to be separated and the two phases (mobile and stationary) are weak, and they are hydrogen bonds, dipole-dipole interactions, dipole-induced dipole interactions, Van der Waals forces, Coulomb attraction and steric interactions. The mechanisms of separation are closely linked to the types of interaction.

The mobile phase must meet some requirements such as: immiscibility with the stationary phase, ability to solubilize the sample, compatibility with the detector, low viscosity, low corrosivity, high purity, low volatility and controlled pH.

The elution is also defined as isocratic, if the same solvent or a mobile phase consisting of different solvents maintain the same composition during the elution, or gradient, if the composition of the mobile phase during the analysis changes.

Loading of a column varies between analytical and preparative HPLC; normally micrograms of substance are used in analytical HPLC while milligrams are used in preparative HPLC. In any case it is important that the substance to be injected is well dissolved in appropriate solvent.

Among the advantages of this technique, we find: the reduced size of the column, which avoids problems of longitudinal deviations (movements of the longitudinal mobile phase) and the presence of alternative paths, the flow rate of the mobile phase (passage of the mobile phase through the column) that is constant and adjustable, the execution speed that is reduced. In addition, greater accuracy and precision thanks to the small amounts of compound required for the analysis is found.

2.1.1 HPLC: instrumentation

The components of the HPLC equipment are (Figure 10):

- The containers of the mobile phase, downstream of which there is often a degassing system that prevents the formation of gas bubbles at the exit of the column, which may interfere with the performance of the detector.

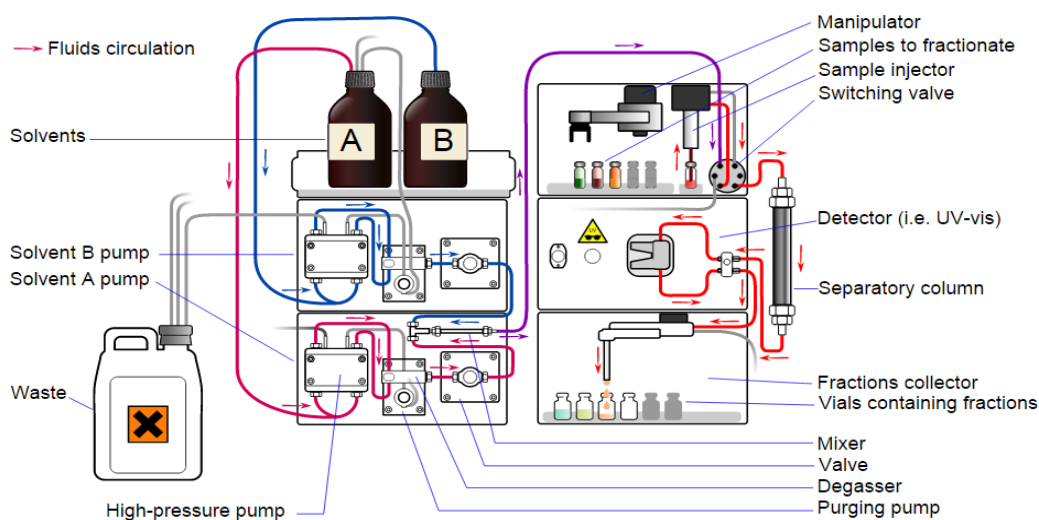


Figure 10. HPLC instrumentation

- The pumps that allow the flow of the mobile phase through the column to the exit, where the detector is located. Considering the small size of the stationary phase, the presence of a pumping system allows to speed up the separative process and to obtain a better resolution.
- The sample introduction system.
- The column, the only part of the instrument in which the separation of analytes takes place.
- The detector that's usually a UV-VIS detector; it records the absorbance of analytes in real time, based on their ability to absorb visible UV radiation, in a wavelength range between 190 nm and 820 nm, providing both qualitative and quantitative information.

2.1.2 Pumping System

The ideal characteristics of an HPLC pump are: ability to work at high pressures; maintaining a constant and pulsation-free flow; good reproducibility; corrosion resistance.

There are three main types of pumps:

Alternative pump: can be either single piston or pair of pistons. The pistons move back and forth inside a tight cylinder and work at staggered times. The solvent flow is regulated by two valves that open and close in synchrony with the piston. This system is the one most frequently used because the costs are low and allows a good versatility and adaptability to changing gradient during the analysis.

Screw-driven syringe pump: it consists of a cylinder, inside which the solvent is located, pushed by a piston. The latter is driven by a motor connected to a "worm" screw that allows you to keep the flow constant and easily controllable. It has, however, disadvantages like high costs, a large footprint and poor tank capacity.

Pneumatic or constant pressure pump: the solvent is contained in a flexible vessel compressed from the outside with a gas under pressure. Unlike the other two pumps, the output capacity and the pressure are limited and, in addition, the flow speed depends on the viscosity of the solvent. However, it has a number of advantages, including the low costs, the ease of use.

2.1.3 System for the Introduction of the Sample

The most used sample loading system in HPLC is the one that uses an external capillary, of known volume, called a "sample loop". This method allows to obtain a high reproducibility of injection of the sample, moreover it can be used for preparative, semi-preparative and analytical analyses, thanks to the presence of interchangeable loops, characterized by variations in injection volume from 1 μ l to 5000 μ l.

The sample is injected with a special syringe by holding the septum present in the system, favoring the entry into an injection chamber. At this point, acting on the injection valve, the flow can be diverted through the "sample loop" containing the injected sample, allowing the entry into the analytical column. This system allows the mobile phase to flow from the pump to the column, injecting the solution directly into the loop.

2.1.4 Columns

Between the injector and the column there is the pre-column, whose main task is to "mechanical filter" because it removes any impurities, undissolved particles and contaminants, prolonging the life of an analytical column. It has an internal composition similar to that of the column although the particle sizes are larger, to minimize the pressure drop at the extremes.

The stationary phase is packed in a column usually made of stainless steel or polymers, (Polyether ether ketone -PEEK), materials resistant to the application of high pressures. The analytical column has a length varying between 5 and 25 cm, an internal diameter between 3 and 5 mm and internally contains particles of homogeneous size and characterized by a very fine grain size, from 3 to 10 μm . Column fills are mainly of two types: film particles, consisting of a non-porous spherical core (silica or glass) coated with a thin layer of microporous and porous microparticles that ensure greater efficiency and have a greater load capacity of the sample. The most used filling materials are silica, alumina, styrene-divinylbenzene copolymers, ion exchange resins.

One of the most used column types is the C18 column where the support is based on hydrolyzed silica. The silanol groups reacted with the appropriate alkyl halide ($\text{C}_{18}\text{H}_{37}\text{Cl}$), but due to steric hindrance a part of the hydroxyls remains free; then a pickling reaction with trimethylchlorosilane, to avoid the presence of centers of excessive polarity is used. The result is a silica granule functionalized with alkyl chains that form a fluid monomolecular layer. The stationary phase is liquid as it is a chemically bound stationary phase.

The advantages of this type of stationary phase lie in the high mechanical stability and in the high-pressure resistance.

2.1.5 Detectors

There are several types of detectors, including electrochemical detectors, detectors based on refractive index change, diffuse light detectors in evaporation, but the most used are those based on the sample's ability to absorb UV and/or visible light.

A good detector must have a number of features, such as adequate sensitivity, good stability and reproducibility, linear response for multiple orders of magnitude, short response time, high ease of use and reliability. Moreover, it must have uniformity of response towards all analytes or, conversely, high specificity for particular compounds, preferably non-destructive detection and small internal volume to avoid band widening.

The detectors usually have an optical path between 2 mm and 10 mm and volumes between 0.5 μl and 10 μl . The most commonly used spectral region is that of UV, especially with wavelengths ranging

from 190 nm to 380 nm, infrared and visible regions are more rarely used. Mercury, deuterium or tungsten lamps are common.

Nowadays, diode array detectors are preferred, called "diode-arrays", which allow to measure in real time the entire UV spectrum of the analyte.

Spectrometric detectors are also widespread, which are able to identify the analytes at the HPLC column output based on their mass, resulting in coupled HPLC-mass spectrometer (HPLC-MS) systems.

2.1 Mass Spectrometry

The mass spectrometry is an analytical technique used for qualitative and quantitative analysis. The wide use of this method is linked to its extreme sensitivity, selectivity, specificity, speed and efficiency.

The principle on which it is based is that a molecule in the gas phase is ionized by the detachment of an electron; in this way a radical cation (molecular ion) is formed, which is partly fragmented by generating neutral radicals, which the instrument does not detect, and cations and radical cations (fragment ions). The molecular ion and the various ions that originate by fragmentation are discriminated on the basis of their mass/charge ratio and revealed by a detector. The result is the mass spectrum, which represents the relative abundance of ions as a function of their mass/charge ratio (m/z).

Each molecule therefore has its own characteristic and specific fragmentation, which depends both on the nature of the molecule and on the operating conditions of ionization. This technique makes it possible to measure molecular masses (both nominal and exact) and to obtain fragmentation profiles that are specific to each compound. It is possible through this analysis to identify the structure formula of unknown compounds, even in the presence of small quantities.

2.2.1 Mass Spectrometer: instrumentation

The mass spectrometer (Fig. 11) consists of a series of basic elements:

- System for sample introduction
- Ionization source: ion generation system
- Analyzer: separates ions according to their m/z ratio
- Detector: detects ions emerging from the analyzer and measures their abundance
- Data processing system

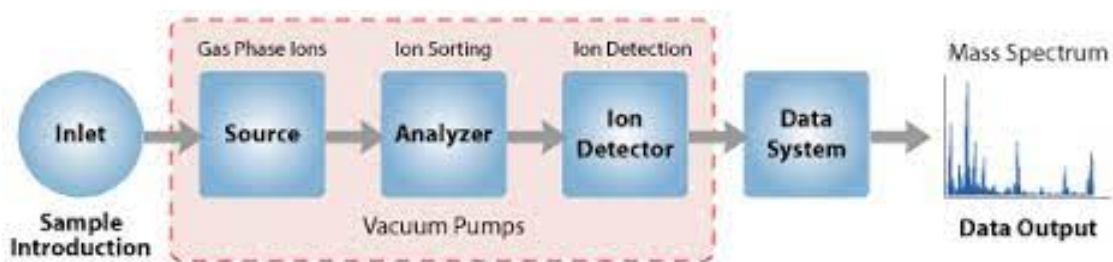


Figure 11. Scheme of a mass spectrometer (http://www.premierbiosoft.com/tech_notes/mass-spectrometry.html)

The mass spectrometer operates under high vacuum conditions (10^{-6} - 10^{-5} Torr) because the impact between ions and atmospheric gas could cause a loss of ionization.

2.2.2 Introduction of the Sample

The introduction of the sample (in the order of micrograms) into the mass spectrometer may take place in the solid state, in the liquid state or in the gaseous state. Solid samples can be found in volatile or non-volatile form. In the first case the samples are introduced into the ionization chamber with the help of a vacuum-tight heating probe; the non-volatile ones are dissolved in a solvent and analyzed through an ionization system such as the technique called "thermospray" or "electrospray". The liquid sample can be introduced via an HPLC system located upstream of the spectrometer or via an infusion pump (direct introduction). Finally, the gaseous samples are introduced through a gas chromatography system, to separate the mixture of interest, and through the use of flow control valves.

2.2.3 Ionization Source

The sample must be ionized in a special ionization chamber to be analyzed, where the electron beam is produced by an ionic source that varies depending on the technique used. Among the various devices, some allow only positive fragments to be analyzed, while others allow the detection of negative ions (anions).

In addition, some ionization techniques operate at high energy and lead to a strong fragmentation ("hard" techniques), while others operate at low energy, producing a lower number of ions ("soft" techniques).

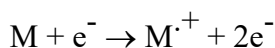
Ionization can be carried out by these systems:

1. Electronic impact (EI)
2. Chemical ionization (CI)
3. Electrospray (ESI)

- Ionization by electronic impact

Starting from an incandescent tungsten filament, an electron beam is generated; these move towards the anode and hit the electron sphere of the molecule, transferring the energy necessary for the loss of an electron and generating a radical cation.

In this way the molecular ion M^+ is formed according to this reaction:



The molecular ion mass does not differ significantly from the mass of the starting molecule M . In the mass spectrum, the molecular ion peak is called the molecular peak. Through the collision with electrons, it has acquired an energy that can fragment; the fragments of the molecule come from a positively charged ion, so they can be positive or neutral loads. The positive ions pass through a series of plates drilled in the center, called accelerator plates, with increasing positive potential, and they are then ejected through an exit slit. The ions are generated at a very high energy level and there may be extensive fragmentation, so this ionization technique is classified as a "hard" technique.

- Chemical ionization

This technique is mainly used for molecules such as hydrocarbons, esters, alcohols, amines, amino acids and small peptides that by means of EI would give an excessive fragmentation, not making the molecular peak visible to the spectrum. This technique is based on the interaction of the vaporized sample with an ionized reagent; the quasi-molecular ion ($M+H^+$) is obtained, increased by a unit of mass with respect to the molecular ion. The quasi-molecular ion has a lower tendency to rupture than the electronically impacted molecular ion. Chemical ionization is therefore classified as a "soft" technique.

- Electrospray

In the electrospray system the sample is passed through a capillary tube under tension. In this way the sample is nebulized and ionized: droplets of liquid form, which, thanks to a coaxial flow of inert gas, generate a spray; the latter is positively charged and moves into a capillary kept vacuum and negative potential. On the way to the analyzer the solvent from the droplet begins to evaporate thanks to a reverse flow of nitrogen, kept at a temperature of about 300° C. This generates a population of single, unsolved positive ions moving towards the analyzer, passing through the sampler cone and a low-pressure zone. Electrospray produces little fragmentation, so it is a "soft" technique that is usually used as an interface for HPLC-MS.

2.2.4 Analyzer

The analyzer allows to differentiate the ions generated, according to their mass/charge ratio. Among the most common are:

- Magnetic analyzer: consists of a tube approximately 1 meter long, with a given radius of curvature and immersed in a magnetic field. The ions coming out of the ionization chamber enter the analyzer tube and, due to the effect of the magnetic field, undergo a deviation from their rectilinear trajectory (deflection phenomenon). The new curvilinear trajectory has a radius of curvature that is directly proportional to the momentum of the ion and inversely proportional to the magnetic field. Thus, for a certain value of the magnetic field and the potential, there will be only one value of mass for which the deflection radius coincides with the radius of curvature of the tube; only the ions that have this value of mass are able to exit the tube. Operating at constant potential and through a scan of the magnetic field it is possible to make ions at different mass exit from the tube at different times. This type of analyser allows to achieve better resolutions.

- Quadrupole analyzer: consists of four cylindrical metal bars which delimit the path followed by ions from the ionization chamber and directed to the detector. The bars are held to an oscillating electromagnetic potential so that, when the two vertical bars have positive potential, the horizontal bars have negative potential, and vice versa. The ions, accelerated by the accelerator plates, enter the tunnel delimited by the bars and are repelled by positive poles and attracted by negative poles. However, due to the oscillation of the quadrupole, the ions assume a zig-zag trajectory and end up unloading on one of the bars, except those that, for a certain value of oscillation frequency, have a kinetic energy such that the motion becomes sinusoidal and can exit the tunnel and enter the detection system. By scanning the oscillation frequency of the field, it is possible to extract ions with increasing molecular mass.

- Ion trap analyzer: consists of three electrodes (in practice there is an annular electrode placed between two semi-spherical input and output electrodes) which serve to trap and accumulate ions in a small cavity; the ion trap, in order to obtain a high sensitivity. The two side electrodes have a small hole in the center, through which the ions pass. The mass spectrum is generated by varying the electric potential in order to eject the ions in sequence, from the trap towards the detector, according to a mass/charge (m/z) increasing value.

- Time-of-flight analyzer: the principle on which it is based is that ions of different mass/charge value have equal energy, but different speeds after acceleration in the ionization chamber. As a result, each ion passes through the analyzer using a different time.

2.2.5 Detector

The detector collects ions and generates an electrical signal proportional to their abundance. The generated signal is then digitized and converted into mass spectrum thanks to a data analysis system. The detector is usually electric and is able to perceive only a value of m/z at a time. In the case of an electro-multiplier detector, the inner surface is covered with an electro-emissive material that, when hit by an ion, emits an electron. The electron is in turn accelerated towards the surface, causing the emission of another electron, generating a cascade effect. This system leads to a remarkable amplification of the signal, up to a million times.

2.2.6 HPLC-MS Coupling

The mass spectrometry coupled to liquid chromatography represents the cutting-edge technology for the detection and characterization of organic molecules, becoming one of the most powerful analytical tools of modern times. The mass spectrometer coupled to the liquid chromatograph allows the detection of eluted species in the liquid phase from a column. The main problem encountered in this technique was to couple the mass spectrometer, which requires a gas phase sample, with liquid chromatography, which requires the liquid phase sample. The problem was overcome by vaporizing the sample and removing most of the solvent, as it generates a volume of gas that is 10-1000 times greater than that of the gas transport in gas chromatography.

Currently the most widely used method is based on the electrospray ionization system at atmospheric pressure, in conditions of low flow speed. The HPLC system is usually a microsized capillary LC system with flow rates around microliters per minute ($\mu\text{l}/\text{min}$). Alternatively, some interfaces allow higher flow rates, ranging from 1 to 2 ml/min , which are typical of conventional HPLC conditions. By combining HPLC with mass spectrometry, you can also isolate unsolved peaks and monitor only a selected mass. This technique then provides information about molecular mass, structural information, and accurate quantitative analysis.

2.3 Nuclear Magnetic Resonance Spectroscopy

Nuclear Magnetic Resonance Spectroscopy (NMR) is an instrumental analytical technique that provides detailed information on the structure of molecules by observing the behavior of atomic

nuclei in a magnetic field. After immersing the molecule in a strong magnetic field, the absorption of a radio frequency radiation (100 to 1000 MHz) is measured, which causes nuclear spin transitions in particular atoms such as ^1H or ^{13}C .

Using the NMR technique, we can observe only nuclei that have a nuclear magnetic moment of spin that is oriented like the needle of a compass in an applied magnetic field.

Nuclear spin is generated by the protons and neutrons that make up the nucleus. These particles have $1/2$ spin and behave as if they were rotating around their axis.

In some atoms (such as ^{12}C) protons and neutrons are present in even numbers, so the spins are all paired, one in opposition to the other and the atomic nucleus has spin result I equal to zero.

In other atoms, (such as ^1H , ^{13}C) protons or neutrons are present in odd numbers and therefore at least one nucleon is unpaired and the nucleus has a non-zero resulting spin I .

As the applied field B_0 increases, the frequency of Larmor increases and the energy difference between the two levels increases, too. Since, however, this difference in energy is very small, the population of nuclei in the two states is practically identical with a very small prevalence for the low energy state, aligned with the field.

The few excess nuclei, aligned with the magnetic field B_0 , allow to generate the NMR signal.

2.3.1 Energy Absorption

If the sample is irradiated with an electromagnetic radiation frequency equal to the Larmor frequency, there is an interaction of the magnetic component of the radiation with the nuclear magnetic moments (also these oscillating at the Larmor frequency). The energy of the radiation can thus be transferred to the nuclei. Each absorption of radiation involves a change of orientation of the nuclear spin that passes from aligned with the field to opposite the field. When this spin transition occurs, it is said that the nuclei are in resonance with the applied radiation, hence the name of Nuclear Magnetic Resonance, NMR.

2.3.2 Production of the NMR Signal

In the first NMR instruments, the analysis was performed by irradiating the sample, immersed in the magnetic field B_0 , with a beam of radio waves of increasing frequency in order to excite in sequence all the nuclei under examination and then the magnitude of the absorbed radiation was recorded. This technique, however, is too slow and is no longer used.

In modern FT-NMR instruments the signal is generated with the pulse method and the Fourier transform. With this technique all the nuclei of a species are simultaneously excited by a radio

frequency pulse that contains all the necessary frequency range, the data are then processed at the computer with the technique of the Fourier transform.

The essential steps to obtain the NMR spectrum of a sample using the FT-NMR pulse technique are as follows:

- 1) Introduction of the sample into a strong B_0 magnetic field to orient the nuclear spins and produce an excess of nuclei with the spin aligned to the field.
- 2) Application of a radio frequency pulse to produce an excess of excited nuclei with spin as opposed to the field (duration: some microseconds).
- 3) FID recording, the signal emitted by the nuclei while the nuclear spins return to equilibrium (duration: about one second).

The collected signal is an oscillating signal with frequency ν , the Larmor frequency of the nucleus under examination, which dampens over time and is called FID, Free Induction Decay.

- 4) Mathematical processing of data by computer, applying the Fourier transform, to obtain the NMR spectrum as a function of frequencies.

Starting from a graph as a function of time, the FID, we get a new graph as a function of frequencies, called the NMR spectrum, which shows the frequency absorbed and then emitted by the hydrogen atoms in the molecule.

If the sample contains nuclei with different resonance frequencies, these are all excited at the same time by the radio frequency pulse, and therefore the collected FID signal is a complex curve, called interferogram, given by the combination of several simple FID, one for each frequency absorbed by the nuclei.

In order to go back to the single frequencies that have generated the complex FID path, by combining with each other, it is necessary to apply a mathematical procedure, called Fourier transform, that allows to pass from the graph as a function of time, the FID, to the graph as a function of the frequencies, the NMR spectrum.

2.3.3 Chemical Shift

The various hydrogen atoms absorb at slightly different frequencies depending on their chemical surroundings. A hydrogen atom, in fact, depending on the electronegativity of the atom to which it is linked, can be more or less immersed in its own electrons of bond. These are charged particles and, when subjected to the B_0 magnetic field, produce an electronic circulation that generates a small bi-induced magnetic field opposite the much stronger one applied.

If hydrogen is bound to low-electronegative atoms, it is more immersed in the bonding electrons and feels a more intense bi-induced magnetic field, which decreases more the applied field and then undergoes the transition to a lower frequency.

If, on the other hand, the proton is bound to more electron-negative atoms, it is less shielded by the bonding electrons and is invested by a weaker induced field and thus feels a more intense effective field and absorbs at higher frequencies.

The frequency change absorbed is called chemical shift. To quantify the chemical shift, it is necessary to identify a reference hydrogen to which to associate the zero value of the scale. By convention, zero has been attributed to the hydrogens of tetramethylsilane $\text{Si}(\text{CH}_3)_4$ which are among the most strongly shielded, due to the low electronegativity of silicon and for this reason the chemical shifts of normal organic molecules are always positive.

Absolute chemical shift is the difference between the absorbed frequency (in Hz) of the test hydrogen and that of the hydrogen of tetramethylsilane, taken as a reference.

The relative chemical shift measured in ppm (Hz/MHz) is used, which is independent of the applied field, so it is equal in all NMR instruments whatever the intensity of the applied magnetic field. For ^1H -NMR, the scale extends from 0 to 12 ppm; for ^{13}C -NMR it is much larger and covers the range 0-220 ppm.

2.3.4 Peak Area

A further feature of ^1H -NMR spectroscopy is that the signal strength is proportional to the number of hydrogens that generate the signal; that is, the peak area (the integral) is directly proportional to the number of hydrogens that produced them. Integrations are given as the simplest integers that are obtained from the ratio between the areas of the peaks

In ^{13}C -NMR spectrometry, however, the area of the peaks is not related to the number of carbons that produce that signal due to the way the signal is collected, so areas are not taken into account in spectrum interpretation.

2.3.5 NMR Spectrometer: instrumentation

The commercial spectrometers used are of two types:

- Continuous wave spectrometers
- Pulse spectrometers, which in turn are divided into two subcategories:
 - 1) Time domain pulse spectrometers
 - 2) Fourier transform pulse spectrometers

Continuous wave instruments use magnets (usually permanent magnets or electromagnets) that produce a field of a few tenths of Tesla.

They were almost supplanted in 1970 by Fourier transform spectrometers, which, despite being more expensive than continuous wave spectrometers, are now predominant in the market.

- Continuous wave spectrometers

In spectral analysis, to observe many nuclei, you have to vary either the amplitude of B_0 , or the frequency of the B_1 radio frequency pulse.

To analyze the different nuclei contained in the sample, the continuous wave spectrometers use two techniques:

- 1) Change in frequency

The amplitude of B_1 is kept constant, while the frequency is varied. By analyzing two different nuclei, they are characterized by different resonance frequencies (ν_1, ν_2).

- 2) Change in the force of the field

The frequency of B_1 is fixed at a reference value for a particular nucleus, while the amplitude of the field B_0 is varied by the current circulating in the adjustment coils.

- Pulse spectrometer

In these instruments, a radio frequency pulse B_1 (fixed frequency) directed at an angle to B_0 is periodically sent to the sample immersed in a fixed B_0 field.

To avoid saturation of the spin system the pulses must have a small duration, usually less than $10\mu\text{s}$.

Between one impulse and another, an interval of more than one second is usually expected to allow complete relaxation of the magnetization at the application of the next impulse.

The signal detected by the coil, which between an RF pulse and the other decays over time, is the FID.

The FID knows its maximum value after applying the pulse and decays exponentially to zero after the pulse is terminated due to relaxation.

- Fourier transform pulse spectrometers

Their operation is similar to that seen for spectrometers in the time domain, as they also send radio frequency pulses to the sample, with the difference that the FID is digitized and the Fourier transform is performed on the obtained samples.

By performing the Fourier transform, we can pass from a representation in the time domain to a representation in the frequency domain, that is, to the signal spectrum.

The block diagram of the architecture of Fourier transform spectrometers is shown in Figure 12.

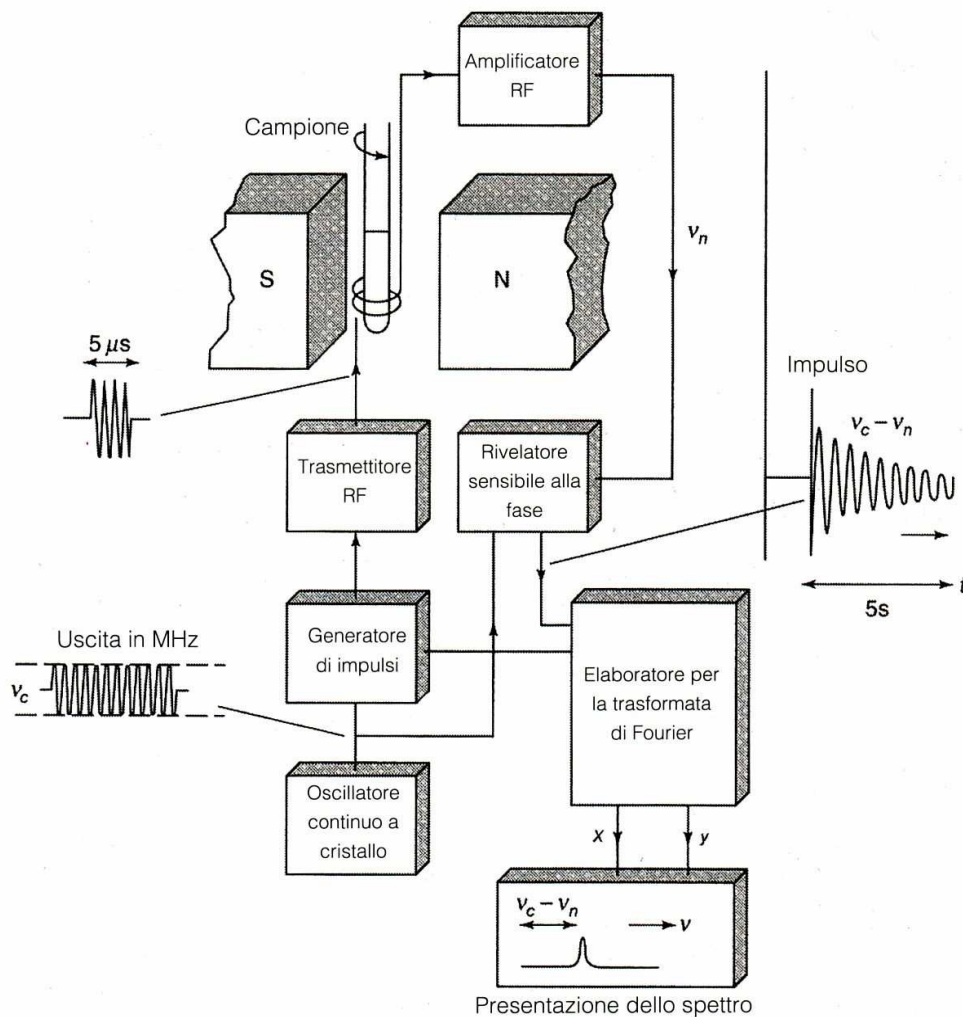


Figure 12. Scheme of the Fourier transform spectrometer

The pulse generator, after receiving a signal composed of the v_c radiation produced by a crystal continuous oscillator, sends the radio frequency pulse to the RF transmitter (transmitting coil).

The coil is intended to send the pulse to the sample.

Once the RF pulse has ceased, the same coil that was used with the transmitter function is now placed in the receiver function to capture the decay signal.

The FID, once received by the coil, is amplified and transmitted to a phase-sensitive detector, which makes the difference between the v_c crystal signal and the v_n nuclear signals to give an output signal in the time domain.

The signal in the time domain will be sampled and then on the acquired samples the Fourier transform will be performed in order to obtain the signal spectrum.

2.3.6 Magnets

The sensitivity and resolution of the various spectrometers depend on their magnet.

The three important characteristics of a magnet are the strength, stability and homogeneity of the field produced.

By examining a sample with nuclei of different elements within it, it is important that the strength of the B_0 field is high in order to achieve high resolution.

Moreover, having higher B_0 values increases the excess of population in the low state of energy with a consequent increase in amplitude of the NMR signal which depends on the square of B_0 .

There are three different types of magnets:

1. Permanent

They are the least expensive magnets, do not require electric currents to produce the field, but suffer from not high field stability. Field variations can be caused by changes in temperature.

The strength of the field produced is also low and can vary between 0.4 and 1.4 T.

2. Electromagnets

They are huge and more expensive than permanent magnets. However, they reach higher B_0 values than permanent magnets and even superconductors with values up to 34 T.

However, to reach such high field values they require large currents, which give rise to dissipative effects in the form of heat.

3. Superconductors

The intensity of the field produced varies between 6 and 18 T.

The advantages of this type of magnets are high values of B_0 , great stability, acceptable operating cost and small size compared to electromagnets.

The cylindrical solenoid is immersed in liquid helium inside the Dewar container which includes an outer coating filled with liquid nitrogen. Thanks to this system, it is possible to ensure a temperature of 4 K in order to nullify the electrical resistance and ensure the behavior of the wire as a superconductor.

Having canceled the resistance, you can ensure a strong and stable magnetic field.

2.3.7 Systems to Ensure the Stability of the Magnetic Field

In order to ensure the stability of the magnetic field, the locking system is adopted, which consists of a coupling of the magnetic field.

First, a nucleus, that gives rise to a strong NMR (lock signal) signal at different frequencies than those of the other nuclei of interest, is chosen.

The lock signal frequency is constantly monitored and compared with the reference frequency produced by the radio frequency oscillator.

When the B_0 field changes, the difference between the lock signal and the reference frequency is sent to coils placed in the magnet to increase or decrease the B_0 field of the amount needed to re-establish the coupling between the two values.

The reference substance may be external (external lock) to the sample to be analyzed, or contained as a solvent within the sample (internal lock).

In current monitoring systems, deuterium is used as a reference signal.

To ensure the homogeneity of the field, or its uniformity in the region of space containing the sample, two other methods are used:

- Adjustment coils: the shape of the magnetic field can be varied within small limits by passing currents through pairs of metal spirals.
- Sample rotation: this technique consists in rotating the sample around its longitudinal axis using an air flow that moves a turbine inserted into the tube containing the sample.

2.3.8 Systems to Reduce Noise Overlapping on the NMR Signal

In order to obtain a good signal in such a way that the noise does not have a significant effect in the measurement, we try to make the signal-to-noise ratio S/N as large as possible. Radio frequency pulses are sent at high power with a series of RF filters, so as to pass the useful signal to RF and eliminate the noise that falls outside the filter band.

As an alternative, you can adopt another technique called CAT or signal averaging, that consists in making more scans, sum the n signals obtained and then divide the resulting by n .

2.3.9 Processing the Collected Data

After the NMR signal data has been collected in the computer's memory, various processes can be performed that raise the sensitivity or improve the shape of the peaks in the frequency domain.

2.3.10 Probes for the Sample

The purpose of the sample probe is to keep the material to be analyzed, contained in a glass tube, in a fixed position at which the field is homogeneous.

In addition, it contains the turbine to rotate the sample, temperature variation systems, and the transmission and receiving coils.

2.3.11 Digitation

The signal from the RF amplifier (v_n) is sent to a phase sensitive detector which operates the subtraction between the signal from the v_c oscillator and the NMR v_n signal.

The detector, by subtracting, transforms the v_n radio frequency signal into an audio signal, so that digitation is easier.

Then, according to the Nyquist theorem, the audio signal will be sampled at a frequency of at least twice the frequency of the signal.

Finally, the transform of Fourier will be executed on the acquired signals.

2.4 Fluorescence Assay to Test CFTR Activity

2.4.1 Basics of YFP Proteins

The anion sensitivity of yellow fluorescent protein (YFP) can be used to perform cellular assays for the functional evaluation of anionic channels and transporters. YFP, derived by mutagenesis from GFP (green fluorescent protein), has a pocket, located near the chromophore, which is capable of binding anions such as Cl^- , I^- , Br^- , thiocyanate and nitrate. The anion bond makes the chromophore non-fluorescent, thereby extinguishing the YFP. It must be considered that anions do not bind YFP with equal affinity: in particular I^- is a better ligand than Cl^- . This feature is the basis of cellular assays in which the exchange between Cl^- and I^- through anionic channels and transporters is visualized through fluorescence variations.

For this type of test, the original YFP is not used, but mutants generated later to improve their sensitivity to I^- (Jayaraman et al., 1999; Galiotta et al., 2001).

The YFP protein cannot enter the cells by "loading", but must be introduced by stable or transient transfection. The channel or transporter to be evaluated (e.g. CFTR) may already be present in the target cells or may be introduced into the same cells by transfection together with YFP.

2.4.2 Principle of the Test

Cells expressing the YFP protein (or a mutant thereof), balanced in a physiological saline solution, are exposed to a high concentration of I^- (usually 100 mM). As soon as added, the I^- begins to enter the cell through ion channels or carrier permeable to it. The influence of I^- determines a progressive quenching of the fluorescence due to the binding with the YFP protein. The greater the transport of I^- (therefore the activity of the channel or the carrier under test), the faster the extinguishing of the fluorescence will be. The YFP test is therefore a kinetic-dependent test in which cell fluorescence should be measured without interruption, before and after the addition of I^- . It is not necessary to

acquire the signal until the maximum shutdown because the required data is the initial speed of shutdown. Sampling of the first 15-30 seconds after the addition of I^- is sufficient to evaluate the transport.

Chapter 3: Experimental Section

3.1 Background

In the Laboratory of Organic Synthesis and Mass Spectrometry at the CEBR, where I did my PhD thesis period, molecules belonging to the class of aminoarilthiazoles (AATs) had been studied. AATs had shown activity in previous studies (Pedemonte et al., 2011; Pesce et al., 2015), in particular exhibiting a dual function both as correctors and as potentiators. This property favored its use, not only on mutation F508del- CFTR, that causes the defect of “trafficking”, but also on mutations G1349D and G551D, which cause the defect of "gating".

In addition, many AATs showed synergistic action when tested in the presence of VX-809. In fact, the action of some AATs combined with VX-809, on cell lines used as a model, was able to generate a marked rescue of the CFTR protein.

In order to develop molecules with greater efficacy, activity and safety than the currently compounds “ligand-based” and QSAR studies have been conducted to identify a number of chemo-descriptors belonging to different classes of active correctors studied in the literature. Thanks to this approach a mathematical model that could predict the biological behavior of a certain corrector was produced (Liessi et al., 2018).

This equation was then used as a filter for the rational design of new structures to be synthesized and tested as F508del-CFTR correctors. In particular, a first library of compounds defined as "hybrids" obtained by merging the suitably modified portion of VX-809 and AATs has been designed (Fig. 13).

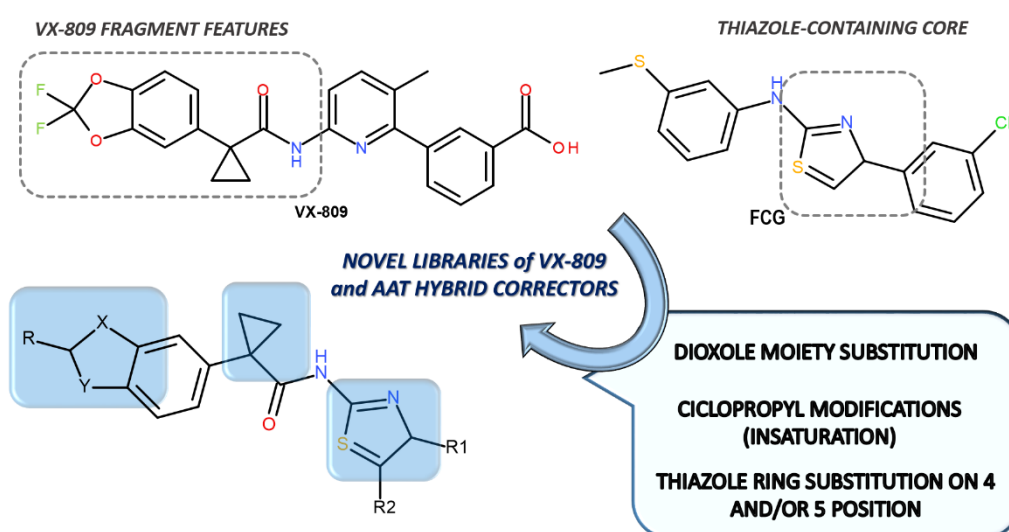


Figure 13. Design of VX-809 and AATs' Hybrids.

Most of the compounds have been synthesized by conjugating dioxolcyclopropanecarboxylic acid with 2-aminothiazoles or suitably modified amino derivatives (Liessi et al., 2018).

Maintaining the benzodioxole group of VX-809 appears a recurrent strategy also taking into account the results obtained with GLPG-2222 (Fig. 14) (Wang et al., 2018) and with other correctors described by AbbVie and Galapagos companies, in which this substituent was tethered to the chroman or to tetrahydropyran ring (Kym et al., 2016).

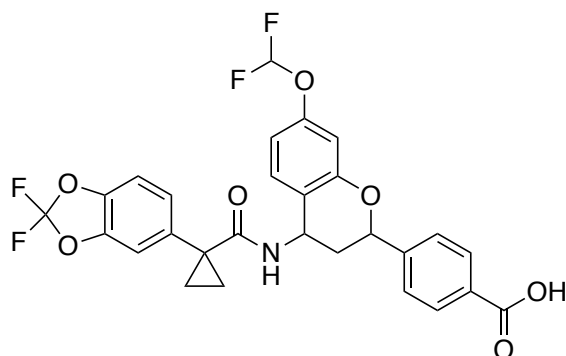


Figure 14. Structure of GLPG-2222.

The activity as correctors of a first series of hybrid compounds designed using the mathematical filter described above is shown in figure 15.

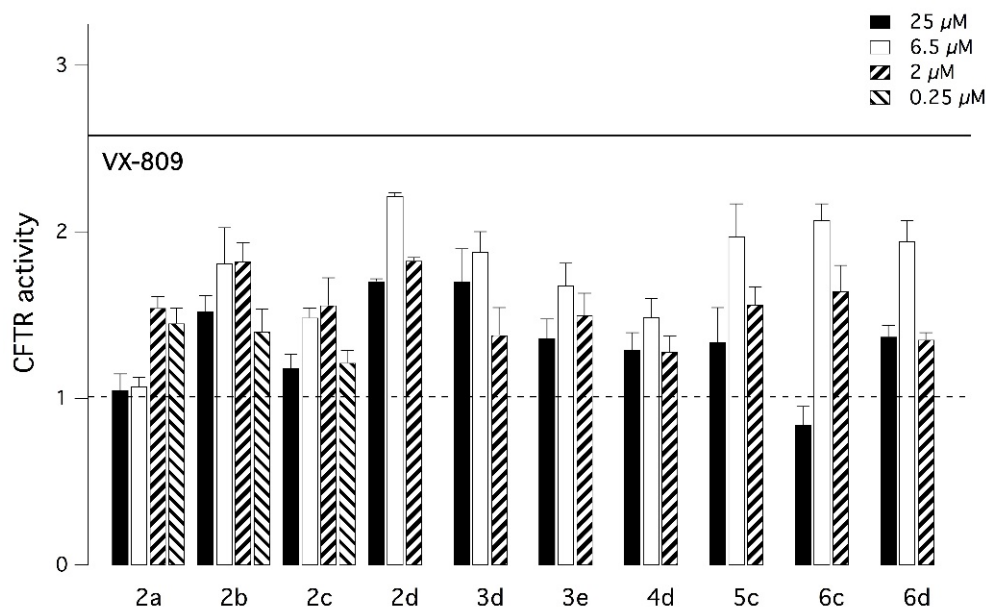


Figure 15. Effect of more active compounds on CFTR rescue. The bar graph shows the normalized activity after 24h of treatment of the compounds, tested at different concentrations, on CFBE41o cells transfected with F508del-CFTR. The activity was measured with the YFP test. The horizontal

non dotted line indicates the level of activity of cells treated with the VX-809 corrector (1 μM). The dotted line indicates the activity of cells treated only with DMSO (Liessi N. et al., 2018).

For some compounds a good activity can be observed compared to the medium (treatment with DMSO), confirming that the compounds belonging to this library maintained the functional interactions established by VX-809 and providing significant activities as correctors. Among them, a number of analogues was identified featuring values in terms of CFTR rescue ability comprised between 0.09 and 0.2 μM , with compound **2a** being the most active ($\text{EC}_{50} = 0.087 \mu\text{M}$).

3.2 Aim of the Thesis

The aim of my thesis is to synthesize, characterize and purify new active and potent molecules assayed in biological tests as F508del-CFTR correctors, useful alone or in association with other drugs to allow the rescue of the CFTR protein.

In particular I started by the structure of compound **2a**, in Fig. 16, previously developed by my Team and I modified every portion to obtain a functional backbone to decorate.

Based on the previous data (Liessi et al., 2018), in which the thiazole ring was modified at different positions, we have identified that the most active compound **2a** ($\text{EC}_{50} = 0.087 \mu\text{M}$) was characterized by a substitution at position 5 of the thiazole ring with benzoyl group and phenyl ring linked at the thiazole position 4.

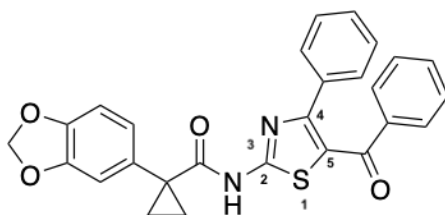


Figure 16. Structure of compound **2a**

In addition, my Team has already demonstrated that substitution at position 5 of the thiazole ring was necessary for a good activity, since the most active derivatives of the previous series contained a substituent at position 5 (Liessi et al., 2018).

I divided the promising compound **2a** in three portions to study as every moiety influenced the biological activity (Figure 17).

In fact, compound **2a** can be divided into three fragments that can be studied one at time.

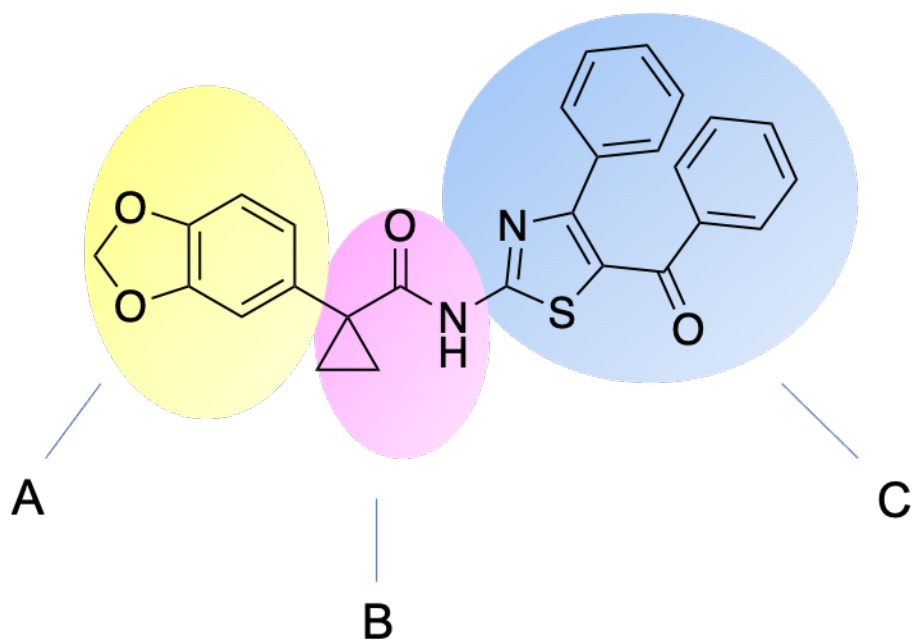


Figure 17. Considered portion to examine compound **2a**. Portion A in yellow is the benzo[d][1,3]dioxole; portion B in pink is the cyclopropane carboxamide; portion C in light blue is the aminothiazole cycle.

I have studied in order:

- The role of the benzo[d][1,3]dioxole (portion A)
- The role of the cyclopropane carboxamide (moiety B)
- The modification on the substituents of the thiazole (cycle C)

Only in the last condition, I obtained two different libraries of compounds in which I have studied first the substitutions at position 5 and then the substitution at position 4 of the thiazole ring (Fig.18).

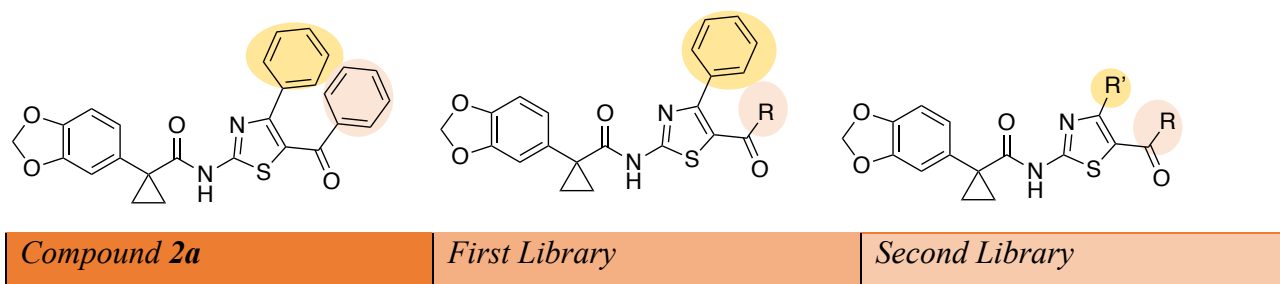


Figure 18. Libraries of compounds derived by the modification of portion C in compound **2a**

In add, the group of Computational Chemist of Department of Pharmacy proceed with molecular docking studies focused on the prototype **2a**, to explore the structure-activity relationship (SAR) within the hybrid series and to point out novel beneficial chemical substitutions to decorate the

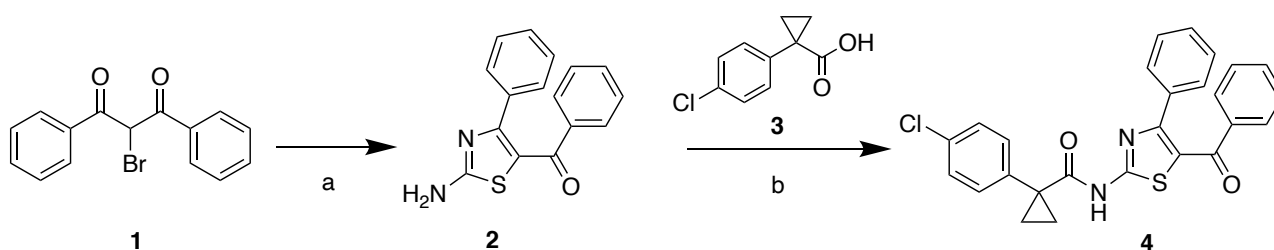
thiazole ring. Moreover, the selection of the most promising compounds to be synthesized has been performed also taking into account the information and mathematical prediction of the QSAR model previously built and published.

All designed compounds were synthesized and tested to investigate the structure-activity relationships as correctors of F508del-CFTR. By using the YFP functional assay on F508del-CFTR CFBE41o- cells, we tested the compounds after 24 h incubation at three different concentrations to determine the EC₅₀ values of the compounds as correctors of F508del-CFTR. Activity was then compared to that of cells treated with vehicle alone (DMSO) or with the corrector VX-809 (1 μM).

Molecular docking studies were also carried out to study how my hybrids bind “in silico” to CFTR, particularly on the NBD1 portion, and compared to the docking of VX-809.

3.3 Chemistry

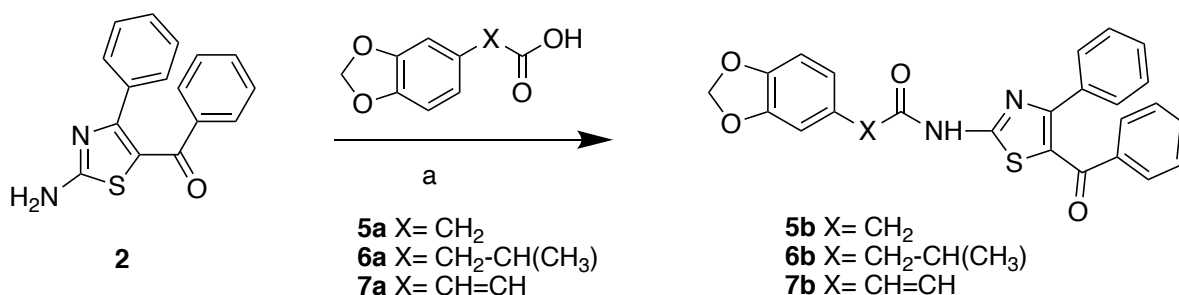
First, I decided to synthesize a compound in which I replaced the benzodioxole portion (portion A) with another aromatic ring (compound **4**). For the compound **4** a traditional Hantzsch protocol was used to furnish (2-amino-4-phenylthiazol-5-yl)(phenyl)methanone **2**. In particular it was achieved in high yield by the condensation of bromo-1-,3-diphenylpropane-1,3-dione **1** with thiourea in refluxing ethanol. The aminothiazole was conjugated with 1-(4-chlorophenyl)cyclopropanecarboxylic acid **3** with HATU/DIPEA activation in anhydrous N, N- DMF to afford the derivative **4** in good yield (40-50%) (Scheme1).



Scheme 1. Reagents and conditions: a) thiourea, ethanol, reflux, 2 h; 75% b) HATU, DIPEA, N,N-DMF, 50°C, 18-24 h, 40-45%

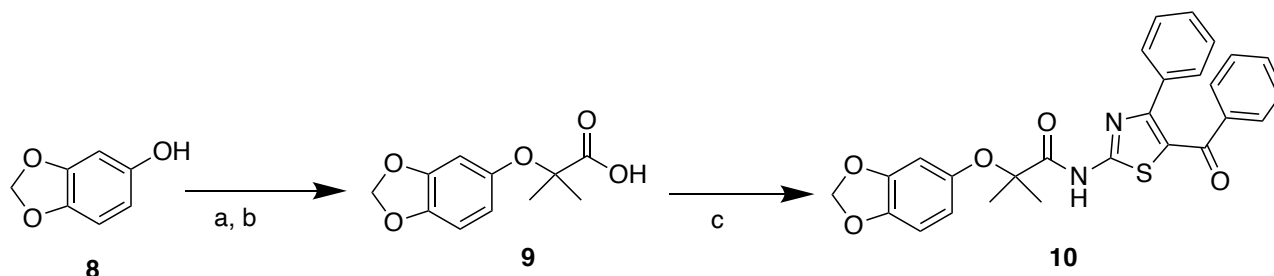
To obtain the compounds with different portion B as **5b**, **6b** and **7b**, the synthesis of amide derivatives of 2-aminothiazoles were achieved by reaction of **2** with the suitable carboxylic derivatives (**5a-7a**)

with HATU/ DIPEA activation in anhydrous N,N - DMF leading to final compounds in good yields (45%) (Scheme 2).



Scheme 2. Reagents and conditions: a) HATU, DIPEA, N,N- DMF, 50°C, 18- 24h, 45%

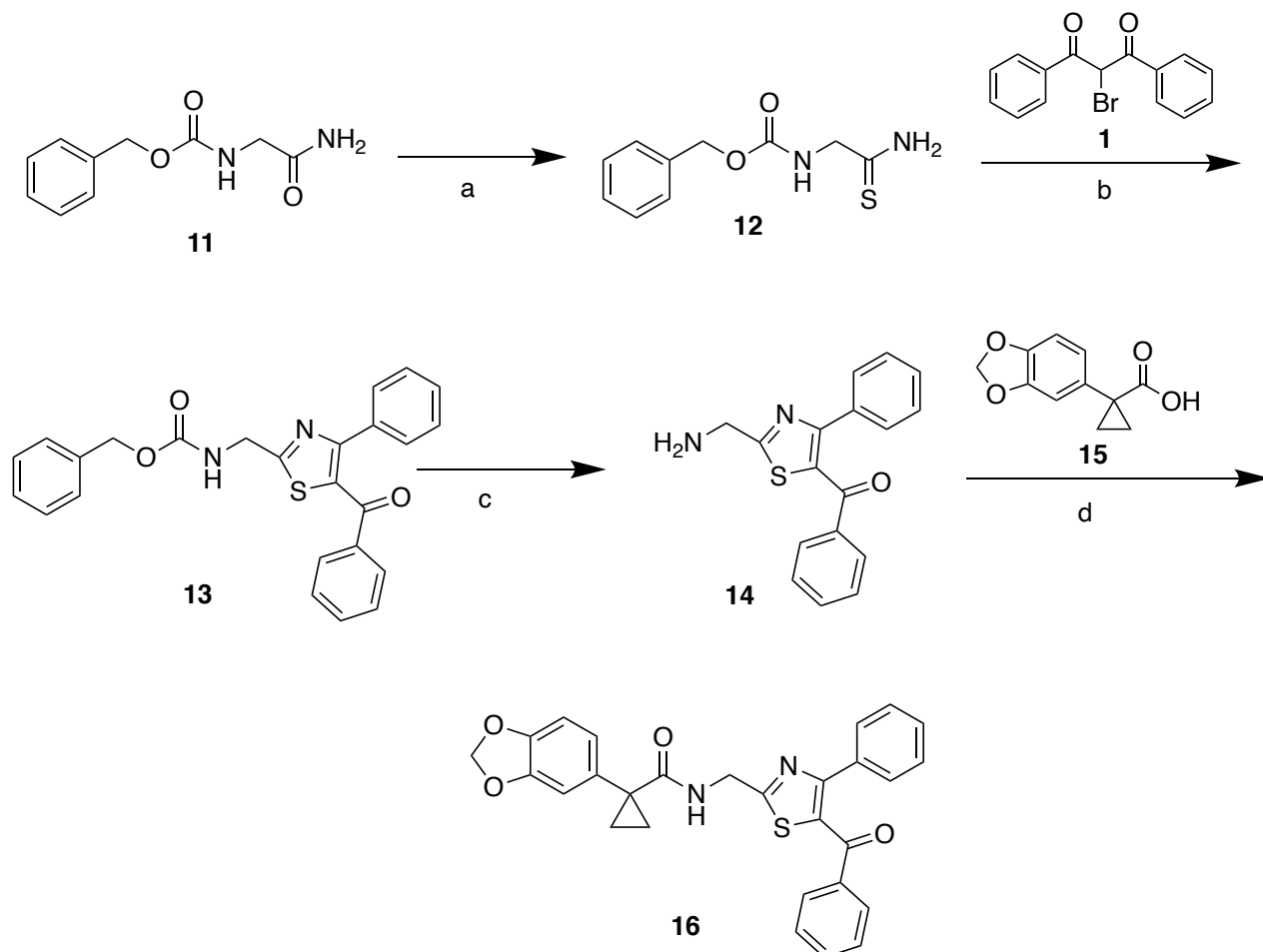
Then, I explored the role of the portion B synthesizing ethyl 2-(benzo[d][1,3]dioxol-5-yloxy)-2-methylpropanoate **10** that was prepared by reaction of ethyl-2-bromoisobutyrate and benzo[d][1,3]dioxol-5-ol **8** in anhydrous N,N - DMF at room temperature in the presence of K₂CO₃. Hydrolysis of substituted ester under aqueous basic conditions yielded acid derivative **9**. Amide coupling of **9** with 2-amino-4-phenylthiazol-5-yl)(phenyl)methanone **2** afforded final compound **10** in low yield (22%) (Scheme 3).



Scheme 3. Reagents and conditions: a) ethyl- 2- bromoisobutyrate, K₂CO₃, N,N-DMF, RT, 16 h; b) KOH 6N, ACN, 60° C, 3 h, 61%; c) (2-amino-4-phenylthiazol-5-yl)(phenyl)methanone, HATU, DIPEA, N,N-DMF, 50°C, 24h, 22%

Finally, to complete the study of the portion B, I decided to synthesize the compound **16** in which the thiazole ring (portion C) was separated from the amide group (portion B) by a methylene. To obtain compound **16**, N-benzoyloxycarbonyl glycineamide **11** was thionated with Lawesson reagent in toluene at reflux to give benzyl (2-amino-2-thioxoethyl)carbamate **12**. Compound **12** condensed with the appropriate alpha-bromodione **1** in ethanol, at reflux, to obtain the thiazole ring protected with the benzoyl group **13**. Then, benzyl ((5-benzoyl-4-phenylthiazol-2-yl)methyl)carbamate **13** was

deprotected with acid solution and the product **14** reacted with 1-(benzo[*d*][1,3]dioxol-5-yl)cyclopropane-1-carboxylic acid **15**, via activation of carboxylic group with uronium salts, to give the final compound **16** in low yield (23%) (Scheme 4).

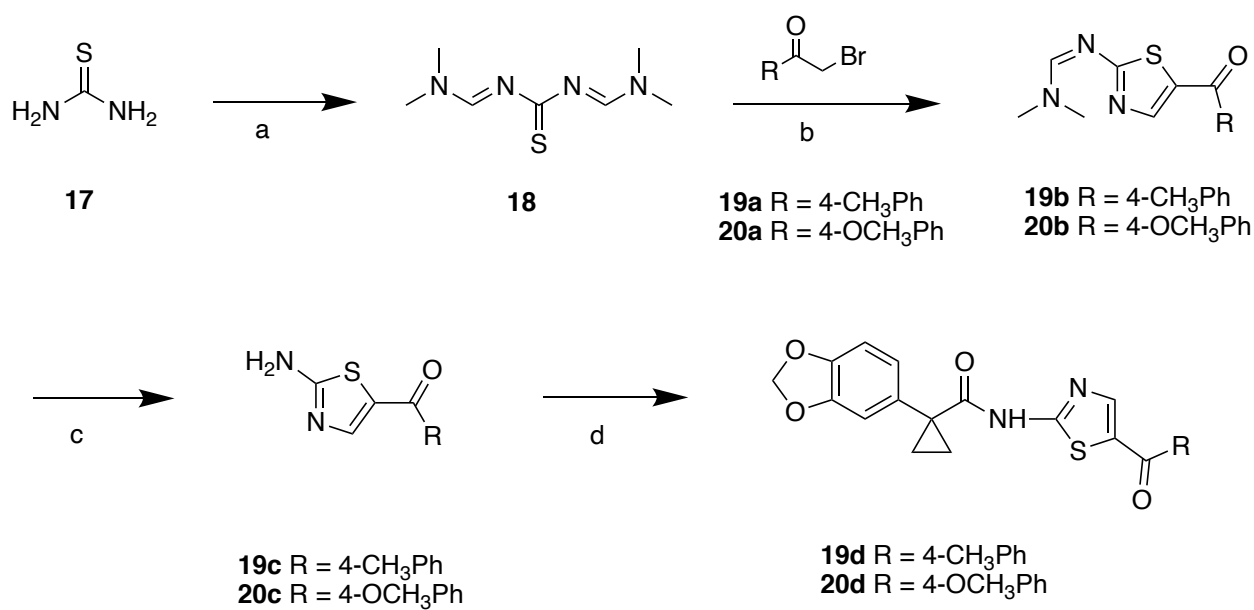


Scheme 4. Reagents and conditions: (a) Lawesson reagent, toluene, 110°C, 4 h; (b) EtOH, reflux, 1-2 h; (c) HBr/ CH₃COOH 33%, 70°C, 24h; (d) HATU, DIPEA, N,N-DMF, 45°C, 24h (23%).

After this, I started to study the portion C evaluating the importance of a phenyl ring at position 4 of the thiazole cycle. For this purpose, I synthesized compound **19d** and **20d**. For the synthesis of these compounds (Scheme 5), the synthetic strategy hinged on a reaction between a substituted thiazole in position 5 and cyclopropanecarboxylic acid derivative. The functionalized thiazoles used for the substitution step were obtained via adaption of reported thiazole synthesis (Bodio et al., 2011). Thiourea **17** was quantitatively activated as bis-thiazadiene **18** with excess of commercially available *N,N*-dimethylformamide dimethylacetal in methanol. The thiazole ring was formed after addition of the corresponding alpha-bromoketones **19a** and **20a** in tetrahydrofuran (THF). Intermediates **19b-20b**, which were not isolated, were deprotonated “in situ” by addition of triethylamine. The second imine,

used here as a protecting group, was subsequently removed with methylamine in water to form the expected products **19c** and **20c** in good yield.

The final products **19d** and **20d** were obtained by condensation of the 2-amino-thiazole with the carboxylic group of cyclopropanecarboxylic acid derivatives as previously described (Scheme 4) in good yields (30-50%).



Scheme 5. Reagents and conditions: a) N, N- Dimethyl formamide dimethyl acetal, DCM, reflux, 4 h; b) THF, TEA, RT to reflux, 18-20 h; c) 33% aq CH₃NH₂, THF, rt, 24 h; d) HATU, DIPEA, N,N-DMF, 50° C, 24-36 h (30- 50%).

To synthesize derivatives **29**, **30** and **31** and all the compounds of the first library (**32** – **58**) I applied the same synthetic route reported in Scheme 6, but starting from aliphatic, heteroaromatic, heterocycle or aromatic haloketones (Scheme 4) (For R groups see the table 5 and 6).

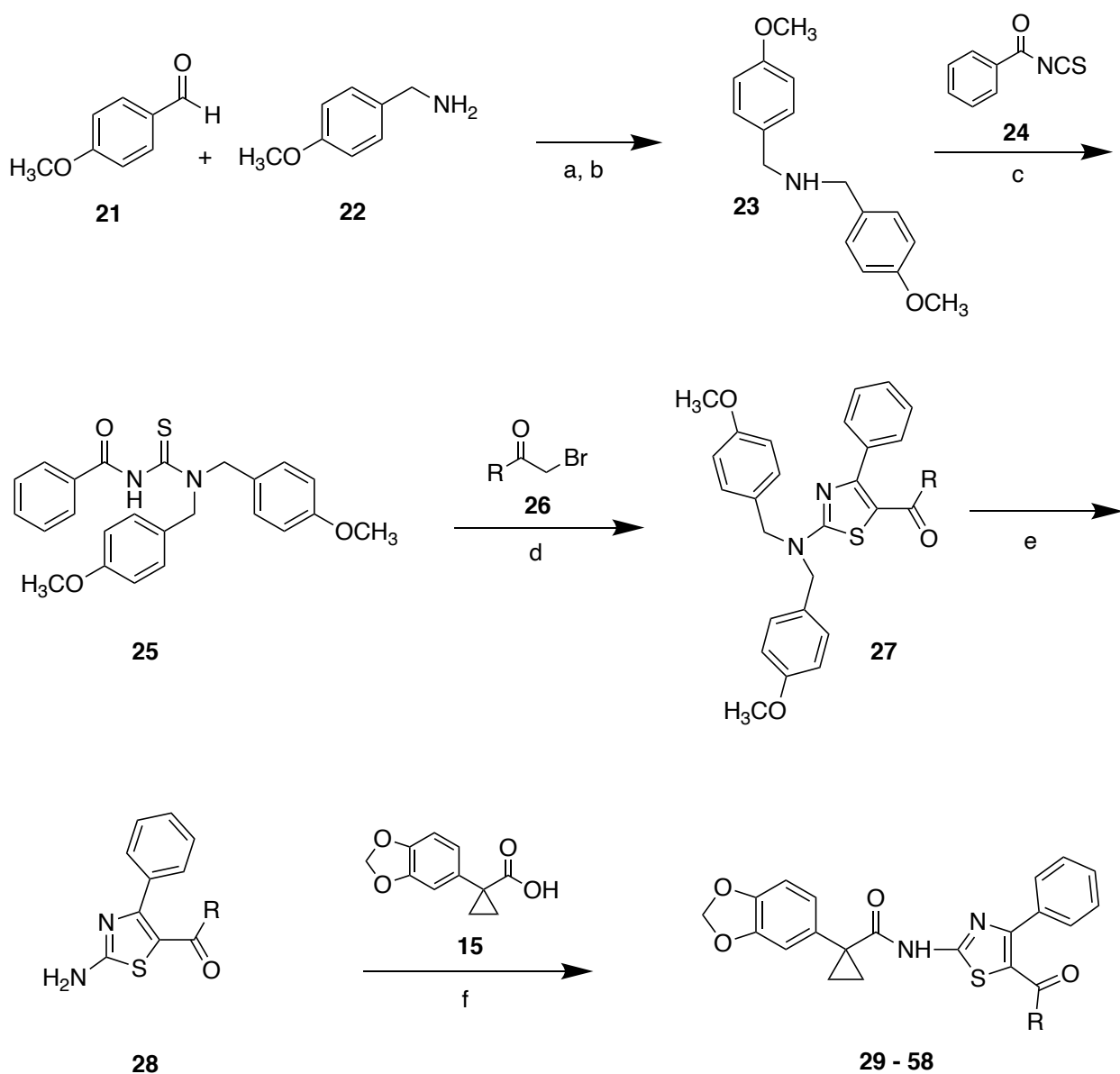
To obtain the similar backbone, I synthesize first the aminothiazole portion, utilizing a convergent synthesis in accord with the Wang protocol, with some modifications (Wang et al., 2014) and then I conjugated the thiazole portion with 1-(benzo[d][1,3] dioxol-5-yl)cyclopropanecarboxylic acid. A protected carbamothioyl amide was conjugated with substituted α -bromoketone, to obtain a selective introduction of the substituent groups on the thiazole ring.

The reaction of 4-(methoxy)benzaldehyde **21** and 1-[4- (methoxy)phenyl]methanamine **22** heated in refluxing methanol and followed by the reduction with NaBH₄, gives bis((4-(methoxy) phenyl)methyl)amine **23** in high yield (90%) .

Bis ((4-(methoxy) phenyl) methyl) amine **23** condensed with benzoylisothiocyanate **24**, to give a protected carbamothioyl amide **25** in high yield (> 50%).

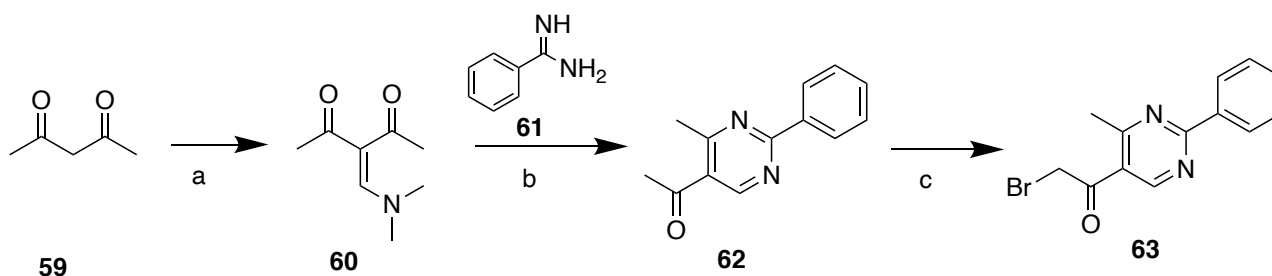
Condensation of protected carbamothioyl amide **25** and α -halo ketone **26** in N,N-DMF, afforded the thiazolic derivatives **27**, this step, followed by deprotection in acid conditions and long times, give the aminothiazole **28** which was then further conjugated with 1-(benzo[d][1,3]dioxol-5-yl)cyclopropanecarboxylic acid **15** to produce the desired analogues **29 – 58** in low yields (11-38%) (Scheme 6).

This last synthetic step was achieved by reaction of 2-amino- thiazole with the carboxylic group of cyclopropane carboxylic acid derivatives with uronium salt activation in anhydrous solvents.



Scheme 6. Reagents and conditions: (a) methanol, reflux, 3 h; (b) NaBH₄, 0 °C to RT, 10 h; (c) acetone, 0 °C, 2 h; (d) N,N-DMF, 85 °C, 3 h; (e) TFA, 100 °C, 36-48h; (f) HATU, DIPEA, N,N-DMF, 50 °C, 24-48 h (11-38%).

In details, to obtain compound **46** belonging to the first library, I had to synthesize the bromo-ketones **63** with a particular procedure; I started from acetylacetone **59** that condensed with an excess of N,N-dimethylformamide dimethyl acetal (DMF-DMA) to give enamine **60**. The reaction between enamine **60** and benzimidamine **61** afforded the corresponding pyrimidine derivatives **62**. Compound **62** is brominated at position alpha of the ketone group with copper (II) bromide in a selective manner to obtain compound **63** (Scheme 7).

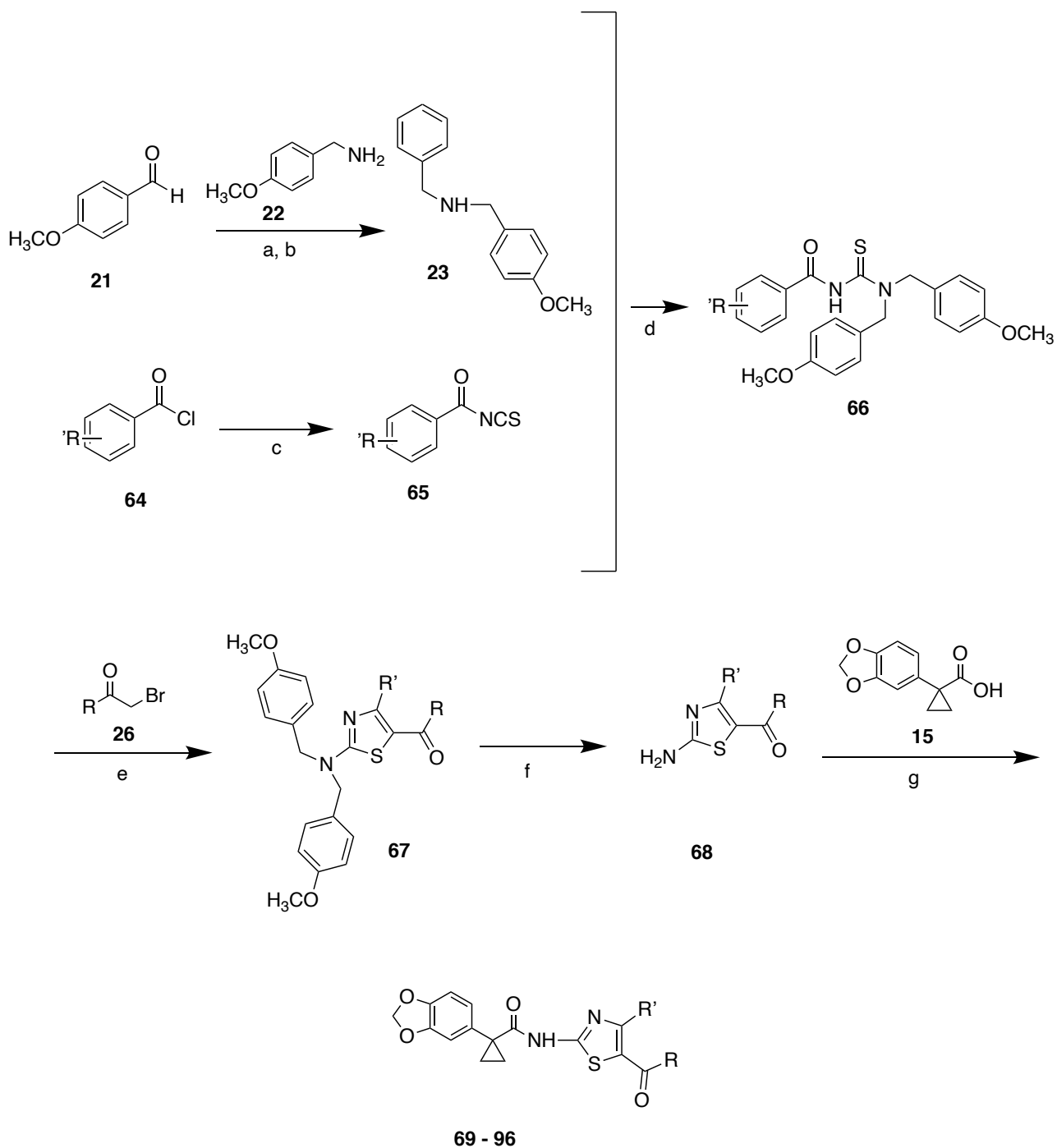


Scheme 7. Reagents and conditions: (a) DMF- DMA, 100°C, 2 h; (b) EtOH, reflux, 3 h; (c) CuBr₂, dioxane, 50°C, 1 h, then 85°C, 30 minutes.

Once obtained the desired bromo-ketone, it reacts with compound **25**, as previously cited in scheme 6, to obtain the final product **46**.

To synthesize compounds of the second library (**69 – 96**), with different substituents on the phenyl at position 4, I utilized a similar scheme of synthesis with a modification in the first steps of the reaction. The appropriate acyl chloride **64** reacts with ammonium thiocyanate in acetone to give the decorated thiocyanate **65**.

Condensation of thiocyanate **65** with bis(4-methoxybenzyl)amine **23**, achieved in the same way described, allows a protected carbamothioyl amide **66** in high yield (>50%) to be obtained. Compound **66** condensed with the appropriate alpha bromo-ketones **26** in DMF to give the protected 2-aminothiazole **67**. The amino group of **67** was deprotected in acid condition and long time to afford compound **68**. In the last step, aminothiazole **68** is conjugated with 1-(benzo[d][1,3]dioxol-5-yl)cyclopropanecarboxylic acid **15** via activation of acid group with uronium salts to obtain the desired products **69-96** (Scheme 8).



Scheme 8. Reagents and condition: (a) MeOH, reflux, 3 h; (b) NaBH₄, 0 °C to RT, 10 h; (c) NH₄SCN, acetone, 0°C, 2 h; (d) acetone, RT, 2- 3 h; (e) N,N-DMF, 85 °C, 3 h; (f) TFA, 100 °C, 36-48h; (g) HATU, DIPEA, N,N-DMF, 50 °C, 24-48 h (16 - 43%).

3.4 CFTR assay

CFBE41o- cells expressing F508del-CFTR and halide-sensitive yellow fluorescent protein (HS-YFP) are plated on 96-well transparent black microplates (Corning Life Sciences, Acton, MA) at a density of 50,000 cells/well and held at 37 °C in 5% CO₂ for 24 hours. For the corrector assay, the CFBE41o- cells are treated for 24 hours with the compounds to be tested, with or without the VX-809 as the reference corrector. At the time of testing, the culture medium is removed and the cells are gently washed with saline solution (PBS) complete with divalent ions (137 mm NaCl, 2.7 mm KCl, 1 mm CaCl₂, 0.5 mm MgCl₂, 1.5 mm KH₂PO₄, 8.1 mm Na₂HPO₄ at pH 7.4). After washing, the cells are incubated for 25 minutes at 37° C with 60 µl of PBS plus 20 µm of forskolin (which stimulates the production of intracellular cAMP, to maximize phosphorylation of the CFTR protein) and 50 µm of genistein (as a potentiator).

At the time of testing, CFBE41o- or FRT cells are transferred to a microplate reader (FluoStar Galaxy; BMG Labtech) to determine the activity of CFTR. The microplate reader is equipped with high quality YFP excitation (HQ500/20X: 500 10 nm) and emission (HQ535/30M: 535 15 nm) filters (Chroma Technology Corp., Brattleboro, VT). The test consists of a continuous fluorescence reading for 14 seconds, 2 seconds before and 12 seconds after injection of a solution containing I- (165 µl of PBS modified with Cl- replaced by I-; the final concentration of I- in the well is 100 mm). After background subtraction (i.e., cell-free basal fluorescence), the data is normalized with respect to the initial fluorescence values. To determine fluorescence quenching (QR) due to I- influence, the data corresponding to the final 10 seconds for each well are interpolated with an exponential function to derive the initial slope (df/dt).

Cell cultures:

- Bronchial epithelial cell line CFBE41o⁻ in which F508del-CFTR is co-expressed with the halide-sensitive yellow fluorescent protein (HS-YFP), grown with MEM (Minimum essential medium) soil.
- FRT cells in which HS-YFP and F508del-CFTR are co-expressed, cultivated with soil Coon's modified Ham's F-12.

Both media are added with fetal calf serum 10%, glutamine 2 mm, penicillin 100 U/ml and streptomycin 100 g/ml.

Chapter 4: Results and Discussion

4.1 Role of the Portion A and of the Portion B

I divided the structure of the progenitor compound **2a** in three parts and first of all I studied the role of portion A and B in modifying the activity.

In particular, portion A and B were modified one a time.

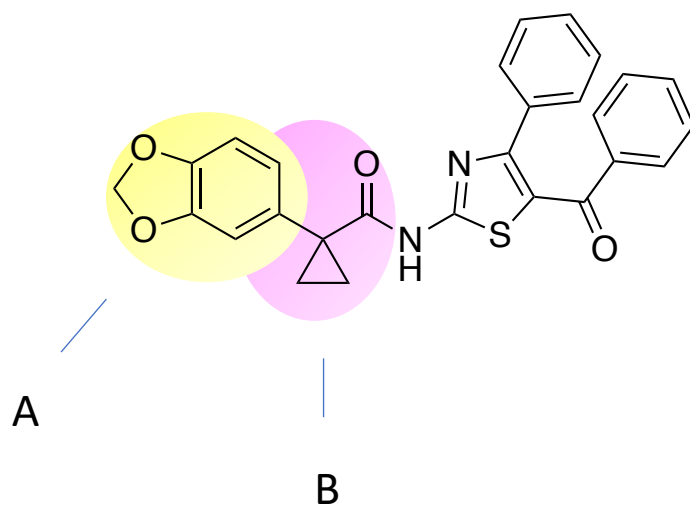


Figure 19. Structure of the progenitor compound **2a**. Portion A and portion B are highlighted in yellow and in pink. These portions were modified one at a time to extrapolate their role in the corrector activity in F508del-CFTR.

I started to investigate the role of the benzo[d][1,3]dioxole (A), hence, I replaced it by p-chlorophenyl and I obtained the compound **4**, not active (Table 2).

This data confirmed the results obtained by Doiron (Doiron et al.; 2019) on VX-809 and analogues; in fact, substituting the benzodioxole portion of both VX-809 and of one of its structural analogues (in which the pyridine ring was replaced by a phenyl) with a methoxyphenyl, the corrector activity turned out of approximately 50% reduced.

I can conclude that the portion A is fundamental for the biological activity.

Then I examined portion B, keeping intact the aminothiazole core of **2a** (portion C) and the benzo[d][1,3]dioxole portion (portion A). I've synthesized 4 molecules in which I have modified the cyclopropane carboxamide:

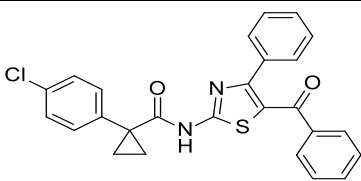
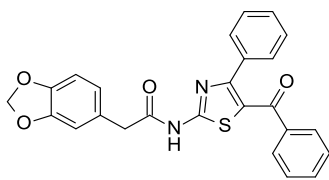
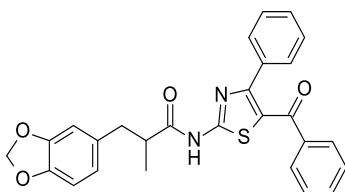
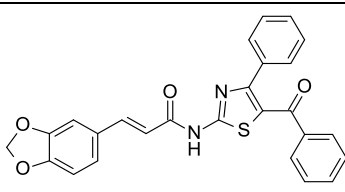
- Compound **5b** without the cyclopropane ring
- Compound **6b** without the cyclopropane ring and with isobutyramide portion
- Compound **7b** without the cyclopropane ring and with acrylamide portion
- Compound **10** without the cyclopropane ring and with aryloxy-2-methylpropanamide moiety

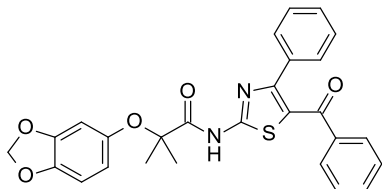
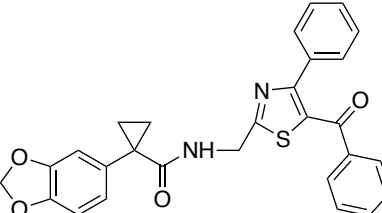
In all the cases compounds were not active as correctors (Table 2).

Thanks to this information I can confirm the importance of the benzo[d][1,3]dioxole cyclopropane carboxamide moiety for corrector activity.

Finally, I synthesized compound **16** (Table 2), in which the carboxy amide (portion B) has been spaced by a methylene from the thiazole core (portion C), to increase the distance between portion B and C, but this modification led to a compound not active.

Table 2- Compounds with modifications to study the importance of the benzo[d][1,3]dioxole cyclopropane carboxamide moiety (A+B) for corrector activity

| Compound | Structure | Activity |
|-----------|---|-----------|
| 4 |  | No Active |
| 5b |  | No Active |
| 6b |  | No Active |
| 7b |  | No Active |

| | | |
|----|---|-----------|
| 10 |  | No Active |
| 16 |  | No Active |

4.2 Role of the Portion C

Finally, I studied the role of the aminothiazole portion (portion C, fig. 20).

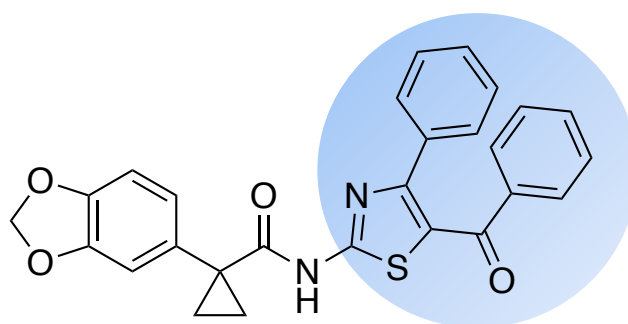
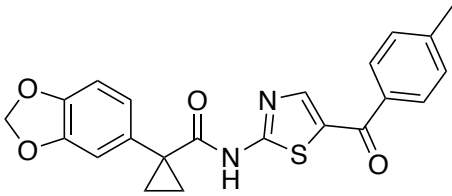
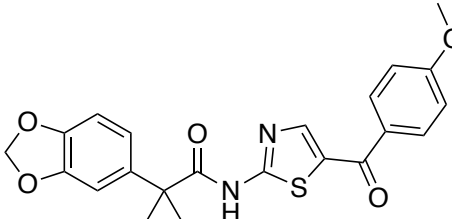


Figure 20. Structure of the progenitor compound **2a**. Portion C is highlighted in light blue. Portion C was modified with different chemical groups to study how different functional groups impacted on the corrector activity in F508del-CFTR.

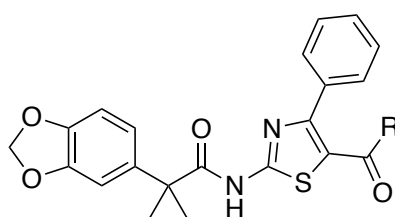
First, I have demonstrated that the C-4 aryl group of the 2-aminothiazole is crucial for activity, as its removal, in **19d** ($EC_{50} = 2.57 \mu\text{M}$) and **20d** ($EC_{50} = 9.3 \mu\text{M}$) led to decreasing activity with respect to the progenitor ($EC_{50} = 0.087 \mu\text{M}$) (Table 3).

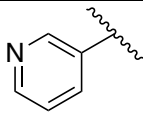
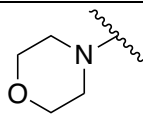
Then I decided to fix the aromatic ring in 4 and to study only the modification at position 5, with the aim to obtain correctors with an increased potency and activity, in comparison with compound **2a**.

Table 3 – Compounds without substituents at position 4 of the thiazole cycle

| Compound | Structure | EC ₅₀ (μM) |
|----------|--|-----------------------|
| 19d |  | 2.57 |
| 20d |  | 9.3 |

Therefore, I inserted a different keto group respect to the benzoyl one, as an aliphatic like methyl in **29**, heteroaromatic like pyridine in **30** and heterocycle like morpholine in **31** (Table 4). All the substitutions were made in the same position. Only compound **30** (EC₅₀= 0.79 μM) had a certain activity, while compound **29** (EC₅₀= 2.72 μM) and, overall, **31** (EC₅₀ = 8.5 μM) led to decreasing activity with respect to the progenitor **2a** (EC₅₀= 0.087 μM), demonstrating the importance of the benzoyl group at position 5 on the thiazole ring.

Table 4 – Hybrids with the replacement of the phenyl ring in 5 with different moieties

| Compound | R | EC ₅₀ (μM) |
|----------|---|-----------------------|
| 29 | -CH ₃ | 2.72 |
| 30 |  | 0.79 |
| 31 |  | 8.50 |

Understood both the importance of the phenyl ring in position 4 and the benzoyl in 5, I explored several substitutions in the phenyl ring at position 5, obtaining a first library of compounds with modifications in 5 and leaving the ring unchanged in 4 (see Table 5).

At first, I examined the *para* position so, I introduced a small group like *p*-methoxy, obtaining a weak active molecule **32** ($EC_{50} = 0.45\mu\text{M}$) respect the progenitor **2a** ($EC_{50} = 0.087\mu\text{M}$). Then, the replacement of the *p*-methoxy with its bioisoster, *p*-thiomethyl in compound **33**, led to an increase in potency ($EC_{50} = 0.10\mu\text{M}$).

After that, I lengthened the alkyl portion of compound **32**, inserting a *p*-propoxy group, in this way, I obtained compound **34** ($EC_{50} = 0.017\mu\text{M}$), that shows an increased activity respect the progenitor **2a**. Finally, I introduced a *p*-trifluoromethoxy, increasing the lipophilicity, and I obtained compound **35** of weak activity ($EC_{50} = 0.36\mu\text{M}$).

I then synthesized a further series of hybrids characterized by the presence of the carboxyl group; by inserting an acid group in *para*, a not active molecule **36** was obtained ($EC_{50} = 7,31\mu\text{M}$); the same result was evaluated with an amide group **37**, while the esterification of the acid group with ethanol results in a more active compound **38** ($EC_{50} = 0.41\mu\text{M}$), although in this series I have not obtained any promising compounds.

Since in the first series the compound **34** with aliphatic chain showed a good activity, I synthesized a compound with *p*-pentyl substituent **39** (lacking of the ethereal bridge), but unfortunately, I have not achieved improvements in the activity ($EC_{50} = 0.43\mu\text{M}$).

The presence of a hetero atom between the alkyl chain and the aromatic ring seems to be ameliorative for the activity of the molecule, so I tried to insert a tertiary amino group, obtaining compound **40** with good activity ($EC_{50} = 0.21\mu\text{M}$), although less than **2a**.

I have therefore inserted in *para* position, a bulky halogen like bromine **41**, without obtaining any improvement in the activity ($EC_{50} = 0.53\mu\text{M}$).

Finally, I synthesized a small series of compounds that have another cycle in *para*, like a *p*-phenyl, obtaining one of the most active molecules of the library **42** ($EC_{50} = 0.07\mu\text{M}$), an aromatic heterocycle that resulted in a molecule **43** that is not so active ($EC_{50} = 1.06\mu\text{M}$) and an aliphatic heterocycle in which the heteroatom is directly linked to the phenyl, obtaining a partially active compound **44** ($EC_{50} = 0.37\mu\text{M}$). Then, by introducing a sterically bulkier ring, like a benzodioxol **45**, I obtained a molecule with a good activity ($EC_{50} = 0.11\mu\text{M}$). Finally, I synthesize a compound in which between the ketone group and the phenyl ring, I placed a pyrimidine ring **46**, creating a bulkier substituent with a good activity ($EC_{50} = 0.28\mu\text{M}$).

To understand the importance of the position of the substituent, I moved some groups from the *para* position to the *meta* one.

The presence of the methoxy group in *meta* gave a compound **47** more active than the analogue *para* substituted ($EC_{50} = 0.10\mu\text{M}$ vs $0.45\mu\text{M}$); so, I moved the same group in *ortho* **48**, confirming also in this case, a better activity ($EC_{50} = 0.14\mu\text{M}$).

Moving the bromine from the *para* position to the *meta*, **49**, an increase of the activity was observed ($EC_{50} = 0.18\mu\text{M}$ vs $0.53\mu\text{M}$); therefore, I synthesized a compound that brought in *meta* position, a less bulky halogen, like the fluorine **50**, increasing the activity ($EC_{50} = 0.13\mu\text{M}$).

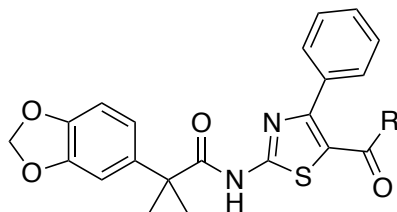
About compound **34**, on the other hand, the same substituent in *meta*, instead of *para*, provides compound **51** with a good activity ($EC_{50} = 0.16\mu\text{M}$), but not comparable with **34**, which is the most active of the entire series. The same situation I observed with the *m*-phenyl **52** ($EC_{50} = 0.25\mu\text{M}$).

In the last round of substitutions, I've been dealing with compounds that are bisubstituted on phenyl. Compound **53** with a methoxy group in *para* and a second methoxy group in *ortho*, show a weak activity ($EC_{50} = 0.40\mu\text{M}$), but also in this case moving the methoxy group from the *para* position to the *meta*, **54**, I observed an increase in the activity ($EC_{50} = 0.11\mu\text{M}$). Keeping the *p*-methoxy and inserted a halogen in *meta*, as in compound **55**, there is no improvement in the activity ($EC_{50} = 0.41\mu\text{M}$).

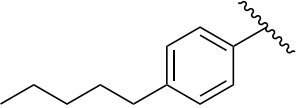
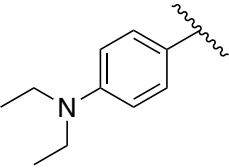
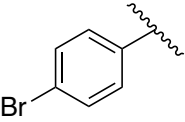
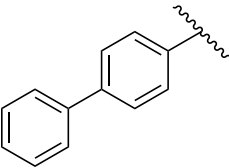
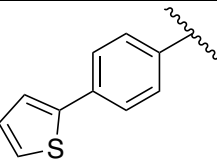
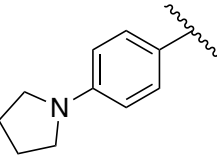
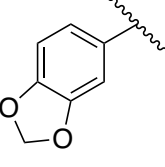
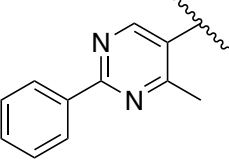
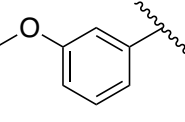
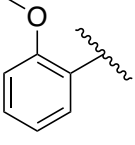
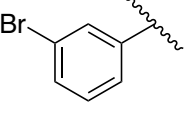
I replaced the methoxy group with a more hydrophilic group, like the hydroxy, and substituted the *meta* position, first, with an unsaturated alkyl chain in compound **56** and then, with a more polar group **57**, obtaining good results only in the first case ($EC_{50} = 0.28\mu\text{M}$ and $13.7\mu\text{M}$). Finally, I

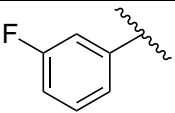
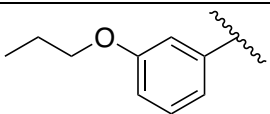
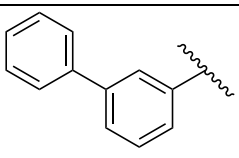
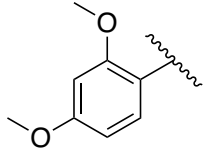
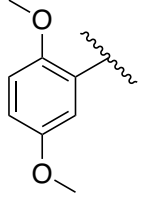
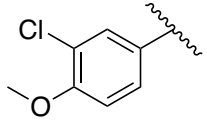
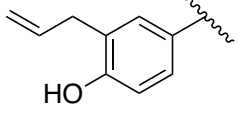
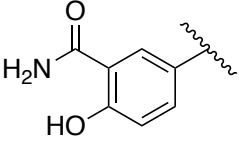
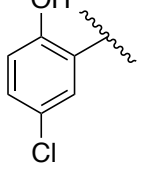
moved the hydroxy group from the *para* to the *ortho* position and simultaneously I inserted a halogen in *meta*, in compound **58**, but in this case, the activity has been lost ($EC_{50} = 1.60 \mu\text{M}$). Only the mono-substituted molecules with the halogen in *meta* ($EC_{50} = 0.18 \mu\text{M}$ and $0.13 \mu\text{M}$) maintain the activity.

Table 5 - First Library of Hybrids with different pattern of substitutions at position 5 of the thiazole ring



| Compound | R | EC_{50} (μM) |
|----------|---|-----------------------------|
| 32 | | 0.45 |
| 33 | | 0.10 |
| 34 | | 0.017 |
| 35 | | 0.36 |
| 36 | | 7.31 |
| 37 | | Not active |
| 38 | | 0.41 |

| | | |
|----|---|------|
| 39 |  | 0.43 |
| 40 |  | 0.21 |
| 41 |  | 0.53 |
| 42 |  | 0.07 |
| 43 |  | 1.06 |
| 44 |  | 0.37 |
| 45 |  | 0.11 |
| 46 |  | 0.28 |
| 47 |  | 0.10 |
| 48 |  | 0.14 |
| 49 |  | 0.18 |

| | | |
|----|---|-------|
| 50 |  | 0.13 |
| 51 |  | 0.16 |
| 52 |  | 0.25 |
| 53 |  | 0.40 |
| 54 |  | 0.11 |
| 55 |  | 0.41 |
| 56 |  | 0.28 |
| 57 |  | 13.70 |
| 58 |  | 1.60 |

I have therefore synthesized a second library of hybrids taking into account some information deduced from substituents in position 5 and applying modifications at position 4 at the thiazole ring (Table 6). As previously reported, the phenyl in 4 was maintained because its presence is fundamental for the corrector activity, so I decorated the phenyl ring in 4 with different substituents. In this way I obtained other information about the relationship with structure and corrector biological activity.

I choose to maintain the active chemical groups, used in the previous library, as the *p*-methoxy; the *m*-methoxy; the *p*-thiomethyl; the *p*-phenyl and the *p*-pyrrolidine.

First, I inserted a *p*-methoxy group in 4 on the backbone of compound **2a** and I obtained a molecule **69** showing a decreased activity ($EC_{50} = 0.35 \mu\text{M}$) respect to **2a** ($EC_{50} = 0.087 \mu\text{M}$). Then, I fixed the *para*-methoxy in 4 working on substitution in 5, as:

a *p*-methoxy **70** ($EC_{50} = 0.064 \mu\text{M}$)

a *p*-trifluoromethoxy **71** ($EC_{50} = 0.14 \mu\text{M}$).

a *p*-thiomethyl **72** ($EC_{50} = 0.10 \mu\text{M}$)

a *p*-phenyl **73** ($EC_{50} = 0.14 \mu\text{M}$)

a *p*-pyrrolidine **74** ($EC_{50} = 0.033 \mu\text{M}$) and

a *m*-methoxy **75** ($EC_{50} = 0.12 \mu\text{M}$)

to evaluate as this substituent (*p*-methoxy) can influence the activity.

In all the cases the substitution in 4, at the presence of a substituent on the benzoyl group in 5, resulted beneficial in the activity of the molecules. In particular compounds **70** with the *p*-methoxy and **74** with the *p*-pyrrolidine demonstrated to be more active than the progenitor **2a**.

I synthesized a second pattern of hybrids in which I studied the influence of the methoxy group in *meta*, at position 4. In this case, when at position 5 is present a *p*-methoxy **76** the molecule is active ($EC_{50} = 0.19 \mu\text{M}$), but the activity decreased moving the methoxy group from the *para* to the *meta* position **77** ($EC_{50} = 0.21 \mu\text{M}$) and with thiomethyl **78** ($EC_{50} = 0.36 \mu\text{M}$). The activity resulted also decreased with a second cycle, as the *p*-phenyl **79** ($EC_{50} = 0.74 \mu\text{M}$) and the *p*-pyrrolidine **80** ($EC_{50} = 0.60 \mu\text{M}$). In all these cases the presence of the methoxy group in *meta* respect than in *para* in 4, lead to a lowering in the activity.

The only molecule that shown a good activity in this series was decorated with a *p*-trifluoromethoxy group **81** in 5 ($EC_{50} = 0.037 \mu\text{M}$).

Then, the importance of the methoxy group on the phenyl ring in 4 was broadened by synthesizing analogues moving the methoxy group in *ortho*. Based on the promising effects shown by the compounds wearing in 5 *p*-methoxy and *p*-trifluoromethoxy, I maintained the same functional groups and I obtained two compounds, **82** and **83** respectively, still active ($EC_{50} = 0.22 \mu\text{M}$ and $0.15 \mu\text{M}$), although the *para* and *meta* substitutions were optimal.

I therefore studied if a polar group could give beneficial effect on the bioactivity, so I synthesized two molecules with *p*-hydroxy in 4; I chose to maintain the *p*-methoxy **84** and *p*-trifluoromethoxy **85** groups at position 5. The activities of these compounds are lower than the analogues with *p*-OCH₃ in 4, as **70** and **71** (EC₅₀ = 0.24 μM and 0.36 μM respect to 0.064 μM and 0.14 μM). So, I can conclude that an increased polarity at position 4 of the hybrid leads to a decreasing in activity.

Then, I investigated the effects of elongation of the chain in 4 on the bioactivity. I synthesized two molecules decorated on the phenyl ring in 4 with *p*-butoxy group and I maintained *p*-methoxy **86** and *p*-trifluoromethoxy groups **87** in 5; they have similar values of EC₅₀ = 0.29 μM and 0.28 μM, but I observed a decrease in the bioactivity, again, in comparison to the analogue with *p*-OCH₃ in 4 (compounds **70** and **71**). So, the elongation of the alkyl chain in 4 is detrimental.

Finally, I decide to deepen the study about best compounds of the first library, as the hybrids substituted in 5 with the *p*-phenyl **42** (EC₅₀ = 0.07 μM), the *p*-thiomethyl **33** (EC₅₀ = 0.10 μM) and the *m*-methoxy **47** (EC₅₀ = 0.10 μM) groups.

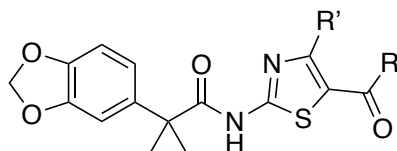
Regarding the structure with the *p*-phenyl in 5, the presence in 4 of a *p*-methoxy **73** and of a *m*-methoxy **79**, as previously seen, led in the first case to an active compound while in the second give a significant decrease in activity. So, different pattern of substitutions in 4 as a *p*-ester **88**, *p*-thiomethyl **89** and a pyridine **90**, gave interesting results (EC₅₀ = 0.12 μM - 0.13 μM - 0.13 μM), although none of them are as active as compound **42**. On the contrary, the presence of a *p*-chloride **91**, a more lipophilic group, led to a decrease in activity (EC₅₀ = 0.64 μM).

Then, I examined the compound with the methoxy group in *meta* position in 5. As already seen, the presence of a *p*-methoxy group in 4 gives a compound **75** with good activity (EC₅₀ = 0.12 μM), while with the insertion of *m*-methoxy group in 4, as in compound **77**, the activity is slightly decreased (EC₅₀ = 0.21 μM). Expanding this series, I insert new groups like a *p*-thiomethyl **92**, a *p*-chloride **93** and a pyrrolidine **94** but, in all the cases the activity was decreased (EC₅₀ = 0,28 μM – 0.37 μM – 1.52 μM).

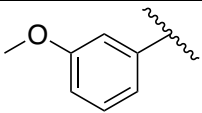
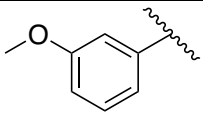
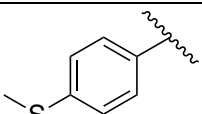
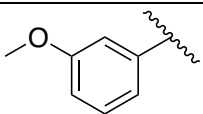
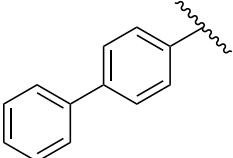
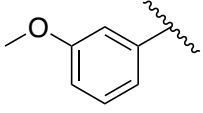
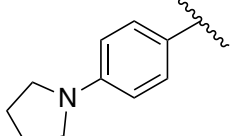
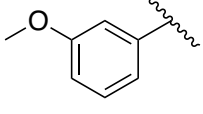
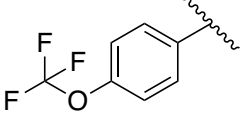
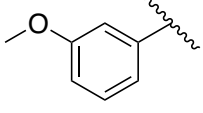
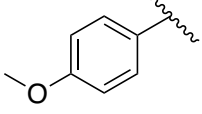
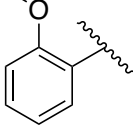
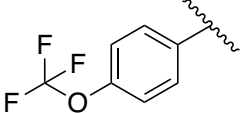
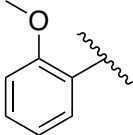
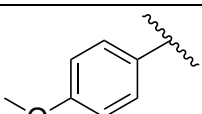
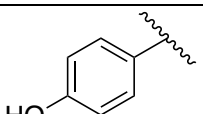
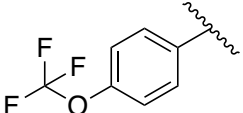
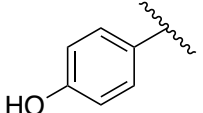
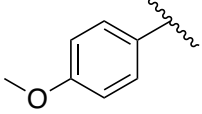
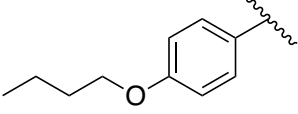
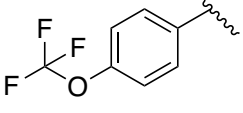
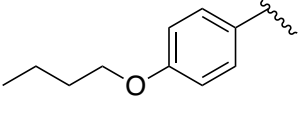
Eventually, I considered the molecule containing the thiomethyl in 5. The insertion of a *p*-methoxy group in 4, as in compound **72**, didn't change the activity, while the presence of a *m*-methoxy group **78** had a detrimental effect. The derivative with two symmetric thiomethyl in *para* position of the phenyl rings **95** caused a decrease in the activity (EC₅₀ = 0.30 9μM). Finally, I synthesized a

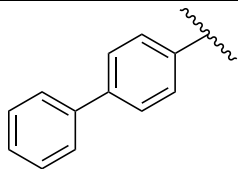
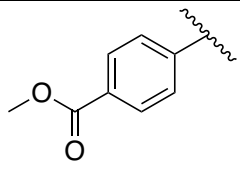
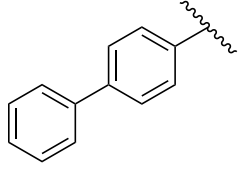
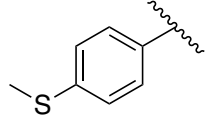
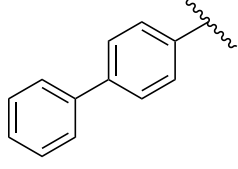
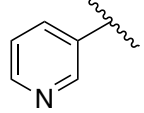
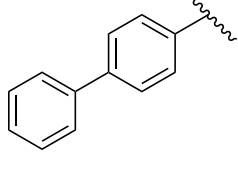
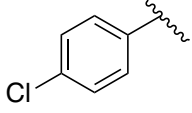
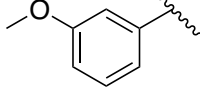
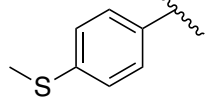
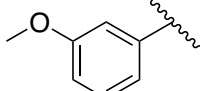
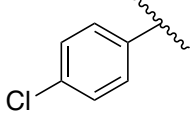
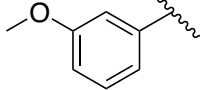
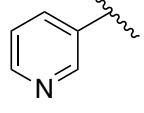
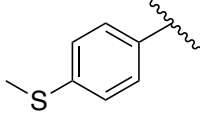
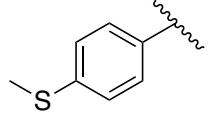
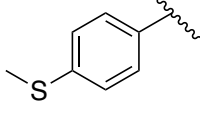
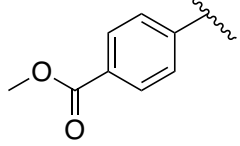
compound containing the *p*- methyl carboxylate **96** in position 4, that shown a higher activity ($EC_{50} = 0.076 \mu\text{M}$) if compared to many of this library.

Table 6 – Second Library of Hybrids with modifications at position 4 and 5 of the thiazole ring



| Compound | R (5) | R' (4) | EC_{50} (μM) |
|----------|-------|--------|-----------------------------|
| 69 | | | 0.35 |
| 70 | | | 0.064 |
| 71 | | | 0.14 |
| 72 | | | 0.10 |
| 73 | | | 0.14 |
| 74 | | | 0.033 |
| 75 | | | 0.12 |
| 76 | | | 0.19 |

| | | | |
|----|---|--|-------|
| 77 |  |  | 0.21 |
| 78 |  |  | 0.36 |
| 79 |  |  | 0.74 |
| 80 |  |  | 0.6 |
| 81 |  |  | 0.037 |
| 82 |  |  | 0.22 |
| 83 |  |  | 0.15 |
| 84 |  |  | 0.24 |
| 85 |  |  | 0.36 |
| 86 |  |  | 0.29 |
| 87 |  |  | 0.28 |

| | | | |
|----|---|--|-------|
| 88 |  |  | 0.12 |
| 89 |  |  | 0.13 |
| 90 |  |  | 0.13 |
| 91 |  |  | 0.64 |
| 92 |  |  | 0.28 |
| 93 |  |  | 0.37 |
| 94 |  |  | 1.52 |
| 95 |  |  | 0.30 |
| 96 |  |  | 0.076 |

4.3 Discussion

I compared the results obtained by the hybrids belonging of the first library, with the phenyl ring in 4 free, and by the hybrids of the second library, with different pattern of substitutions in 4, fixed the same functional group on the benzoyl ring in 5.

The presence of a *p*-methoxy group on the benzoyl group in 5 is always accepted, if the phenyl in 4 was substituted with any chemical group, like methoxy moiety in *para* **70** ($EC_{50}=0.064\ \mu\text{M}$), in *meta* **76** ($EC_{50}=0.19\ \mu\text{M}$) and *ortho* **82** ($EC_{50}=0.22\ \mu\text{M}$) position or a *p*-hydroxy **84** ($EC_{50}=0.24\ \mu\text{M}$) and *p*-butoxy **86** ($EC_{50}=0.29\ \mu\text{M}$) groups. In add, when there's a *p*-methoxy in 5 the activity is higher when the ring in 4 take a functional group respect the analogue **32** unsubstituted in 4 ($EC_{50}=0.35\ \mu\text{M}$).

In the presence of a *p*-trifluoromethoxy in 5 the compound is well tolerated with a substituent in 4 as methoxy group in *para* **71** ($EC_{50}=0.14\ \mu\text{M}$), in *meta* **81** ($EC_{50}=0.037\ \mu\text{M}$) and in *ortho* **83** ($EC_{50}=0.15\ \mu\text{M}$) or a *p*-butoxy **87** ($EC_{50}=0.28\ \mu\text{M}$), and the activity ameliorates respect the analogue unsubstituted **35** in 4 ($EC_{50}=0.36\ \mu\text{M}$); on the contrary with a more polar group **85** in 4, as the hydroxy moiety, the activity is the same of the hybrid of the first series ($EC_{50}=0.36\ \mu\text{M}$).

In the presence of a *p*-thiomethyl in 5, there is no precise trend because while with a *p*-methoxy **72** in 4 the activity is maintained ($EC_{50}=0,10\ \mu\text{M}$), as the unsubstituted analogue **33** in 4 ($EC_{50}=0.10\ \mu\text{M}$), with a *p*-ester **96** the activity is really increased ($EC_{50}=0.076\ \mu\text{M}$), but with a *p*-thiomethyl **95** or a *m*-methoxy **78** the activity is decreased ($EC_{50}=0.30\ \mu\text{M}$ and $0.36\ \mu\text{M}$).

With the *p*-pyrrolidine ring in 5, the presence of a *p*-methoxy group **74** in 4 is very advantageous ($EC_{50}=0.033\ \mu\text{M}$), on the contrary moving the methoxy group from the *para* to the *meta* position **80** is detrimental ($EC_{50}=0.6\ \mu\text{M}$) respect the analogue with the phenyl ring unsubstituted **44** in 4 ($EC_{50}=0.37\ \mu\text{M}$).

Regarding the *m*-methoxy group in 5 the corrector activity is higher if the phenyl in 4 is without substituents as in compound **47** ($EC_{50}=0.10\ \mu\text{M}$).

At last, with the *p*-phenyl in 5, the biological activity resulted decreased with a function group decorating the ring in 4 respect compound **42** ($EC_{50}=0.07\ \mu\text{M}$), but the introduction of some substituents as the *p*-methoxy **73** ($EC_{50}=0.14\ \mu\text{M}$), the *p*-methyl ester **88** ($EC_{50}=0.12\ \mu\text{M}$), the *p*-thiomethyl **89** ($EC_{50}=0.13\ \mu\text{M}$) and the *p*-pyridine **90** ($EC_{50}=0.13\ \mu\text{M}$) preserve the activity, even if the insertion of *p*-chloride **91** ($EC_{50}=0.64\ \mu\text{M}$) and *m*-methoxy **79** ($EC_{50}=0.74\ \mu\text{M}$) are detrimental for the activity.

These data taken together have allowed me to identify which portions of the molecule are fundamental in furnish the corrector activity and to identify some hybrids that can become a starting point for developing new molecules with better activity.

4.4 Further Biological Assays on the First Library Hybrids

I selected the most active compounds belonging to the first library to subject them to further investigations, as:

- the trans epithelial electrical resistance and potential difference measurements (TEER/PD), to study the ability of the novel derivates to rescue F508del-CFTR on primary cultures of human bronchial epithelial cells, from a CF patient homozygous for the F508del mutation;
- the Western blot (WB), to evaluate biochemically the rescue of processing defect;
- the surface plasmon resonance (SPR) to evaluate the effective capacity of the compounds to bind F508del-CFTR in collaboration with .

I choose **33** ($EC_{50}= 0.10 \mu\text{M}$) and **42** ($EC_{50} = 0.07 \mu\text{M}$) to test in TEER/PD and in WB assays.

These biochemical tests have been conducted at U.O.C of Molecular Genetic (G. Gaslini).

Epithelia for 24 h were treated with test compounds at different concentrations: **33** (5 - 0.5 - 0.05 μM), **42** (10 - 1 - 0.1 μM), and with a positive control as VX-809 1 μM or vehicle alone (DMSO) as negative control, and then assayed.

Trans epithelial electrical resistance was measured before and after stimulation with forskolin (20 μM) plus genistein (50 μM) to totally activate CFTR. It was then measured after addition of the CFTR inhibitor PPQ-102 (30 μM) to fully block CFTR activity.

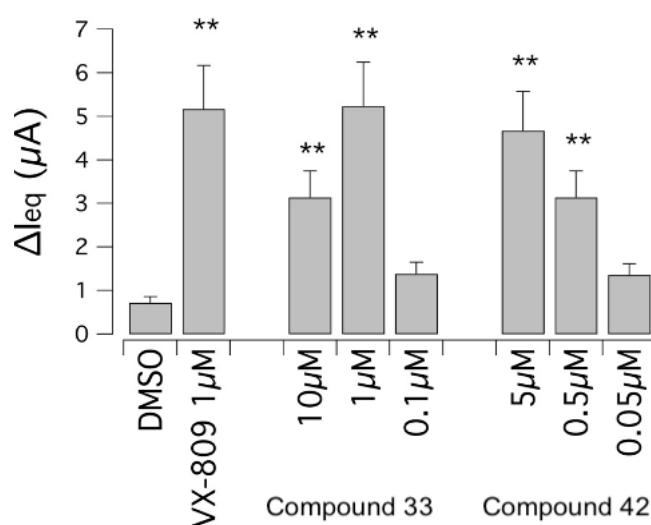


Figure 21. Compounds **33** and **42** rescue F508del-CFTR activity in primary bronchial epithelia.

The graph reports the equivalent short-circuit current (calculated from TEER/PD measurements) in F508del/F508del bronchial epithelia, treated for 24 h with test compounds at the indicated

concentration, or VX-809 (1 μ M), or vehicle alone (DMSO). Data are expressed as means \pm SD, n = 3.

The bar graphs of Figure 21 show the delta between the values of electrical resistance measured before and after CFTR inhibition, converted into its reciprocal conductance.

As it appears evident, long-term treatment of CF primary bronchial epithelia with compounds **33** and **42** significantly increased both CFTR-mediated conductance and equivalent short-circuit current.

Then, the selected compounds **33** and **42** were assayed in the WB to evaluate F508del-CFTR expression pattern. In WB, CFTR protein is detected as two bands:

- band B, of approximately 150 kDa, that corresponds to partially glycosylated CFTR residing in the ER;
- band C, of approximately 170 kDa, that is the fully processed (mature) CFTR that has passed through the Golgi.

The prevalent form in cells expressing WT CFTR is band C. Lysates of cells expressing F508del-CFTR show primarily band B, consistent with the severe trafficking defect caused by the mutation. F508del-CFTR/HS-YFP expressing CFBE41o-cells were treated with DMSO as vehicle alone, with test compounds **33** and **42** (0.5 μ M) or with the positive control VX-809 (1 μ M), to evaluate the effect of hybrid compounds on CFTR electrophoretic mobility. After 24 h, cells were lysed and lysates were subjected to SDS-PAGE followed by western blotting.

Western blot images were analyzed with ImageJ software. For each lane, CFTR bands, analyzed as ROI, were quantified after normalization for GAPDH to account for total protein loading.

Treatment of F508del-CFTR cells with corrector VX-809 significantly enhanced expression of mature CFTR (band C), resulting in a change in the C band/B band ratio. Similarly, also the treatment with my compounds resulted in a significant increase in the C band/B band ratio, comparable to that obtained following treatment with VX-809 (Figure 22).

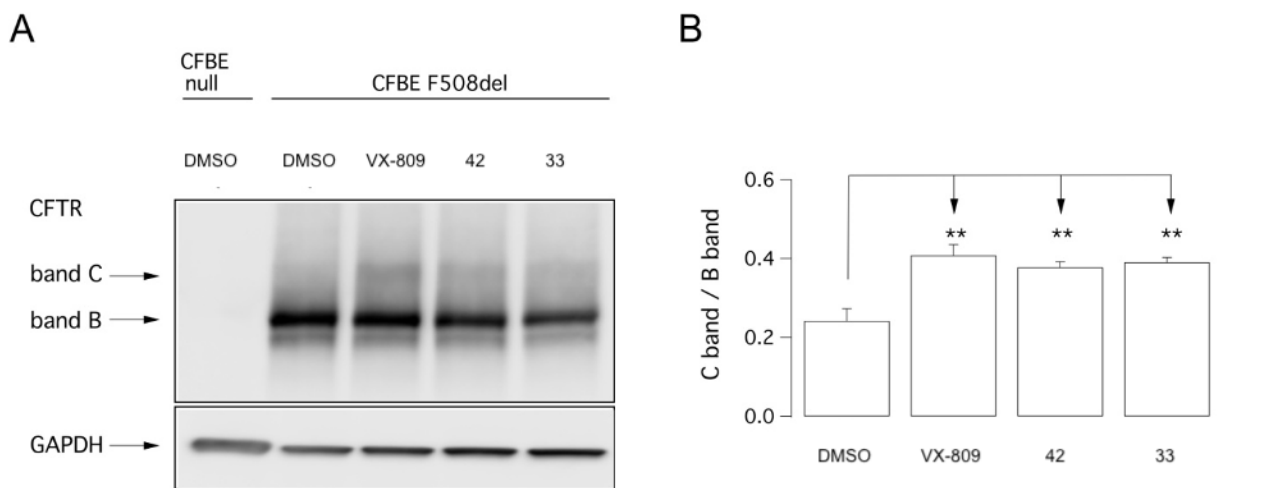


Figure 22. Biochemical analysis of the F508del-CFTR expression pattern.

(A) Electrophoretic mobility of F508del-CFTR in 2 different preparations of CFBE41o- cells, treated for 24 hours with vehicle or test compounds (0.5 μ M) or VX-809 (1 μ M). Arrows indicate complex-glycosylated (band C) and core-glycosylated (band B) forms of CFTR protein. (B) The bar graph reports the densitometric analysis (means \pm SEM, n = 3) of band C/band B ratio normalized to GAPDH. **P < 0.01 versus control (ANOVA with Dunnett's post hoc test).

To demonstrate in which part of the protein these structures are linked and probably that the mechanism of action of our hybrids involved the direct interaction with the mutated protein we exploit the potential of surface plasmon resonance (SPR) to evaluate the effective capacity of the compounds to bind CFTR protein. Hence, I selected two different compounds **34** (0.017 μ M) and **42** (0.07 μ M) to bind to F508del-CFTR, exploiting a biosensor recently described by D'Ursi (D'Ursi et al., 2019), in which the mutated protein was immobilized in membrane-like lipid vesicles as to resemble the F508del-CFTR environment *in vivo*.

Increasing concentrations of **34** and of **42** were injected onto the biosensor containing F508del-CFTR provided saturable and dose-dependent binding curves (Fig. 23) that allowed to calculate the Kd values. Kd resulted equal to 38.2 ± 5.1 mM for **34** and 89.3 ± 35.3 mM for **42**.

VX-809 was used as a positive control and bound F508del-CFTR with similar affinity (Kd value equal to 72.8 ± 19.5 mM) in the same experimental condition.

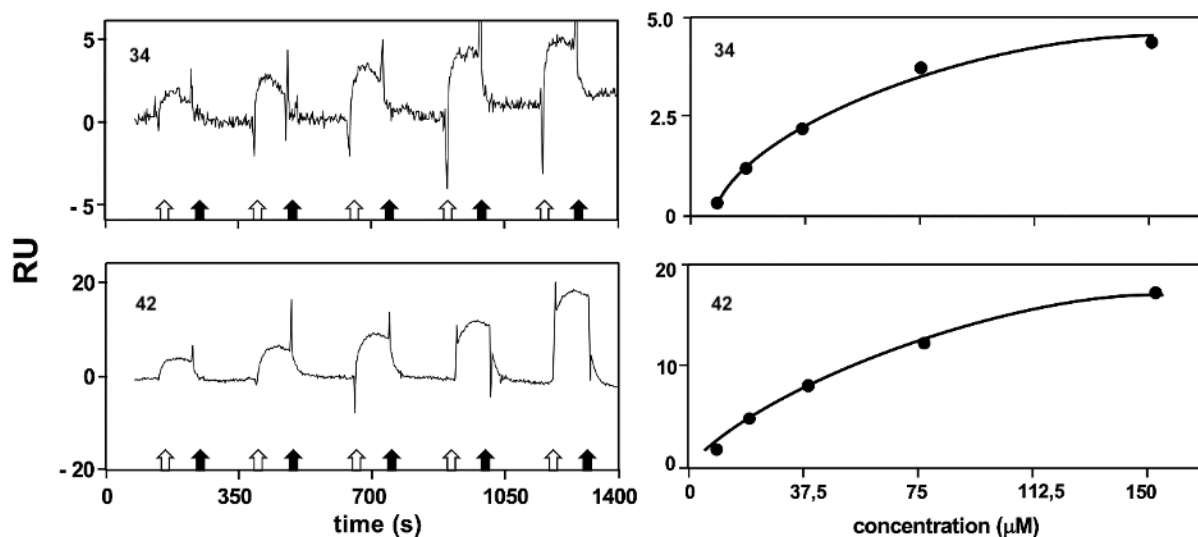


Figure 23. Left panels: Blank-subtracted sensor-grams derived from a single cycle analysis of **34** (upper panel) or of **42** (lower panel) both at 9.4, 18.8, 40, 37.5, 75, 150 μM injected on the F508del-CFTR biosensor. White and black arrows point to the start and end of the injections, respectively. Right panels: Steady-state analysis of **34** (upper panel) or of **42** (lower panel) injected onto the F508del-CFTR-containing biosensor (same doses as above). The results shown are representative of other three that gave similar results.

Finally, to confirm the hypothesis that my hybrids act as corrector of type 1, I decided to test some of my compounds in combinations with VX-809 and VX-661 (the commercial drug available as type 1 correctors), to verify that they did not present any additive or synergistic effects. So, we tested **33**, **34**, **42** in combination with VX-809 and VX-661, in CFBE41o-cells stably expressing F508del-CFTR in the YFP functional assay. Cells were treated for 24 h with single test compounds or their combinations and then assayed (Fig. 24). No additive or synergistic effect was observed when combining **33**, **34** and **42** with VX-809 or VX-661, supporting the hypothesis that all these compounds possibly share the same binding site.

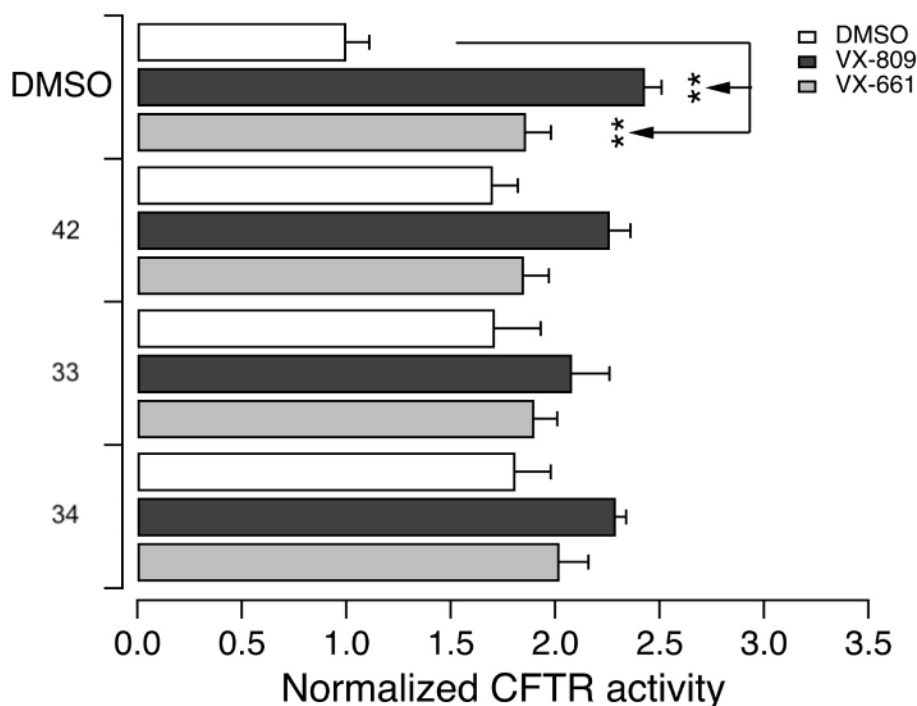


Figure 24. Analysis of corrector combinations. F508del-CFTR activity determined in CFBE41o-cells with the HS-YFP.

Cells were treated with **42** (0.2 μM), **33** (1 μM), **34** (1 μM), VX-809 (1 μM) or VX-661 (10 μM), as single agents or as combinations. ****P** < 0.01 (ANOVA with Tukey's post hoc test).

4.5 Further Biological Assays on the Second Library Hybrids

To corroborate the corrector activity of these new derivatives, I choose the most active compounds to test in further biochemical assay.

I selected **74** (EC_{50} = 0.033 μM) and **81** (EC_{50} = 0.037 μM) to test the ability of these compounds to rescue F508del-CFTR on well-differentiated primary cultures of human bronchial epithelial cells. Test were performed on cells from two different F508del homozygous subjects (donor codes: HBE73 and HBE93) by using electrophysiological techniques.

Bronchial epithelia were then treated for 24 hours with DMSO vehicle alone as negative control, or with compounds **74**, **81** (50 nM and 1 μM), or with VX-809 as positive control (at the same concentrations used for test compounds).

The following day, epithelia were mounted in Ussing chambers for measurement of chloride transepithelial transport by short-circuit current measurements. After blocking epithelial sodium channel (ENaC) activity with amiloride, cells treated with vehicle (DMSO) showed little CFTR function, as indicated by the small response to the membrane-permeable cAMP analog CPT-cAMP and the potentiator VX-770. The low activity of F508del-CFTR in the apical membrane was

confirmed by adding the selective CFTR inhibitor, CFTRinh-172, which caused a relatively small current drop.

As expected, 24 h incubation with corrector VX-809 resulted in dose-dependent significant F508del-CFTR rescue, as evidenced by the marked current increase elicited by stimulation with CPT-cAMP and VX-770 and the amplitude of the current drop caused by CFTRinh-172.

Epithelia treated with **74** and **81** showed significant increase in CFTR-dependent function as compared to DMSO-treated epithelia, although the rescue observed was lower than that achieved following treatment with VX-809.

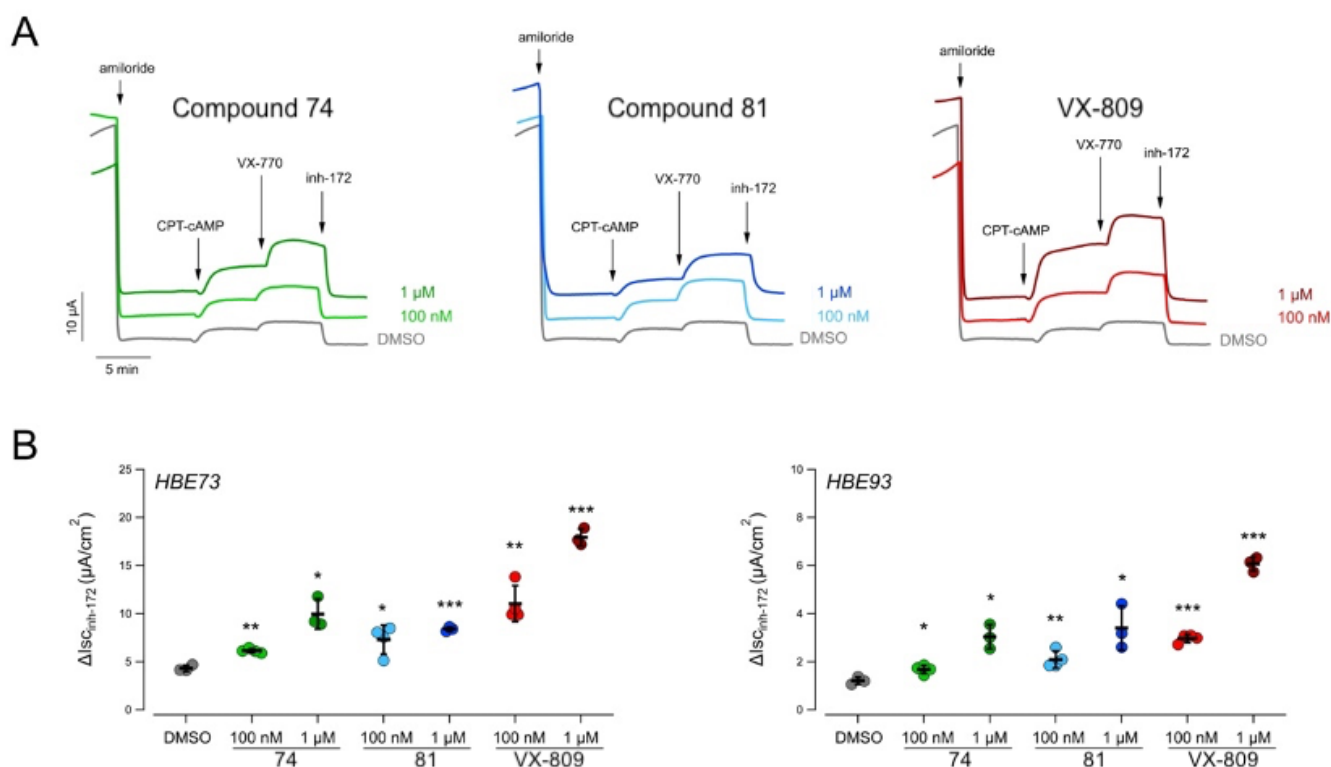


Figure 25. Evaluation of the effect of hybrid derivatives **74** and **81** on F508del-CFTR activity measured on human primary bronchial epithelia derived from two CF patients.

A. Representative traces from Ussing chamber recordings of human primary bronchial epithelia derived from a homozygous F508del patient (donor code: HBE73) following 24 h treatment with DMSO alone or indicated test compounds.

B. Dot plots summarizing CFTR-mediated currents from Ussing chamber recordings of human primary bronchial epithelia derived from two homozygous F508del patients (donor codes: HBE73 and HBE93) treated as described in A. Analysis of variance was calculated for the groups. Asterisks indicate statistical significance versus negative control: * $P < 0.05$; ** $P < 0.01$; *** $P < 0.001$.

Then, 3 hybrids, as **70** ($EC_{50} = 0.064 \mu\text{M}$), **74** ($EC_{50} = 0.033 \mu\text{M}$) and **81** ($EC_{50} = 0.037 \mu\text{M}$) were utilized to biochemically study the rescue of the trafficking defect by analyzing the electrophoretic mobility of mutant CFTR protein.

In addition, to estimate the effect of our molecules on CFTR expression pattern, we treated F508del-CFTR/HS-YFP expressing CFBE41o-cells for 24 h with test compounds **70**, **74** and **81** (50 nM and 1 μM) VX-809 as positive control or DMSO as vehicle alone.

The next day, cells were lysed and the obtained lysates were subjected to SDS-PAGE followed by western blotting. Western blot images were analyzed with ImageJ software. CFTR bands, analyzed as ROI, were quantified in each lane after normalization for GAPDH as loading control. The treatment of F508del-CFTR cells with **70**, **74** and **81** resulted in a significant enhancement in the C band/B band ratio, similar to that with VX-809, see Figure 26.

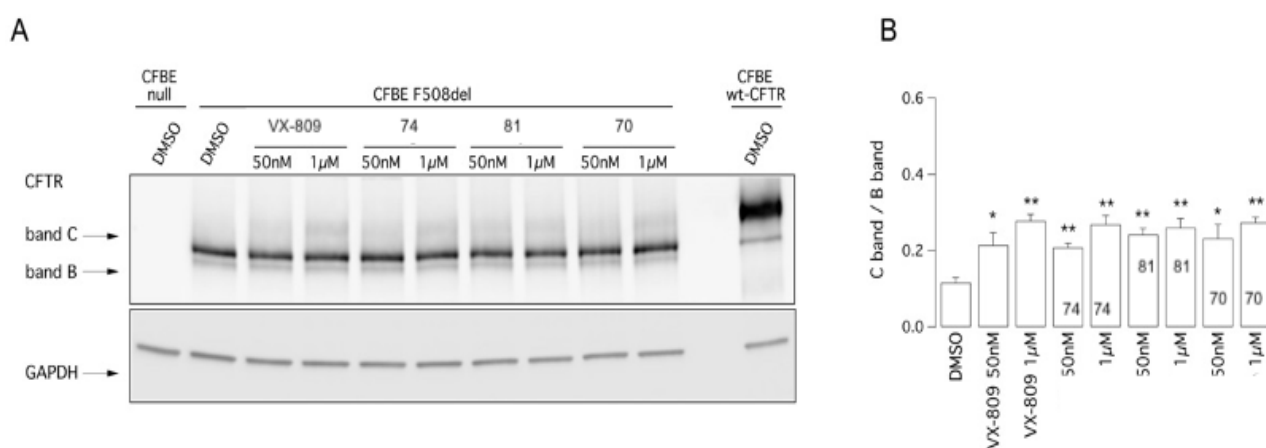


Figure 26. Biochemical analysis of the F508del-CFTR expression pattern.

A. The Western Blot image shows the electrophoretic mobility of F508del-CFTR in CFBE41o-cells, treated for 24 h with vehicle alone or test compounds (as indicated). Arrows indicate mature, complex-glycosylated (band C) and immature, core-glycosylated (band B) forms of CFTR protein.

B. Quantification of the C band / B band ratio in experiments as in A. Data are shown as mean \pm SD ($n = 3$ independent experiments). Asterisks indicate statistical significance versus negative control: * $P < 0.05$; ** $P < 0.01$.

I have previously shown that the combination of our hybrids with VX-809 or VX-661 showed no additive or synergistic effect, sustaining the concept that all these hybrids may have the same binding site.

Now, to further characterize the activity of these novel compounds, we tested the novel derivatives **70**, **74** and **81**, along with VX-809 as positive control, in combination with VX-445 (3 μM), at today

considered a type 3 corrector, in CFBE41o-cells stably expressing F508del-CFTR by using the YFP functional assay.

Cells were treated for 24 h with test compounds at different concentrations, in combination with VX-445 (3 μ M), and then assayed after maximal stimulation of F508del-CFTR in the presence of forskolin (20 μ M) plus VX-770 (1 μ M). The three novel derivatives as well as VX-809 showed a clear additive effect with VX-445, in particular the combinations based on **74** and **81** were as effective as the combination with the positive control VX-809 in terms of maximal rescue and activity at low concentration (Fig. 27). These results can further confirm the putative mechanism of action of our hybrids, as type 1 correctors.

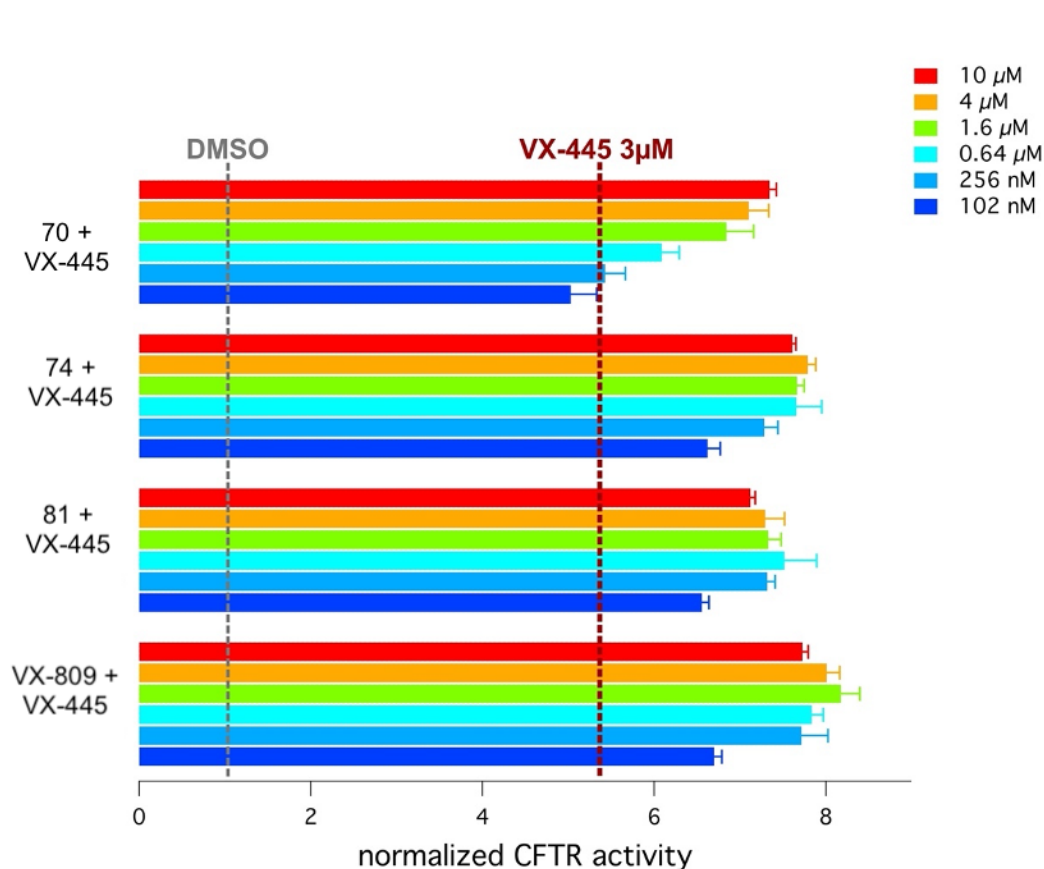


Figure 27. Functional analysis of corrector combinations. F508del-CFTR activity was determined in CFBE41o- cells with stable expression of the HS-YFP. Cells were treated for 24 h with VX-445 (3 μ M) alone or in combination with **70**, or **74**, or **81**, or VX-809 at different concentrations (from 102 nM to 10 μ M). The YFP-based assay was performed after stimulation of CFTR activity with forskolin (20 μ M) plus VX-770 (1 μ M).

4.6 Molecular Docking Studies

Beyond QSAR prediction, the computational chemist group of the Pharmacy Department performed preliminary docking studies to gain further useful information to guide the rational design of new **2a** analogues.

In this context, the research group of University of Brescia by Rusnati, SPR studies performed with the corrector VX-809 on F508del-NBD1, molecular docking and dynamics simulations. These studies supported a key role played at the NBD1 - CFTR by the corrector VX-809 to rescue CFTR and demonstrated a strong agreement between the theoretical prediction and the experimental SPR-based data (Rusnati et al., 2018).

Then, the computational chemist team of Genova proceeded to apply molecular docking studies around the human F508del-CFTR NBD1 domain and described two putative binding positioning for the corrector VX-809, namely POS1 and POS2.

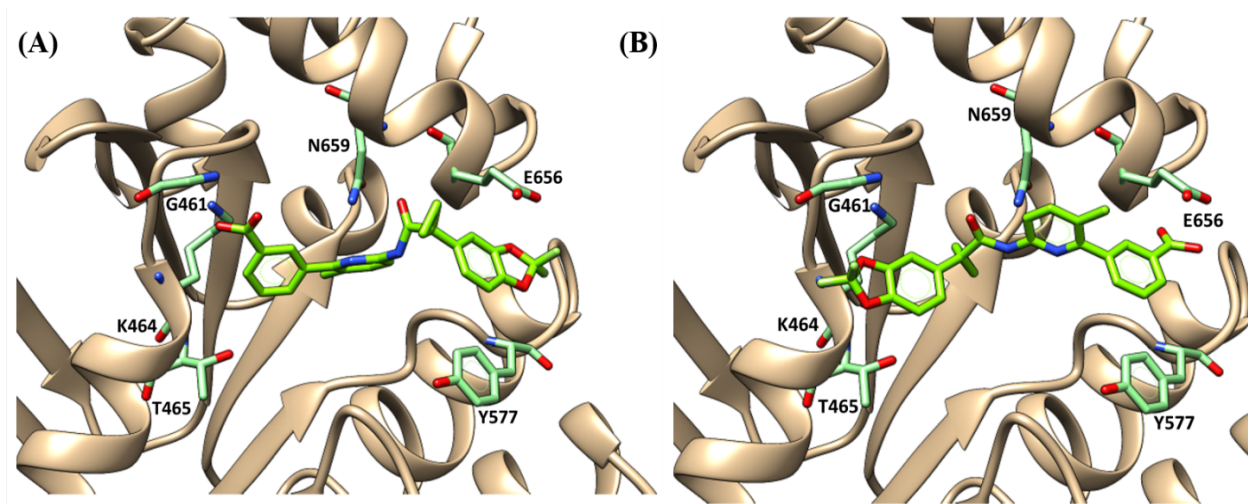


Fig. 28. Selected docking poses of VX-809 within the CFTR hNBD1 domain as POS1 (A) and POS2 (B). The most important residues are labelled.

As shown in Fig. 28A (POS1), the oxygen atom of the carboxamide group of VX-809 is involved in one H-bond with the N659 side- chain, while the carboxylic group is engaged in H-bonds with T460 and G461 and in ionic contacts with K464. The aromatic rings of VX-809 occupy the protein pocket delimited by S573, G576, V603 and A655, exhibiting van der Waals contacts while the benzo-dioxole core is projected towards Y577 and E656.

Concerning POS2 (Fig. 28B), two H-bonds with the key residues K464 and T465 are formed by the two oxygen atoms of the benzodioxole core. The negatively charged carboxylic group of the corrector is H-bonded to the backbone of E656. The overall positioning recognized as POS2 allowed VX-809 to occupy the same binding pocket described for POS1, since the aromatic rings and all the substituents are placed in proximity to the previously cited G461, V603, A655 and N659.

Then, compound **2a** was examined, showing a docking mode similar to those of VX-809 in POS2. So, our computational team performed also docking studies on my hybrids to better investigate their putative mechanism of action. Here, I report the molecular docking of some of the best compounds in the libraries.

The most potent compound **34** displayed a similar docking positioning with those observed for VX-809, highlighting the importance of bulky, flexible and quite lipophilic groups linked at the benzoyl moiety. The benzodioxole moiety of **34** is H-bonded to G461, K464 and T465, while the oxygen atom of the benzoyl group displays contacts with the backbone of E656 and the propoxy group features hydrophobic contacts with the aromatic ring of Y577.

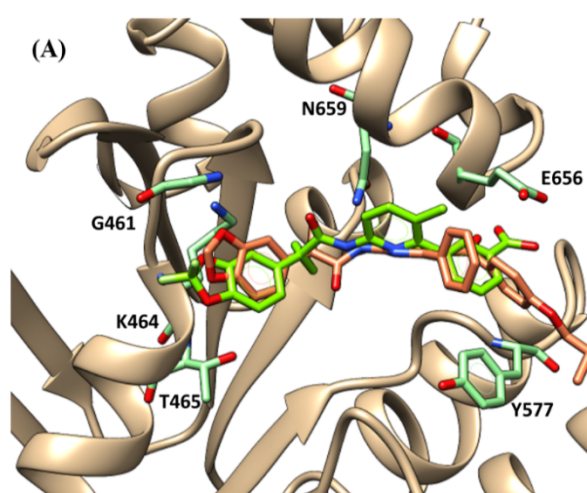


Figure 29. Docking mode of **34** (C atom; orange) in comparison with that of VX-809 (C atom; light green) (A) at the hNBD1 domain of the F508del CFTR mutant.

This kind of docking mode was shared by most of the other promising hybrids, such as **33** featuring a thiomethyl group onto the para position of the benzoyl substituent.

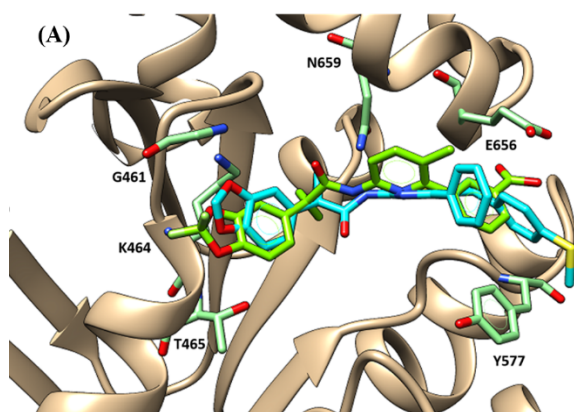


Figure 30. Docking mode of **33** (C atom; dark cyan) (A) in comparison with that of VX-809 (C atom; light green) (A) at the hNBD1 domain of the F508del CFTR mutant.

Analogues of compound **33**, as compound **72** ($EC_{50} = 0.10 \mu\text{M}$) and **96** ($EC_{50} = 0.076 \mu\text{M}$), bearing a p-OCH₃ or a p-methyl ester phenyl in position 4 of the thiazole ring, got comparable or higher potency than the precursor **33**. As shown in Figure 31, the derived docking poses for all of them guarantee contacts with the protein region delimited by W1063, V1293, and K1351, in add, compound **96** more potent than **72**, exhibits additional H-bonds with I177 and E267

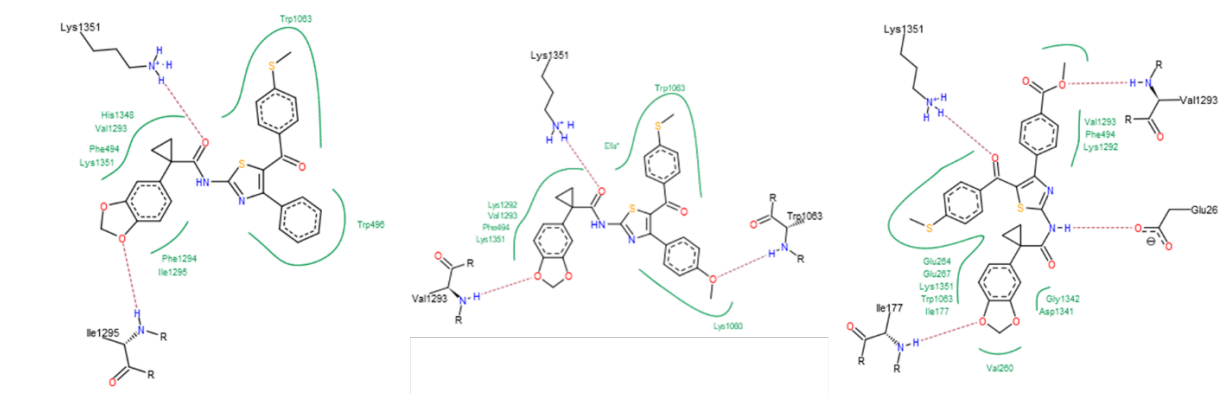


Figure 31. Docking positioning (starting from left) of the hybrid precursor **33** and of the newly synthesized analogues **72** and **96** at the modelled F508del-CFTR.

Compound **42** ($EC_{50} = 0.07 \mu\text{M}$) is characterized by the biaryl moiety and displayed a switched positioning fig. 32, probably caused by the steric hindrance due to the bulky biaryl group. In any case, this docking mode allowed maintaining the aforementioned key contacts with N659, K464 and T465 while interaction with E656 or Y577 appeared to be both involved in stabilizing the compound at the hNBD1 domain.

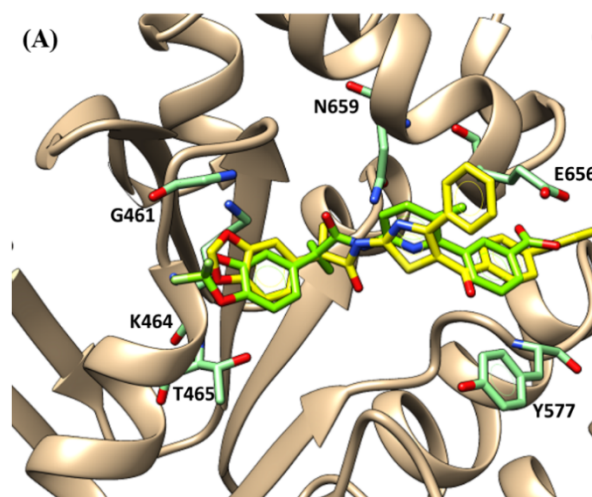


Figure 32. Docking mode of **42** (C atom; yellow) in comparison with that of VX-809 (C atom; light green) (A) at the hNBD1 domain of the F508del CFTR mutant.

The analogues of compound **42** with same bi-aryl motif in **5** showed good corrector ability only when combined with small H-bonding groups at the para position of the phenyl ring at position 4.

In accordance with these data, the most promising derivatives, disclosed in the second library of molecules, featured a methoxy substituted phenyl ring tethered at the position 4 of the main thiazole, as described for compounds **70** ($EC_{50} = 0.064 \mu\text{M}$), **74** ($EC_{50} = 0.033 \mu\text{M}$), and **81** ($EC_{50} = 0.037 \mu\text{M}$). Here, I reported the docking mode of compound **74**, the most potent molecule of this last series. Compound **74**, displaying the p-OCH₃-phenyl substituent in position 4, moved this portion of the corrector towards the same crevice of the protein, interacting with the surrounding residues W1063. It maintained the key contacts with K1351 thanks to the carboxamide group, and it was H-bonded by the benzodioxole oxygen atoms to I1296, (Figure 33).

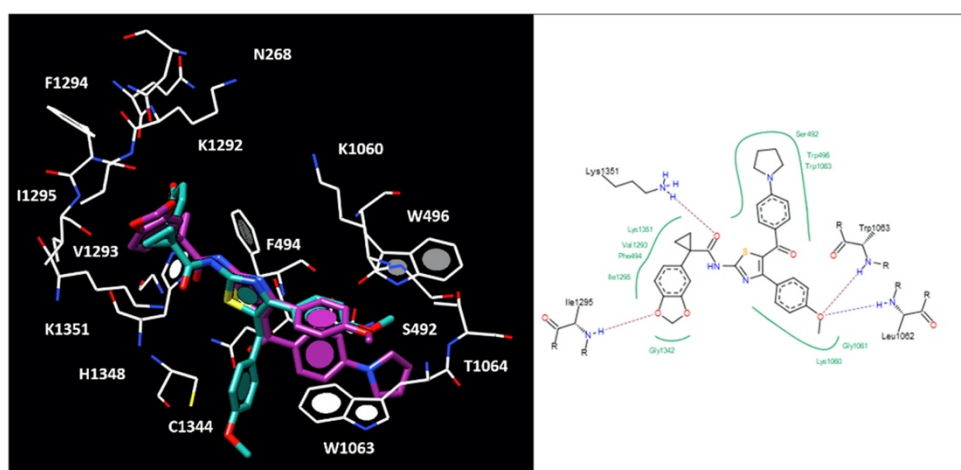


Figure 33. Docking positioning at the modelled F508del-CFTR of **9b** (C atom; light sea green) and **74** (C atom; purple).

In addition, it shown further H-bonds with L1062 by means of the methoxy group in **4**. It should be noticed that the bulkier substituent in **5** of **74** was projected towards the deeper crevice delimited by W496, K1060, and W1063, featuring π - π stacking.

Conclusion

In this work, I started from a molecule previously synthesized in my laboratory, named **2a** ($EC_{50} = 0,087 \mu\text{M}$), and active as a corrector against F508del-CFTR and I synthesized analogues taking into account each structural portion to understand which moieties were needed to maintain biological activity. Once determined the backbone of the molecule, I proceeded through the decoration of the two aromatic rings with different functional groups, obtaining two different libraries of molecules, in order to optimize the corrector activity and obtain more potent compounds.

The synthesis, characterization and purification of each molecule was followed by functional biological tests and in particular the most active compounds were subjected to further biochemical tests, obtaining the following information about my new compounds:

- they bind directly to the CFTR protein (confirmed by SPR as observed in silico through molecular docking studies)
- they increase the rescue of the trafficking defect of CFTR (confirmed by WB)
- they may be classified as type 1 correctors (having no additive effect /synergy with VX-809, type 1 corrector taken as reference, but showing such effect with VX-445, type 3 corrector as reference; docking studies confirm the binding of compounds with NBD1, too).

In this work in which a multidisciplinary approach was utilized, merging computational, synthetic and biological methods, it was possible to obtain more potent compounds than the progenitor compound **2a**, as compound **34** ($0.017 \mu\text{M}$), **42** ($0.07 \mu\text{M}$), **74** ($0.033 \mu\text{M}$), **81** ($EC_{50} = 0.037 \mu\text{M}$) and **70** ($0.064 \mu\text{M}$), exploitable also in combination with other molecules with different mechanism of action against the mutation F508del-CFTR. My approach highlighted the effectiveness of VX-809-like derivatives, exhibiting the thiazole main core, as endowed with F508del CFTR corrector ability

Experimental

Chemistry

Reagents and solvents were purchased from Sigma Aldrich, Alfa Aesar, VWR and Zentek used as received unless otherwise indicated.

Solvent removal was accomplished with a rotary evaporator at ca.10e50 Torr. The analytical instrument used was an Agilent 1260 HPLC. The analytical HPLC column was a Phenomenex C18 Luna (4.6 250 mm, 5 mm).

The preparative HPLC was Agilent 1260 Infinity preparative HPLC and the column used for preparative chromatography was a Phenomenex C18 Luna (21.2 x 250 mm, 15 mm). The analysis of the intermediates and the raw products was performed by liquid chromatography-electrospray mass spectrometry (HPLC-ESI-MS) using an Agilent 1100 series LC/MSD ion trap instrument.

HRMS experiments were performed using Q Exactive Orbitrap instrument by Thermo Scientific.

The nuclear magnetic resonance (NMR) spectrometer was a Varian Gemini 200 MHz.

The proton spectra were acquired at 200 MHz while carbon spectra were acquired at 50 MHz, at room temperature. Chemical shifts are reported in δ units (ppm) relative to TMS as an internal standard.

Coupling constants (J) are reported in Hertz (Hz).

All the raw powders obtained were purified with preparative HPLC using the following gradient: from 0 to 5 min at 20% eluent B, then from 5 min to 40 min to 100% eluent B, from 40 to 45 min at 100% eluent B. Eluent A was water with 0.1% formic acid (FOA) and eluent B was acetonitrile with 0.1% FOA. All analogues submitted for testing were judged to be of 95% or higher purity based on analytical HPLC/MS analysis.

Compound purity was determined by integrating peak areas of the liquid chromatogram, monitored at 254 nm.

2-amino-4-phenylthiazol-5-yl(phenyl)methanone (2)

2-bromo-1, 3- diphenylpropano-1, 3-dione 10 (300.3 mg, 1 mmol) and thiourea (77 mg, 1 mmol) in anhydrous EtOH (2 ml) was stirred at reflux until the reaction was judged complete (about 2 h) (HPLC-MS).

The solvent was concentrated under reduced pressure and the mixture partitioned between dichloromethane and H₂O. The organic layer was washed with brine and dried over anhydrous Na₂SO₄. The organic phases were concentrated in vacuum and the crude product, verified by HPLC and MS was purified with preparative HPLC to give the final product as white solid with purity higher than 95% ,as confirmed by HPLC-MS (211 mg, 75%).

¹H NMR (200 MHz, DMSO-d₆) δ 7.98 (s, 2H, NH₂); 7.42-7.35 (m, 2H, arom); 7.32-7.26 (m, 1H, arom); 7.23 (m, 2H, arom); 7.17 (m, 3H, arom); 7.11 (m, 2H, arom).

¹³C NMR (75 MHz, DMSO-d₆) δ 188.5, 170.9, 157.9, 138.5, 133.8, 131.7, 129.6, 128.5, 128.3, 127.7, 127.3, 122.5.

HRMS (ESI) calculated for C₁₆H₁₃N₂OS [M + H]⁺ 281.0743, found 281.0761.

N-(5-benzoyl-4-phenylthiazol-2-yl)-1-(4-chlorophenyl)cyclopropanecarboxamide (4)

A mixture of 1-(4-chlorophenyl)cyclopropanecarboxylic acid (21.0 mg, 0.1 mmol), HATU (38 mg, 0.1 mmol) and DIPEA (38 μL, 0.1 mmol) was dissolved in anhydrous N,N-DMF (1 mL) and stirred for few minutes. To the solution 2-amino-(4-phenylthiazol-5-yl) phenylmethanone 11 (28 mg, 0.1 mmol) was added. The reaction was stirred at 50 °C for 36 hours. After completeness, the mixture was purified by using preparative HPLC. The title compound was obtained as pale brown oil with purity of >95% confirmed by HPLC-MS (23 mg, 50%).

¹H NMR (200 MHz, DMSO-d₆): δ 11.98 (s, 1H, broad, NH); 7.88-6.79 (m, 13H, arom); 1.73-1.45 (m, 2H, cyclopr); 1.43-1.16 (m, 2H, cyclopr).

¹³C NMR (50 MHz, DMSO-d₆): δ 188.2, 171.8, 159.7, 153.1, 146.8, 146.3, 138.5, 131.6, 129.2, 128.7, 127.8, 124.2, 123.1, 121.3, 118.4, 113.0, 110.2, 107.8, 100.6, 30.2, 15.5.

HRMS (ESI) calculated for C₂₆H₂₀ClN₂O₂S : [M + H]⁺ 459.09339; found 459.09273

2-(benzo[d][1,3]dioxol-5-yl)-*N*-(5-benzoyl-4-phenylthiazol-2-yl)acetamide (5b)

2-(benzo[d][1,3]dioxol-5-yl)acetic acid (18 mg, 0.1 mmol), DIPEA (38 μL, 0.1 mmol) and HATU (42 mg, 0.1 mmol) were dissolved in anhydrous N,N-DMF (1 mL). Then, to the solution was added 2-amino-(4-phenylthiazol-5-yl) phenylmethanone 11 (28 mg, 0.1 mmol). The reaction was heated to 50 °C for 15 hours. The purification of the final product was performed by preparative HPLC to obtain the title compound as pale-yellow oil with purity of >95% as confirmed by HPLC-MS (20 mg, 45%).

¹H NMR (200 MHz, DMSO-d₆): δ 11.87 (s, 1H, broad, NH); 7.81-6.84 (m, 13H, arom); 6.00 (s, 2H, OCH₂O); 3.12 (s, 2H, ArCH₂C(O)).

¹³C NMR (50 MHz, DMSO-d₆): δ 188.4, 171.5, 159.7, 158.3, 152.7, 146.8, 146.3, 138.5, 131.8, 129.3, 128.7, 127.9, 124.3, 123.2, 121.3, 118.5, 113.1, 110.3, 107.8, 100.6, 41.7.

HRMS (ESI) calculated for C₂₅H₁₉N₂O₄S : [M + H]⁺ 443.10654; found 443.10554

3-(benzo[d][1,3]dioxol-5-yl)-*N*-(5-benzoyl-4-phenylthiazol-2-yl)-2-methylpropanamide (6b)

3-(benzo[d][1,3]dioxol-5-yl)-2-methylpropanoic acid (21 mg, 0.1 mmol) was dissolved in 1 mL of anhydrous N, N- DMF with HATU (38 mg, 0.1 mmol) and DIPEA (38 μ L, 0.1 mmol). The reaction was stirred at room temperature and after 5 min and 2-amino-(4-phenylthiazol-5-yl) phenylmethanone 11 (28 mg, 0.1 mmol) was added. The solution was heated to 50 °C until completeness (about 20 h). The purification of the final product was performed by preparative HPLC. The title compound, afforded as pale-yellow oil, had a purity of >95% as confirmed by HPLC-MS (21 mg, 45%).

^1H NMR (200 MHz, DMSO-d₆): δ 11.98 (s, 1H, broad, NH); 7.82-6.79 (m, 13H, arom); 6.01 (s, 2H, OCH₂O); 2.96 (m, 1H, CH); 2.78 (d, J = 6.2 Hz, 2H, ArCH₂); 1.18 (d, 3H, J = 6.8 Hz, CH₃).

^{13}C NMR (50 MHz, DMSO-d₆): δ 187.6, 171.3, 159.7, 159.1, 153.1, 146.8, 146.3, 138.4, 131.8, 129.2, 128.7, 127.9, 124.2, 123.2, 121.2, 118.4, 112.8, 110.2, 107.8, 100.6, 40.4, 36.8, 16.1.

HRMS (ESI) calculated for C₂₇H₂₃N₂O₄S : [M + H]⁺ 471.13784; found 471.13753

(Z)-3-(benzo[d][1,3]dioxol-5-yl)-N-(5-benzoyl-4-phenylthiazol-2-yl)acrylamide (7b)

((Z)-3-(benzo[d][1,3]dioxol-5-yl)acrylic acid (19 mg, 0.1 mmol), HATU (38 mg, 0.1 mmol) and DIPEA (38 μ L, 0.1 mmol) were dissolved in anhydrous N,N- DMF (1 mL) and stirred for 5 min. Then, 2-amino-(4-phenylthiazol-5-yl) phenylmethanone 11 (28 mg, 0.1 mmol) was added. The mixture was heated to 50 °C overnight and then purified by preparative HPLC. The final product was afforded as a pale brown oil with purity of >95% as confirmed by HPLC-MS (18 mg, 40%).

^1H NMR (200 MHz, DMSO-d₆): δ 12.02 (s, 1H, broad, NH); 7.86-6.75 (m, 13H, arom); 6.34 (d, J = 8.6 Hz, H, CH=); 6.22 (d, J = 8.6 Hz, H, CH=); 6.05 (s, 2H, OCH₂O).

^{13}C NMR (50 MHz, DMSO-d₆): δ 188.1, 172.1, 159.7, 158.0, 153.2, 146.8, 146.3, 144.3, 138.4, 131.8, 129.3, 128.7, 127.9, 127.7, 124.1, 123.2, 121.2, 118.5, 112.8, 110.2, 107.8, 100.6.

HRMS (ESI) calculated for C₂₆H₁₈N₂O₄S : [M + H]⁺ 454.09872; found 454.09772

2-(benzo[d][1,3]dioxol-5-yloxy)-N-(5-benzoyl-4-phenylthiazol-2-yl)-2-methylpropanamide (10)

Benzo[d][1,3]dioxol-5-ol 15 (138.0 mg, 1 mmol) and K₂CO₃ (414 mg, 3 mmol) were dissolved in N,N- DMF (1 mL). The solution was stirred for 10 min at room temperature and then ethyl 2-bromo-2-methylpropanoate (176 μ l, 1.2 mmol) was added. The resulting reaction mixture was stirred at room temperature for 16 h. The residue was taken up in EtOAc and washed with H₂O and brine, dried over Na₂SO₄, and concentrated under reduced pressure to afford the product, ethyl 2-(benzo[d][1,3]dioxol-5-yloxy)-2-methylpropanoate, as a yellow oil (176.0 mg, 70%).

Ethyl 2-(benzo[d][1,3]dioxol-5-yloxy)-2-methylpropanoate was dissolved in ACN (2 mL) and KOH 6N was added dropwise (1 mL). The reaction was stirred at T= 60 °C until complete hydrolysis (about 3h).

The mixture was then cooled to room temperature and concentrated under reduced pressure. The residue was taken up in H₂O, acidified with 1N HCl and extracted with EtOAc / NaHCO₃ 1N (3 x 3 mL). The combined organic layers were washed with brine, dried over Na₂SO₄, and concentrated under reduced pressure to afford 2-(benzo[d][1,3]dioxol-5-yloxy)-2-methylpropanoic acid 16 (136.0 mg, 61%).

To a solution of 2-(benzo[d][1,3]dioxol-5-yloxy)-2-methylpropanoic acid (33.6 mg, 0.15 mmol) in N,N-DMF, HATU (51.3 mg, 0.15 mmol) and DIPEA (57.7 μL, 0.15 mmol) were added and stirred for 5 minutes at room temperature. Then, 2-amino-(4-phenylthiazol-5-yl) phenylmethanone 11 (42 mg, 0.15 mmol) was added and the resulting mixture stirred to T = 50°C for 24 h.

The final product was purified by preparative HPLC, and the peak of interest was concentrated under vacuum to obtain 2-(benzo[d][1,3]dioxol-5-yloxy)-N-(5-benzoyl-4-phenylthiazol-2-yl)-2-methylpropanamide as a yellow powder, with purity of >95% as determined by HPLC-MS (15.9 mg, 22%).

¹H NMR (200 MHz, DMSO-d₆): δ 11.89 (s, 1H, broad, NH); 7.87-6.73 (m, 17H, arom); 6.02 (s, 2H, OCH₂O); 1.22 (s, 6H, 2CH₃).

¹³C NMR (50 MHz, DMSO-d₆): δ 186.8, 171.9, 159.7, 159.1, 152.8, 146.8, 146.3, 143.2, 138.5, 135.6, 132.6, 131.8, 130.6, 129.2, 128.7, 127.9, 127.3, 126.7, 125.7, 124.2, 123.2, 121.2, 118.6, 112.9, 110.2, 107.8, 100.6, 58.2, 22.5.

HRMS (ESI) calculated for C₂₇H₂₃N₂O₅S : [M + H]⁺ 487.13276; found 487.13252

1-(benzo[d][1,3]dioxol-5-yl)-N-((5-benzoyl-4-phenylthiazol-2-yl)methyl)cyclopropane-1-carboxamide (16)

N-benzyloxycarbonyl glycinamide (208.2 mg, 1 mmol) was solved in toluene and stirred for few minutes; then Lawesson reagent was added portionwise (323.5 mg, 0.8 mmol). The reaction was stirred at 110°C for 4 hours. Then toluene was removed in vacuum, and ethyl acetate and NaOH (aq) 1% were added to the mixture; organic phase and aqueous phase were separated and the aqueous phase was extracted with ethyl acetate for 3 times (3 x 5 mL). The organic phases were combined, dried over Na₂SO₄, and concentrated under reduced pressure to afford benzyl (2-amino-2-thioethyl)carbamate (180 mg, 80%).

Benzyl (2-amino-2-thioethyl)carbamate (112 mg, 0.5 mmol) was dissolved in absolute EtOH (2mL) and a solution of 2-bromo-1,3-diphenylpropane-1,3-dione (151 mg, 0.5 mmol) solved in EtOH

was added dropwise. The reaction is maintained at reflux for 2 h. Then, the solvent was removed and the mixture was taken up in EtOAc and washed with H₂O (3 x 5 mL), dried over Na₂SO₄, concentrated under reduced pressure and lyophilized to obtain benzyl ((5-benzoyl-4-phenylthiazol-2-yl)methyl)carbamate (175.6 mg, 82%).

Benzyl ((5-benzoyl-4-phenylthiazol-2-yl)methyl)carbamate (175.6 mg, 0.4 mmol) was dissolved in a solution of HBr / Acetic acid 33% (4mL) and stirred at 70°C for 24 - 48 h. The mixture was taken up in ethyl acetate and washed with an aqueous saturated solution of bicarbonate (3 x 5 mL). The organic phase was discarded, then the aqueous layer was extracted with ethyl acetate for 2 times. This organic phase was dried over Na₂SO₄, concentrated under reduced pressure and lyophilized to give (2-(aminomethyl)-4-phenylthiazol-5-yl)(phenyl)methanone (25mg, 21%).

Benzo[1,3]dioxol-5-yl-cyclopropanecarboxylic acid (21.0 mg, 0.1 mmol), HATU (34.2 mg, 0.09 mmol) and DIPEA (38 µL, 0.1 mmol) were resuspended in anhydrous N,N- DMF (1 mL) at room temperature. After 5 min a solution of (2-(aminomethyl)-4-phenylthiazol-5-yl)(phenyl)methanone (25 mg, 0.09 mg) in N,N- DMF was added, and the resulting mixture was heated to 50 °C for 24 hours. Preparative HPLC was used to purify the final product. The peak of interest was concentrated to obtain a powder with a purity higher than >95%, as confirmed by HPLC-MS (10.0 mg, 23%).

1-(Benzo[d][1,3]dioxol-5-yl)-N-(5-(4-methylbenzoyl) thiazol-2-yl)cyclopropanecarboxamide (19d)

N,N-Dimethyl formamide dimethyl acetal (1036 mL, 7.8 mmol) was added to a suspension of thiourea (198 mg, 2.6 mmol) in DCM (2 mL). The mixture was heated at reflux for 4 h. The solvent was removed and the residue was crystallized from diethyl ether to obtain (1E, 1' E)-N',N'' -thiocarbonylbis (N,N-dimethylformimidamide) (400 mg, 83%). ESI-MS: m/z 187.1 (M þ H) þ.

(1E, 1'E)-N',N'' -Thiocarbonylbis-N,N-dimethylformimidamide (100 mg, 0.53 mmol) was suspended in THF (1 mL) and 2-bromo- methylacetophenone (113 mg, 0.53 mmol) was added. The mixture was stirred at room temperature for 15 min and then TEA (147 mL, 1.16 mmol) was added and the mixture was heated at reflux for 18 h. The mixture was concentrated under vacuum and after extraction with EtOAc (3 x 3 mL), washed with H₂O (3 x 2 mL). The organic phase was dried over Na₂SO₄, concentrated under reduced pressure to obtain (Z)-N'-(5-(4-methylbenzoyl) thiazol-2-yl)-N,N- dimethylformimidamide (108 mg, 70%). ESI-MS: m/z 273.1 (M þ H) þ.

A 33% (wt./wt.) aqueous methylamine (400 mL) was added to a solution of (Z)-N'-(5-(4-methylbenzoyl)thiazol-2-yl)-N,N-dimethylformimidamide (101 mg, 0,37 mmol) in THF (1 mL) and the mixture was stirred for 24 h at room temperature. The mixture was concentrated under vacuum and after extraction with EtOAc (3 x 3 mL), washed with H₂O (3 x 2 mL). The organic phase was dried over Na₂SO₄, concentrated under reduced pressure to obtain a pale, yellow oil. Crystallization

in acetonitrile furnishes (2-aminothiazol-5-yl) (p-tolyl)methanone (36 mg, 45%). ESI-MS: m/z 219.1 [M⁺H]⁺.

Benzo [1,3]dioxol-5-yl-cyclopropanecarboxylic acid (33 mg, 0.16 mmol) was resuspended in anhydrous N,N-DMF (1 mL), HATU (61 mg, 0.16 mmol) and DIPEA (56 mL, 0.16 mmol) were added. After 5 min, (2-aminothiazol-5-yl) (p-tolyl) methanone (35 mg, 0.16 mmol) in anhydrous N,N-DMF (500 mL) was added. The reaction was kept at T = 50° C until completeness (about 24 h). The mixture was concentrated under vacuum and after extraction with EtOAc (3 x 3 mL), washed with H₂O (3 x 2 mL). The organic phase was dried over Na₂SO₄, concentrated under reduced pressure and purified by preparative HPLC. The peak of interest was concentrated to obtain the title compound as pale, yellow solid with purity of >95% as determined by HPLC-MS (32.4 mg, 50%).

¹H NMR (200 MHz, DMSO-d₆): δ 11.87 (s, broad, 1H, NH); 8.05 (s, 1H, arom); 7.81e6.78 (m, 7H, arom); 6.04 (s, 2H OCH₂O); 2.32 (s, 3H, CH₃); 1.81e1.42 (m, 2H, CH₂, cyclopr); 1.41e1.00 (m, 2H, CH₂, cyclopr).

¹³C NMR (50 MHz, DMSO-d₆) δ 186.2, 173.6, 146.8, 146.3, 137.0, 133.1, 129.6, 129.1, 121.3, 110.8, 107.2, 101.2, 30.3, 24.6, 15.5.

HRMS (ESI) calculated for C₂₂H₁₉N₂O₄S: [M⁺H]⁺ 407.10654; found 407.10608.

1-(Benzo[d][1,3]dioxol-5-yl)-N-(5-(4-methoxybenzoyl)thiazol-2-yl)cyclopropanecarboxamide (20d)

(1E, 1'E)-N',N''-Thiocarbonylbis-N,N-dimethylformimidamide (100 mg, 0.53 mmol) was suspended in DCM (1 mL) and 2-bromo-4-methoxyacetophenone (121 mg, 0.53 mmol) was added. The mixture was stirred at room temperature for 15 min and then TEA (147 mL, 1.16 mmol) was added. The mixture was heated at reflux for about 20 h. At the end of the reaction the solution was concentrated under vacuum and after extraction with EtOAc (3 x 3 mL), washed with H₂O (3 x 2 mL). The organic phase was dried over Na₂SO₄, concentrated under reduced pressure to obtain (Z)-N'-(5-(4-methoxybenzoyl)thiazol-2-yl)-N,N-dimethylformimidamide (108 mg, 70%).

ESI-MS: m/z 290.1 [M⁺H]⁺.

A 33% (wt./wt.) aqueous methylamine (600 mL) was added to a solution of (Z)-N'-(5-(4-methoxybenzoyl)thiazol-2-yl)-N,N-dimethylformimidamide (108 mg, 0.37 mmol) in THF (1 mL) and the mixture was stirred for 24 h at room temperature. The solution was then concentrated under vacuum and after extraction with EtOAc (3 x 3 mL), washed with H₂O (3 x 2 mL). The organic phase was dried over Na₂SO₄, concentrated under reduced pressure to obtain a yellow oil. Crystallization in acetonitrile furnishes (2-aminothiazol-5-yl) (4-methoxyphenyl)methanone (46 mg, 53%). MS ESI-MS: m/z 235.1 [M⁺H]⁺.

Benzo [1,3]dioxol-5-yl-cyclopropanecarboxylic acid (39 mg, 0.19 mmol) was resuspended in anhydrous N,N- DMF (1 mL), HATU (72 mg, 0.19 mmol) and DIPEA (66 mL, 0.19 mmol) were added. After 5 min, (2-aminothiazol-5-yl) (4-methoxyphenyl)methanone (45 mg, 0.19 mmol) in anhydrous N,N- DMF (500 mL) was added. The reaction was kept at T= 50° C until completeness (about 36 h).

The mixture was concentrated under vacuum and after extraction with EtOAc (3 x 3 mL), washed with H₂O (3 x 2 mL). The organic phase was dried over, concentrated under reduced pressure and purified by preparative HPLC. The peak of interest was concentrated to obtain the title compound as brown solid with purity of >95% as determined by HPLC-MS (26.6 mg, 33%).

¹H NMR (200 MHz, DMSO-d₆): d 11.87 (s, broad, 1H, NH); 8.08 (s, 1H, arom); 7.79e6.81 (m, 7H, arom); 6.04 (s, 2H OCH₂O); 3.89 (s, 3H, CH₃); 1.78e1.41 (m, 2H, CH₂, cyclopr); 1.40e1.03 (m, 2H, CH₂, cyclopr).

¹³C NMR (50 MHz, DMSO-d₆) d 182.7, 171.9, 146.9, 146.3, 137.1, 133.0, 129.7, 128.8, 121.4, 110.8, 107.2, 101.2, 55.9, 30.3, 15.5.

HRMS (ESI) calculated for C₂₂H₁₉N₂O₅S: [M⁺ H]⁺ 423.10146; found 423.10098.

N-(5-Acetyl-4-phenylthiazol-2-yl)-1-(benzo[d][1,3]dioxol-5-yl)cyclopropanecarboxamide (29)

A mixture of (4-methoxyphenyl) methanamine (535 mL, 4 mmol) and 4-(methoxy)benzaldehyde (595 mL, 4.8 mmol) in methanol (2 mL) was heated to reflux for 3 h, then cooled to T= 0° C, NaBH₄ (228 mg, 6 mmol) was added portion wise to the reaction and the resulting mixture was stirred at room temperature for about 10 h. Solvent was removed under reduced pressure and the residue was partitioned between ethyl acetate (EtOAc) and H₂O. The combined organic layers were washed with H₂O, and then dried over anhydrous Na₂SO₄. After filtration, solvent was removed in vacuum to afford bis [4-methoxyphenyl]methylamine (962 mg, 94%) as a colorless oil which was used in the next step without further purification. ESI-MS: m/z 258.0 [M⁺H]⁺.

To a solution of benzoylisothiocyanate (140 mL, 1 mmol) in acetone (1 mL) cooled at T = 0° C, bis [4-methoxyphenyl]methyl- amine (257 mg, 1 mmol) in acetone (1 mL) was added at this temperature and stirred for an additional 1 h.

The mixture was concentrated under reduced pressure, to afford N-(bis(4-methoxybenzyl) carbamothioyl)benzamide (398 mg, 95%) as yellow sticky oil which was used in the next step without further purification. ESI-MS: m/z 421.0 [M⁺H]⁺.

A solution of 1-bromopropan-2-one (68.0 mg, 0.5 mmol) and N-(bis(4-methoxybenzyl)carbamothioyl)- benzamide (210 mg, 0.5 mmol) in N, N- DMF (3 mL) was stirred at T = 85° C for 3 h. After cooling to room temperature, the mixture was partitioned between EtOAc

and H₂O. The organic layer was washed with brine and dried over anhydrous Na₂SO₄. After filtration, solvent was removed in vacuum and the residue was stirred in trifluoroacetic acid (TFA) (4 mL) at T= 80° C for 24 - 36 h until complete deprotection. Most of TFA was removed under reduced pressure. The residue was then neutralized with NaHCO₃ 1 N, and then extracted with EtOAc for 3 times. The combined organic layers were washed with brine and dried over anhydrous Na₂SO₄. After filtration, the solution was concentrated and further crystallized in acetonitrile to afford 1-(2-amino-4-phenylthiazol-5-yl)ethan-1-one (77 mg, 71%) as a brown solid. ESI-MS: m/z 328.1 [M⁺H]⁺.

Benzo [1,3]dioxol-5-yl-cyclopropanecarboxylic acid (20.6 mg, 0.1 mmol) was resuspended in anhydrous N,N - DMF (1 mL); HATU (38 mg, 0.1 mmol) and DIPEA (35 mL, 0.2 mmol) were added. The reaction was vigorously stirred for 5 min and (32.7 mg, 0.1 mmol) in anhydrous N,N- DMF (500 mL) 1-(2-amino-4-phenylthiazol-5-yl)ethan-1-one (22.0 mg, 0,1 mmol) was added. The reaction was kept at T = 50° C until completeness (18 - 24 h) and then purified by preparative HPLC. The peak of interest was concentrated to obtain the title compound as yellow solid with purity of >95% as determined by HPLC-MS (9.6 mg, 24%).

¹H NMR (200 MHz, DMSO-d₆): δ 11.94 (s, broad, 1H, NH); 7.64e6.59 (m, 8H, arom); 6.02 (s, 2H OCH₂O); 2.62 (s, 3H, CH₃); 1.74e1.43 (m, 2H, CH₂, cyclopr); 1.40e1.16 (m, 2H, CH₂, cyclopr).

¹³C NMR (50 MHz, DMSO-d₆) δ 192.5, 180.4, 164.2, 151.0, 146.8, 146.3, 137.0, 131.9, 129.2, 128.7, 127.5, 116.0, 110.2, 107.6, 101.2, 30.3, 29.7, 15.6.

HRMS (ESI) calculated for C₂₂H₁₉N₂O₄S: [M⁺H]⁺ 407.10655; found 407.10611.

1-(Benzo[d][1,3]dioxol-5-yl)-N-(5-nicotinoyl-4-phenylthiazol-2-yl)cyclopropanecarboxamide (30)

Compound **30** (16 mg, 34%) was prepared from (2-amino-4-phenylthiazol-5-yl) (pyridin-3-yl)methanone (28 mg, 0.1 mmol) and benzo [1,3]dioxol-5-yl-cyclopropanecarboxylic acid (20.6 mg, 0.1 mmol) in the same manner as described for compound **29** until completeness (24 h) as brown oil.

¹H NMR (200 MHz, DMSO-d₆): δ 12.04 (s, broad, 1H, NH); 8.62e8.22 (m, 3H, arom); 7.93e6.76 (m, 9H, arom); 6.06 (s, 2H OCH₂O); 1.73e1.41 (m, 2H, CH₂, cyclopr); 1.37e1.02 (m, 2H, CH₂, cyclopr).

¹³C NMR (50 MHz, DMSO-d₆) δ 178.8, 171.5, 164.3, 155.0, 151.7, 146.9, 146.3, 141.8, 138.3, 136.9, 133.2, 129.2, 128.7, 127.5, 124.4, 116.0, 111.8, 107.8, 101.2, 30.3, 15.5.

HRMS (ESI) calculated for C₂₆H₂₀N₃O₄S: [M⁺H]⁺ 470.11745; found 470.11708.

12_ABCD_24ABC #454-484 RT: 7.95-8.48 AV: 31 SB: 180 4.20-7.34 NL: 2.78E8
T: FTMS + p ESI Full ms [250.0000-700.0000]

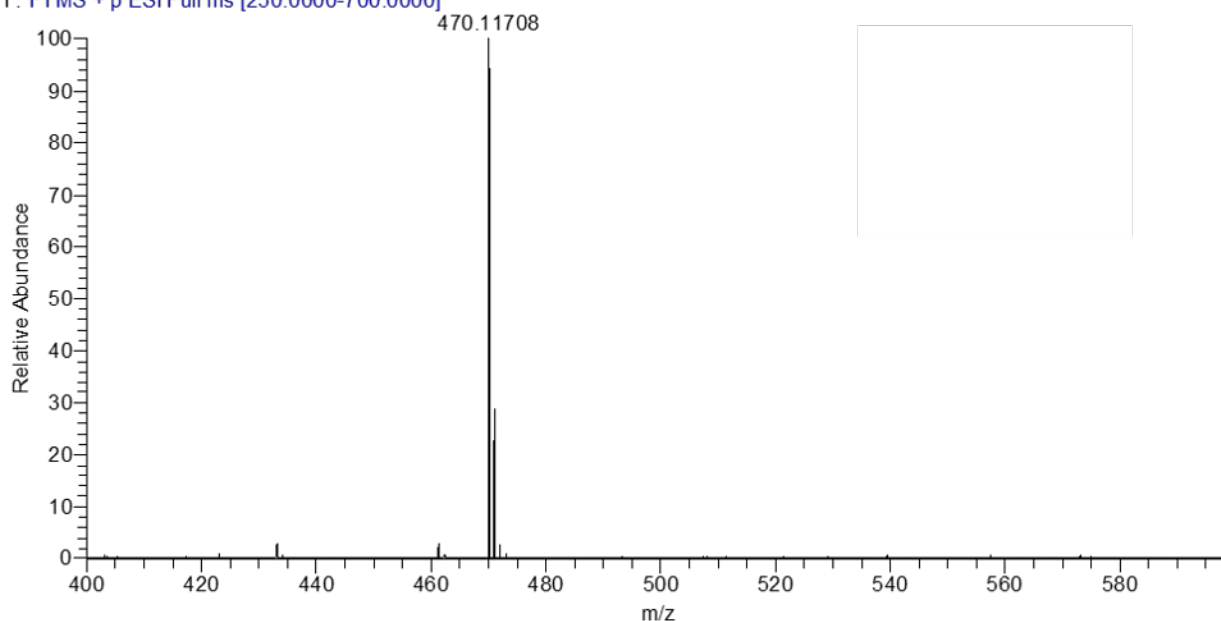


Figure 34. HRMS spectra of compound **30**

1-(Benzo[d][1,3]dioxol-5-yl)-N-(5-(morpholine-4-carbonyl)-4-phenylthiazol-2-yl)cyclopropanecarboxamide (31)

Compound **31** (12.8 mg, 27%) was prepared from (2-amino-4-phenylthiazol-5-yl)(morpholino)methanone (29 mg, 0.1 mmol) and benzo [1,3]dioxol-5-yl-cyclopropanecarboxylic acid (20.6 mg, 0.1 mmol) in the same manner as described for compound **29** until completeness (24 h) as yellow solid.

¹H NMR (200 MHz, DMSO-d₆): δ 11.91 (s, broad, 1H, NH); 7.72e6.58 (m, 8H, arom); 6.03 (s, 2H OCH₂O); 3.72 (t, J 1/4 6.8, 4H, OCH₂O); 2.67 (t, J 1/4 6.8, 4H, NCH₂); 1.78e1.43 (m, 2H, CH₂, cyclopr); 1.41e1.06 (m, 2H, CH₂, cyclopr).

¹³C NMR (50 MHz, DMSO-d₆) δ 176.3, 169.8, 162.5, 151.2, 146.9, 146.4, 137.0, 131.1, 129.2, 128.7, 127.5, 116.0, 110.8, 10.2, 101.2, 56.2, 42.8, 30.3, 15.6.

HRMS (ESI) calculated for C₂₅H₂₄N₃O₅S: [M + H]⁺ 478.14366; found 478.14327.

1-(Benzo[d][1,3]dioxol-5-yl)-N-(5-(4-methoxybenzoyl)-4-phenylthiazol-2-yl)cyclopropanecarboxamide (32)

Compound **32** (18.9 mg, 38%) was prepared from (2-amino-4-phenylthiazol-5-yl)(4-methoxyphenyl)methanone (31 mg, 0.1 mmol) and benzo [1,3]dioxol-5-yl-cyclopropanecarboxylic acid (20.6 mg, 0.1 mmol) in the same manner as described for compound **29** as brown solid.

¹H NMR (200 MHz, DMSO-d₆): δ 11.80 (s, broad, 1H, NH), 7.78e6.92 (m, 12H, arom), 6.04 (s, 2H OCH₂O), 3.76 (s, 3H, OCH₃), 1.63e1.42 (m, 2H, CH₂, cyclopr), 1.41e1.16 (m, 2H, CH₂, cyclopr).

^{13}C NMR (50 MHz, DMSO- d_6): d 187.2, 162.5, 159.0, 154.8, 146.9, 146.3, 131.8, 131.2, 129.7, 128.8, 128.1, 127.5, 123.2, 113.1, 110.2, 107.8, 100.6, 97.2, 55.1, 30.2, 15.4.

HRMS (ESI) calculated for $\text{C}_{28}\text{H}_{23}\text{N}_2\text{O}_5\text{S}$: $[\text{M} + \text{H}]^+$ 499.13276; found 499.13224.

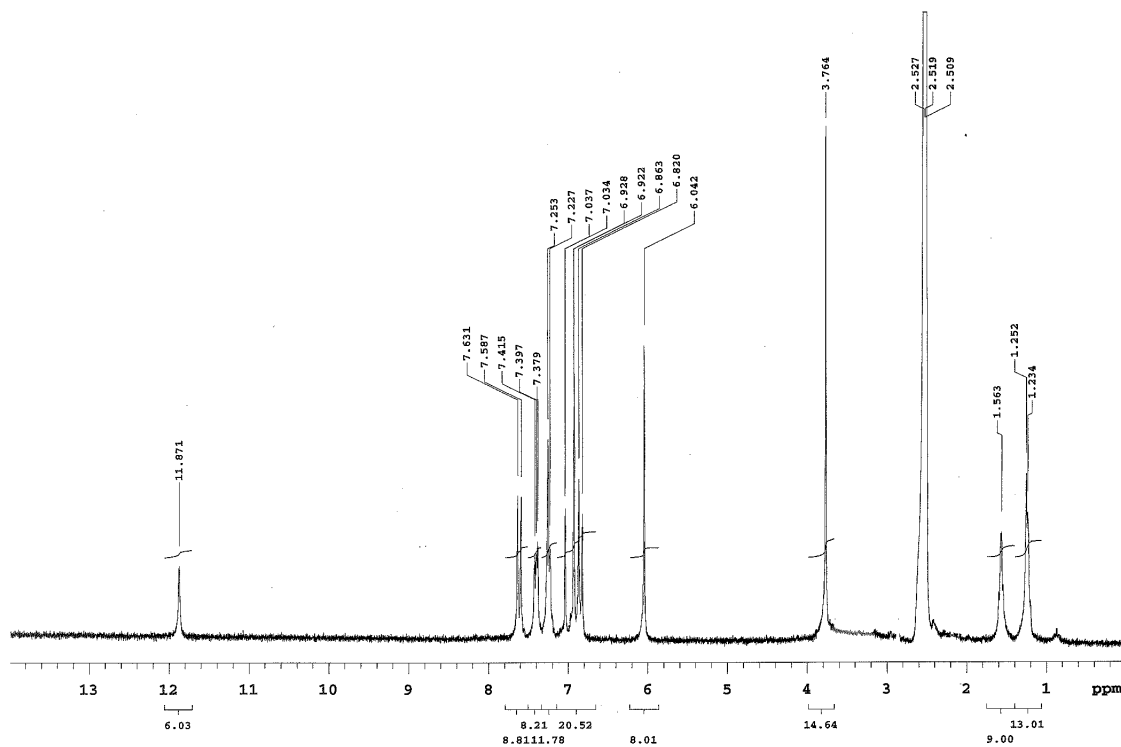


Figure 35. ^1H NMR spectra of compound 32

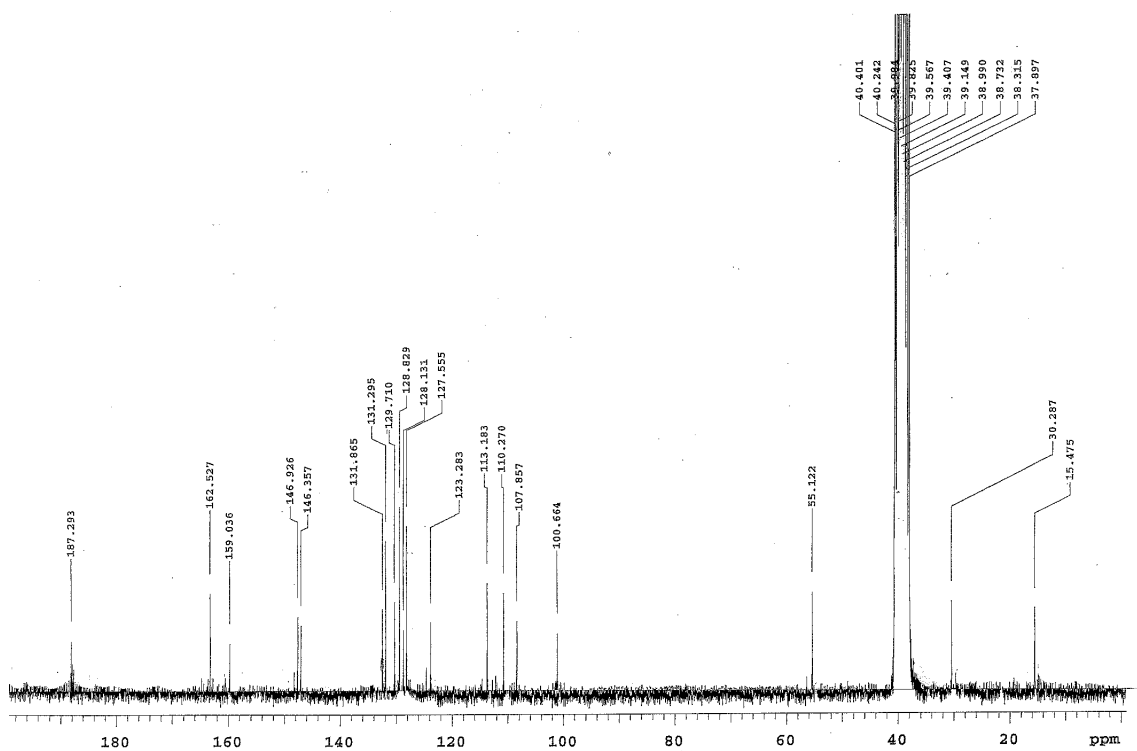


Figure 36. ^{13}C NMR spectra of compound **32**

1-(Benzo[d][1,3]dioxol-6-yl)-N-(5-(4-(methylthio)benzoyl)-4-phenylthiazol-2-yl)cyclopropanecarboxamide (33)

Compound **33** (12.7 mg, 25%) was prepared from (2-amino-4-phenylthiazol-5-yl) (4-(methylthio)phenyl) methanone (32.7 mg, 0.1 mmol) and benzo [1,3]dioxol-5-yl-cyclopropanecarboxylic acid (20.6 mg, 0.1 mmol) in the same manner as described for compound **29** as yellow solid.

^1H NMR (200 MHz, DMSO- d_6): δ 11.89 (s, broad, 1H, NH); 7.71e6.57 (m, 12H, arom); 6.02 (s, 2H OCH₂O); 2.37 (s, 3H, SCH₃); 1.68e1.42 (m, 2H, CH₂, cyclopr); 1.40e1.09 (m, 2H, CH₂, cyclopr).

^{13}C NMR (50 MHz, DMSO- d_6): δ 187.3, 165.7, 158.6, 153.9, 146.9, 146.3, 131.8, 130.9, 129.6, 128.9, 128.1, 127.4, 123.1, 114.5, 110.2, 107.8, 100.6, 98.7, 51.8, 30.3, 15.5.

HRMS (ESI) calculated for C₂₈H₂₃N₂O₄S₂: [M + H]⁺ 515.10992; found 515.10971.

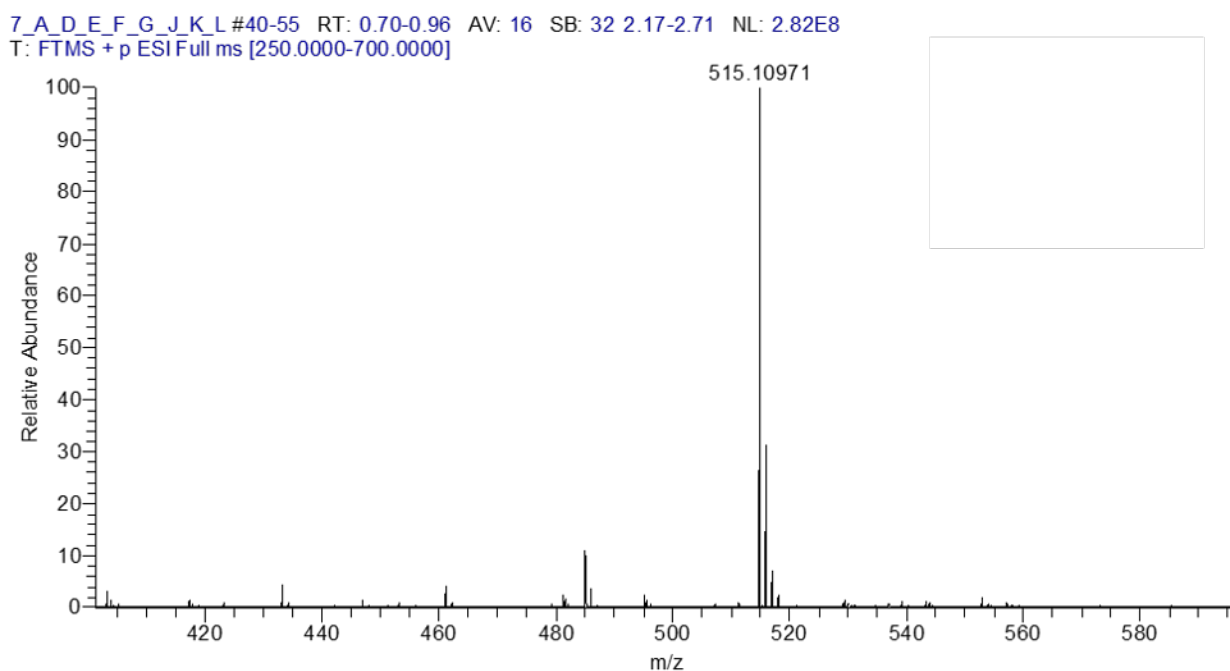


Figure 37. HRMS spectra of compound **33**

1-(Benzo[d][1,3]dioxol-5-yl)-N-(4-phenyl-5-(4-propoxybenzoyl)thiazol-2-yl)cyclopropanecarboxamide (34)

Compound **34** (9.6 mg, 18%) was prepared from (2-amino-4-phenylthiazol-5-yl) (4-propoxyphenyl) methanone (34 mg, 0.1 mmol) and benzo [1,3]dioxol-5-yl-cyclopropanecarboxylic acid (20.6 mg, 0.1 mmol) in the same manner as described for compound **29** as pale, yellow solid.

¹H NMR (200 MHz, DMSO-d₆): d 11.94 (s, broad, 1H, NH); 7.65e6.58 (m, 12H, arom); 6.01 (s, 2H OCH₂O); 3.93 (t, 2H, J 1/4 7.0, OCH₂CH₂); 1.85e1.44 (m, 4H, 2H, OCH₂CH₂, p 2H, CH₂, cyclopr); 1.41e1.09 (m, 2H, CH₂, cyclopr); 0.96 (t, 3H, J 1/4 7.0, CH₂CH₃).

¹³C NMR (50 MHz, DMSO-d₆): d 178.1, 164.7, 156.5, 153.8, 146.9, 146.4, 132.2, 131.3, 129.6, 128.9, 128.2, 127.5, 123.1, 113.6, 110.2, 107.8, 100.6, 99.2, 57.8, 30.3, 22.7, 15.4.

HRMS (ESI) calculated for C₃₀H₂₇N₂O₅S: [M p H]⁺ 527.16406; found 527.16388.

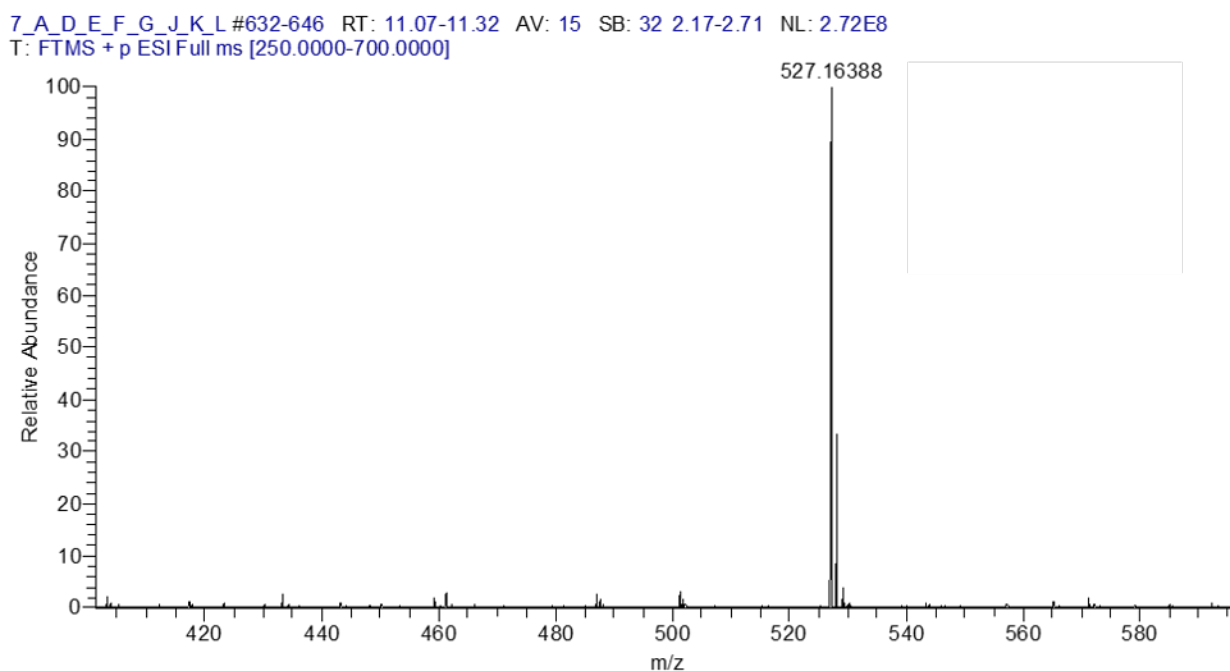


Figure 38. HRMS spectra of compound **34**

1-(Benzo[d][1,3]dioxol-5-yl)-N-(4-phenyl-5-(4-(trifluoromethoxy)benzoyl)thiazol-2-yl)cyclopropanecarboxamide (35)

Compound **35** (12.5 mg, 23%) was prepared from (2-amino-4-phenylthiazol-5-yl) (4-(trifluoromethoxy)phenyl)methanone (36 mg, 0.1 mmol) and benzo [1,3]dioxol-5-yl-cyclopropanecarboxylic acid (20.6 mg, 0.1 mmol) in the same manner as described for compound **29** as pale brown solid.

¹H NMR (200 MHz, DMSO-d₆): d 12.03 (s, broad, 1H, NH), 7.76e6.79 (m, 12H, arom), 6.05 (s, 2H OCH₂O), 1.65e1.43 (m, 2H, CH₂, cyclopr), 1.41e1.04 (m, 2H, CH₂, cyclopr).

¹³C NMR (50 MHz, DMSO-d₆): d 187.6, 172.5, 160.4, 154.9, 146.9, 146.3, 136.3, 133.6, 131.7, 130.8, 129.2, 128.2, 127.2, 124.4, 123.2, 119.8, 110.2, 107.8, 100.6, 30.3, 15.5.

HRMS (ESI) calculated for C₂₈H₂₀F₃N₂O₅S: [M p H]⁺ 553.10449; found 553.10404.

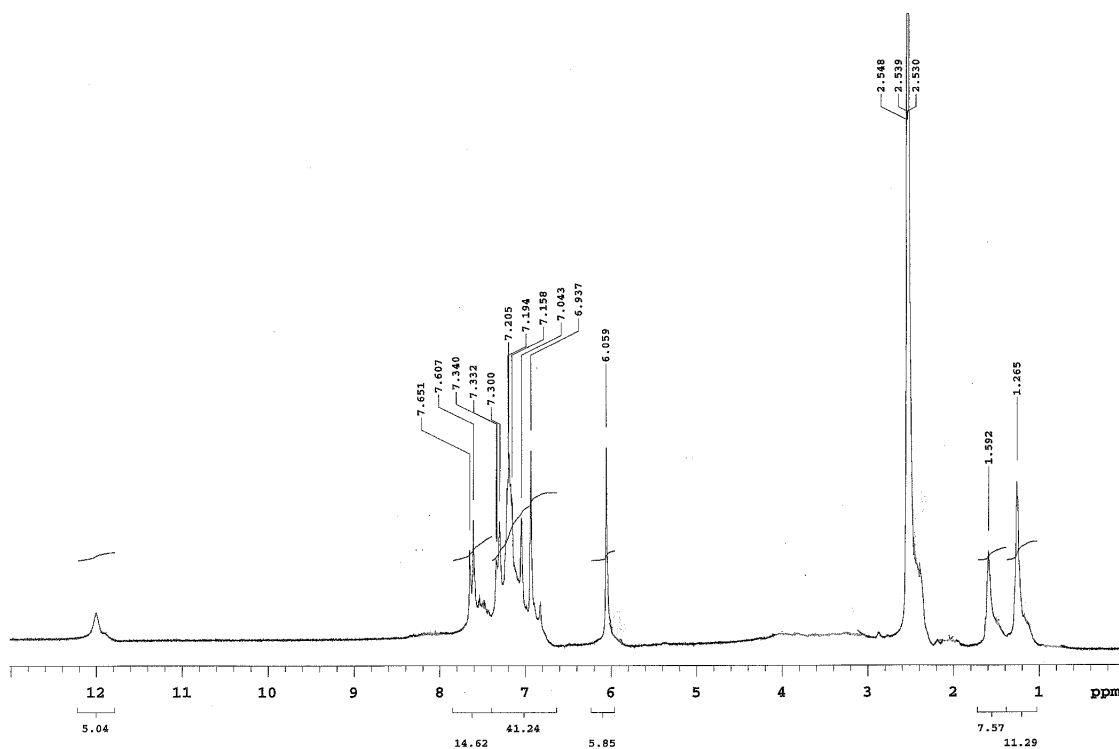


Figure 39. ^1H NMR spectra of compound 35

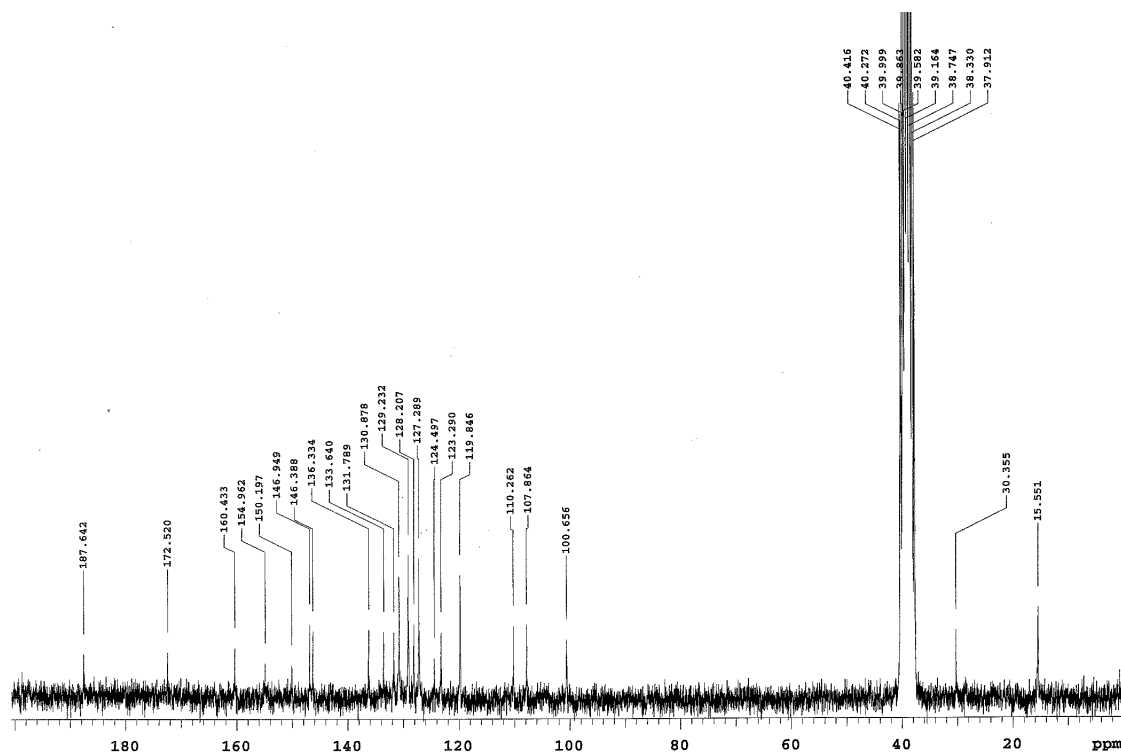


Figure 40. ^{13}C NMR spectra of compound 35

4-(2-(1-(Benzo[d][1,3]dioxol-5-yl) cyclopropanecarboxamido)-4-phenylthiazole-5-carbonyl) benzoic acid (36)

Compound **36** (9.9 mg, 19%) was prepared from 4-(2-amino-4- phenylthiazole-5-carbonyl)benzoic acid (32.4 mg, 0.1 mmol) and benzo [1,3]dioxol-5-yl-cyclopropanecarboxylic acid (20.6 mg, 0.1 mmol) in the same manner as described for compound **29** as brown solid.

¹H NMR (200 MHz, DMSO-d₆): δ 13.18 (s, 1H, broad, COOH); 11.99 (s, broad, 1H, NH); 8.02e6.73 (m, 12H, arom); 6.03 (s, 2H OCH₂O); 1.68e1.43 (m, 2H, CH₂, cyclopr); 1.40e1.05 (m, 2H, CH₂, cyclopr).

¹³C NMR (50 MHz, DMSO-d₆): δ 187.7, 171.6, 168.8, 154.6, 146.9, 146.3, 137.0, 131.3, 130.2, 129.4, 128.7, 128.2, 127.5, 123.1, 113.1, 110.2, 107.8, 100.6, 30.3, 15.5.

HRMS (ESI) calculated for C₂₈H₂₁N₂O₆S: [M + H]⁺ 513.11202; found 513.11179.

4-(2-(1-(Benzo[d] [1,3]dioxol-5-yl) cyclopropanecarboxamido)-4-phenylthiazole-5-carbonyl)-N-methylbenzamide (37)

Compound **37** (12 mg, 11%) was prepared from 4-(2-amino-4- phenylthiazole-5-carbonyl)-N-methylbenzamide (68 mg, 0.2 mmol) and benzo [1,3]dioxol-5-yl-cyclopropanecarboxylic acid (41 mg, 0.20 mmol) in the same manner as described for compound **29** as brown oil.

¹H NMR (200 MHz, DMSO-d₆): δ 12.01 (s, 1H, broad, NH); 11.75 (s, broad, 1H, NH); 7.71e6.63 (m, 12H, arom); 6.03 (s, 2H OCH₂O); 2.43 (s, 3H, CH₃N); 1.72e1.46 (m, 2H, CH₂, cyclopr); 1.42e1.11 (m, 2H, CH₂, cyclopr).

¹³C NMR (50 MHz, DMSO-d₆): δ 187.8, 172.3, 167.8, 154.1, 146.8, 146.3, 136.6, 131.8, 130.3, 129.3, 128.8, 128.1, 127.5, 123.2, 113.5, 110.2, 107.8, 100.6, 38.5, 30.3, 15.5.

HRMS (ESI) calculated for C₂₉H₂₄N₃O₅S:[M + H]⁺ 526.14366; found 526.14343.

Ethyl4-(2-(1-(benzo[d][1,3]dioxol-5-yl) cyclopropanecarboxamido)-4-phenylthiazole-5-carbonyl)benzoate (38)

Compound **38** (18.4 mg, 34%) was prepared from ethyl 4-(2- amino-4-phenylthiazole-5-carbonyl) benzoate (35.2 mg, 0.1 mmol) and benzo [1,3]dioxol-5-yl-cyclopropanecarboxylic acid (20.6 mg, 0.1 mmol) in the same manner as described for compound **29** as brown solid.

¹H NMR (200 MHz, DMSO-d₆): δ 12.05 (s, broad, 1H, NH), 7.84e6.82 (m, 12H, arom), 6.03 (s, 2H OCH₂O), 4.45 (q, J 1/4 7.2, 2H, OCH₂CH₃), 1.67e1.48 (m, 2H, CH₂, cyclopr), 1.41e1.04 (5H, m, 2H, CH₂, cyclopr + superimposed t, J 1/4 7.2, 3H, OCH₂CH₃).

^{13}C NMR (50 MHz, DMSO- d_6): δ 188.2, 172.5, 164.5, 160.5, 155.0, 146.9, 146.3, 141.1, 133.6, 131.9, 131.7, 129.5, 128.7, 128.3, 128.2, 127.3, 124.3, 123.2, 110.2, 107.8, 100.6, 60.7, 30.3, 15.5, 13.6.

HRMS (ESI) calculated for $\text{C}_{30}\text{H}_{25}\text{N}_2\text{O}_6\text{S}$: $[\text{M} + \text{H}]^+$ 541.14332; found 541.14314.

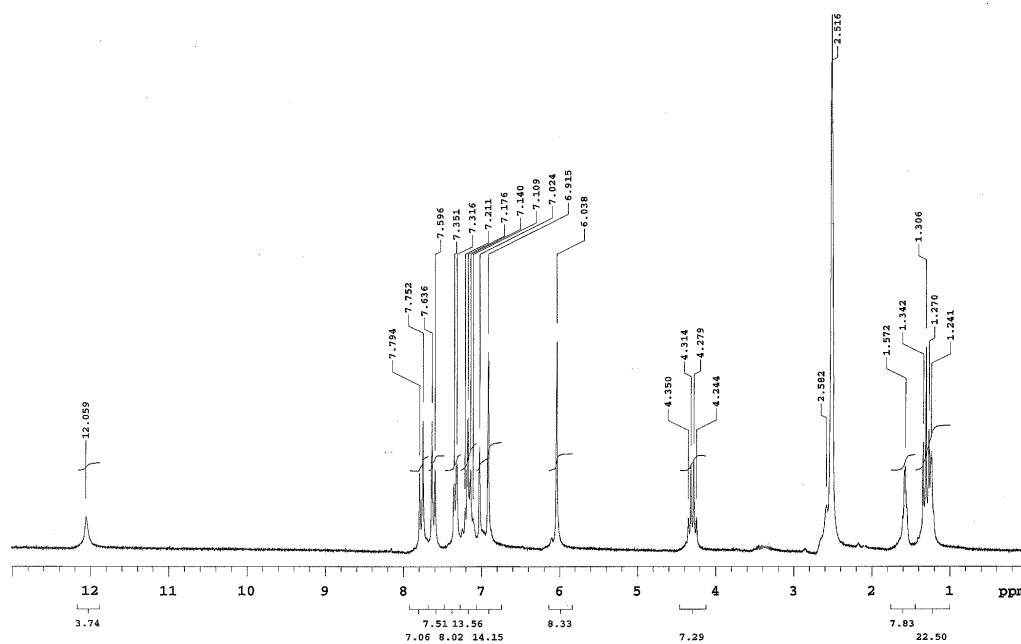


Figure 41. ^1H NMR spectra of compound 38

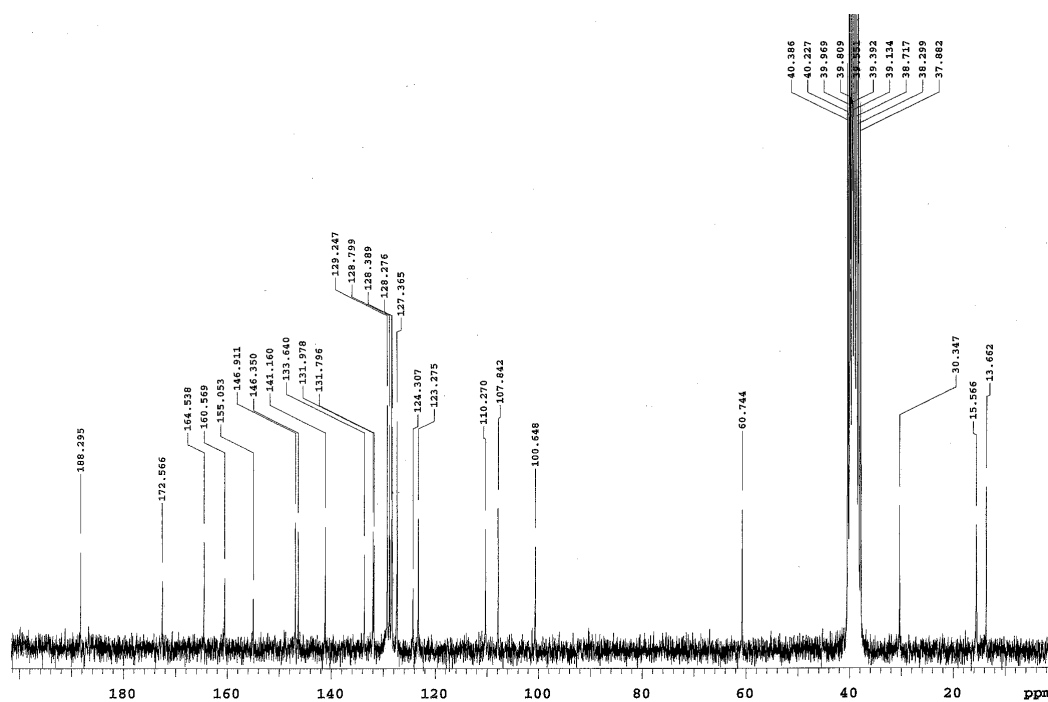


Figure 42. ^{13}C NMR spectra of compound 38

1-(Benzo[d][1,3]dioxol-5-yl)-N-(5-(4-pentylbenzoyl)-4-phenylthiazol-2-yl)cyclopropanecarboxamide (39)

Compound **39** (13.5 mg, 25%) was prepared from (2-amino-4-phenylthiazol-5-yl) (4-pentylphenyl)methanone (35 mg, 0.1 mmol) and benzo [1,3]dioxol-5-yl-cyclopropanecarboxylic acid (20.6 mg, 0.1 mmol) in the same manner as described for compound **29** as pale, yellow solid.

¹H NMR (200 MHz, DMSO-d₆): δ 11.90 (s, broad, 1H, NH), 7.61e6.76 (m, 12H, arom), 6.05 (s, 2H OCH₂O), 1.65e1.42 (m, 2H, CH₂, cyclopr), 1.41e1.05 (m, 6H, 2H, CH₂, cyclopr & 4H, CH₂CH₂), 0.98e0.72 (m, 7H, CH₂CH₂CH₃).

¹³C NMR (50 MHz, DMSO-d₆): δ 188.4, 172.3, 159.5, 174.2, 146.9, 146.3, 134.8, 133.8, 131.8, 128.9, 128.8, 128.0, 127.6, 127.3, 124.3, 123.2, 110.2, 107.8, 100.6, 34.5, 30.3, 30.1, 29.7, 28.5, 21.5, 15.4, 13.4.

HRMS (ESI) calculated for C₃₂H₃₁N₂O₄S: [M + H]⁺ 539.20044; found 539.20018.

1-(Benzo[d][1,3]dioxol-5-yl)-N-(5-(4-(diethylamino)benzoyl)-4-phenylthiazol-2-yl)cyclopropanecarboxamide (40)

Compound **40** (12.5 mg, 23%) was prepared from (2-amino-4-phenylthiazol-5-yl) (4-(diethylamino)phenyl)methanone (35 mg, 0.1 mmol) and benzo [1,3]dioxol-5-yl-cyclopropanecarboxylic acid (20.6 mg, 0.1 mmol) in the same manner as described for compound **29** as white solid.

¹H NMR (200 MHz, DMSO-d₆): δ 11.94 (s, broad, 1H, NH), 7.79e6.85 (m, 12H, arom), 6.05 (s, 2H OCH₂O), 2.83 (q, 4H, J 1/4 6.8, NCH₂), 1.65e1.41 (m, 2H, CH₂, cyclopr), 1.40e1.09 (m, 2H, CH₂, cyclopr), 1.04 (t, 6H, J 1/4 6.8, CH₃CH₂N).

¹³C NMR (50 MHz, DMSO-d₆): δ 188.3, 172.3, 163.2, 160.6, 155.2, 146.9, 146.3, 134.2, 133.7, 131.9, 131.6, 129.2, 128.7, 128.3, 128.1, 127.4, 124.3, 123.1, 110.2, 107.8, 100.6, 51.8, 30.3, 15.5, 13.8.

HRMS (ESI) calculated for C₃₁H₃₀N₃O₄S: [M + H]⁺ 540.19569; found 540.19544.

1-(Benzo[d][1,3]dioxol-5-yl)-N-(5-(4-bromobenzoyl)-4-phenylthiazol-2-yl)cyclopropanecarboxamide (41)

Compound **41** (17.5 mg, 32%) was prepared from (2-amino-4-phenylthiazol-5-yl) (4-bromophenyl)methanone (35.9 mg, 0.1 mmol) and benzo [1,3]dioxol-5-yl-cyclopropanecarboxylic acid (20.6 mg, 0.1 mmol) in the same manner as described for compound **29** as brown solid.

¹H NMR (200 MHz, DMSO-d₆) δ 12.02 (s, 1H, NH), 7.68e6.91 (m, 12H, arom), 6.06 (s, 2H, OCH₂O), 1.72e1.44 (m, 2H, CH₂, cyclopr), 1.38e1.12 (m, 2H, CH₂, cyclopr).

^{13}C NMR (50 MHz, DMSO- d_6) δ , 187.8, 172.4, 160.2, 154.5, 146.9, 146.3, 136.3, 133.6, 131.8, 130.7, 130.6, 129.2, 128.3, 127.4, 125.8, 124.1, 123.3, 110.2, 107.8, 100.6, 30.3, 15.5.

HRMS (ESI) calculated for $\text{C}_{27}\text{H}_{20}\text{BrN}_2\text{O}_4\text{S}$: $[\text{M} + \text{H}]^+$ 547.03271; found 547.03215.

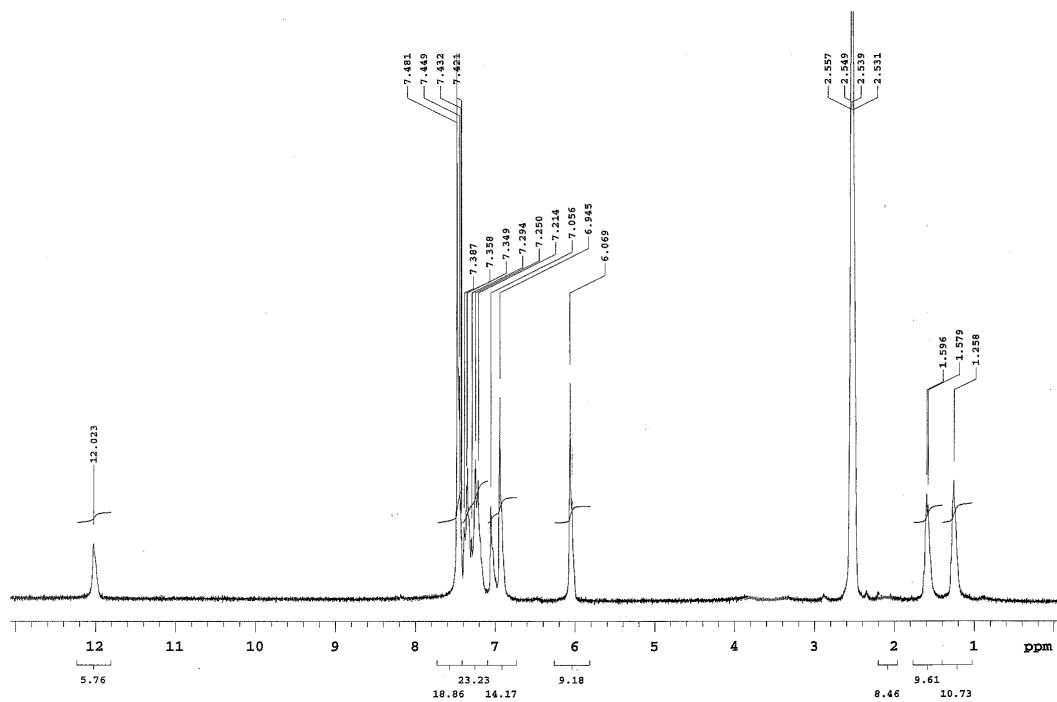


Figure 43. ^1H NMR spectra of compound 41

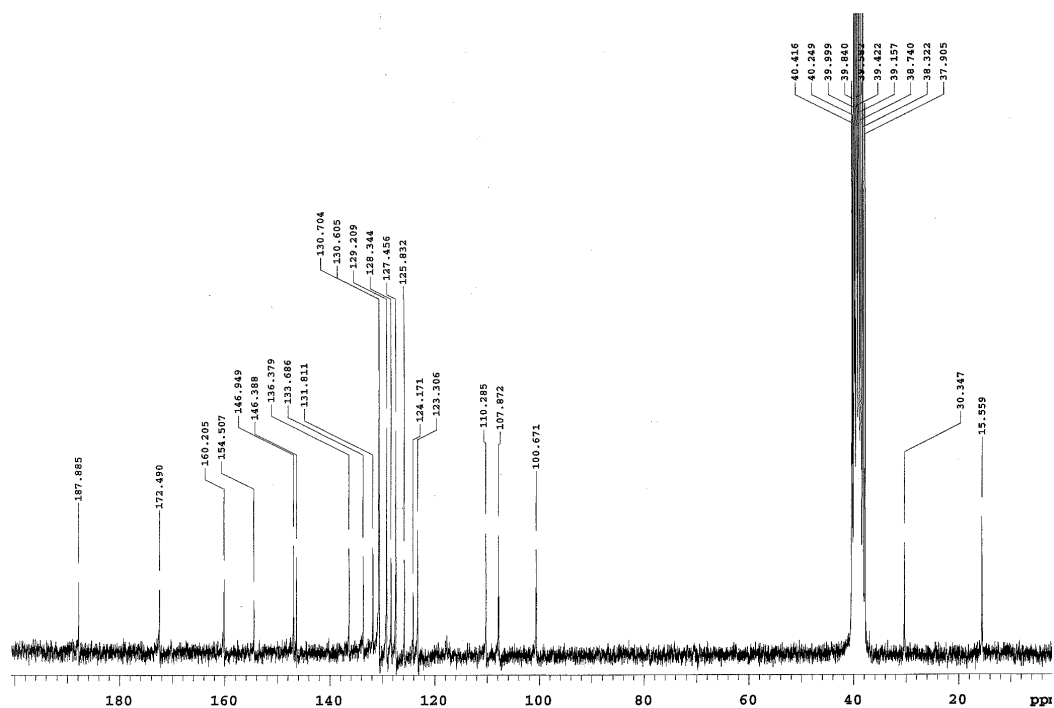


Figure 44. ^{13}C NMR of compound 41

N-(5-([1,10-biphenyl]-4-carbonyl)-4-phenylthiazol-2-yl)-1-(benzo[*d*][1,3]dioxol-5-yl)cyclopropanecarboxamide (42)

Compound **42** (15.3 mg, 28%) was prepared from [1, 10- biphenyl]-4-yl (2-amino-4-phenylthiazol-5-yl)methanone (35.7 mg, 0.1 mmol) and benzo [1,3]dioxol-5-yl-cyclo- propanecarboxylic acid (20.6 mg, 0.1 mmol) in the same manner as described for compound **29**, as a yellow solid.

¹H NMR (200 MHz, DMSO-*d*₆): d 12.01 (s, 1H, broad, NH); 7.92e6.76 (m, 17H, arom); 6.05 (s, 2H OCH₂O); 1.78e1.44 (m, 2H, CH₂, cyclopr); 1.42e1.08 (m, 2H, CH₂, cyclopr).

¹³C NMR (50 MHz, DMSO-*d*₆): d 188.2, 172.2, 156.8, 153.2, 146.9, 146.3, 140.7, 137.9, 133.2, 131.3, 129.3, 128.9, 128.2, 127.4, 123.1, 110.2, 107.8, 100.6, 30.3, 15.4.

HRMS (ESI) calculated for C₃₃H₂₅N₂O₄S: [M + H]⁺ 545.15349; found 545.13351.

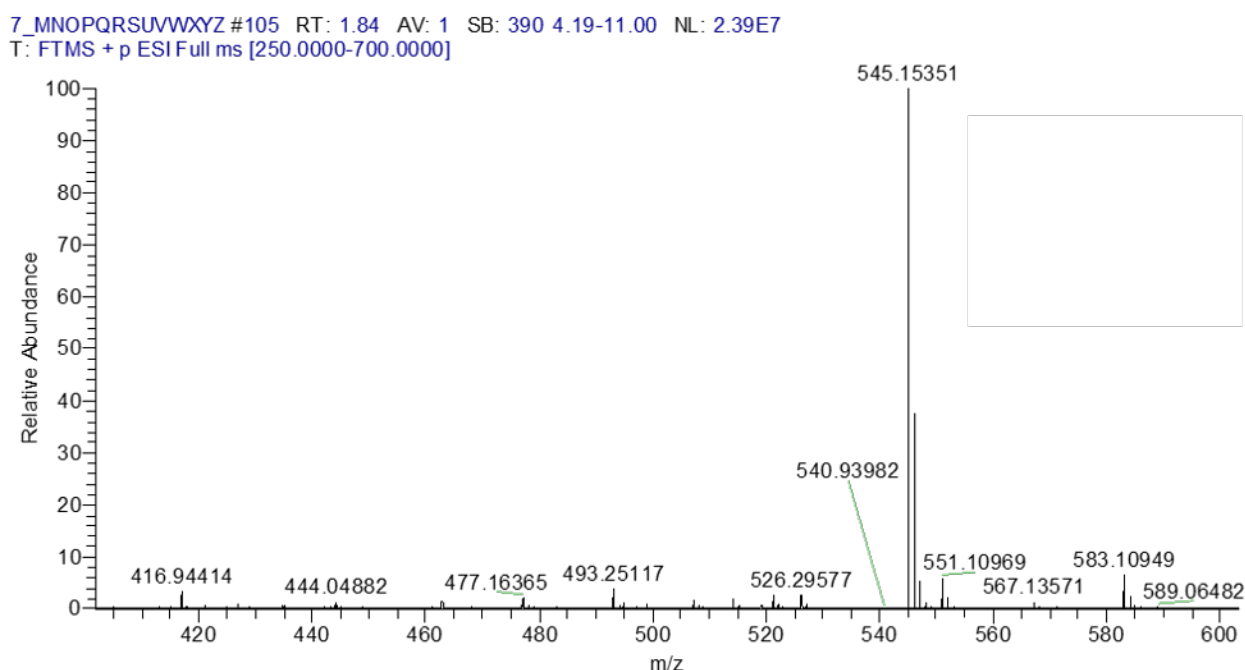


Figure 45. HRMS spectra of compound **42**

1-(Benzo[*d*][1,3]dioxol-5-yl)-*N*-(4-phenyl-5-(4-(thiophen-2-yl)benzoyl)thiazol-2-yl)cyclopropanecarboxamide (43)

Compound **43** (11.7 mg, 21%) was prepared from (2-amino-4- phenylthiazol-5-yl) (4-(thiophen-2-yl) phenyl)methanone (36.2 mg, 0.1 mmol) and benzo [1,3]dioxol-5-yl-cyclo- propanecarboxylic acid (20.6 mg, 0.1 mmol) in the same manner as described for compound **29** as brown oil.

¹H NMR (200 MHz, DMSO-*d*₆): d 11.96 (s, 1H, broad, NH); 7.95e6.73 (m, 15H, arom); 6.04 (s, 2H OCH₂O); 1.73e1.42 (m, 2H, CH₂, cyclopr); 1.40e1.05 (m, 2H, CH₂, cyclopr).

¹³C NMR (50 MHz, DMSO-*d*₆): d 176.8, 172.1, 159.7, 154.3, 146.9, 146.2, 137.6, 137.0, 133.4, 131.7, 131.3, 129.6, 128.8, 128.2, 127.5, 123.2, 113.4, 110.2, 107.8, 100.6, 30.3, 15.5.

HRMS (ESI) calculated for C₃₁H₂₃N₂O₄S₂: [M + H]⁺ 551.10992; found 551.10971.

1-(Benzo[d][1,3]dioxol-5-yl)-N-(4-phenyl-5-(4-(pyrrolidin-1-yl)benzoyl)thiazol-2-yl)cyclopropanecarboxamide (44)

Compound **44** (11.5 mg, 21%) was prepared from (2-amino-4-phenylthiazol-5-yl) (4-(pyrrolidin-1-yl)phenyl) methanone (35 mg, 0.1 mmol) and benzo [1,3]dioxol-5-yl-cyclopropanecarboxylic acid (20.6 mg, 0.1 mmol) in the same manner as described for compound **29** as pale yellow oil.

¹H NMR (200 MHz, DMSO-d₆): δ 12.08 (s, 1H, broad, NH); 7.82e6.75 (m, 12H, arom); 6.01 (s, 2H, OCH₂O); 2.97 (m, 4H, CH₂N); 1.88e1.43 (m, 6H, 4H CH₂CH₂, 2H, CH₂, cyclopr); 1.40e1.12 (m, 2H, CH₂, cyclopr).

¹³C NMR (50 MHz, DMSO-d₆): δ 187.7, 170.3, 160.2, 154.7, 146.9, 146.3, 131.8, 131.0, 129.6, 128.7, 128.2, 127.5, 123.3, 113.2, 110.2, 107.8, 100.6, 48.2, 30.3, 18.6, 15.4.

HRMS (ESI) calculated for C₃₁H₂₈N₃O₄S: [M + H]⁺ 538.18004; found 538.17987.

1-(Benzo[d][1,3]dioxol-5-yl)-N-(5-(benzo[d][1,3]dioxole-5-carbonyl)-4-phenylthiazol-2-yl)cyclopropanecarboxamide (45)

Compound **45** (15.5 mg, 30%) was prepared from (2-amino-4-phenylthiazol-5-yl) (benzo [d] [1,3] dioxol-5-yl)methanone (32.4 mg, 0.1 mmol) and benzo [1,3]dioxol-5-yl-cyclopropanecarboxylic acid (20.6 mg, 0.1 mmol) in the same manner as described for compound **29** as brown oil.

¹H NMR (200 MHz, DMSO-d₆) δ 12.08 (s, 1H, NH); 7.77e6.68 (m, 11H, arom); 6.07 (s, 2H, OCH₂O); 6.03 (s, 2H, OCH₂O); 1.64e1.41 (m, 2H, CH₂, cyclopr); 1.41e1.00 (m, 2H, CH₂, cyclopr).

¹³C NMR (50 MHz, DMSO-d₆) δ 178.8, 171.4, 159.3, 154.8, 151.5, 146.9, 146.3, 137.0, 131.2, 128.8, 128.1, 127.4, 123.2, 114.6, 110.3, 107.8, 100.6, 30.3, 15.4.

HRMS (ESI) calculated for C₂₈H₂₁N₂O₆S: [M + H]⁺ 513.11203; found 513.11187.

1-(benzo[d][1,3]dioxol-5-yl)-N-(5-(4-methyl-2-phenylpyrimidine-5-carbonyl)-4-phenylthiazol-2-yl)cyclopropane-1-carboxamide (46)

A mixture of (4-methoxyphenyl) methanamine (535 mL, 4 mmol) and 4-(methoxy)benzaldehyde (595 mL, 4.8 mmol) were dissolved in methanol (2 mL) and heated to reflux for 3 h, then cooled to T = 0 ° C, NaBH₄ (228 mg, 6 mmol) was added portion wise to the reaction and the resulting mixture was stirred at room temperature overnight. Methanol was removed in vacuum and the residue was taken up in ethyl acetate (EtOAc). The organic layer was washed with water (3 x 5 mL), and then dried over anhydrous Na₂SO₄. After filtration, solvent was removed to afford bis [4-

methoxyphenyl]methylamine (962 mg, 94%) as a colorless oil which was used in the next step without further purification. ESI-MS: m/z 258.0 [M⁺H]⁺.

To a solution of benzoylisothiocyanate (140 mL, 1 mmol) in acetone (1 mL) cooled at $T = 0^\circ \text{C}$, bis [4-methoxyphenyl]methyl- amine (257 mg, 1 mmol) in acetone (1 mL) was added at this temperature and stirred for 1 h.

The mixture was concentrated under reduced pressure, to afford N-(bis(4-methoxybenzyl) carbamothioyl)benzamide (398 mg, 95%) as yellow sticky oil which was used in the next step without further purification. ESI-MS: m/z 421.0 [M⁺H]⁺.

Then, N,N- dimethylformamide dimethyl acetal (DMF-DMA) (398 μL , 3 mmol) was mixed with acetylacetone (155 μL , 1,5 mmol) and stirred at 100°C for 2 h. Benzimidamide (180,2 mg, 1,5 mmol) dissolved in EtOH, was directly added in the reaction mixture and the reaction was maintained at 75°C for 3 h. The solvent was removed under pressure, the residue was taken up in dichloromethane (DCM) and washed with water for 3 times (3 x 5 mL). The organic phase was dried over anhydrous Na_2SO_4 and after filtration, solvent was removed to obtain 1-(4-methyl-2-phenylpyrimidin-5-yl)ethan-1-one, as a powder (140 mg, 44%).

1-(4-methyl-2-phenylpyrimidin-5-yl)ethan-1-one (140 mg, 0,7 mmol) was brominated with CuBr_2 (312 mg, 1,4 mmol) in dioxane (3 mL). The mixture was stirred at 50°C for 1 h and at 85°C for additional 30 minutes to afford a selective bromination in position alpha of the ketone group. The solvent was evaporated in vacuum and the residue was dissolved in ethyl acetate and washed with water (3 x 5 mL). The organic layer was dried over anhydrous Na_2SO_4 , filtered, the solvent was removed to give 2-bromo-1-(4-methyl-2-phenylpyrimidin-5-yl)ethan-1-one, that was lyophilized (145 mg, 71%).

A solution of 2-bromo-1-(4-methyl-2-phenylpyrimidin-5-yl)ethan-1-one (145 mg, 0.5 mmol) and N-(bis(4-methoxybenzyl)carbamothioyl)- benzamide (210 mg, 0.5 mmol) in N, N- DMF (3 mL) was stirred at $T = 85^\circ \text{C}$ for 3 h. After cooling to room temperature, the mixture was partitioned between EtOAc and H_2O . The organic layer was washed with brine and dried over anhydrous Na_2SO_4 . After filtration, solvent was removed in vacuum and the residue was stirred in trifluoroacetic acid (TFA) (4 mL) at $T = 80^\circ \text{C}$ for 36 h until complete deprotection. Most of TFA was removed under vacuum. The residue was then neutralized with NaHCO_3 1 N, and then extracted with EtOAc for 3 times (3 x 5 mL). The organic phase was washed with brine and dried over anhydrous Na_2SO_4 . After filtration, the solution was concentrated and further crystallized in acetonitrile to afford (2-amino-4-phenylthiazol-5-yl)(4-methyl-2-phenylpyrimidin-5-yl)methanone (75 mg, 40%) as a brown solid.

Benzo [1,3]dioxol-5-yl-cyclopropanecarboxylic acid (20.6 mg, 0.1 mmol) was resuspended in anhydrous N,N - DMF (1 mL); HATU (38 mg, 0.1 mmol) and DIPEA (35 mL, 0.2 mmol) were added.

The reaction was vigorously stirred for 5 min and (2-amino-4-phenylthiazol-5-yl)(4-methyl-2-phenylpyrimidin-5-yl)methanone (37 mg, 0.1 mmol) in anhydrous N,N-DMF (0.5 mL) was added. The reaction was stirred at T= 50° C until completeness (24 h) and then purified by preparative HPLC. The peak of interest was concentrated to obtain the title compound as yellow solid with purity of >95% as determined by HPLC-MS (12 mg, 21%).

1-(Benzo[d][1,3]dioxol-5-yl)-N-(5-(3-methoxybenzoyl)-4-phenylthiazol-2-yl)cyclopropanecarboxamide (47)

Compound **47** (10.8 mg, 22%) was prepared from (2-amino-4-phenylthiazol-5-yl) (3-methoxyphenyl)methanone (31 mg, 0.1 mmol) and benzo [1,3]dioxol-5-yl-cyclopropanecarboxylic acid (20.6 mg, 0.1 mmol) in the same manner as described for compound **29** as pale brown oil.

¹H NMR (200 MHz, DMSO-d₆): δ 12.04 (s, 1H, broad, NH); 7.94e6.76 (m, 12H, arom); 6.04 (s, 2H OCH₂O); 4.01 (s, 3H, CH₃O); 1.71e1.44 (m, 2H, CH₂, cyclopr); 1.40e1.02 (m, 2H, CH₂, cyclopr).

¹³C NMR (50 MHz, DMSO-d₆): δ 177.4, 164.6, 158.4, 154.2, 146.9, 146.2, 131.8, 131.1, 129.7, 128.8, 128.1, 127.4, 123.2, 113.7, 110.2, 107.8, 100.6, 98.1, 55.6, 30.2, 15.4.

HRMS (ESI) calculated for C₂₈H₂₃N₂O₅S: [M + H]⁺ 499.13276; found 499.13245.

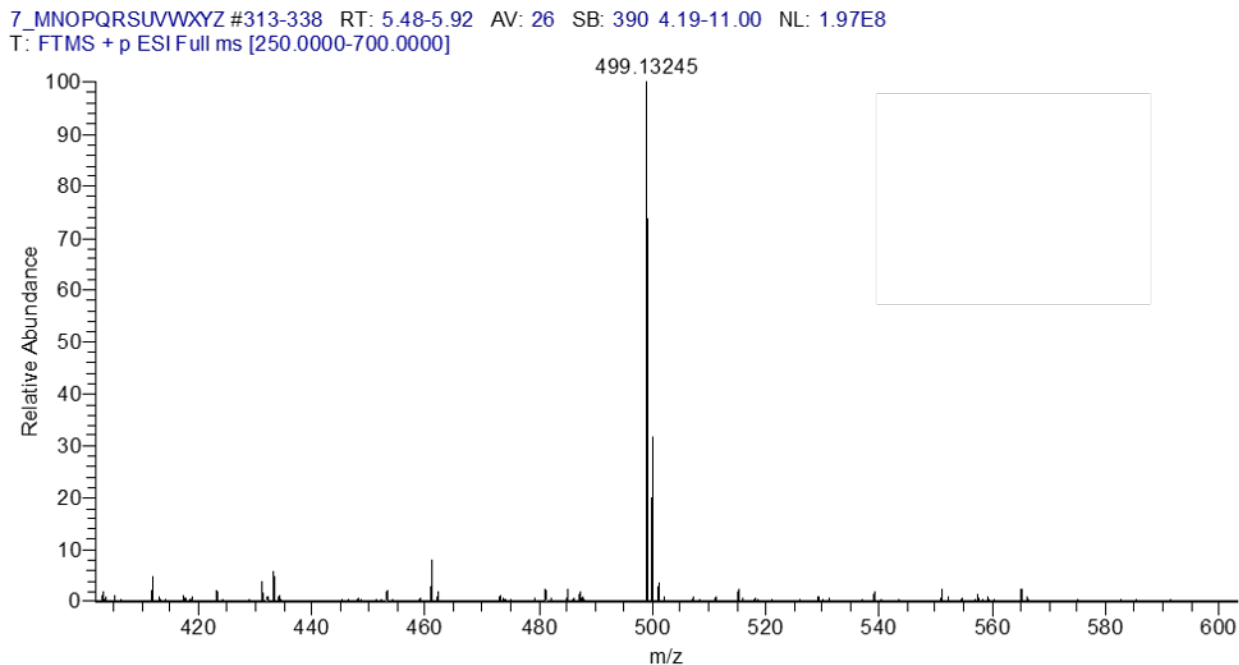


Figure 46. HRMS spectra of compound **47**

1-(Benzo[d][1,3]dioxol-5-yl)-N-(5-(2-methoxybenzoyl)-4-phenylthiazol-2-yl)cyclopropanecarboxamide (48)

Compound **48** (11 mg, 22%) was prepared from (2-amino-4- phenylthiazol-5-yl) (2-methoxyphenyl) methanone (31 mg, 0.1 mmol) and benzo [1,3]dioxol-5-yl-cyclopropanecarboxylic acid (20.6 mg, 0.1 mmol) in the same manner as described for compound **29** as brown oil.

¹H NMR (200 MHz, DMSO-d₆): d 10.97 (s, 1H, broad, NH); 7.68e6.69 (m, 12H, arom); 6.02 (s, 2H OCH₂O); 3.98 (s, 3H, CH₃O); 1.68e1.43 (m, 2H, CH₂, cyclopr); 1.42e1.03 (m, 2H, CH₂, cyclopr).

¹³C NMR (50 MHz, DMSO-d₆): d 175.7, 163.1, 158.9, 154.4, 147.0, 146.3, 131.7, 131.1, 129.6, 128.9, 128.1, 127.5, 123.2, 113.8, 110.2, 107.8, 100.6, 97.7, 55.3, 30.3, 15.5.

HRMS (ESI) calculated for C₂₈H₂₃N₂O₅S: [M + H]⁺ 499.13276; found 499.13276.

1-(Benzo[d][1,3]dioxol-5-yl)-N-(5-(3-bromobenzoyl)-4-phenylthiazol-2-yl)cyclopropanecarboxamide (49)

Compound **49** (16 mg, 29%) was prepared from (2-amino-4- phenylthiazol-5-yl) (3-bromophenyl)methanone (35.9 mg, 0.1 mmol) and benzo [1,3]dioxol-5-yl-cyclopropanecarboxylic acid (20.6 mg, 0.1 mmol) in the same manner as described for compound **29** as pale brown solid.

¹H NMR (200 MHz, DMSO-d₆): d 12.03 (s, 1H, broad, NH); 8.18e6.81 (m, 12H, arom); 6.06 (s, 2H OCH₂O); 1.78e1.45 (m, 2H, CH₂, cyclopr); 1.44e1.05 (m, 2H, CH₂, cyclopr).

¹³C NMR (50 MHz, DMSO-d₆): d 188.3, 172.1, 159.3, 155.3, 146.9, 146.3, 137.0, 131.2, 129.6, 129.0, 128.2, 127.5, 123.3, 114.2, 110.2, 107.8, 100.6, 30.3, 15.5.

HRMS (ESI) calculated for C₂₇H₂₀BrN₂O₄S: [M + H]⁺ 547.03271; found 547.03219.

1-(Benzo[d][1,3]dioxol-5-yl)-N-(5-(3-fluorobenzoyl)-4-phenylthiazol-2-yl)cyclopropanecarboxamide (50)

Compound **50** (13 mg, 27%) was prepared from (2-amino-4- phenylthiazol-5-yl) (3-fluorophenyl)methanone (30 mg, 0.1 mmol) and benzo [1,3]dioxol-5-yl-cyclopropanecarboxylic acid (20.6 mg, 0.1 mmol) in the same manner as described for compound **29** as white solid.

¹H NMR (200 MHz, DMSO-d₆): d 11.93 (s, 1H, broad, NH); 8.01e6.74 (m, 12H, arom); 6.05 (s, 2H OCH₂O); 1.73e1.44 (m, 2H, CH₂, cyclopr); 1.42e1.08 (m, 2H, CH₂, cyclopr).

¹³C NMR (50 MHz, DMSO-d₆): d 188.0, 171.5, 158.7, 156.2, 146.9, 146.3, 137.0, 133.4, 131.1, 129.7, 128.8, 128.2, 127.6, 123.2, 113.8, 110.2, 107.8, 100.6, 30.3, 15.5.

HRMS (ESI) calculated for C₂₇H₂₀FN₂O₄S: [M + H]⁺ 487.11277; found 487.11243.

1-(Benzo[d][1,3]dioxol-5-yl)-N-(4-phenyl-5-(3-propoxybenzoyl)thiazol-2-yl)cyclopropanecarboxamide (51)

3-(Prop-1-yloxy)acetophenone (356 mg, 2 mmol) synthesized starting from 3-hydroxyacetophenone and was brominated with CuBr₂ using the general procedure previously described (Liessi et al., 2018), providing 2-bromo-1-(3-propoxyphenyl)ethanone intermediate (460 mg, 90%). The purity was verified by HPLC-MS without further purification.

A solution of 2-bromo-1-(3-propoxyphenyl)ethanone (128 mg, 0.5 mmol) and N-(bis(4-methoxybenzyl)carbamothioyl)-benzamide (210 mg, 0.5 mmol) in N,N - DMF (3 mL) was stirred at T = 85 °C for 3 h. After TFA deprotection and crystallization in acetonitrile (2-amino-4-phenylthiazol-5-yl) (3-propoxyphenyl)methanone (118 mg, 70%) was isolated. ESI-MS: m/z 339.1 [M⁺H]⁺.

(2-Amino-4-phenylthiazol-5-yl) (3-propoxyphenyl)methanone (34 mg, 0.1 mmol) and benzo [1,3] dioxol-5-ylcyclopropanecarboxylic acid (20.6 mg, 0.1 mmol) was then conjugated in the same manner as described for compound **29** to furnish, after HPLC purification, the title compound as pale brown oil (11 mg, 21%).

HRMS (ESI) calculated for C₃₀H₂₇N₂O₅S: [M⁺H]⁺ 527.16406; found 527.16385.

N-(5-([1,10-biphenyl]-3-carbonyl)-4-phenylthiazol-2-yl)-1-(benzo[d][1,3]dioxol-5-yl)cyclopropanecarboxamide (**52**)

1-([1,10-Biphenyl]-3-yl)ethanone (196 mg, 1 mmol) was brominated with N-bromosuccinimide (NBS) using the general procedure previously described (Liessi et al; 2018) providing [1,10 - biphenyl]-3-carbonyl bromide intermediate (202 mg, 73%). The purity was verified by HPLC-MS without further purification.

A solution of [1,10 -biphenyl]-3-carbonyl bromide intermediate (130 mg, 0.5 mmol) and N-(bis(4-methoxybenzyl)carbamothioyl)- benzamide (230 mg, 0.5 mmol) in N,N - DMF (3 mL) was stirred at T = 85°C for 3 h. After TFA deprotection and crystallization in acetonitrile [1,10-biphenyl]- 3-yl (2-amino-4-phenylthiazol-5-yl)methanone (60,5 mg, 34%) was isolated. ESI-MS: m/z 357.1 [M⁺H]⁺.

[1,10 -Biphenyl]-3-yl (2-amino-4-phenylthiazol-5-yl)methanone (36 mg, 0.1 mmol) and benzo [1,3] dioxol-5-yl-cyclo- propanecarboxylic acid (20.6 mg, 0.1 mmol) was then conjugated in the same manner as described for compound **29** to furnish, after HPLC purification, the title compound as pale, yellow solid (12.5 mg, 23%).

¹H NMR (200 MHz, DMSO-d₆): δ 12.01 (s, 1H, broad, NH) 8.27e6.82 (m, 17H, arom); 6.04 (s, 2H OCH₂O); 1.69e1.42 (m, 2H, CH₂, cyclopr); 1.41e1.03 (m, 2H, CH₂, cyclopr).

¹³C NMR (50 MHz, DMSO-d₆): δ 187.9, 171.8, 157.4, 153.3, 146.9, 146.3, 141.7, 137.8, 137.2, 131.3, 129.4, 128.8, 128.1, 127.5, 123.1, 110.2, 107.8, 100.6, 30.3, 15.6.

HRMS (ESI) calculated for C₃₃H₂₅N₂O₄S: [M⁺H]⁺ 515.15349; found 545.15331.

1-(Benzo[d][1,3]dioxol-5-yl)-N-(5-(2,4-dimethoxybenzoyl)-4-phenylthiazol-2-yl)cyclopropanecarboxamide (53)

Compound **53** (18.1 mg, 34%) was prepared from (2-amino-4- phenylthiazol-5-yl) (2,4-dimethoxyphenyl)methanone (34 mg, 0.1 mmol) and benzo [1,3]dioxol-5-yl-cyclopropanecarboxylic acid (20.6 mg, 0.1 mmol) in the same manner as described for compound **29** as brown solid.

¹H NMR (200 MHz, DMSO-d₆) δ 11.98 (s, 1H, NH); 7.62e6.64 (m, 11H, arom); 6.04 (s, 2H, OCH₂O); 3.73 (s, 3H, OCH₃); 3.62 (s, 3H, OCH₃); 1.70e1.45 (m, 2H, CH₂, cyclopr); 1.39e1.09 (m, 2H, CH₂, cyclopr).

¹³C NMR (50 MHz, DMSO-d₆) δ 176.4, 170.6, 160.2, 155.3, 152.2, 146.9, 146.3, 133.8, 131.4, 128.9, 128.2, 126.7, 123.2, 117.8, 113.6, 110.2, 107.8, 100.6, 55.4, 55.2, 30.3, 15.5.

HRMS (ESI) calculated for C₂₉H₂₅N₂O₆S: [M + H]⁺ 529.14332; found 529.14298.

1-(Benzo[d][1,3]dioxol-5-yl)-N-(5-(2,5-dimethoxybenzoyl)-4-phenylthiazol-2-yl)cyclopropanecarboxamide (54)

Compound **54** (13.8 mg, 26%) was prepared from (2-amino-4- phenylthiazol-5-yl) (2,5-dimethoxyphenyl)methanone (35 mg, 0.1 mmol) and benzo [1,3]dioxol-5-yl cyclopropanecarboxylic acid (20.6 mg, 0.1 mmol) in the same manner as described for compound **29** as brown solid.

¹H NMR (200 MHz, DMSO-d₆) δ 11.85 (s, 1H, NH), 7.47e6.53 (m, 11H, arom); 6.02 (s, 2H, OCH₂O); 3.64 (s, 3H, OCH₃); 3.47 (s, 3H, OCH₃); 1.72e1.47 (m, 2H, CH₂, cyclopr); 1.37e1.16 (m, 2H, CH₂, cyclopr).

¹³C NMR (50 MHz, DMSO-d₆) δ 172.3, 160.4, 155.2, 152.2, 149.9, 146.9, 146.3, 133.5, 131.7, 128.8, 128.1, 126.7, 123.3, 117.0, 113.5, 111.9, 110.3, 107.8, 100.6, 55.3, 55.2, 30.3, 15.5.

HRMS (ESI) calculated for C₂₉H₂₅N₂O₆S: [M + H]⁺ 529.14332; found 529.14301.

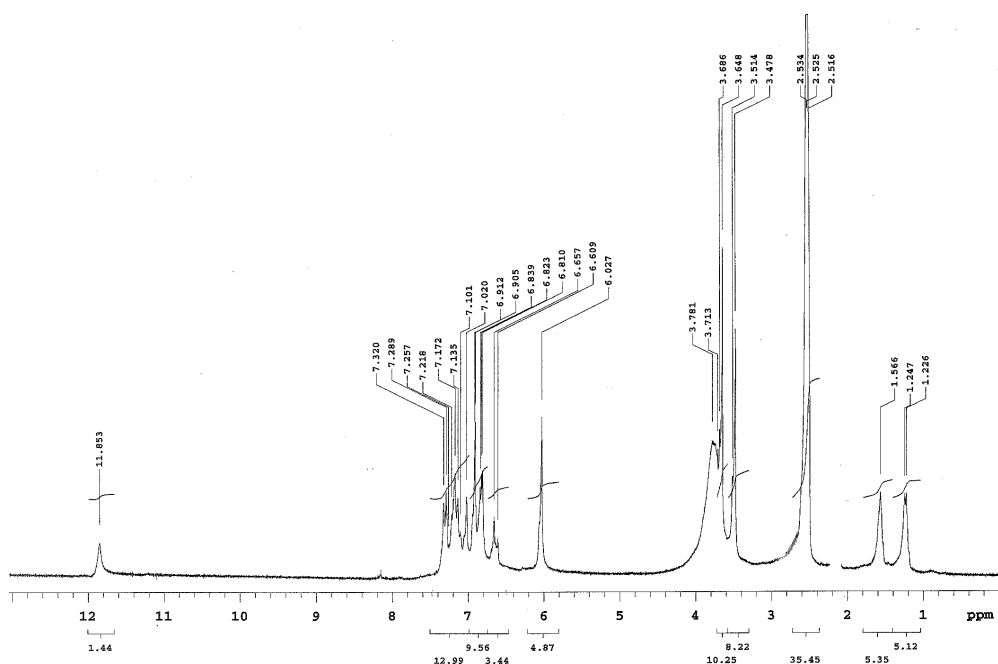


Figure 47. ^1H NMR spectra of compound **54**

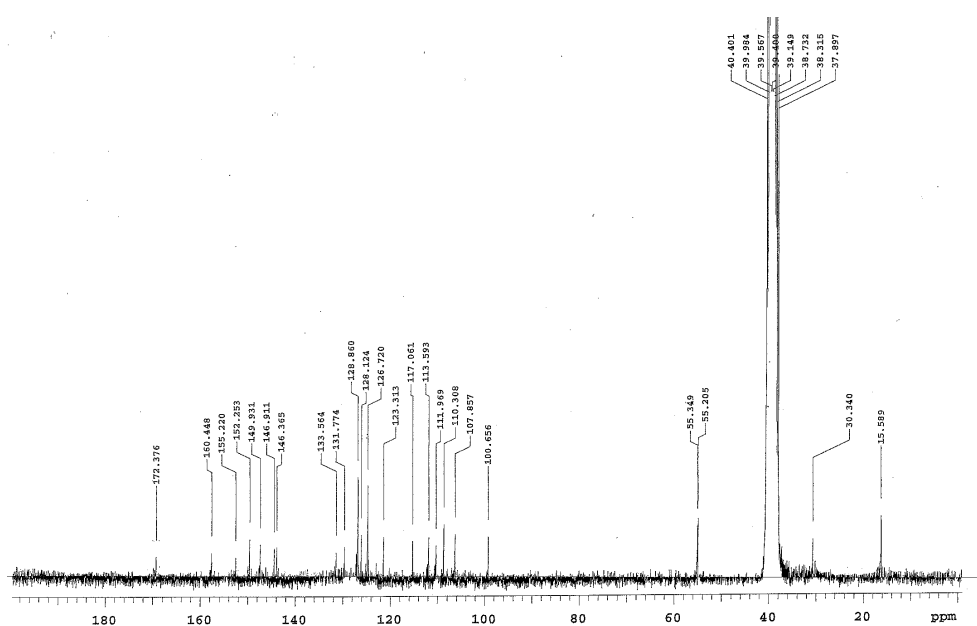


Figure 48. ^{13}C NMR of compound **54**

1-(Benzo[d][1,3]dioxol-5-yl)-N-(5-(3-chloro-4-methoxybenzoyl)-4-phenylthiazol-2-yl)cyclopropanecarboxamide (55)

Compound **55** (14.5 mg, 27%) was prepared (2-amino-4-phenylthiazol-5-yl) (3-chloro-4-methoxyphenyl)methanone (40 mg, 0.1 mmol) and benzo [1,3]dioxol-5-yl-cyclopropanecarboxylic acid (20.6 mg, 0.1 mmol) in the same manner as described for compound **29** as brown oil.

¹H NMR (200 MHz, DMSO-d₆) δ 12.14 (s, 1H, NH); 8.03e6.75 (m, 11H, arom); 6.06 (s, 2H, OCH₂O); 3.77 (s, 3H, OCH₃); 1.78e1.46 (m, 2H, CH₂, cyclopr); 1.42e1.10 (m, 2H, CH₂, cyclopr).

¹³C NMR (50 MHz, DMSO-d₆) δ 184.5, 171.5, 162.2, 156.8, 153.1, 146.8, 146.3, 140.5, 137.2, 131.2, 128.8, 128.2, 123.3, 118.1, 113.6, 110.2, 107.7, 100.6, 55.3, 30.3, 15.6.

HRMS (ESI) calculated for C₂₈H₂₂ClN₂O₅S: [M + H]⁺ 533.09379; found 533.09336

N-(5-(3-allyl-4-hydroxybenzoyl)-4-phenylthiazol-2-yl)-1-(benzo[d][1,3]dioxol-5-yl)cyclopropanecarboxamide (56)

Compound **56** (10 mg, 19%) was prepared from (3-allyl-4-hydroxyphenyl) (2-amino-4-phenylthiazol-5-yl)methanone (34 mg, 0.1 mmol) and benzo [1,3]dioxol-5-yl-cyclopropanecarboxylic acid (20.6 mg, 0.1 mmol) in the same manner as described for compound **29** as brown oil.

¹H NMR (200 MHz, DMSO-d₆) δ 12.02 (s, 1H, NH); 9.73 (s, 1H, OH); 7.88e6.72 (m, 11H, arom); 6.05 (s, 2H, OCH₂O); 5.95e5.61 (m, 1H, CH₂CH=CH₂); 4.92e4.68 (m, 2H, CH₂CH=CH₂); 3.18 (d, J = 15.2, 2H, CH₂CH=CH₂); 1.77e1.43 (m, 2H, CH₂, cyclopr); 1.42e1.14 (m, 2H, CH₂, cyclopr).

¹³C NMR (50 MHz, DMSO-d₆) δ 178.4, 170.5, 161.1, 156.2, 152.9, 146.9, 146.3, 145.2, 136.9, 136.5, 131.2, 128.8, 128.3, 123.4, 114.2, 110.2, 107.8, 100.6, 34.9, 30.3, 15.6.

HRMS (ESI) calculated for C₃₀H₂₅N₂O₅S: [M + H]⁺ 525.14841; found 525.14803.

5-(2-(1-(Benzo[d][1,3]dioxol-5-yl)cyclopropanecarboxamido)-4-phenylthiazole-5-carbonyl)-2-hydroxybenzamide (57)

Compound **57** (12.5 mg, 24%) was prepared from 5-(2-amino-4-phenylthiazole-5-carbonyl)-2-hydroxybenzamide (34 mg, 0.1 mmol) and benzo [1,3]dioxol-5-yl-cyclopropanecarboxylic acid (20.6 mg, 0.1 mmol) in the same manner as described for compound **29** as brown oil.

¹H NMR (200 MHz, DMSO-d₆) δ 11.89 (s, 1H, NH); 11.38 (s, 1H, OH); 8.55 (s, 2H, NH₂); 7.64e6.68 (m, 11H, arom); 6.05 (s, 2H, OCH₂O); 1.72e1.42 (m, 2H, CH₂, cyclopr); 1.42e1.05 (m, 2H, CH₂, cyclopr).

¹³C NMR (50 MHz, DMSO-d₆) δ 180.4, 172.6, 168.3, 159.7, 155.5, 152.8, 146.9, 146.3, 137.1, 131.3, 128.9, 128.2, 126.7, 123.4, 113.9, 110.2, 107.7, 100.6, 30.3, 15.5.

HRMS (ESI) calculated for C₂₈H₂₂N₃O₆S: [M + H]⁺ 528.12292; found 528.12282.

1-(Benzo[d][1,3]dioxol-5-yl)-N-(5-(5-chloro-2-hydroxybenzoyl)-4-phenylthiazol-2-yl)cyclopropanecarboxamide (58)

Compound **58** (11.2 mg, 11%) was prepared from (2-amino-4-phenylthiazol-5-yl) (5-chloro-2-hydroxyphenyl)methanone (66 mg, 0.19 mmol) and benzo [1,3]dioxol-5-yl-cyclopropanecarboxylic acid (39 mg, 0.19 mmol) in the same manner as described for compound **29** as brown oil.

¹H NMR (200 MHz, DMSO-d₆) δ 12.06 (s, 1H, NH); 10.84 (s, 1H, OH); 8.01e6.71 (m, 11H, arom); 6.05 (s, 2H, OCH₂O); 1.73e1.45 (m, 2H, CH₂, cyclopr); 1.43e1.05 (m, 2H, CH₂, cyclopr).

¹³C NMR (50 MHz, DMSO-d₆) δ 185.6, 172.7, 160.9, 155.9, 153.3, 146.9, 146.2, 141.8, 137.3, 131.1, 128.9, 128.1, 123.2, 117.5, 113.8, 110.2, 107.7, 100.6, 30.3, 15.5.

HRMS (ESI) calculated for C₂₇H₂₀ClN₂O₅S: [M + H]⁺ 519.07814; found 519.07781.

1-(benzo[d][1,3]dioxol-5-yl)-N-(5-benzoyl-4-(4-methoxyphenyl)thiazol-2-yl)cyclopropane-1-carboxamide (69)

4-methoxybenzoyl chloride (270.8 μL, 2 mmol) was dissolved in acetone and at this solution was added ammonium thiocyanate (304.4 mg, 4 mmol) at T= 0°C. After two hours, bis(4-methoxybenzyl)amine (620.0 mg, 2.4 mmol), obtained by 4-(methoxy)benzaldehyde and (4-methoxyphenyl)methanamine as already described [28], was added to the mixture and the reaction was stirred at room temperature. After completion of the reaction, as monitored by HPLC, acetone was removed by rotavapor and to the residue were added ethyl acetate (EtOAc) and H₂O. The organic layers were washed with water (3 x 3.5 mL), dried over anhydrous Na₂SO₄ and filtered. Ethyl acetate was removed under reduced pressure to give N-(bis(4-methoxybenzyl)carbamothioyl)-4-methoxybenzamide (720.0 mg, 80%) as yellow oil, that was used in the next step without further purification.

2-bromo-1-phenylethan-1-one (39.8 mg, 0.2 mmol) was dissolved in N,N-DMF and N-(bis(4-methoxybenzyl)carbamothioyl)-4-methoxybenzamide (90.1 mg, 0.2 mmol) was added; the reaction was heated to 85 °C for 2 hours. The mixture was cooled to room temperature and then, ethyl acetate and water were added. The organic phase was washed with brine, dried over anhydrous Na₂SO₄ and filtered. After removing solvent in vacuum, the product obtained was resuspended in trifluoroacetic acid (TFA) (4 mL) and stirred at T = 100°C for 48 hours. Most of TFA was evaporated by using rotavapor and a solution of NaHCO₃ 1N was added to neutralize the residue. Then the mixture was extracted by ethyl acetate (3 x 5 mL), the organic phase was dried over anhydrous Na₂SO₄, filtered and concentrated to afford (2-amino-4-(4-methoxyphenyl)thiazol-5-yl)(phenyl)methanone. (2-amino-4-(4-methoxyphenyl)thiazol-5-yl)(phenyl)methanone was crystallized in acetonitrile to give a pure product (45.3 mg, 73%).

A solution of benzo[1,3]dioxol-5-yl-cyclopropanecarboxylic acid (21.0 mg, 0.1 mmol), HATU (34.2 mg, 0.09 mmol) and DIPEA (38 μL, 0.1 mmol) was dissolved in anhydrous N,N-DMF and stirred at

room temperature for 5 min. Then, (2-amino-4-(4-methoxyphenyl)thiazol-5-yl)(phenyl)methanone (31.0 mg, 0.1 mmol) in anhydrous N,N-DMF was added and the mixture was heated to 50 °C for 24 h.

Preparative HPLC was used to purify the product and after concentration of the peak of interest, the final product was obtained with a purity higher than 95%. The purity of the compound was determined by HPLC-MS. Then the product was lyophilised and afforded as a powder (12.5 mg, 25%).

¹H NMR (200 MHz, DMSO-d₆): δ 12.01 (s, 1H, broad, NH); 7.72-6.79 (m, 12H, arom); 6.02 (s, 2H, OCH₂O); 3.64 (s, 3H, OCH₃); 1.63-1.44 (m, 2H, cyclopr); 1.38-1.11 (m, 2H, cyclopr).

¹³C NMR (50 MHz, DMSO-d₆): δ 188.2, 171.8, 159.8, 159.1, 153.8, 146.8, 146.3, 138.5, 131.8, 130.6, 128.8, 126.4, 123.2, 121.1, 118.4, 113.1, 112.6, 110.2, 107.8, 100.6, 54.6, 30.2, 15.4.

HRMS (ESI) calculated for C₂₈H₂₃N₂O₅S : [M + H]⁺ 499.13276; found 499.13264

1-(benzo[d][1,3]dioxol-5-yl)-N-(5-(4-methoxybenzoyl)-4-(4-methoxyphenyl)thiazol-2-yl)cyclopropane-1-carboxamide (70)

Compound **70** (13.5 mg, 26%) was obtained from (2-amino-4-(4-methoxyphenyl)thiazol-5-yl)(4-methoxyphenyl)methanone (34.0 mg, 0.1 mmol) and benzo[1,3]dioxol-5-yl-cyclopropanecarboxylic acid (20.6 mg, 0.1 mmol) in the same manner as described for compound **69**.

¹H NMR (200 MHz, DMSO-d₆): δ 11.91 (s, 1H, broad, NH); 7.53-6.72 (m, 11H, arom); 6.02 (s, 2H, OCH₂O); 3.62 (s, 3H, OCH₃); 3.57 (s, 3H, OCH₃); 1.64-1.42 (m, 2H, cyclopr); 1.39-1.10 (m, 2H, cyclopr).

¹³C NMR (50 MHz, DMSO-d₆): δ 186.4, 172.2, 159.7, 159.1, 158.3, 153.7, 146.8, 146.3, 138.6, 135.1, 131.7, 128.8, 126.2, 124.5, 123.2, 121.3, 118.3, 113.8, 112.6, 110.2, 107.8, 100.6, 54.7, 30.2, 15.4.

HRMS (ESI) calculated for C₂₉H₂₅N₂O₆S : [M + H]⁺ 529.14332; found 529.14552

1-(benzo[d][1,3]dioxol-5-yl)-N-(4-(4-methoxyphenyl)-5-(4(trifluoromethoxy)benzoyl)thiazol-2-yl)cyclopropane-1-carboxamide (71)

Compound **71** (10 mg, 17%) was obtained from (2-amino-4-(4-methoxyphenyl)thiazol-5-yl)(4-(trifluoromethoxy)phenyl)methanone (39.4 mg, 0.1 mmol) and benzo[1,3]dioxol-5-yl-cyclopropanecarboxylic acid (20.6 mg, 0.1 mmol) in the same manner as described for compound **69**.

¹H NMR (200 MHz, DMSO-d₆): δ 12.01 (s, 1H, broad, NH); 7.76-6.82 (m, 11H, arom); 6.03 (s, 2H, OCH₂O); 3.66 (s, 3H, OCH₃); 1.65-1.40 (m, 2H, cyclopr); 1.37-1.08 (m, 2H, cyclopr).

^{13}C NMR (50 MHz, DMSO- d_6): δ 188.1, 172.3, 159.2, 153.4, 146.8, 146.3, 144.6, 139.9, 133.5, 131.8, 131.4, 129.2, 128.1, 126.2, 123.9, 123.2, 122.7, 121.1, 118.4, 112.9, 110.2, 107.8, 100.6, 54.6, 30.2, 15.4.

HRMS (ESI) calculated for $\text{C}_{29}\text{H}_{22}\text{F}_3\text{N}_2\text{O}_6\text{S}$: $[\text{M} + \text{H}]^+$ 583.11506; found 583.11454

1-(benzo[d][1,3]dioxol-5-yl)-N-(4-(4-methoxyphenyl)-5-(4-(methylthio)benzoyl)thiazol-2-yl)cyclopropane-1-carboxamide (72)

Compound **72** (14.7 mg, 27%) was obtained from (2-amino-4-(4-methoxyphenyl)thiazol-5-yl)(4-(methylthio)phenyl)methanone (0.1 mmol, 35.6 mg) and benzo[1,3]dioxol-5-yl-cyclopropanecarboxylic acid (20.6 mg, 0.1 mmol) in the same manner as described for compound **69**.

^1H NMR (200 MHz, DMSO- d_6): δ 11.84 (s, 1H, broad, NH); 7.59-6.69 (m, 11H, arom); 6.02 (s, 2H, OCH $_2$ O); 3.68 (s, 3H, OCH $_3$); 2.45 (s, 3H, SCH $_3$); 1.62-1.46 (m, 2H, cyclopr); 1.35-1.14 (m, 2H, cyclopr).

^{13}C NMR (50 MHz, DMSO- d_6): δ 187.7, 172.2, 159.2, 159.1, 153.1, 146.8, 146.3, 144.4, 133.3, 131.8, 130.4, 129.2, 126.1, 124.0, 123.2, 122.8, 112.9, 110.2, 107.8, 100.6, 54.7, 30.2, 15.4, 13.5.

HRMS (ESI) calculated for $\text{C}_{29}\text{H}_{25}\text{N}_2\text{O}_5\text{S}_2$: $[\text{M} + \text{H}]^+$ 545.12048; found 545.11966

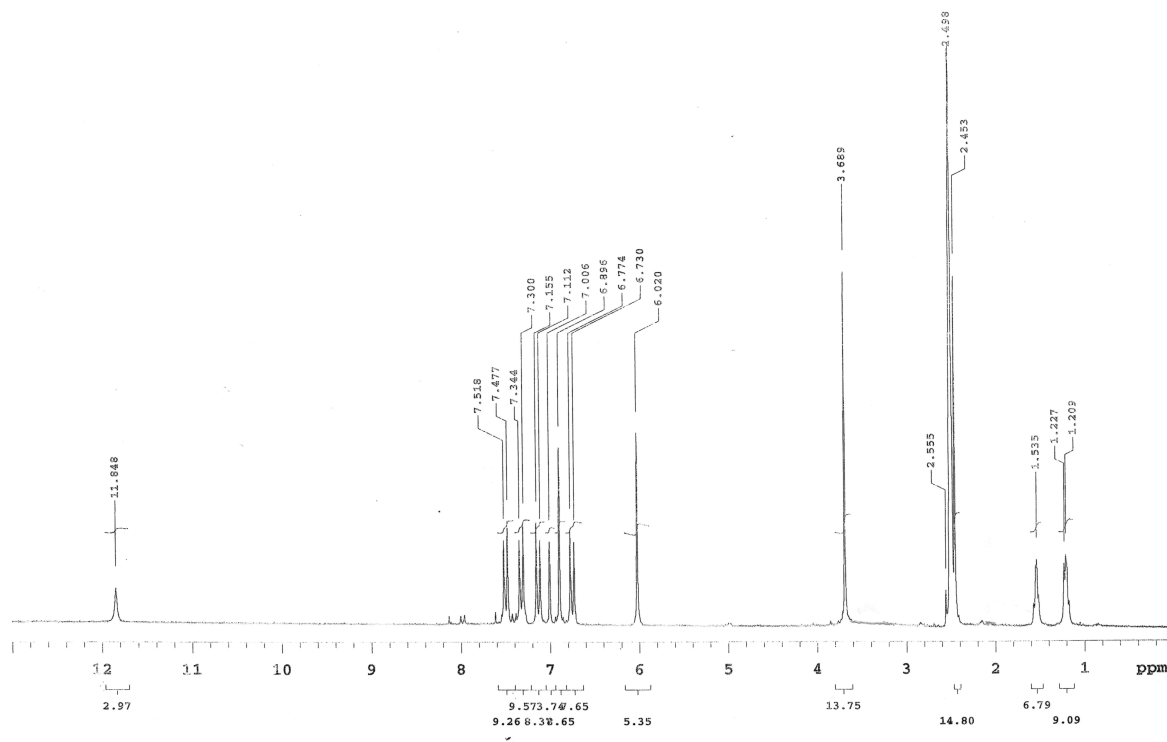


Figure 49. ^1H NMR spectra of compound **72**.

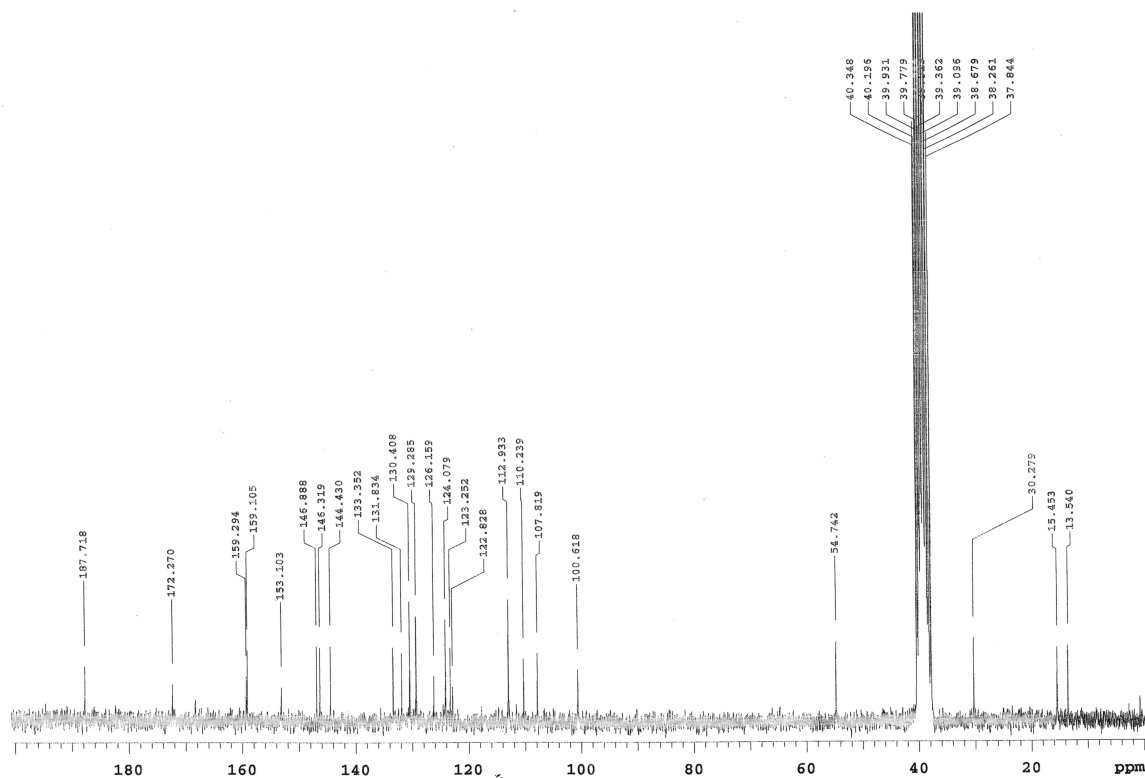


Figure 50. ¹³C NMR spectra of compound **72**.

N-(5-([1,1'-biphenyl]-4-carbonyl)-4-(4-methoxyphenyl)thiazol-2-yl)-1-(benzo[*d*][1,3]dioxol-5-yl)cyclopropane-1-carboxamide (**73**)

Compound **73** (13.2 mg, 23%) was obtained from [1,1'-biphenyl]-4-yl(2-amino-4-(4-methoxyphenyl)thiazol-5-yl)methanone (38.0 mg, 0.1 mmol) and benzo[1,3]dioxol-5-yl-cyclopropanecarboxylic acid (20.6 mg, 0.1 mmol) in the same manner as described for compound **69**.

¹H NMR (200 MHz, DMSO-*d*₆): δ 11.91 (s, 1H, broad, NH); 7.86-6.65 (m, 16H, arom); 6.03 (s, 2H, OCH₂O); 3.64 (s, 3H, OCH₃); 1.62-1.46 (m, 2H, cyclopr); 1.34-1.07 (m, 2H, cyclopr).

¹³C NMR (50 MHz, DMSO-*d*₆): δ 188.3, 172.3, 159.6, 159.1, 153.9, 146.9, 146.3, 143.3, 138.5, 136.2, 131.8, 130.5, 129.3, 128.6, 127.9, 126.4, 126.2, 125.8, 123.2, 112.8, 110.2, 107.8, 100.6, 54.6, 30.2, 15.5.

HRMS (ESI) calculated for C₃₄H₂₇N₂O₅S : [M + H]⁺ 575.16405; found 575.16323

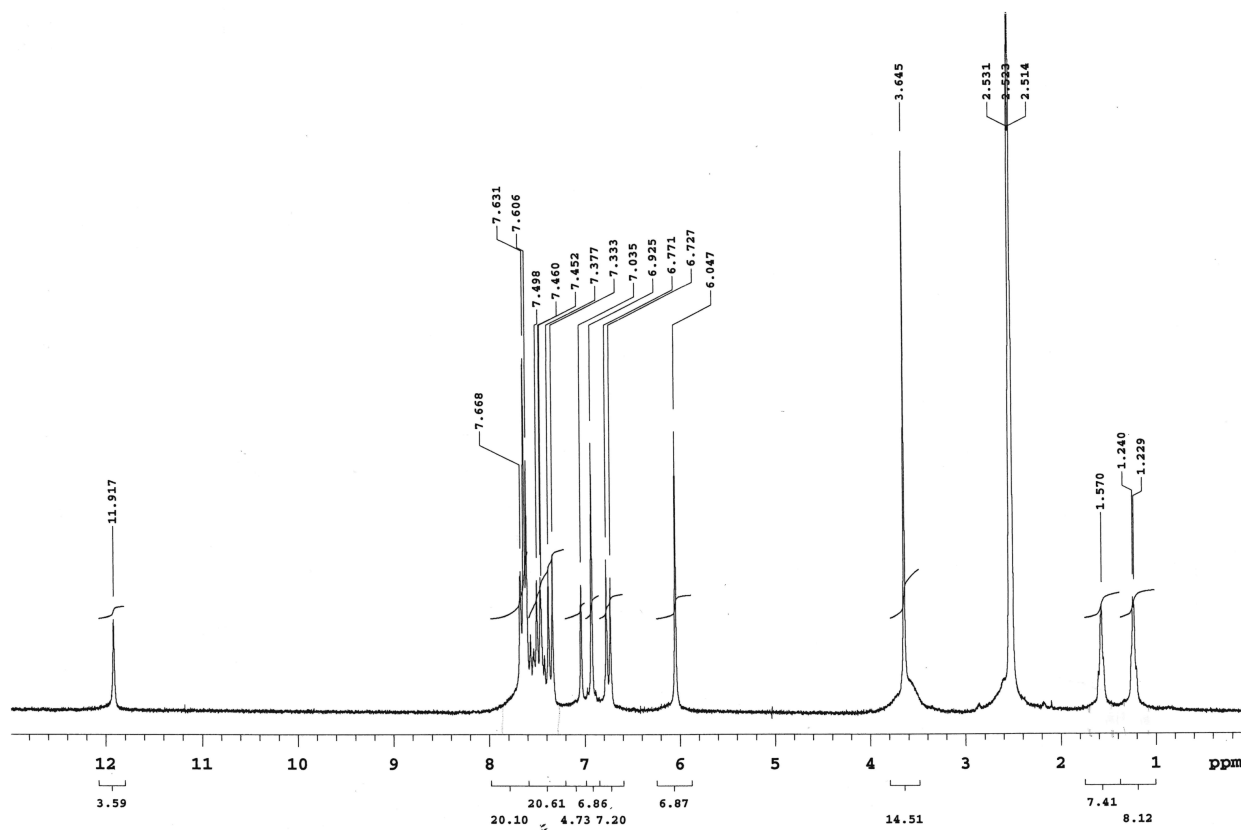


Figure 51. ^1H NMR of compound 73.

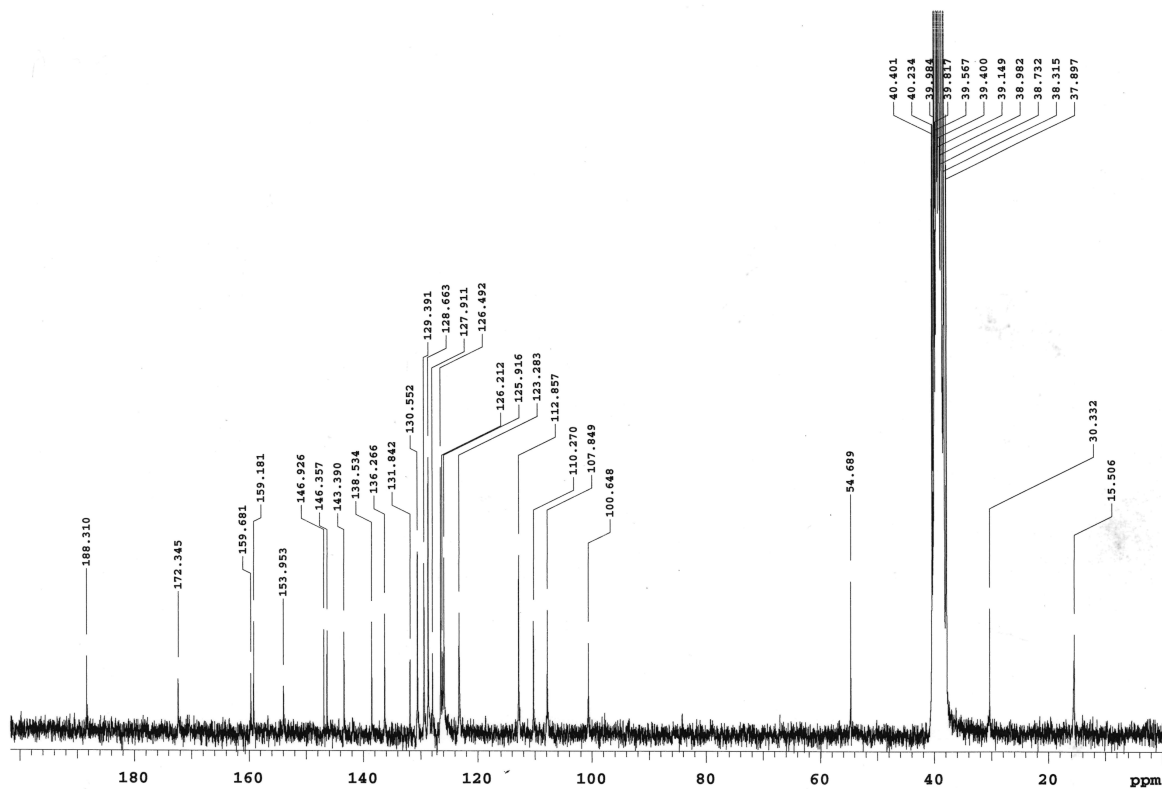


Figure 52. ^{13}C NMR spectra of compound 73.

1-(benzo[d][1,3]dioxol-5-yl)-N-(4-(4-methoxyphenyl)-5-(4-(pyrrolidin-1-yl)benzoyl)thiazol-2-yl)cyclopropane-1-carboxamide (74)

Compound **74** (11.4 mg, 20%) was obtained from (2-amino-4-(4-methoxyphenyl)thiazol-5-yl)(4-(pyrrolidin-1-yl)phenyl)methanone (38.0 mg, 0.1 mmol) and benzo[1,3]dioxol-5-yl-cyclopropanecarboxylic acid (20.6 mg, 0.1 mmol) in the same manner as described for compound **69**. ¹H NMR (200 MHz, DMSO-d₆): δ 11.64 (s, 1H, broad, NH); 7.81-6.37 (m, 11H, arom); 6.04 (s, 2H, OCH₂O); 3.72 (s, 3H, OCH₃); 3.56-3.19 (m, 4H, pyr); 2.18-1.85 (m, 4H, pyr); 1.76-1.12 (m, 6H, 2h pyr + 4H, cyclopr).

¹³C NMR (50 MHz, DMSO-d₆): δ 186.1, 171.9, 158.7, 157.5, 150.4, 149.4, 146.9, 146.3, 131.9, 131.5, 129.7, 126.5, 123.5, 123.2, 122.7, 113.1, 110.3, 107.8, 100.6, 54.7, 46.9, 30.2, 24.4., 15.3.

HRMS (ESI) calculated for C₃₂H₃₀N₃O₅S : [M + H]⁺ 568.19060; found 568.18943

1-(benzo[d][1,3]dioxol-5-yl)-N-(5-(3-methoxybenzoyl)-4-(4-methoxyphenyl)thiazol-2-yl)cyclopropane-1-carboxamide (75)

Compound **75** (22.7 mg, 43%) was obtained from (2-amino-4-(4-methoxyphenyl)thiazol-5-yl)(3-methoxyphenyl)methanone (34.0 mg, 0.1 mmol) and benzo[1,3]dioxol-5-yl-cyclopropanecarboxylic acid (20.6 mg, 0.1 mmol) in the same manner as described for compound **69**.

¹H NMR (200 MHz, DMSO-d₆): δ 11.86 (s, 1H, broad, NH); 7.30-6.61 (m, 11H, arom); 6.01 (s, 2H, OCH₂O); 3.67 (s, 3H, OCH₃); 3.61 (s, 3H, OCH₃); 1.60-1.42 (m, 2H, cyclopr); 1.28-1.04 (m, 2H, cyclopr).

¹³C NMR (50 MHz, DMSO-d₆): δ 188.4, 172.3, 159.7, 159.1, 158.3, 153.9, 146.8, 146.3, 138.6, 131.8, 130.5, 128.9, 126.2, 123.2, 123.1, 121.0, 118.3, 113.0, 112.7, 110.2, 107.8, 100.6, 54.7, 30.2, 15.4.

HRMS (ESI) calculated for C₂₉H₂₅N₂O₆S : [M + H]⁺ 529.14332; found 529.14276

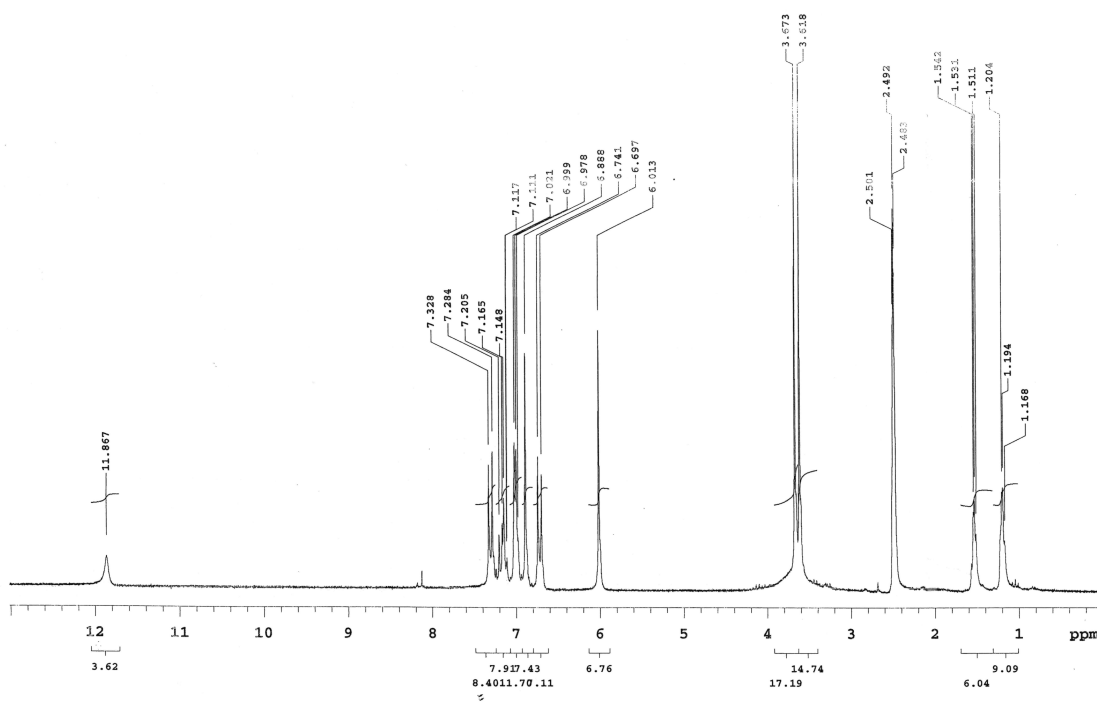


Figure 53. ^1H NMR spectra of compound 75.

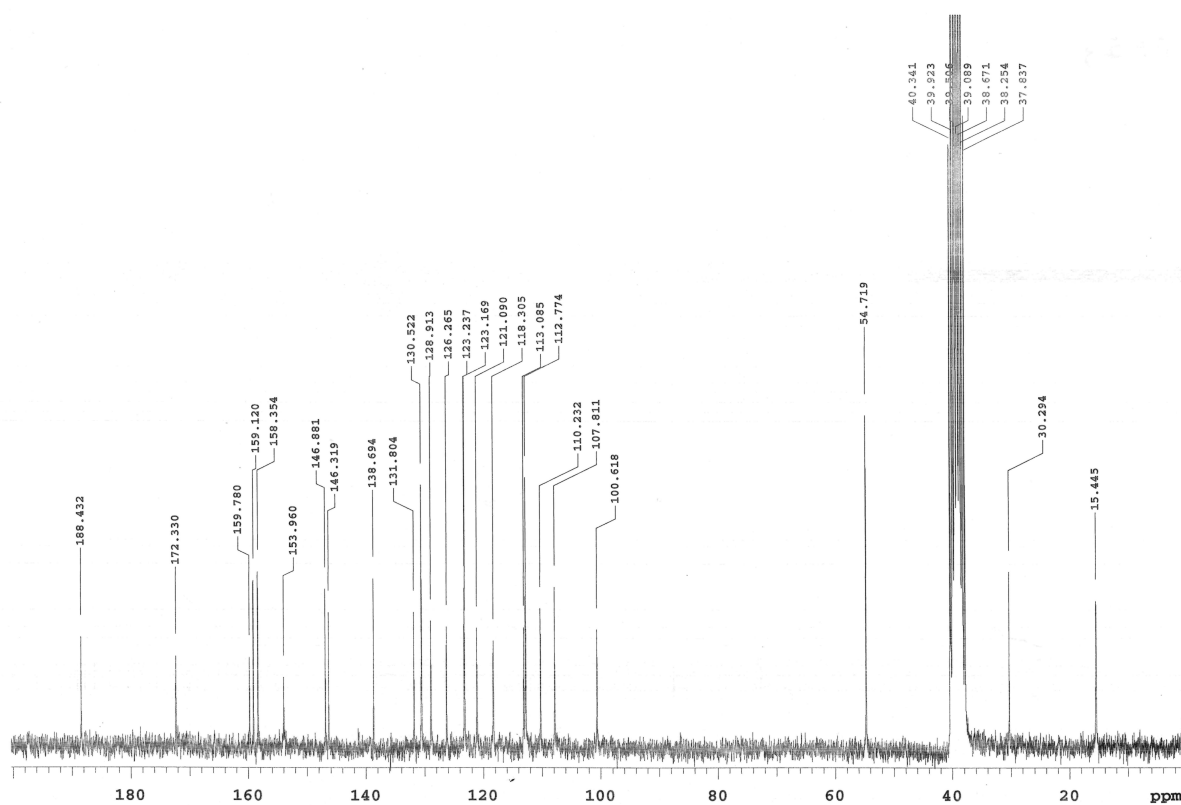


Figure 54. ^{13}C NMR of compound 75.

1-(benzo[d][1,3]dioxol-5-yl)-N-(5-(4-methoxybenzoyl)-4-(3-methoxyphenyl)thiazol-2-yl)cyclopropane-1-carboxamide (76)

Ammonium thiocyanate (152.2 mg, 2 mmol) was added to a solution of 3-methoxybenzoyl chloride (141.0 μ L, 1 mmol) in acetone (1.5 mL) and the mixture was stirred at $T = 0^{\circ}\text{C}$ for 2 hours.

To the suspension was added bis(4-methoxybenzyl)amine (308.0 mg, 1.2 mmol) and the reaction was stirred at room temperature. After completion, acetone was removed in vacuum; the residue was added to EtOAc and water. The organic phases were washed with H_2O (3 x 3 mL), then dried over anhydrous Na_2SO_4 , filtered and evaporated to afford N-(bis(4-methoxybenzyl)carbamothioyl)-3-methoxybenzamide (347.0 mg, 77%) as yellow oil, that was used in the next step without further purification.

2-bromo-1-(4-methoxyphenyl)ethan-1-one (45.0 mg, 0.2 mmol) was dissolved in N,N-DMF and N-(bis(4-methoxybenzyl)carbamothioyl)-3-methoxybenzamide (90.1 mg, 0.2 mmol) was added; the reaction was heated to 85°C for 3 hours. The mixture was cooled to room temperature and was extracted by ethyl acetate and washed with H_2O (3 x 3 mL). The organic layer was dried over anhydrous Na_2SO_4 and filtered. Ethyl acetate was removed by rotavapor. The compound was resuspended in TFA (about 5 mL) and heated to 100°C until complete deprotection (36 h). Most of TFA was evaporated in vacuum, then, a solution of NaHCO_3 1N was added to the residue to neutralize the acid and the product was extracted with EtOAc (3 x 5 mL). The organic phase was washed with brine, dried over anhydrous Na_2SO_4 and filtered. After concentration, (2-amino-4-(3-methoxyphenyl)thiazol-5-yl)(4-methoxyphenyl)methanone was crystallized in acetonitrile (47.2 mg, 69%).

Benzo[1,3]dioxol-5-yl-cyclopropanecarboxylic acid (21.0 mg, 0.1 mmol) was dissolved in anhydrous N,N-DMF (1 mL) with DIPEA (38 μ L, 0.1 mmol) and HATU (34.2 mg, 0.09 mmol). After 5 min, a solution of (2-amino-4-(3-methoxyphenyl)thiazol-5-yl)(4-methoxyphenyl)methanone (35.0 mg, 0.11 mmol) was added portion wise to the mixture. The reaction was heated to 50°C and stirred until completeness (24 h). The mixture was purified by preparative HPLC to afford the title compound with purity higher than 95%, as confirmed by HPLC-MS. (13.5 mg, 26%).

^1H NMR (200 MHz, DMSO- d_6): δ 11.85 (s, 1H, broad, NH); 7.68-6.86 (m, 11H, arom); 6.01 (s, 2H, OCH_2O); 3.61 (s, 3H, OCH_3); 3.58 (s, 3H, OCH_3); 1.67-1.43 (m, 2H, cyclopr); 1.39-1.11 (m, 2H, cyclopr).

^{13}C NMR (50 MHz, DMSO- d_6): δ 187.8, 172.4, 159.7, 159.2, 158.4, 153.9, 146.8, 146.3, 138.5, 131.8, 130.5, 128.9, 126.3, 123.2, 121.2, 118.4, 113.2, 112.7, 110.2, 107.8, 100.6, 54.7, 30.2, 15.4.

HRMS (ESI) calculated for $\text{C}_{29}\text{H}_{25}\text{N}_2\text{O}_6\text{S}$: $[\text{M} + \text{H}]^+$ 529.14332; found 529.14262

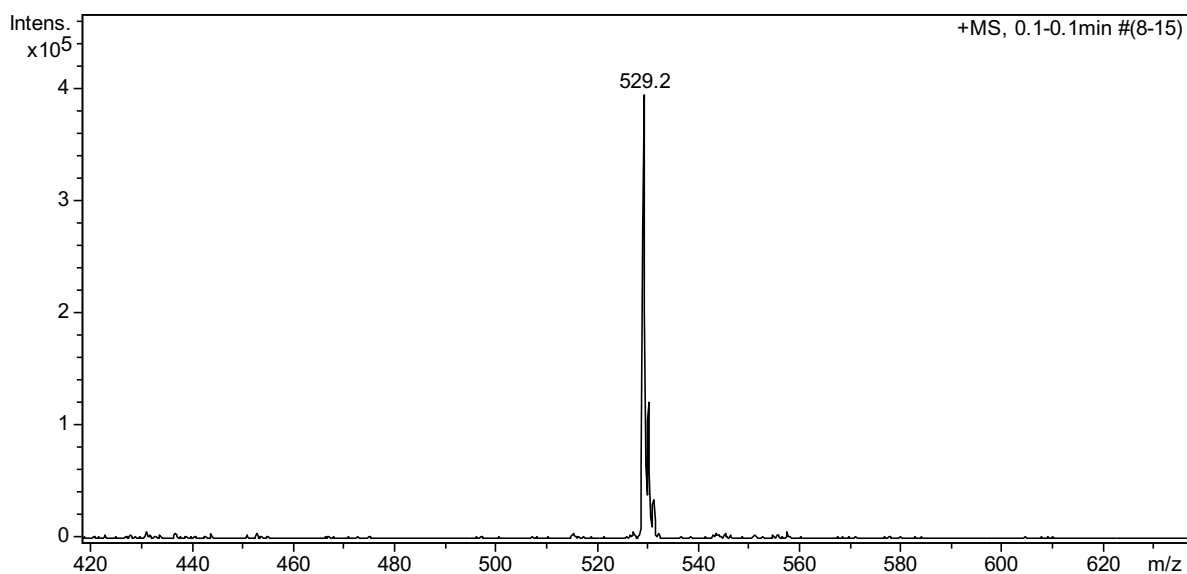


Figure 55. MS spectra of compound **76**.

1-(benzo[d][1,3]dioxol-5-yl)-N-(5-(3-methoxybenzoyl)-4-(3-methoxyphenyl)thiazol-2-yl)cyclopropane-1-carboxamide (77)

Compound **77** (22.3 mg; 42%) was obtained from (2-amino-4-(3-methoxyphenyl)thiazol-5-yl)(3-methoxyphenyl)methanone (34.0 mg, 0.1 mmol) and benzo[1,3]dioxol-5-yl-cyclopropanecarboxylic acid (20.6 mg, 0.1 mmol) in the same manner as described for compound **76**.

¹H NMR (200 MHz, DMSO-d₆): δ 11.93 (s, 1H, broad, NH); 7.28-6.71 (m, 11H, arom); 6.01 (s, 2H, OCH₂O); 3.58 (s, 3H, OCH₃); 3.56 (s, 3H, OCH₃); 1.65-1.41 (m, 2H, cyclopr); 1.38-1.12 (m, 2H, cyclopr).

¹³C NMR (50 MHz, DMSO-d₆): δ 188.5, 172.4, 159.9, 158.2, 153.7, 146.8, 146.3, 138.5, 135.1, 131.7, 128.8, 128.4, 124.6, 123.2, 121.4, 121.0, 118.5, 114.6, 113.9, 112.9, 110.2, 107.8, 100.6, 54.6, 54.5, 30.2, 15.4

HRMS (ESI) calculated for C₂₉H₂₅N₂O₆S : [M + H]⁺ 529.14332; found 529.14270

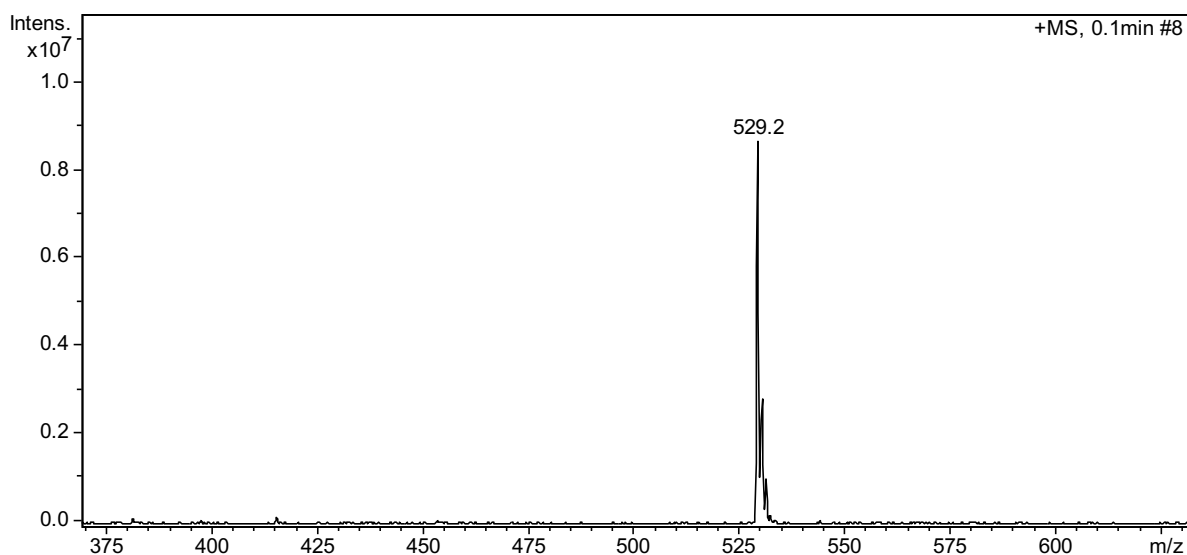


Figure 56. MS spectra of compound **77**.

1-(benzo[d][1,3]dioxol-5-yl)-N-(4-(3-methoxyphenyl)-5-(4-(methylthio)benzoyl)thiazol-2-yl)cyclopropane-1-carboxamide (78)

Compound **78** (18.5 mg, 34%) was obtained from (2-amino-4-(3-methoxyphenyl)thiazol-5-yl)(4-(methylthio)phenyl)methanone (35.6 mg, 0.1 mmol) and benzo[1,3]dioxol-5-yl-cyclopropanecarboxylic acid (20.6 mg, 0.1 mmol) in the same manner as described for compound **76**.

¹H NMR (200 MHz, DMSO-d₆): δ 11.91 (s, 1H, broad, NH); 7.50-6.73 (m, 11H, arom); 6.01 (s, 2H, OCH₂O); 3.60 (s, 3H, OCH₃); 2.44 (s, 3H, SCH₃); 1.62-1.41 (m, 2H, cyclopr); 1.36-1.10 (m, 2H, cyclopr).

¹³C NMR (50 MHz, DMSO-d₆): δ 187.7, 172.3, 159.3, 158.2, 152.6, 146.8, 146.3, 144.6, 134.9, 133.1, 131.8, 129.2, 128.6, 124.2, 123.2, 121.3, 114.6, 113.9, 110.2, 107.8, 100.6, 54.5, 30.2, 15.4, 13.5.

HRMS (ESI) calculated for C₂₉H₂₅N₂O₅S₂ : [M + H]⁺ 545.12048; found 545.11985

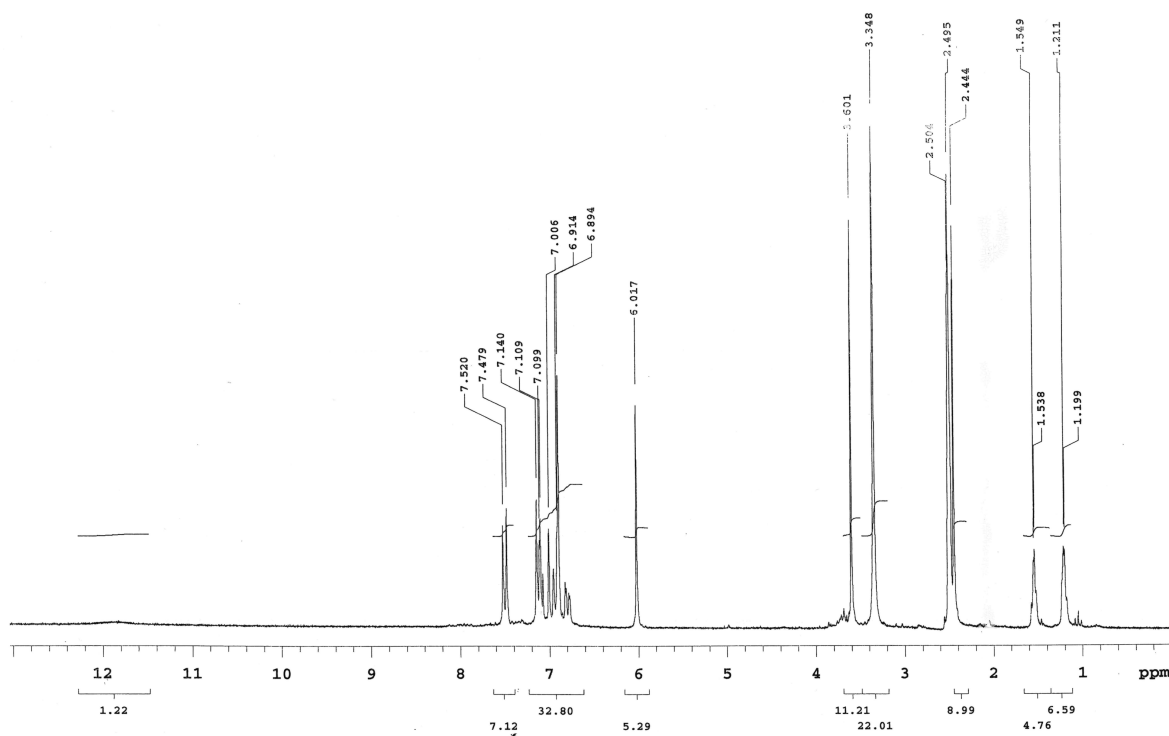


Figure 57. ^1H NMR spectra of compound 78.

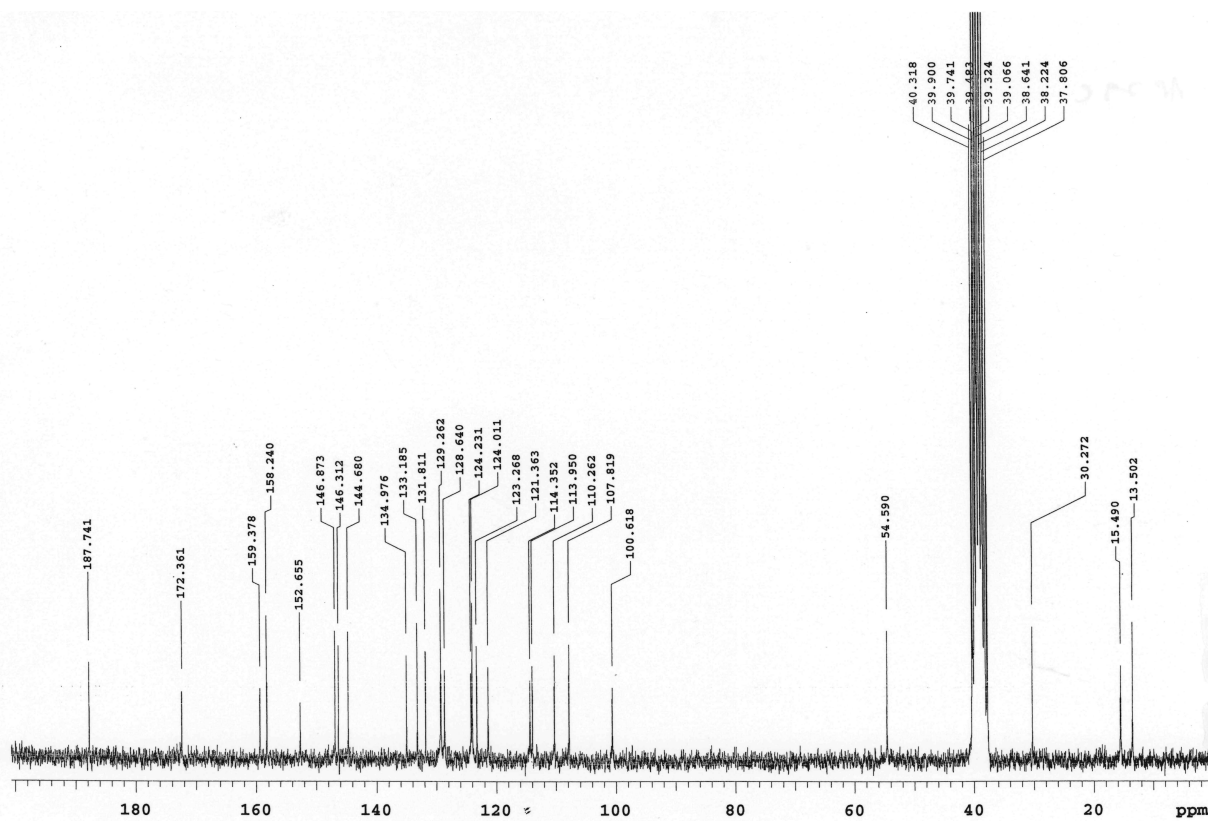


Figure 58. ^{13}C NMR spectra of compound 78.

N-(5-([1,1'-biphenyl]-4-carbonyl)-4-(3-methoxyphenyl)thiazol-2-yl)-1-(benzo[*d*][1,3]dioxol-5-yl)cyclopropane-1-carboxamide (**79**)

Compound **79** (12.7 mg, 22%) was obtained from [1,1'-biphenyl]-4-yl(2-amino-4-(3-methoxyphenyl)thiazol-5-yl)methanone (38.6 mg, 0.1 mmol) and benzo[1,3]dioxol-5-yl-cyclopropanecarboxylic acid ((20.6 mg, 0.1 mmol) in the same manner as described for compound **76**.

¹H NMR (200 MHz, DMSO-*d*₆): δ 11.82 (s, 1H, broad, NH); 7.88-6.69 (m, 16H, arom); 6.01 (s, 2H, OCH₂O); 3.59 (s, 3H, OCH₃); 1.68-1.40 (m, 2H, cyclopr); 1.38-1.12 (m, 2H, cyclopr).

¹³C NMR (50 MHz, DMSO-*d*₆): δ 188.2, 171.8, 159.7, 159.2, 152.7, 146.9, 146.3, 143.7, 138.4, 136.0, 131.8, 130.6, 129.4, 128.6, 127.9, 126.5, 126.2, 125.9, 123.6, 123.2, 110.2, 107.8, 100.6, 54.7, 30.3, 15.5.

HRMS (ESI) calculated for C₃₄H₂₇N₂O₅S : [M + H]⁺ 575.16405; found 575.16313

1-(benzo[*d*][1,3]dioxol-5-yl)-*N*-(4-(3-methoxyphenyl)-5-(4-(pyrrolidin-1-yl)benzoyl)thiazol-2-yl)cyclopropane-1-carboxamide (**80**)

Compound **80** (11.4 mg, 20%) was obtained from (2-amino-4-(3-methoxyphenyl)thiazol-5-yl)(4-(pyrrolidin-1-yl)phenyl)methanone (38.0 mg, 0.1 mmol) and benzo[1,3]dioxol-5-yl-cyclopropanecarboxylic acid (20.6 mg, 0.1 mmol) in the same manner as described for compound **76**.

¹H NMR (200 MHz, DMSO-*d*₆): δ 11.78 (s, 1H, broad, NH); 7.80-6.48 (m, 11H, arom); 6.02 (s, 2H, OCH₂O); 3.60 (s, 3H, OCH₃); 3.51-3.15 (m, 4H, pyr); 2.22-1.86 (m, 4H, pyr); 1.72-1.15 (m, 6H, 2H pyr + 4H, cyclopr).

¹³C NMR (50 MHz, DMSO-*d*₆): δ 186.3, 172.3, 158.7, 157.4, 150.6, 149.4, 146.8, 146.3, 131.8, 131.4, 129.6, 126.5, 123.5, 123.1, 122.7, 113.0, 110.3, 107.8, 100.6, 54.6, 46.8, 30.2, 24.4, 15.3.

HRMS (ESI) calculated for C₃₂H₃₀N₃O₅S : [M + H]⁺ 568.19060; found 568.18983

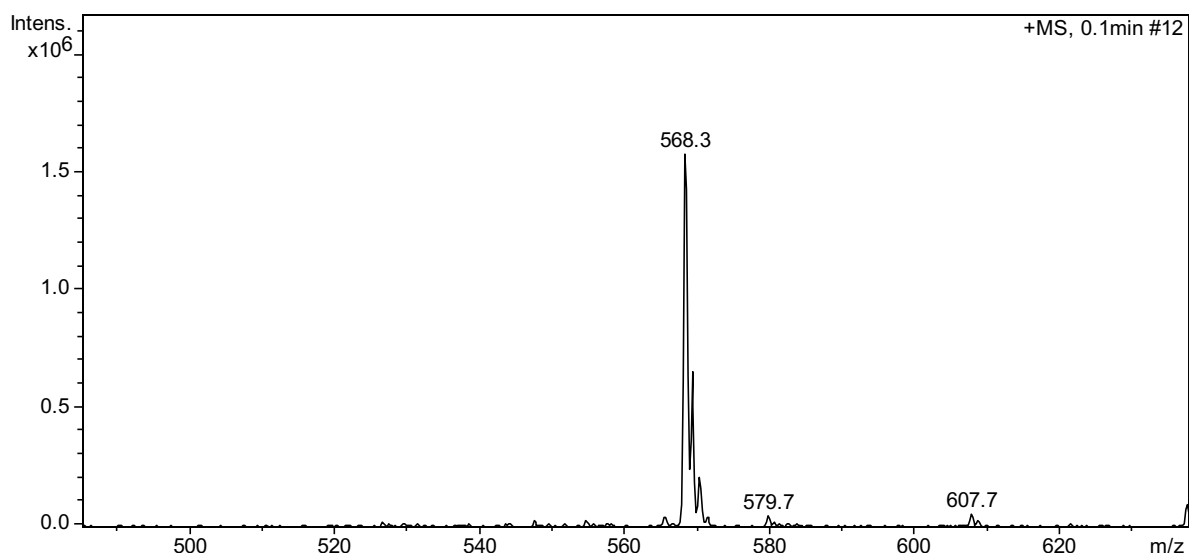


Figure 59. MS spectra of compound **80**.

1-(benzo[d][1,3]dioxol-5-yl)-N-(4-(3-methoxyphenyl)-5-(4-(trifluoromethoxy)benzoyl)thiazol-2-yl)cyclopropane-1-carboxamide (81)

Compound **81** (12.0 mg, 21%) was obtained from ((2-amino-4-(3-methoxyphenyl)thiazol-5-yl)(4-(trifluoromethoxy)phenyl)methanone (39.0 mg, 0.1 mmol) and benzo[1,3]dioxol-5-yl-cyclopropanecarboxylic acid ((20.6 mg, 0.1 mmol) in the same manner as described for compound **76**.

¹H NMR (200 MHz, DMSO-d₆): δ 12.00 (s, 1H, broad, NH); 7.74-6.82 (m, 11H, arom); 6.02 (s, 2H, OCH₂O); 3.61 (s, 3H, OCH₃); 1.70-1.44 (m, 2H, cyclopr); 1.42-1.11 (m, 2H, cyclopr).

¹³C NMR (50 MHz, DMSO-d₆): δ 187.6, 172.3, 159.6, 153.5, 146.8, 146.3, 144.6, 140.1, 133.7, 131.8, 131.3, 129.3, 128.3, 126.2, 123.4, 123.2, 122.9, 122.6, 121.1, 118.3, 112.9, 110.2, 107.8, 100.6, 54.7, 30.2, 15.4.

HRMS (ESI) calculated for C₂₉H₂₂F₃N₂O₆S : [M + H]⁺ 583.11506; found 583.11445

1-(benzo[d][1,3]dioxol-5-yl)-N-(5-(4-methoxybenzoyl)-4-(2-methoxyphenyl)thiazol-2-yl)cyclopropanecarboxamide (82)

2-methoxybenzoyl chloride was synthesized as previously described [40] with some modification. Briefly, to a solution of 2-methoxybenzoic acid (152 mg, 1 mmol) in anhydrous dichloromethane (DCM) (2 mL) were added few drops of N,N -DMF and thionyl chloride (198 μL, 2.5 mmol) at T= 0°C. The reaction was stirred at T= 80 °C for 2 hours and then at T= 50 °C overnight. The reaction mixture was concentrated in vacuum to afford the crude 2-methoxybenzoyl chloride, controlled with GC-MS, as yellow oil (150 mg, 88%). A mixture of 2-methoxybenzoyl chloride (68 mg, 0.4 mmol)

in acetone (1 mL) and ammonium thiocyanate (60.8 mg, 0.8 mmol) was stirred for about 2 h, at T = 0°C.

Bis(4-methoxybenzyl)amine (128.5 mg, 0.5 mmol) was added to the reaction and the resulting mixture was stirred for 3 h at room temperature. Acetone was removed by rotavapor and EtOAc and H₂O were added to the residue. The organic phase was washed with water (3 x 3.5 mL), dried over anhydrous Na₂SO₄, filtered and concentrated under reduced pressure to afford N-(bis(4-methoxybenzyl)carbamothioyl)-2-methoxybenzamide (150.0 mg, 83%), a yellow oil, that was used in the next step without further purification.

To a solution of 2-bromo-1-(4-methoxyphenyl)ethanone (56.0 mg, 0.2 mmol) in N,N - DMF was added portionwise N-(bis(4-methoxybenzyl)carbamothioyl)-2-methoxybenzamide (50.0 mg, 0.2 mmol) and the resulting mixture was stirred at T = 85°C for 3 h. At room temperature, to the mixture were added EtOAc and H₂O. The organic layers were washed with brine, dried over anhydrous Na₂SO₄, filtered and concentrated. The residue was stirred in TFA (4 mL) and heated to 100°C for 48 hours. Most of TFA was removed in vacuum and the residue was neutralized using a solution of NaHCO₃ 1N. The extraction of the compound was performed with EtOAc (3 x 5 mL) and then the layers were washed with brine, dried over anhydrous Na₂SO₄ and filtered. After concentration, (2-amino-4-(2-methoxyphenyl)thiazol-5-yl)(4-methoxyphenyl)methanone was used in the next step without purification (45.0 mg, 66%).

Benzo [1,3] dioxol-5-yl-cyclopropanecarboxylic acid (21.0 mg, 0.1 mmol), HATU (34.2 mg, 0.09 mmol) and DIPEA (38 µL, 0.1mmol) were dissolved in in 1 mL of anhydrous N,N - DMF.

After few minutes a solution of (2-amino-4-(2-methoxyphenyl)thiazol-5-yl)(4-methoxyphenyl)methanone (34 mg, 0.1 mmol) was added portionwise to the reaction and the resulting mixture was stirred at T = 50 °C (36 h). The purification was made by preparative HPLC. The peak of interest was concentrated to give the final product with purity of >95% as confirmed by HPLC-MS (12.0 mg, 23%).

¹H NMR (200 MHz, DMSO-d₆): δ 11.76 (s, 1H, broad, NH); 7.71-6.88 (m, 11H, arom); 6.02 (s, 2H, OCH₂O); 3.65 (s, 3H, OCH₃); 3.61 (s, 3H, OCH₃); 1.73-1.45 (m, 2H, cyclopr); 1.42-1.09 (m, 2H, cyclopr).

¹³C NMR (50 MHz, DMSO-d₆): δ 188.1, 171.7, 159.6, 159.2, 157.9, 153.8, 146.8, 146.2, 138.5, 131.8, 131.0, 128.9, 126.3, 123.5, 123.2, 121.1, 118.4, 113.2, 112.7, 110.2, 107.8, 54.7, 53.9, 30.2, 15.4.

HRMS (ESI) calculated for C₂₉H₂₅N₂O₆S : [M + H]⁺ 529.14332; found 529.14266

1-(benzo[d][1,3]dioxol-5-yl)-N-(4-(2-methoxyphenyl)-5-(4-(trifluoromethoxy)benzoyl)thiazol-2-yl)cyclopropanecarboxamide (83)

Compound **83** (15.1 mg, 26 %) was obtained from (2-amino-4-(2-methoxyphenyl)thiazol-5-yl)(4-(trifluoromethoxy)phenyl)methanone (39 mg, 0.1 mmol) and benzo [1,3]dioxol-5-yl-cyclopropanecarboxylic acid (20.6 mg, 0.1 mmol) in the same manner as described for compound **82**. ¹H NMR (200 MHz, DMSO-d₆): δ 11.92 (s, 1H, broad, NH); 7.75-6.91 (m, 11H, arom); 6.03 (s, 2H, OCH₂O); 3.66 (s, 3H, OCH₃); 1.68-1.42 (m, 2H, cyclopr); 1.40-1.13 (m, 2H, cyclopr).

¹³C NMR (50 MHz, DMSO-d₆): δ 187.2, 172.1, 159.5, 153.4, 146.8, 146.3, 144.5, 140.1, 133.6, 131.8, 131.2, 129.3, 128.1, 126.2, 123.3, 123.2, 122.7, 122.6, 121.1, 118.3, 112.9, 110.2, 107.8, 100.6, 54.7, 30.2, 15.5.

HRMS (ESI) calculated for C₂₉H₂₂F₃N₂O₆S : [M + H]⁺ 583.11506; found 583.11478

1-(benzo[d][1,3]dioxol-5-yl)-N-(4-(4-hydroxyphenyl)-5-(4-methoxybenzoyl)thiazol-2-yl)cyclopropane-1-carboxamide (84)

4-(benzyloxy)benzoyl chloride (246.0 mg, 1 mmol) was dissolved in acetone and at this solution was added ammonium thiocyanate (152.0 mg, 2 mmol) at T= 0°C. After two hours, bis(4-methoxybenzyl)amine (310.0 mg, 1.2 mmol), was added to the mixture and the reaction was stirred at room temperature. After completion of the reaction, as monitored by HPLC, acetone was removed by rotavapor and to the residue were added ethyl acetate (EtOAc) and H₂O. The organic layers were washed with water (3 x 3.5 mL), dried over anhydrous Na₂SO₄ and filtered. Ethyl acetate was removed under reduced pressure to give 4-(benzyloxy)-N-(bis(4-methoxybenzyl)carbamothioyl)benzamide (420.0 mg, 80%) as yellow oil, that was used in the next step without further purification.

2-bromo-1-(4-methoxyphenyl)ethan-1-one (45.5 mg, 0.2 mmol) was dissolved in N,N- DMF and 4-(benzyloxy)-N-(bis(4-methoxybenzyl)carbamothioyl)benzamide (105.2 mg, 0.2 mmol) was added; the reaction was heated to 85 °C for 2 hours. The mixture was cooled to room temperature and then, ethyl acetate and water were added. The organic phase was washed with brine, dried over anhydrous Na₂SO₄ and filtered. After removing solvent in vacuum, the product obtained was resuspended in TFA (4 mL) and stirred at T = 100°C for 48 hours, to complete deprotection of both amine and hydroxy groups. Most of TFA was evaporated by using rotavapor and a solution of NaHCO₃ 1N was added to neutralize the residue. Then the mixture was extracted by ethyl acetate (3 x 5 mL), the organic phase was dried over anhydrous Na₂SO₄, filtered and concentrated to afford (2-amino-4-(4-hydroxyphenyl)thiazol-5-yl)(4-methoxyphenyl)methanone, that was crystallized in acetonitrile to give a pure product (47.2 mg, 72%).

A solution of benzo[1,3]dioxol-5-yl-cyclopropanecarboxylic acid (21.0 mg, 0.1 mmol), HATU (34.2 mg, 0.09 mmol) and DIPEA (38 μ L, 0.1 mmol) was dissolved in anhydrous N,N - DMF and stirred at room temperature for 5 min. Then, (2-amino-4-(4-hydroxyphenyl)thiazol-5-yl)(4-methoxyphenyl)methanone (33.0 mg, 0.1 mmol) in anhydrous N,N - DMF was added and the mixture was heated to 50 °C for 24 h.

The mixture was extracted in ethyl acetate and washed with water (3 x 5 mL). Then, the organic phase was dried over anhydrous Na₂SO₄, filtered and concentrated. The residue was resuspended in a solution of ACN (1 mL) and NaOH 10% at room temperature for 3 h, to hydrolase the undesired ester formed between the free hydroxy group and the benzo[1,3]dioxol-5-yl-cyclopropanecarboxylic acid. The solvent was removed by rotavapor, the residue was taken to acid pH with HCl 2N to give a precipitate that was washed three times with water.

Preparative HPLC was used to purify the final product and after concentration of the peak of interest, the product was obtained with a purity higher than 95% . The purity of the compound was determined by HPLC-MS . Then the product was lyophilised and afforded as a powder (12.5 mg, 24%).

1-(benzo[d][1,3]dioxol-5-yl)-N-(4-(4-hydroxyphenyl)-5-(4-(trifluoromethoxy)benzoyl)thiazol-2-yl)cyclopropane-1-carboxamide (85)

Compound **85** (15.1 mg, 26%) was obtained from (2-amino-4-(4-hydroxyphenyl)thiazol-5-yl)(4-(trifluoromethoxy)phenyl)methanone (38 mg, 0.1 mmol) and benzo [1,3]dioxol-5-yl-cyclopropanecarboxylic acid (20.6 mg, 0.1 mmol) in the same manner as described for compound **84**.

1-(benzo[d][1,3]dioxol-5-yl)-N-(4-(4-butoxyphenyl)-5-(4-methoxybenzoyl)thiazol-2-yl)cyclopropane-1-carboxamide (86)

A mixture of ammonium thiocyanate (152.2 mg, 2 mmol) and 4-butoxybenzoyl chloride (190.0 μ L, 1 mmol) in acetone (2.0 mL) was stirred at T = 0°C for 2 hours.

To the suspension was added bis(4-methoxybenzyl)amine (308.0 mg, 1.2 mmol) and the reaction was stirred at room temperature. After completion, acetone was removed in vacuum; the residue was added to EtOAc. The organic phases were washed with H₂O (3 x 3 mL), dried over anhydrous Na₂SO₄, filtered and evaporated to obtain N-(bis(4-methoxybenzyl)carbamothioyl)-4-butoxybenzamide (310.0 mg, 63%) as yellow oil, that was used in the next step without further purification.

2-bromo-1-(4-methoxyphenyl)ethan-1-one (45.0 mg, 0.2 mmol) was dissolved in N,N - DMF and N-(bis(4-methoxybenzyl)carbamothioyl)-4-butoxybenzamide (98.1 mg, 0.2 mmol), solved in N,N -

DMF, was added dropwise; the reaction was heated to 85°C for 3 hours. The mixture was cooled to room temperature and was extracted by ethyl acetate and washed with H₂O (3 x 3 mL). The organic layer was dried over anhydrous Na₂SO₄ and filtered. Ethyl acetate was removed by rotavapor. The compound was resuspended in TFA (about 5 mL) and heated to 100°C until complete deprotection (48 h). Most of TFA was evaporated in vacuum, then, a solution of NaHCO₃ 1N was added to the residue to neutralize the acid and the product was extracted with EtOAc (3 x 5 mL). The organic layer was washed with brine, dried over anhydrous Na₂SO₄ and filtered. After concentration, (2-amino-4-(4-butoxyphenyl)thiazol-5-yl)(4-methoxyphenyl)methanone was crystallized in acetonitrile (35.0 mg, 46%).

Benzo[1,3]dioxol-5-yl-cyclopropanecarboxylic acid (21.0 mg, 0.1 mmol) was dissolved in anhydrous N,N - DMF (1 mL) with DIPEA (38 µL, 0.1mmol) and HATU (34.2 mg, 0.09 mmol). After 5 min, a solution of (2-amino-4-(4-butoxyphenyl)thiazol-5-yl)(4-methoxyphenyl)methanone (35.0 mg, 0.09 mmol) was added portion wise to the mixture. The reaction was heated to 50 °C and stirred until completeness (24 h). The mixture was purified by preparative HPLC to afford the title compound with purity higher than 95%, as confirmed by HPLC-MS. (10.5 mg, 20%).

1-(benzo[d][1,3]dioxol-5-yl)-N-(4-(4-butoxyphenyl)-5-(4-(trifluoromethoxy)benzoyl)thiazol-2-yl)cyclopropane-1-carboxamide (87)

Compound **87** (13.0 mg, 21%) was obtained from (2-amino-4-(4-butoxyphenyl)thiazol-5-yl)(4-(trifluoromethoxy)phenyl)methanone (43.0 mg, 0.1mmol) and benzo [1,3]dioxol-5-yl-cyclopropanecarboxylic acid (20.6 mg, 0.1 mmol) in the same manner as described for compound **86**.

Methyl 4-(5-([1,1'-biphenyl]-4-carbonyl)-2-(1-(benzo[d][1,3]dioxol-5-yl)cyclopropane-1-carboxamido)thiazol-4-yl)benzoate (88)

Methyl 4-(chlorocarbonyl)benzoate (198.6 mg, 1 mmol) was dissolved in acetone (1 mL) and ammonium thiocyanate (152.2 mg, 2 mmol) was added at 0°C; the reaction was stirred for about 2 h, at this temperature.

Bis(4-methoxybenzyl)amine (308.4 mg, 1.2 mmol) was added to the reaction and the resulting mixture was stirred for 2 h, at room temperature. The mixture was concentrated under reduced pressure and the residue was diluted by water and extracted with EtOAc. The organic phase was dried over anhydrous Na₂SO₄ and filtered. After concentration, methyl 4-((bis(4-

methoxybenzyl)carbamothioyl)carbamoyl)benzoate was afforded (254.0 mg, 53%), as a yellow oil, that was used in the next step without further purification.

A solution of 1-([1,1'-biphenyl]-4-yl)-2-bromoethan-1-one (55.0 mg, 0.2 mmol) and methyl 4-((bis(4-methoxybenzyl)carbamothioyl)carbamoyl)benzoate (95.7 mg, 0.2 mmol) in N,N - DMF was stirred at T = 85°C. After 3 hours, the mixture was cooled to room temperature, diluted in water and extracted with EtOAc (3 x 5 mL). The organic layer was dried over anhydrous Na₂SO₄ and filtered. Solvent was removed by rotavapor and the residue was resuspended in TFA (4 mL) and heated to 100°C for 48 h. The reaction was concentrated by rotavapor and the residue was neutralized preparing a solution of NaHCO₃ 1N. The mixture was extracted with EtOAc (3 x 5 mL), the organic layers were dried over anhydrous Na₂SO₄ and filtered.

After concentration, methyl 4-(5-([1,1'-biphenyl]-4-carbonyl)-2-aminothiazol-4-yl)benzoate was crystallized in absolute ethanol (45.6 mg, 55%).

A mixture of benzo[1,3]dioxol-5-yl-cyclopropanecarboxylic acid (21.0 mg, 0.1 mmol), DIPEA (38 µL, 0.1 mmol) and HATU (34.6 mg, 0.09 mmol) was dissolved in anhydrous N,N - DMF.

After few minutes a solution of methyl 4-(5-([1,1'-biphenyl]-4-carbonyl)-2-aminothiazol-4-yl)benzoate (41.5 mg, 0.1 mmol) was added to the reaction and the resulting mixture was stirred at T = 50 °C for 42 hours. To purify the product, preparative HPLC was used and it allowed to obtain the title compound with purity higher than 95% as confirmed by HPLC-MS (12.7 mg, 21%).

¹H NMR (200 MHz, DMSO-d₆): δ 11.87 (s, 1H, broad, NH); 7.81-6.63 (m, 16H, arom); 6.02 (s, 2H, OCH₂O); 4.06 (s, 3H, CH₃O); 1.72-1.44 (m, 2H, cyclopr); 1.40-1.15 (m, 2H, cyclopr).

¹³C NMR (50 MHz, DMSO-d₆): δ 188.2, 172.3, 166.4, 159.6, 159.1, 153.4, 146.9, 146.3, 143.4, 138.5, 136.1, 131.8, 130.5, 129.2, 128.4, 127.9, 126.4, 125.9, 123.2, 121.2, 118.5, 112.8, 110.2, 107.8, 100.6, 52.5, 30.3, 15.5.

HRMS (ESI) calculated for C₃₅H₂₇N₂O₆S : [M + H]⁺ 603.15897; found 603.15834

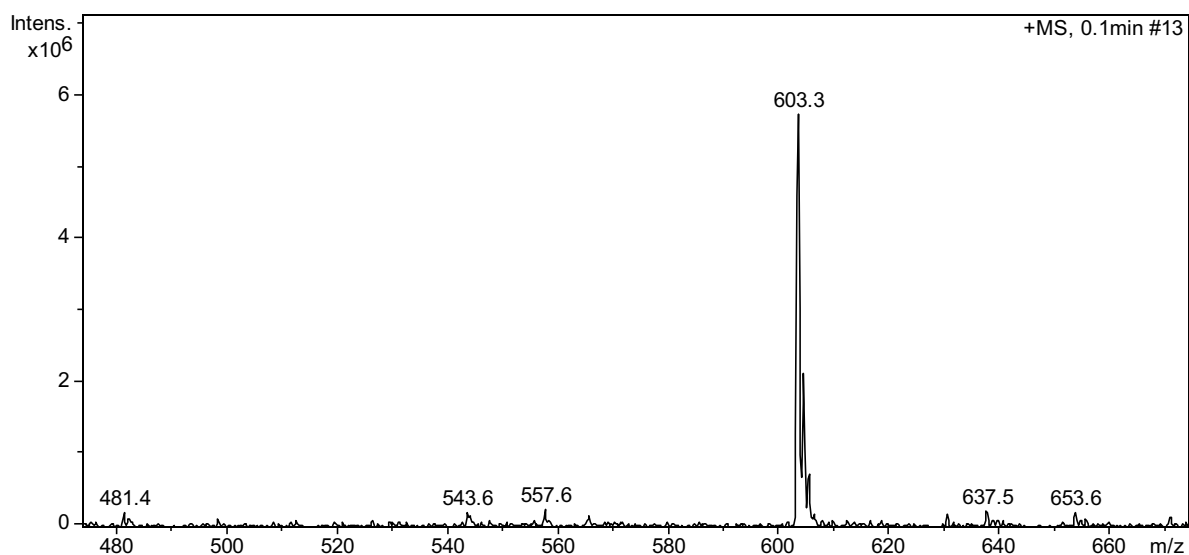


Figure 60. MS spectra of compound **88**.

N-(5-([1,1'-biphenyl]-4-carbonyl)-4-(4-(methylthio)phenyl)thiazol-2-yl)-1-(benzo[*d*][1,3]dioxol-5-yl)cyclopropane-1-carboxamide (**89**)

To a solution of 4-methylthiobenzoic acid (80 mg, 0.5 mmol) in anhydrous dichloromethane (DCM) (2 mL) were added few drops of N,N - DMF and thionyl chloride (91 μ L, 1.25 mmol) at T = 0°C. The reaction was stirred at T = 80 °C and then at T = 50°C overnight. The reaction mixture was concentrated in vacuum to afford crude 4-(methylthio)benzoyl chloride, controlled with GC-MS, as colourless oil (75 mg, 81%).

A mixture of 4-(methylthio)benzoyl chloride (75 mg, 0.4 mmol) in acetone (1 mL) and ammonium thiocyanate (60.8 mg, 0.8 mmol) was stirred for about 2 h, at T= 0°C.

Bis(4-methoxybenzyl)amine (128.5 mg, 0.5 mmol) was added to the reaction and the resulting mixture was stirred for 3 h at room temperature. The solvent was evaporated by rotavapor and the residue was diluted with water and extract with EtOAc (3 x 5 mL). The organic phase was dried over anhydrous Na₂SO₄ and filtered. Solvent was removed in vacuum to give N-(bis(4-methoxybenzyl)carbamothioyl)-4-(methylthio)benzamide (131.0 mg, 70%), a yellow oil, that was used in the next step without further purification.

To a solution of 1-([1,1'-biphenyl]-4-yl)-2-bromoethan-1-one (55.0 mg, 0.2 mmol) in N,N - DMF was added portionwise N-(bis(4-methoxybenzyl)carbamothioyl)-4-(methylthio)benzamide (93.3 mg, 0.2 mmol) and the resulting mixture was heated to 85°C. After 2 hours the reaction was completed as monitored by HPLC, cooled to room temperature and the mixture was partitioned between EtOAc and H₂O. The organic layer was washed with brine and dried over anhydrous Na₂SO₄. The organic phase was filtered and ethyl acetate was evaporated by rotavapor. The residue was resuspended in TFA (4 mL) and heated to 100°C for 48 hours. TFA was evaporated in vacuum and the residue was

neutralized with a solution of NaHCO₃ 1N. After having extracted with EtOAc (3 x 3 mL), the organic layers were dried over anhydrous Na₂SO₄ and filtered.

After concentration, [1,1'-biphenyl]-4-yl(2-amino-4-(4-(methylthio)phenyl)thiazol-5-yl)methanone was crystallized in acetonitrile (52.3 mg, 65%).

Benzo[1,3]dioxol-5-yl-cyclopropanecarboxylic acid (21.0 mg, 0.1 mmol), HATU (34.2 mg, 0.09 mmol) and DIPEA (38 μL, 0.1 mmol) were resuspended in anhydrous N,N - DMF (1 mL) at room temperature. After 5 min a solution of [1,1'-biphenyl]-4-yl(2-amino-4-(4-(methylthio)phenyl)thiazol-5-yl)methanone (40.0 mg, 0.1 mmol) was added and the resulting mixture was heated to 50 °C for 40 hours. Preparative HPLC was used to purify the final product. The peak of interest was concentrated to obtain a powder with a purity higher than >95%, as confirmed by HPLC-MS (13.0 mg, 22%).

¹H NMR (200 MHz, DMSO-d₆): δ 11.89 (s, 1H, broad, NH); 7.85-6.70 (m, 16H, arom); 6.04 (s, 2H, OCH₂O); 2.48 (s, 3H, SCH₃); 1.69-1.43 (m, 2H, cyclopr); 1.38-1.09 (m, 2H, cyclopr).

¹³C NMR (50 MHz, DMSO-d₆): δ 188.1, 172.1, 159.6, 159.2, 152.8, 146.9, 146.3, 144.2, 138.5, 135.9, 131.8, 130.7, 129.4, 128.6, 127.9, 126.2, 125.8, 123.2, 121.2, 118.4, 114.7, 112.8, 110.2, 107.8, 100.6, 30.3, 14.5.

HRMS (ESI) calculated for C₃₄H₂₇N₂O₄S₂ : [M + H]⁺ 591.141216; found 591.14013

N-(5-([1,1'-biphenyl]-4-carbonyl)-4-(pyridin-3-yl)thiazol-2-yl)-1-(benzo[d][1,3]dioxol-5-yl)cyclopropane-1-carboxamide (90)

A solution of nicotinoyl chloride (141.6 mg, 1 mmol) in acetone (1 mL) was cooled at T = 0°C and then ammonium thiocyanate (152.2 mg, 2 mmol) was added and stirred for 2 h, at this temperature. Bis(4-methoxybenzyl)amine (308.0 mg, 1.2 mmol) was added to the reaction and the resulting mixture was stirred for 2 h at room temperature. Acetone was evaporated under vacuum, the residue was diluted with water and extracted with EtOAc. The organic layers were dried over anhydrous MgSO₄ and filtered. After concentration, N-(bis(4-methoxybenzyl)carbamothioyl)nicotinamide (312.0 mg, 74%), was afforded as a yellow oil, that was used in the next step without further purification.

A solution of N-(bis(4-methoxybenzyl)carbamothioyl)nicotinamide (84.3 mg, 0.2 mmol) and 1-([1,1'-biphenyl]-4-yl)-2-bromoethan-1-one (55.0 mg, 0.2 mmol) in N,N - DMF was heated to 85°C until completes. To the mixture were added EtOAc and H₂O. The organic layer was dried over anhydrous Na₂SO₄ and filtered. After concentration, the residue was dissolved in TFA (4 mL) and heated to 100°C. After complete deprotection, TFA was removed by rotavapor and to the residue was added a solution of NaHCO₃ 1N to neutralize the residual acid. The compound was extracted with EtOAc (3 x 5 mL) and then, the organic phases were dried over anhydrous Na₂SO₄.

After concentration, [1,1'-biphenyl]-4-yl(2-amino-4-(pyridin-3-yl)thiazol-5-yl)methanone was crystallized in acetonitrile (48.6 mg, 68%).

[1,1'-biphenyl]-4-yl(2-amino-4-(pyridin-3-yl)thiazol-5-yl)methanone (35.7 mg, 0.1 mmol) was dissolved in anhydrous N,N - DMF and a mixture of benzo[1,3]dioxol-5-yl-cyclopropanecarboxylic acid (21.0 mg, 0.1 mmol), HATU (34.2 mg, 0.09 mmol) and DIPEA (38 μ L, 0.1 mmol) in N,N - DMF was added to the solution, after 5 minutes of activation .

The resulting mixture was heated to 50 $^{\circ}$ C for 48 h. The purification of the final product was made by preparative HPLC to obtain a compound with a purity higher than 95% as confirmed by HPLC-MS (11.0 mg, 20%).

1 H NMR (200 MHz, DMSO- d_6): δ 12.01 (s, 1H, broad, NH); 8.03-6.98 (m, 16H, arom); 6.05 (s, 2H, OCH₂O); 1.79-1.48 (m, 2H, cyclopr); 1.42-1.12 (m, 2H, cyclopr).

13 C NMR (50 MHz, DMSO- d_6): δ 187.8, 172.2, 159.7, 159.1, 153.4, 149.3, 147.7, 146.3, 138.5, 136.0, 131.9, 131.3, 129.2, 128.7, 127.9, 126.2, 124.0, 123.2, 121.2, 118.4, 112.9, 110.2, 107.8, 100.6, 30.2, 15.5.

HRMS (ESI) calculated for C₃₂H₂₃N₃O₄S : [M + H]⁺ 545.14091; found 546.14856

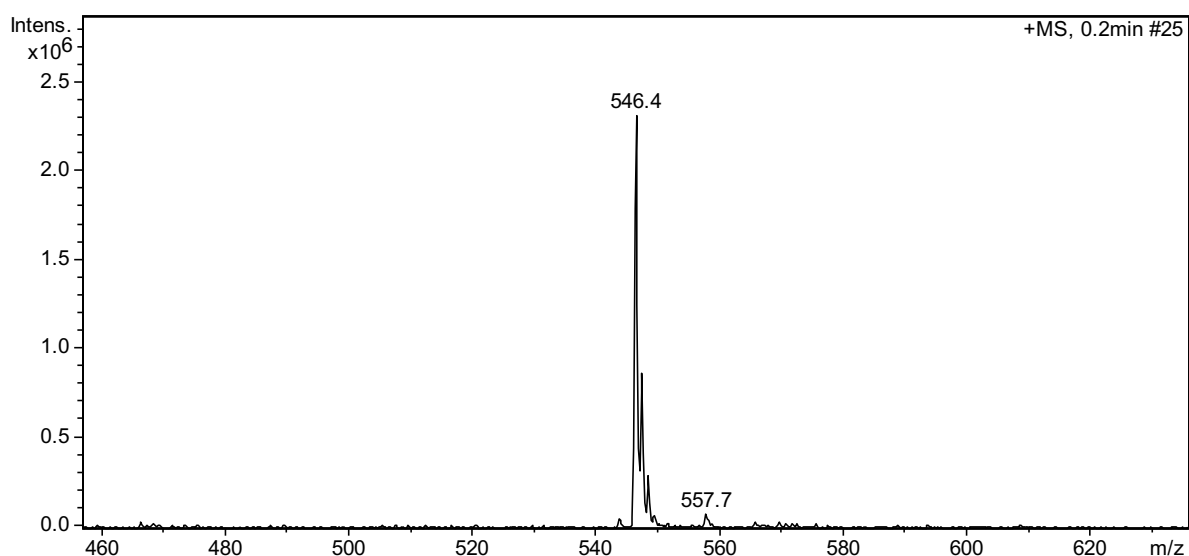


Figure 61. MS spectra of compound **90**.

N-(5-([1,1'-biphenyl]-4-carbonyl)-4-(4-chlorophenyl)thiazol-2-yl)-1-(benzo[*d*][1,3]dioxol-5-yl)cyclopropane-1-carboxamide (**91**)

To a solution of 4- chlorobenzoyl chloride (102.6 μ L, 0.8 mmol) in acetone (1 mL) cooled at T = 0 $^{\circ}$ C, ammonium thiocyanate (121.6 mg, 1.6 mmol) was added and stirred for 2 h at this temperature. Bis(4-methoxybenzyl)amine (246.7 mg, 0.96 mmol) was added to the mixture and the reaction was stirred for 2 h, at room temperature. Solvent was removed, the residue was diluted with water and

then the extraction was made by EtOAc. The organic phase was dried over anhydrous MgSO₄ and filtered. Solvent was removed by rotavapor to obtain N-(bis(4-methoxybenzyl)carbamothioyl)-4-chlorobenzamide (330 mg, 91%) as pale-yellow oil, that was used in the next step without further purification.

1-([1,1'-biphenyl]-4-yl)-2-bromoethan-1-one (55.0 mg, 0.2 mmol) was dissolved in N,N - DMF and N-(bis(4-methoxybenzyl)carbamothioyl)-4-chlorobenzamide (91.0 mg, 0.2 mmol) was added; the mixture was heated to 85°C. After 2 hours the solution was diluted with water and extracted with EtOAc (3 x 5 mL). The organic layer was dried over anhydrous Na₂SO₄ and filtered. After concentration, the residue was resuspended in TFA (4 mL) and heated to 100°C until complete deprotection (36 h). After removing TFA by rotavapor, the residue was neutralized with NaHCO₃ 1N, and then an extraction was made by EtOAc (3 x 5 mL). The organic layers were washed with brine, dried over anhydrous MgSO₄ and filtered. After concentration, [1,1'-biphenyl]-4-yl(2-amino-4-(4-chlorophenyl)thiazol-5-yl)methanone was crystallized in acetonitrile (32.0 mg, 41%).

Benzo[1,3]dioxol-5-yl-cyclopropanecarboxylic acid (16.5 mg, 0.08 mmol) was dissolved in anhydrous N,N - DMF (1 mL) with DIPEA (31 µL, 0.08 mmol) and HATU (27.4 mg, 0.07 mmol). After few minutes, a solution of [1,1'-biphenyl]-4-yl(2-amino-4-(4-chlorophenyl)thiazol-5-yl)methanone (32.0 mg, 0.08 mmol) was added to the solution and the reaction was heated to 50 °C until completeness (36 h). The final product was purified by preparative HPLC. The peak of interest was concentrated and lyophilized to obtain the title compound as a powder with purity of >95% as confirmed by HPLC-MS (14.8 mg, 32,0%).

¹H NMR (200 MHz, DMSO-d₆): δ 11.98 (s, 1H, broad, NH); 7.73-6.81 (m, 16H, arom); 6.01 (s, 2H, OCH₂O); 1.64-1.40 (m, 2H, cyclopr); 1.38-1.12 (m, 2H, cyclopr).

¹³C NMR (50 MHz, DMSO-d₆): δ 187.9, 172.4, 159.9, 152.7, 146.8, 146.3, 143.6, 138.4, 136.0, 132.9, 132.6, 131.7, 130.7, 129.4, 128.6, 127.9, 127.4, 126.5, 125.9, 124.5, 123.2, 110.2, 107.8, 100.6, 30.2, 15.5.

HRMS (ESI) calculated for C₃₃H₂₄ClN₂O₄S : [M + H]⁺ 579.11452; found 579.11385

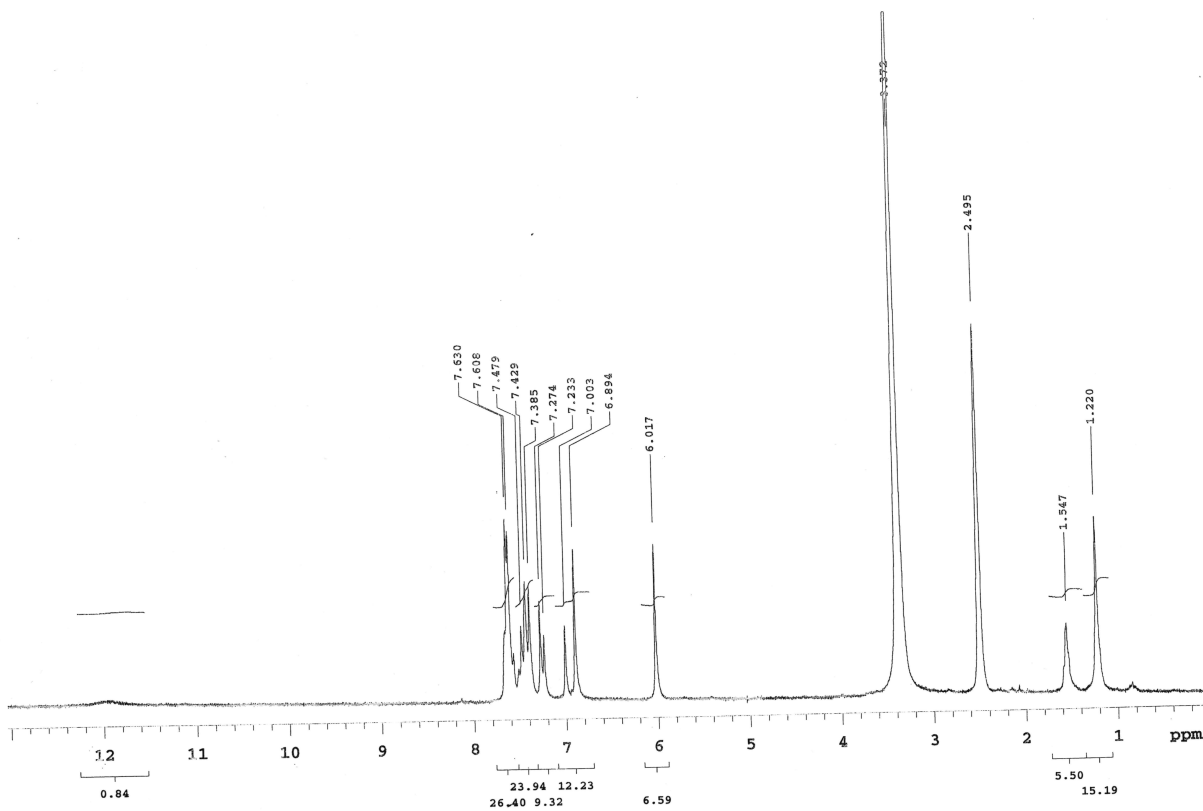


Figure 62. ^1H NMR spectra of compound 91.

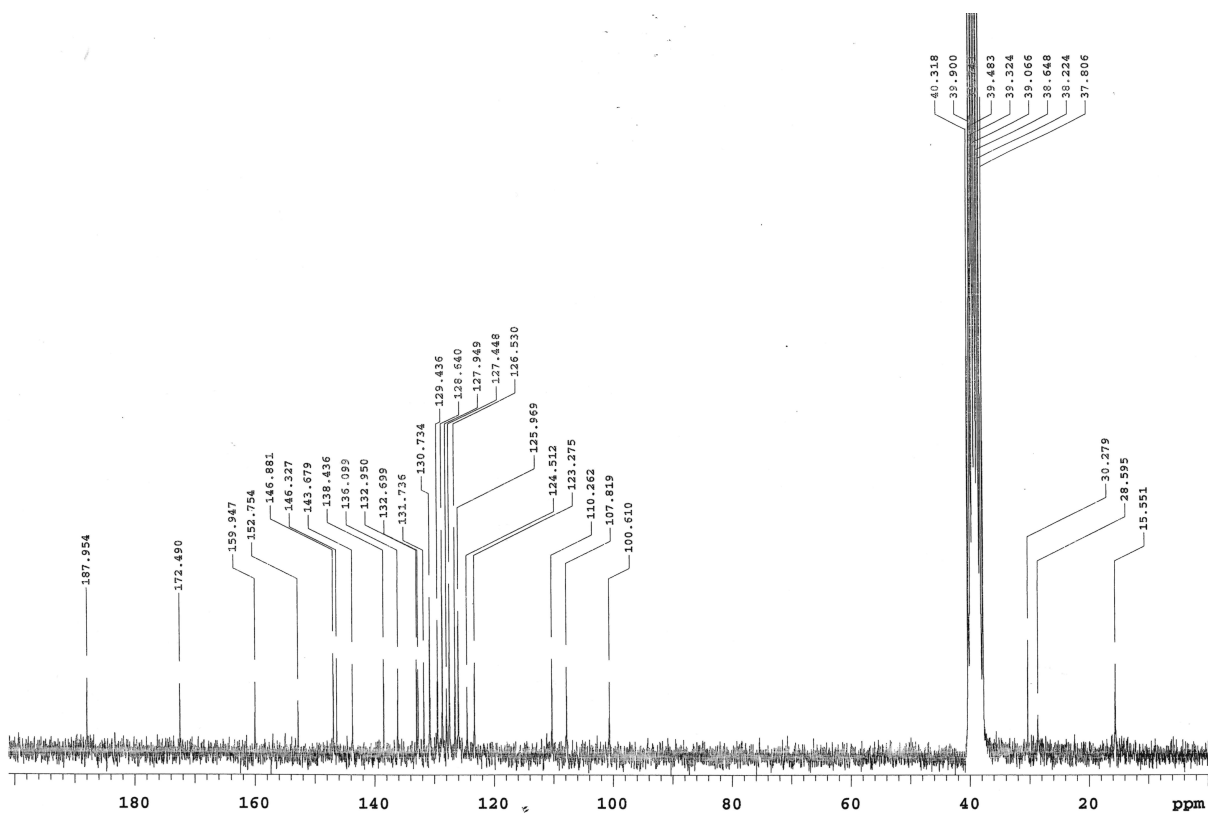


Figure 63. ^{13}C NMR spectra of compound 91.

1-(benzo[d][1,3]dioxol-5-yl)-N-(5-(3-methoxybenzoyl)-4-(4-(methylthio)phenyl)thiazol-2-yl)cyclopropane-1-carboxamide (92)

Compound **92** (13.1 mg, 24%) was obtained from (2-amino-4-(4-(methylthio)phenyl)thiazol-5-yl)(3-methoxyphenyl)methanone (36.0 mg, 0.1 mmol) and benzo[1,3]dioxol-5-yl-cyclopropanecarboxylic acid (20.6 mg, 0.1 mmol) in the same manner as described for compound **89**.

¹H NMR (200 MHz, DMSO-d₆): δ 11.79 (s, 1H, broad, NH); 7.66-6.71 (m, 11H, arom); 6.02 (s, 2H, OCH₂O); 3.60 (s, 3H, OCH₃); 2.44 (s, 3H, SCH₃); 1.65-1.42 (m, 2H, cyclopr); 1.40-1.13 (m, 2H, cyclopr).

¹³C NMR (50 MHz, DMSO-d₆): δ 186.5, 171.9, 159.3, 158.1, 151.5, 146.8, 146.3, 135.1, 133.2, 131.9, 129.3, 128.6, 123.2, 121.2, 115.1, 113.0, 112.8, 110.2, 107.8, 100.6, 54.7, 30.2, 15.4, 13.4.

HRMS (ESI) calculated for C₂₉H₂₅N₂O₅S₂ : [M + H]⁺ 545.12048; found 545.11990

1-(benzo[d][1,3]dioxol-5-yl)-N-(4-(4-chlorophenyl)-5-(3-methoxybenzoyl)thiazol-2-yl)cyclopropane-1-carboxamide (93)

Compound **93** (8.7 mg, 16%) was obtained from (2-amino-4-(4-chlorophenyl)thiazol-5-yl)(3-methoxyphenyl)methanone (34.5 mg, 0.1 mmol) and benzo[1,3]dioxol-5-yl-cyclopropanecarboxylic acid (20.6 mg, 0.1 mmol) in the same manner as described for compound **93**.

¹H NMR (200 MHz, DMSO-d₆): δ 11.98 (s, 1H, broad, NH); 7.84-6.85 (m, 11H, arom); 6.02 (s, 2H, OCH₂O); 3.60 (s, 3H, OCH₃); 1.74-1.46 (m, 2H, cyclopr); 1.41-1.15 (m, 2H, cyclopr).

¹³C NMR (50 MHz, DMSO-d₆): δ 186.9, 172.0, 159.8, 152.7, 146.8, 146.3, 143.6, 138.4, 131.7, 129.4, 128.6, 127.9, 126.3, 124.3, 123.2, 121.2, 112.9, 110.2, 107.8, 100.6, 54.6, 30.2, 15.4.

HRMS (ESI) calculated for C₂₈H₂₂ClN₂O₅S : [M + H]⁺ 533.09378; found 533.09371

1-(benzo[d][1,3]dioxol-5-yl)-N-(5-(3-methoxybenzoyl)-4-(pyridin-3-yl)thiazol-2-yl)cyclopropane-1-carboxamide (94)

Compound **94** (12.5 mg, 25%) was obtained from (2-amino-4-(pyridin-3-yl)thiazol-5-yl)(3-methoxyphenyl)methanone (32.0 mg, 0.1 mmol) and benzo[1,3]dioxol-5-yl-cyclopropanecarboxylic acid (20.6 mg, 0.1 mmol) in the same manner as described for compound **90**.

¹H NMR (200 MHz, DMSO-d₆): δ 11.72 (s, 1H, broad, NH); 8.10-7.02 (m, 11H, arom); 6.05 (s, 2H, OCH₂O); 3.62 (s, 3H, OCH₃); 1.77-1.45 (m, 2H, cyclopr); 1.42-1.16 (m, 2H, cyclopr).

¹³C NMR (50 MHz, DMSO-d₆): δ 187.6, 172.1, 159.8, 159.2, 153.1, 149.3, 147.7, 146.3, 138.6, 135.8, 131.8, 129.2, 128.7, 127.9, 123.4, 123.2, 121.3, 118.4, 112.8, 110.2, 107.8, 100.6, 54.7, 30.2, 15.4.

HRMS (ESI) calculated for C₂₇H₂₂N₃O₅S : [M + H]⁺ 500.12801; found 500.12716

1-(benzo[d][1,3]dioxol-5-yl)-N-(5-(4-(methylthio)benzoyl)-4-(4-(methylthio)phenyl)thiazol-2-yl)cyclopropanecarboxamide (95)

Compound **95** (12 mg, 21%) was obtained from 2-amino-4-(4-(methylthio)phenyl)thiazol-5-yl(4-(methylthio)phenyl)methanone (37.2 mg, 0.1 mmol) and benzo[1,3]dioxol-5-yl-cyclopropanecarboxylic acid (20.6 mg, 0.1 mmol) in the same manner as described for compound **89**.

¹H NMR (200 MHz, DMSO-d₆): δ 11.89 (s, 1H, broad, NH); 7.64-6.71 (m, 11H, arom); 6.01 (s, 2H, OCH₂O); 2.47 (s, 3H, SCH₃); 2.42 (s, 3H, SCH₃); 1.63-1.42 (m, 2H, cyclopr); 1.39-1.14 (m, 2H, cyclopr).

¹³C NMR (50 MHz, DMSO-d₆): δ 187.2, 172.2, 159.8, 159.2, 153.1, 146.8, 146.3, 138.5, 131.9, 129.3, 128.7, 127.9, 124.2, 123.2, 121.3, 118.4, 112.8, 110.2, 107.8, 100.6, 30.2, 15.4, 13.5.

HRMS (ESI) calculated for C₂₉H₂₅N₂O₄S₃ : [M + H]⁺ 561.09763; found 561.09670

Methyl 4-(2-(1-(benzo[d][1,3]dioxol-5-yl)cyclopropane-1-carboxamido)-5-(4-(methylthio)benzoyl)thiazol-4-yl)benzoate (96)

Compound **96** (14.3 mg, 25%) was obtained from methyl 4-(2-amino-5-(4-(methylthio)benzoyl)thiazol-4-yl)benzoate (39.0 mg, 0.1 mmol) and benzo[1,3]dioxol-5-yl-cyclopropanecarboxylic acid (20.6 mg, 0.1 mmol) in the same manner as described for compound **88**.

¹H NMR (200 MHz, DMSO-d₆): δ 11.96 (s, 1H, broad, NH); 7.79-6.78 (m, 11H, arom); 6.01 (s, 2H, OCH₂O); 4.12 (s, 3H, CH₃O); 2.41 (s, 3H, SCH₃); 1.65-1.42 (m, 2H, cyclopr); 1.39-1.12 (m, 2H, cyclopr).

¹³C NMR (50 MHz, DMSO-d₆): δ 188.7, 172.3, 165.7, 159.7, 159.1, 152.4, 146.8, 146.3, 138.6, 131.8, 129.2, 128.6, 127.8, 126.3, 124.1, 123.2, 121.4, 113.1, 110.2, 107.8, 100.6, 52.8, 30.2, 15.4, 13.5.

HRMS (ESI) calculated for C₃₀H₂₅N₂O₆S₂ : [M + H]⁺ 573.11539; found 573.11438

Biological evaluations

Cell culture

The bronchial epithelial cell line CFBE41o-with stable co- expression of F508del-CFTR and the halide-sensitive yellow fluorescent protein (HS-YFP) was cultured with MEM medium supplemented with 10% fetal calf serum, 2 mM L-glutamine, 100 U/mL penicillin, and 100 mg/mL streptomycin.

Fluorescence assay for CFTR activity

CFBE41o-cells with expression of mutant CFTR and HS-YFP were plated on clear-bottom 96-well black microplates (Corning Life Sciences, Acton, MA) at a density of 50,000 cells/well and kept at 37 C in 5% CO₂ for 24 h. For the corrector assay, CFBE41o-cells were treated for further 24 h with compounds and/or VX-809 or VX-661. After treatment, the culture medium was removed and cells in each well were stimulated for 30 min at 37 C with 60 mL PBS (containing 137 mM NaCl, 2.7 mM KCl, 8.1 mM Na₂HPO₄, 1.5 mM KH₂PO₄, 1 mM CaCl₂, and 0.5 mM MgCl₂) plus forskolin (20 mM) and genistein (50 mM).

At the time of assay, microplates carrying CFBE41o-cells were transferred to a microplate's reader (FluoStar Galaxy; BMG Labtech, Offenburg, Germany). The plate reader was equipped with high quality excitation (HQ500/20X: 500 ± 10 nm) and emission (HQ535/30 M: 535 ± 15 nm) filters for YFP (Chroma Technology, Brattleboro, VT). The assay consisted of a continuous 14 s fluorescence reading with 2 s before and 12 s after injection of an iodide containing solution (165 mL of a modified PBS containing I⁻ instead of Cl⁻; final I⁻ concentration in the well: 100 mM). Data were normalized to the initial background-subtracted fluorescence. To determine fluorescence quenching rate associated with I⁻ influx, the final 10 s of data for each well were fitted with an exponential function to extrapolate initial slope (dF/dt).

Dose-response relationships from each experiment were fitted with the Hill equation using the Igor software (WaveMetrics) to calculate EC₅₀, maximal effect, and Hill coefficient.

Transepithelial electrical resistance (TEER) evaluation

Primary bronchial epithelial cells obtained from one patient with CF (homozygous for F508del mutation) were seeded at high density on porous membranes (200.000 cells for 0.33-cm² mini-Transwell inserts (Corning, code 3379) for transepithelial European Journal of Medicinal Chemistry 208 (2020) 112833 electrical resistance (TEER). To test putative correctors, compounds were added to the basolateral medium for 24 h at 37 C and 5% CO₂, before measuring the TEER. Control epithelia were treated with vehicle alone (DMSO). TEER was measured in each well under basal conditions, after ENaC inhibition with apical amiloride (10 mM), after CFTR stimulation with forskolin (10 mM) and genistein (50 mM) on both sides, and after CFTR inhibition with apical PPQ102 (30 mM). After each treatment, we waited 10 min before recording electrical parameters. The TEER values for each well were converted into short-circuit current equivalent by Ohm's law. The TEER values were converted into TEEC.

Biochemical analysis of CFTR expression pattern

CFBE41o-cells stably expressing mutant CFTR and HS-YFP were grown to confluence on 60-mm diameter dishes and treated for 24 h with test compounds or vehicle alone. After 24 h cells were lysed in RIPA buffer containing a complete protease inhibitor (Roche). Cell lysates were subjected to centrifugation at 12000 rpm at 4 C for 10min. Supernatant protein concentration was calculated using the BCA assay (Euroclone) following the manufacturer's instructions. Equal amounts of protein (10 mg) were separated onto gradient (4e15%) Criterion TGX Precast gels (Bio-rad laboratories Inc.), transferred to nitrocellulose membrane with Trans-Blot Turbo system (Bio-rad Laboratories Inc.) and analyzed by Western blotting. Proteins were detected using monoclonal anti-CFTR (596, Cystic Fibrosis Foundation Therapeutics, University of North Carolina, Chapel Hill) or mouse monoclonal anti-GAPDH (cl.6C5; Santa Cruz Biotechnology, Inc) followed by horseradish peroxidase (HRP)-conjugated anti-mouse IgG (Abcam), and subsequently visualized by chemiluminescence using the SuperSignal West Femto Substrate (Thermo Scientific). Chemiluminescence was monitored using the Molecular Imager ChemiDoc XRS System. Images were analyzed with ImageJ software (National Institutes of Health). Bands were analyzed as ROI, normalized against the GAPDH loading control. Data are presented as mean \pm SEM of independent experiments.

Statistics

Each experimental condition was tested in three independent experiments, each one performed with three biological replicates (n 1/4 9). The KolmogoroveSmirnov test was used to evaluate the assumption of normality. Statistical significance of the effect of single treatments on CFTR activity or expression was tested by parametric 1-way ANOVA followed by the Dunnet multiple comparisons test (all groups against the control group) as post-hoc test. In the case of combination of treatments, statistical significance was verified by ANOVA followed by the Tukey test (for multiple comparisons) as post-hoc test. Normally distributed data are expressed as mean \pm SD or mean \pm SEM, as indicated, and significances are two-sided. Differences were considered statistically significant when P was less than 0.05.

Surface plasmon resonance binding assays

His-tagged human intact F508del-CFTR protein purified as described (O' Ryan et al., 2012; Pollock et al., 2014) was provided by Prof. R.C. Ford, Manchester University, UK. Lipids [synthetic phospholipid blend (Dioleoyl) DOPC: DOPS [(7:3 w/w)] were from Avant Polar Lipids (Alabaster, AL). CHAPS and cholesteryl hemi succinate (CHS) Tris salt were from Sigma-Aldrich (St Louis,

MO). Carboxy-methyl dextran CM5 sensor chip, anti-His antibody, 1-ethyl-3-(3-diaminopropyl)-carbodiimide hydrochloride (EDC) and N-hydroxysuccinimide (NHS) were from GE-Healthcare (Milwaukee, WI).

A BIAcore X-100 instrument (GE-Healthcare) was used. The preparation of the biosensor containing F508del-CFTR in a membrane-like lipid environment was prepared as described [38]. Briefly, anti-His antibody was immobilized on a CM5 sensor chip by standard amine-coupling chemistry. After sensor chip equilibration by injection of DOPC:DOPS (7:3 W/W) 0.075 mg/mL, 0.02% CHS, 0.1% CHAPS (DOPC:DOPS running buffer), human His-tagged intact F508del-CFTR (10 mg/mL, Hepes 50 mM, pH 7 containing NaCl 150 mM DOPC: DOPS (7:3 W/W) 363 mg/mL, 0.06% CHS, 0.3% CHAPS (DOPC:DOPS-F508del-CFTR buffer), was injected on the anti-His surface, allowing the capture of about 1125 RU. A sensor chip coated with anti-His antibody alone was used for blank subtraction.

To evaluate their F508del-CFTR-binding capacity, compounds were injected over the sensor chip at increasing concentration in PBS, 0.05% surfactant P20 and 5% DMSO, pH 7.4 (PBS-DMSO) by adopting the single cycle model [46]. Dissociation Constant (K_d) values were calculated by steady state analyses performed by fitting the proper form of Scatchard's equation for the plot of the bound resonance units (RU) at equilibrium versus the compound concentration in solution.

References

Ashlock, M.A.; Olson, E.R. Therapeutics development for cystic fibrosis: a successful model for a multisystem genetic disease. *Annu. Rev. Med.* **2011**, *62*, 107-25. doi: 10.1146/annurev-med-061509-131034. PMID: 21226613.

Baroni, D.; Zegarra-Moran, O.; Svensson, A.; Moran, O. Direct interaction of a CFTR potentiator and a CFTR corrector with phospholipid bilayers. *Eur. Biophys. J.* **2014**, *43*, (6-7), 341-6. doi: 10.1007/s00249-014-0956-y. Epub 2014 Apr 26. PMID: 24771136.

Baatallah, N.; Elbahnsi, A.; Mornon, J.P.; Chevalier, B.; Pranke, I.; Serval, N.; Zelli, R.; Décout, J.L.; Edelman, A.; Sermet-Gaudelus, I.; Callebaut, I.; Hinzpeter, A. Pharmacological chaperones improve intra-domain stability and inter-domain assembly via distinct binding sites to rescue misfolded CFTR. *Cell Mol Life Sci.* **2021**, *78*, (23), 7813-7829. doi: 10.1007/s00018-021-03994-5. Epub 2021 Oct 29. PMID: 34714360.

Bodio, E.; Julienne, K.; Gouin, S.G.; Faivre-Chauvet, A.; Deniaud, D. Efficient synthesis of new tetradentate ligands with potential applications for ⁶⁴Cu PET-imaging. *Bioorg. Med. Chem. Lett.* **2011**, *21*, (3), 924-7. doi: 10.1016/j.bmcl.2010.12.072. Epub 2010 Dec 19. PMID: 21236669.

Bompadre, S.G.; Sohma, Y.; Li, M.; Hwang, T.C. G551D and G1349D, two CF-associated mutations in the signature sequences of CFTR, exhibit distinct gating defects. *J. Gen. Physiol.* **2007**, *129*, (4), 285-98. doi: 10.1085/jgp.200609667. Epub 2007 Mar 12. PMID: 17353351; PMCID: PMC2151620.

Bompadre, S.G.; Li, M.; Hwang, T.C. Mechanism of G551D-CFTR (cystic fibrosis transmembrane conductance regulator) potentiation by a high affinity ATP analog. *J. Biol. Chem.* **2008**, *283*, (9), 5364-9. doi: 10.1074/jbc.M709417200. Epub 2007 Dec 30. PMID: 18167357.

Cant, N.; Pollock, N.; Ford, R.C. CFTR structure and cystic fibrosis. *Int. J. Biochem. Cell. Biol.* **2014**, *52*, 15-25. doi: 10.1016/j.biocel.2014.02.004. Epub 2014 Feb 15. PMID: 24534272.

Castellani, C.; Southern, K.W.; Brownlee, K.; Dankert Roelse, J.; Duff, A.; Farrell, M.; Mehta, A.; Munck A, Pollitt, R.; Sermet-Gaudelus, I.; Wilcken, B.; Ballmann, M.; Corbetta, C.; de Monestrol, I.; Farrell, P.; Feilcke, M.; Férec, C.; Gartner, S.; Gaskin, K.; Hammermann, J.; Kashirskaya, N.;

Loeber, G.; Macek, M. Jr.; Mehta, G.; Reiman, A.; Rizzotti, P.; Sammon, A.; Sands, D.; Smyth, A.; Sommerburg, O.; Torresani, T.; Travert, G.; Vernooij, A.; Elborn, S. European best practice guidelines for cystic fibrosis neonatal screening. *J. Cyst. Fibros.* **2009**, 8, (3), 153-73. doi: 10.1016/j.jcf.2009.01.004. Epub 2009 Feb 26. PMID: 19246252

Castellani, C.; Massie, J.; Sontag, M.; Southern, K.W. Newborn screening for cystic fibrosis. *Lancet Respir Med.* **2016**, 4, (8), 653-661. doi: 10.1016/S2213-2600(16)00053-9. Epub 2016 Apr 1. PMID: 27053341.

Chin, S.; Yang, D.; Miles, A.J.; Eckford, P.D.W.; Molinski, S.; Wallace, B.A.; Bear, C.E. Attenuation of Phosphorylation-dependent Activation of Cystic Fibrosis Transmembrane Conductance Regulator (CFTR) by Disease-causing Mutations at the Transmission Interface. *J. Biol. Chem.* **2017**, 292, (5), 1988-1999. doi: 10.1074/jbc.M116.762633. Epub 2016 Dec 21. PMID: 28003367; PMCID: PMC5290968.

Cholon, D.M.; Quinney, N.L.; Fulcher, M.L.; Esther, C.R. Jr.; Das, J.; Dokholyan, N.V.; Randell, S.H.; Boucher, R.C.; Gentsch, M. Potentiator ivacaftor abrogates pharmacological correction of $\Delta F508$ CFTR in cystic fibrosis. *Sci. Transl. Med.* **2014**, 6, (246), 246ra96. doi: 10.1126/scitranslmed.3008680. PMID: 25101886; PMCID: PMC4272825.

Cipolli, M.; Castellani, C.; Wilcken, B.; Massie, J.; McKay, K.; Gruca, M.; Tamanini, A.; Assael, M.B.; Gaskin, K. Pancreatic phenotype in infants with cystic fibrosis identified by mutation screening. *Arch. Dis. Child.* **2007**, 92, (10), 842-6. doi: 10.1136/adc.2006.107581. Epub 2007 Apr 20. PMID: 17449517; PMCID: PMC2083233.

Cirilli, N.; Raia, V.; Rocco, I.; De Gregorio, F.; Tosco, A.; Salvadori, L.; Sepe, A.O.; Buzzetti, R.; Minicuci, N.; Castaldo, G. Intra-individual biological variation in sweat chloride concentrations in CF, CFTR dysfunction, and healthy pediatric subjects. *Pediatr. Pulmonol.* **2018**, 53, (6), 728-734. doi: 10.1002/ppul.23992. Epub 2018 Apr 2. PMID: 29611353.

Collaco, J.M.; Blackman, S.M.; Raraigh, K.S.; Corvol, H.; Rommens, J.M.; Pace, R.G.; Boelle, P.Y.; McGready, J.; Sosnay, P.R.; Strug, L.J.; Knowles, M.R.; Cutting, G.R. Sources of Variation in Sweat Chloride Measurements in Cystic Fibrosis. *Am. J. Respir. Crit. Care. Med.* **2016**, 194, (11), 1375-1382. doi: 10.1164/rccm.201603-0459OC. PMID: 27258095; PMCID: PMC5148144.

Conner, G.E.; Wijkstrom-Frei, C.; Randell, S.H.; Fernandez, V.E.; Salathe, M. The lactoperoxidase system links anion transport to host defense in cystic fibrosis. *FEBS Lett.* **2007**, 581, (2), 271-8. doi: 10.1016/j.febslet.2006.12.025. Epub 2006 Dec 19. PMID: 17204267; PMCID: PMC1851694.

Cuthbert, A.W. New horizons in the treatment of cystic fibrosis. *Br. J. Pharmacol.* **2011**, 163, (1), 173-83. doi: 10.1111/j.1476-5381.2010.01137.x. PMID: 21108631; PMCID: PMC3085876.

De Jonge, H.R.; Ballmann, M.; Veeze, H.; Bronsveld, I.; Stanke, F.; Tümmler, B.; Sinaasappel, M. Ex vivo CF diagnosis by intestinal current measurements (ICM) in small aperture, circulating Ussing chambers. *J. Cyst. Fibros.* **2004**, 3 Suppl 2, 159-63. doi: 10.1016/j.jcf.2004.05.034. PMID: 15463951.

Derichs, N.; Sanz, J.; Von Kanel, T.; Stolpe, C.; Zapf, A.; Tümmler, B.; Gallati, S.; Ballmann, M. Intestinal current measurement for diagnostic classification of patients with questionable cystic fibrosis: validation and reference data. *Thorax.* **2010**, 65, (7), 594-9. doi: 10.1136/thx.2009.125088. PMID: 20627915.

Doiron, J.E.; Le, C.A.; Ody, B.K.; Brace, J.B.; Post, S.J.; Thacker, N.L.; Hill, H.M.; Breton, G.W.; Mulder, M.J.; Chang, S.; Bridges, T.M.; Tang, L.; Wang, W.; Rowe, S.M.; Aller, S.G.; Turlington, M. Evaluation of 1,2,3-Triazoles as Amide Bioisosteres In Cystic Fibrosis Transmembrane Conductance Regulator Modulators VX-770 and VX-809. *Chemistry.* **2019**, 25, (14), 3662-3674. doi: 10.1002/chem.201805919. Epub 2019 Feb 11. PMID: 30650214; PMCID: PMC6469399.

Donaldson, S.H.; Pilewski, J.M.; Griese, M.; Cooke, J.; Viswanathan, L.; Tullis, E.; Davies, J.C.; Lekstrom-Himes, J.A.; Wang, L.T. VX11-661-101 Study Group. Tezacaftor/Ivacaftor in Subjects with Cystic Fibrosis and F508del/F508del-CFTR or F508del/G551D-CFTR. *Am. J. Respir. Crit. Care Med.* **2018**, 197, (2), 214-224. doi: 10.1164/rccm.201704-0717OC. PMID: 28930490; PMCID: PMC5768901.

Drumm, M.L.; Konstan, M.W.; Schluchter, M.D.; Handler, A.; Pace, R.; Zou, F.; Zariwala, M.; Fargo, D.; Xu, A.; Dunn, J.M.; Darrah, R.J.; Dorfman, R.; Sandford, A.J.; Corey, M.; Zielenski, J.; Durie, P.; Goddard, K.; Yankaskas, J.R.; Wright, F.A.; Knowles, M.R. Gene Modifier Study Group. Genetic modifiers of lung disease in cystic fibrosis. *N. Engl. J. Med.* **2005**, 353, (14), 1443-53. doi: 10.1056/NEJMoa051469. PMID: 16207846.

Dobay, O.; Laub, K.; Stercz, B.; Kéri, A.; Balázs, B.; Tóthpál, A.; Kardos, S.; Jaikumpun, P.; Ruksakiet, K.; Quinton, P.M.; Zsembery, Á. Bicarbonate Inhibits Bacterial Growth and Biofilm Formation of Prevalent Cystic Fibrosis Pathogens. *Front. Microbiol.* **2018**, *9*, 2245. doi: 10.3389/fmicb.2018.02245. PMID: 30283433; PMCID: PMC6157313.

Dupuis, A.; Keenan, K.; Ooi, C.Y.; Dorfman, R.; Sontag, M.K.; Naehrlich, L.; Castellani, C.; Strug, L.J.; Rommens, J.M.; Gonska, T. Prevalence of meconium ileus marks the severity of mutations of the Cystic Fibrosis Transmembrane Conductance Regulator (CFTR) gene. *Genet Med.* **2016**, *18*, (4), 333-40. doi: 10.1038/gim.2015.79. Epub 2015 Jun 18. PMID: 26087176.

D'Ursi, P., Uggeri, M., Urbinati, C., Millo, E., Paiardi, G., Milanese, L., Ford, R. C., Clews, J., Meng, X., Bergese, P., Ridolfi, A., Pedemonte, N., Fossa, P., Orro, A., & Rusnati, M. Exploitation of a novel biosensor based on the full-length human F508del-CFTR with computational studies, biochemical and biological assays for the characterization of a new Lumacaftor/Tezacaftor analogue. *Sensors and Actuators, B: Chemical*, **2019**, 301. <https://doi.org/10.1016/j.snb.2019.127131>

Eckford, P.D.; Ramjeesingh, M.; Molinski, S.; Pasyk, S.; Dekkers, J.F.; Li, C.; Ahmadi, S.; Ip, W; Chung, T.E.; Du, K.; Yeager, H.; Beekman, J.; Gonska, T.; Bear, C.E. VX-809 and related corrector compounds exhibit secondary activity stabilizing active F508del-CFTR after its partial rescue to the cell surface. *Chem Biol.* **2014**, *21*, (5), 666-78. doi: 10.1016/j.chembiol.2014.02.021. Epub 2014 Apr 10. PMID: 24726831.

Edelman, A. Measurement of nasal potential difference in young children with an equivocal sweat test following newborn screening for cystic fibrosis. *Thorax.* **2010**, *65*, (6), 539-44. doi: 10.1136/thx.2009.123422. PMID: 20522854.

El Hiani, Y.; Linsdell, P. Functional Architecture of the Cytoplasmic Entrance to the Cystic Fibrosis Transmembrane Conductance Regulator Chloride Channel Pore. *J. Biol. Chem.* **2015**, *290*, (25), 15855-15865. doi: 10.1074/jbc.M115.656181. Epub 2015 May 5. PMID: 25944907; PMCID: PMC4505492.

Emerson, J.; Rosenfeld, M.; McNamara, S.; Ramsey, B.; Gibson, R.L. Pseudomonas aeruginosa and other predictors of mortality and morbidity in young children with cystic fibrosis. *Pediatr. Pulmonol.* **2002**, 34, (2), 91-100. doi: 10.1002/ppul.10127. PMID: 12112774.

Estabrooks, S.; Brodsky, J.L. Regulation of CFTR Biogenesis by the Proteostatic Network and Pharmacological Modulators. *Int. J. Mol. Sci.* **2020**, 21, (2), 452. doi: 10.3390/ijms21020452. PMID: 31936842; PMCID: PMC7013518.

Farinha, C.M.; Amaral, M.D. Most F508del-CFTR is targeted to degradation at an early folding checkpoint and independently of calnexin. *Mol. Cell. Biol.* **2005**, 25, (12), 5242-52. doi: 10.1128/MCB.25.12.5242-5252.2005. PMID: 15923638; PMCID: PMC1140594.

Farinha, C.M.; Matos, P.; Amaral, M.D. Control of cystic fibrosis transmembrane conductance regulator membrane trafficking: not just from the endoplasmic reticulum to the Golgi. *FEBS J.* **2013**, 280, (18), 4396-406. doi: 10.1111/febs.12392. Epub 2013 Jul 5. PMID: 23773658.

Farinha, C.M.; King-Underwood, J.; Sousa, M.; Correia, A.R.; Henriques, B.J.; Roxo-Rosa, M.; Da Paula, A.C.; Williams, J.; Hirst, S.; Gomes, C.M.; Amaral, M.D. Revertants, low temperature, and correctors reveal the mechanism of F508del-CFTR rescue by VX-809 and suggest multiple agents for full correction. *Chem. Biol.* **2013**, 20, (7), 943-55. doi: 10.1016/j.chembiol.2013.06.004. PMID: 23890012.

Farinha, C.M.; Swiatecka-Urban, A.; Brautigan, D.L.; Jordan, P. Regulatory Crosstalk by Protein Kinases on CFTR Trafficking and Activity. *Front. Chem.* **2016**, 4:1. doi: 10.3389/fchem.2016.00001. PMID: 26835446; PMCID: PMC4718993.

Farinha, C.M.; Canato, S. From the endoplasmic reticulum to the plasma membrane: mechanisms of CFTR folding and trafficking. *Cell. Mol. Life Sci.* **2017**, 74, (1), 39-55. doi: 10.1007/s00018-016-2387-7. Epub 2016 Oct 3. PMID: 27699454.

Fiedorczuk, K.; Chen, J. Mechanism of CFTR correction by type I folding correctors. *Cell.* **2022**, 185, (1), 158-168.e11. doi: 10.1016/j.cell.2021.12.009. PMID: 34995514.

Flass, T.; Narkewicz, M.R. Cirrhosis and other liver disease in cystic fibrosis. *J. Cyst. Fibros.* **2013**, 12, (2), 116-24. doi: 10.1016/j.jcf.2012.11.010. Epub 2012 Dec 20. PMID: 23266093; PMCID: PMC3883947.

Fukuda, R.; Okiyoneda, T. Peripheral Protein Quality Control as a Novel Drug Target for CFTR Stabilizer. *Front. Pharmacol.* **2018**, 9, 1100. doi: 10.3389/fphar.2018.01100. PMID: 30319426; PMCID: PMC6170605.

Galietta, L.V.; Jayaraman, S.; Verkman, A.S. Cell-based assay for high-throughput quantitative screening of CFTR chloride transport agonists. *Am J Physiol Cell Physiol.* **2001**, 281, (5), C1734-42. doi: 10.1152/ajpcell.2001.281.5.C1734. PMID: 11600438.

Gao, X.; Bai, Y.; Hwang, T.C. Cysteine scanning of CFTR's first transmembrane segment reveals its plausible roles in gating and permeation. *Biophys. J.* **2013**, 104, (4), 786-97. doi: 10.1016/j.bpj.2012.12.048. PMID: 23442957; PMCID: PMC3576531.

Giuliano, K.A.; Wachi, S.; Drew, L.; Dukovski, D.; Green, O.; Bastos, C.; Cullen, M.D.; Hauck, S.; Tait, B.D.; Munoz, B.; Lee, P.S.; Miller, J.P. Use of a High-Throughput Phenotypic Screening Strategy to Identify Amplifiers, a Novel Pharmacological Class of Small Molecules That Exhibit Functional Synergy with Potentiators and Correctors. *SLAS Discov.* **2018**, 23, (2), 111-121. doi: 10.1177/2472555217729790. Epub 2017 Sep 12. PMID: 28898585; PMCID: PMC5784457.

Hartl, F.U.; Bracher, A.; Hayer-Hartl, M. Molecular chaperones in protein folding and proteostasis. *Nature.* **2011**, 475, (7356), 324-32. doi: 10.1038/nature10317. PMID: 21776078.

Hanssens, L.S.; Duchateau, J.; Casimir, G.J. CFTR Protein: Not Just a Chloride Channel? *Cells.* **2021**, 10, (11), 2844. doi: 10.3390/cells10112844. PMID: 34831067; PMCID: PMC8616376.

Hoo, A.F.; Thia, L.P.; Nguyen, T.T.; Bush, A.; Chudleigh, J.; Lum, S.; Ahmed, D.; Balfour Lynn, I.; Carr, S.B.; Chavasse, R.J.; Costeloe, K.L.; Price, J.; Shankar, A.; Wallis, C.; Wyatt, H.A.; Wade, A.; Stocks, J.; London Cystic Fibrosis Collaboration. Lung function is abnormal in 3-month-old infants with cystic fibrosis diagnosed by newborn screening. *Thorax.* **2012**, 67, (10), 874-81. doi: 10.1136/thoraxjnl-2012-201747. Epub 2012 Jun 29. PMID: 22752198.

Hudson, R.P.; Dawson, J.E.; Chong, P.A.; Yang, Z.; Millen, L.; Thomas, P.J.; Brouillette, C.G.; Forman-Kay, J.D. Direct Binding of the Corrector VX-809 to Human CFTR NBD1: Evidence of an Allosteric Coupling between the Binding Site and the NBD1:CL4 Interface. *Mol Pharmacol.* **2017**, *92*, (2), 124-135. doi: 10.1124/mol.117.108373. Epub 2017 May 25. PMID: 28546419.

Hwang, T.C.; Yeh, J.T.; Zhang, J.; Yu, Y.C.; Yeh, H.I.; Destefano, S. Structural mechanisms of CFTR function and dysfunction. *J. Gen. Physiol.* **2018**, *150*, (4), 539-570. doi: 10.1085/jgp.201711946. Epub 2018 Mar 26. PMID: 29581173; PMCID: PMC5881446.

Illek, B.; Fischer, H.; Santos, G.F.; Widdicombe, J.H.; Machen, T.E.; Reenstra, W.W. cAMP-independent activation of CFTR Cl channels by the tyrosine kinase inhibitor genistein. *Am. J. Physiol.* **1995**, *268* (4 Pt 1), C886-93. doi: 10.1152/ajpcell.1995.268.4.C886. PMID: 7537452.

Jayaraman, S.; Teitler, L.; Skalski, B.; Verkman, A.S. Long-wavelength iodide-sensitive fluorescent indicators for measurement of functional CFTR expression in cells. *Am J Physiol.* **1999**, *277* (5), C1008-18. doi: 10.1152/ajpcell.1999.277.5.C1008. PMID: 10564094.

Kampinga, H.H.; Craig, E.A. The HSP70 chaperone machinery: J proteins as drivers of functional specificity. *Nat. Rev. Mol. Cell. Biol.* **2010**, *11*, (8), 579-92. doi: 10.1038/nrm2941. Erratum in: *Nat Rev Mol Cell Biol.* 2010 Oct;11(10):750. PMID: 20651708; PMCID: PMC3003299

Kanelis, V.; Hudson, R.P.; Thibodeau, P.H.; Thomas, P.J.; Forman-Kay, J.D. NMR evidence for differential phosphorylation-dependent interactions in WT and DeltaF508 CFTR. *EMBO J.* **2010**, *29*, (1), 263-77. doi: 10.1038/emboj.2009.329. Epub 2009 Nov 19. PMID: 19927121; PMCID: PMC2808376.

Kym, P.R.; Wang, X.; Searle, X.B.; Liu, B.; Yeung, M.C. Preparation of Substituted Tetrahydropyrans as Cystic Fibrosis Transmembrane Conductance Regulator (CFTR) Modulators, **2016**. US20160122331A1.

Konstan, M.W.; McKone, E.F.; Moss, R.B.; Marigowda, G.; Tian, S.; Waltz, D.; Huang, X.; Lubarsky, B.; Rubin, J.; Millar, S.J.; Pasta, D.J.; Mayer-Hamblett, N.; Goss, C.H.; Morgan, W.; Sawicki, G.S. Assessment of safety and efficacy of long-term treatment with combination lumacaftor and ivacaftor therapy in patients with cystic fibrosis homozygous for the F508del-CFTR mutation

(PROGRESS): a phase 3, extension study. *Lancet Respir. Med.* **2017**, 5, (2), 107-118. doi: 10.1016/S2213-2600(16)30427-1. Epub 2016 Dec 21. PMID: 28011037.

Laselva, O.; Bartlett, C.; Gunawardena, T.N.A.; Ouyang, H.; Eckford, P.D.W.; Moraes, T.J.; Bear, C.E.; Gonska, T. Rescue of multiple class II CFTR mutations by elexacaftor+tezacaftor+ivacaftor mediated in part by the dual activities of elexacaftor as both corrector and potentiator. *Eur Respir J.* **2021**, 57, 6, 2002774. doi: 10.1183/13993003.02774-2020. PMID: 33303536; PMCID: PMC8209484.

Liessi, N.; Cichero, E.; Pesce, E.; Arkel, M.; Salis, A.; Tomati, V.; Paccagnella, M.; Damonte, G.; Tasso, B.; Galiotta, L.J.V.; Pedemonte, N.; Fossa, P.; Millo, E. Synthesis and biological evaluation of novel thiazole- VX-809 hybrid derivatives as F508del correctors by QSAR-based filtering tools. *Eur. J. Med. Chem.* **2018**, 144, 179-200. doi: 10.1016/j.ejmech.2017.12.030. Epub 2017 Dec 8. PMID: 29272749.

Linsdell, P.; Hanrahan, J.W. Glutathione permeability of CFTR. *Am. J. Physiol.* **1998**, 275, (1), C323-6. doi: 10.1152/ajpcell.1998.275.1.C323. PMID: 9688865.

Linsdell, P. Structural Changes Fundamental to Gating of the Cystic Fibrosis Transmembrane Conductance Regulator Anion Channel Pore. *Adv. Exp. Med. Biol.* **2017**, 925, 13-32. doi: 10.1007/5584_2016_33. PMID: 27311317.

Liu, F.; Zhang, Z.; Csanády, L.; Gadsby, D.C. Chen, J. Molecular Structure of the Human CFTR Ion Channel. *Cell.* **2017**, 169, (1), 85-95.e8. doi: 10.1016/j.cell.2017.02.024. PMID: 28340353.

Loo, T.W.; Bartlett, M.C.; Clarke, D.M. Corrector VX-809 stabilizes the first transmembrane domain of CFTR. *Biochem. Pharmacol.* **2013**, 86, (5), 612-9. doi: 10.1016/j.bcp.2013.06.028. Epub 2013 Jul 5. PMID: 23835419.

Lukacs, G.L.; Verkman, A.S. CFTR: folding, misfolding and correcting the Δ F508 conformational defect. *Trends Mol. Med.* **2012**, 18, (2), 81-91. doi: 10.1016/j.molmed.2011.10.003. Epub 2011 Dec 3. PMID: 22138491; PMCID: PMC3643519.

Marson, F.A.L.; Bertuzzo, C.S.; Ribeiro, J.D. Classification of CFTR mutation classes. *Lancet Respir. Med.* **2016**, *4*, (8), e37-e38. doi: 10.1016/S2213-2600(16)30188-6. Epub 2016 Jul 1. PMID: 27377414.

Mayer, M.P.; Bukau, B. Hsp70 chaperones: cellular functions and molecular mechanism. *Cell. Mol. Life Sci.* **2005**, *62*, (6), 670-84. doi: 10.1007/s00018-004-4464-6. PMID: 15770419; PMCID: PMC2773841.

McKone, E.F.; Borowitz, D.; Drevinek, P.; Griese, M.; Konstan, M.W.; Wainwright, C.; Ratjen, F.; Sermet-Gaudelus, I.; Plant, B.; Munck, A.; Jiang, Y.; Gilmartin, G.; Davies, J.C. VX08-770-105 (PERSIST) Study Group. Long-term safety and efficacy of ivacaftor in patients with cystic fibrosis who have the Gly551Asp-CFTR mutation: a phase 3, open-label extension study (PERSIST). *Lancet Respir. Med.* **2014**, *2*, (11), 902-910. doi: 10.1016/S2213-2600(14)70218-8. Epub 2014 Oct 9. PMID: 25311995.

Mott, L.S.; Park, J.; Murray, C.P.; Gangell, C.L.; de Klerk, N.H.; Robinson, P.J.; Robertson, C.F.; Ranganathan, S.C.; Sly, P.D.; Stick, S.M. AREST CF. Progression of early structural lung disease in young children with cystic fibrosis assessed using CT. *Thorax.* **2012**, *67*, (6), 509-16. doi: 10.1136/thoraxjnl-2011-200912. Epub 2011 Dec 26. PMID: 22201161.

Mulder, M.P.; Witting, K.; Berlin, I.; Pruneda, J.N.; Wu, K.P.; Chang, J.G.; Merks, R.; Bialas, J.; Groettrup, M.; Vertegaal, A.C.; Schulman, B.A.; Komander, D.; Neefjes, J.; El Oualid, F.; Ovaas, H. A cascading activity-based probe sequentially targets E1-E2-E3 ubiquitin enzymes. *Nat. Chem. Biol.* **2016**, *12*, (7), 523-30. doi: 10.1038/nchembio.2084. Epub 2016 May 16. PMID: 27182664; PMCID: PMC5108872.

Oberdorf, J.; Carlson, E.J.; Skach, W.R. Redundancy of mammalian proteasome beta subunit function during endoplasmic reticulum associated degradation. *Biochem.* **2001**, *40*, (44), 13397-405. doi: 10.1021/bi011322y. PMID: 11683650.

Okuyoneda, T.; Barrière, H.; Bagdány, M.; Rabeh, W.M.; Du, K.; Höhfeld, J.; Young, J.C.; Lukacs, G.L. Peripheral protein quality control removes unfolded CFTR from the plasma membrane. *Science.* **2010**, *329*, (5993), 805-10. doi: 10.1126/science.1191542. Epub 2010 Jul 1. PMID: 20595578; PMCID: PMC5026491.

Okiyoneda, T.; Veit, G.; Dekkers, J.F.; Bagdany, M.; Soya, N.; Xu, H.; Roldan, A.; Verkman, A.S.; Kurth, M.; Simon, A.; Hegedus, T.; Beekman, J.M.; Lukacs, G.L. Mechanism-based corrector combination restores Δ F508-CFTR folding and function. *Nat .Chem. Biol.* **2013**, 9, (7), 444-54. doi: 10.1038/nchembio.1253. Epub 2013 May 12. PMID: 23666117; PMCID: PMC3840170.

O'Ryan, L.; Rimington, T.; Cant, N.; Ford, R.C. Expression and purification of the cystic fibrosis transmembrane conductance regulator protein in *Saccharomyces cerevisiae*. *J Vis Exp.* **2012**, (61), 3860. doi: 10.3791/3860. PMID: 22433465; PMCID: PMC3460588.

Palleros, D.R.; Reid, K.L.; Shi, L.; Welch, W.J.; Fink, A.L. ATP-induced protein-Hsp70 complex dissociation requires K⁺ but not ATP hydrolysis. *Nature.* **1993**, 365, (6447), 664-6. doi: 10.1038/365664a0. PMID: 8413631.

Pedemonte, N.; Lukacs, G.L.; Du, K.; Caci, E.; Zegarra-Moran, O.; Galiotta, L.J.; Verkman, A.S. Small-molecule correctors of defective Δ F508-CFTR cellular processing identified by high-throughput screening. *J. Clin. Invest.* **2005**, 115, (9), 2564-71. doi: 10.1172/JCI24898. Epub 2005 Aug 25. PMID: 16127463; PMCID: PMC1190372.

Pedemonte, N.; Tomati, V.; Sondo, E.; Caci, E.; Millo, E.; Armirotti, A.; Damonte, G.; Zegarra-Moran, O.; Galiotta, L.J. Dual activity of aminoarylthiazoles on the trafficking and gating defects of the cystic fibrosis transmembrane conductance regulator chloride channel caused by cystic fibrosis mutations. *J. Biol. Chem.* **2011**, 286, (17), 15215-26. doi: 10.1074/jbc.M110.184267. Epub 2011 Mar 7. PMID: 21383017; PMCID: PMC3083174.

Pesce, E.; Bellotti, M.; Liessi, N.; Guariento, S.; Damonte, G.; Cichero, E.; Galatini, A.; Salis, A.; Gianotti, A.; Pedemonte, N.; Zegarra-Moran, O.; Fossa, P.; Galiotta, L.J.; Millo, E. Synthesis and structure-activity relationship of aminoarylthiazole derivatives as correctors of the chloride transport defect in cystic fibrosis. *Eur. J. Med. Chem.* **2015**, 99, 14-35. doi: 10.1016/j.ejmech.2015.05.030. Epub 2015 May 28. PMID: 26041577.

Pollock, N.; Cant, N.; Rimington, T.; Ford, R.C. Purification of the cystic fibrosis transmembrane conductance regulator protein expressed in *Saccharomyces cerevisiae*. *J Vis Exp.* **2014**, (87), 51447. doi: 10.3791/51447. PMID: 24893839; PMCID: PMC4181556.

Pranke, I.; Bidou, L.; Martin, N.; Blanchet, S.; Hatton, A.; Karri, S.; Cornu, D.; Costes, B.; Chevalier, B.; Tondelier, D.; Girodon, E.; Coupet, M.; Edelman, A.; Fanen, P.; Namy, O.; Sermet-Gaudelus, I.; Hinzpeter, A. Factors influencing readthrough therapy for frequent cystic fibrosis premature termination codons. *ERJ Open Res.* **2018**, 4, (1), 00080-2017. doi: 10.1183/23120541.00080-2017. Erratum in: *ERJ Open Res.* 2018 Jul 13;4(3): PMID: 29497617; PMCID: PMC5827411.

Quinton PM. Cystic fibrosis: lessons from the sweat gland. *Physiology* **2007**, 22:212-25. doi: 10.1152/physiol.00041.2006. PMID: 17557942.

Quon, B.S.; Rowe, S.M. New and emerging targeted therapies for cystic fibrosis. *BMJ* **2016**, 352, 1–14

Ramsey, K.A.; Ranganathan, S.; Park, J.; Skoric, B.; Adams, A.M.; Simpson, S.J.; Robins-Browne, R.M.; Franklin, P.J.; de Klerk, N.H.; Sly, P.D.; Stick, S.M.; Hall, G.L. AREST CF. Early respiratory infection is associated with reduced spirometry in children with cystic fibrosis. *Am. J. Respir. Crit. Care Med.* **2014**, 190, (10), 1111-6. doi: 10.1164/rccm.201407-1277OC. PMID: 25321321.

Ren, H.Y.; Grove, D.E.; De La Rosa, O.; Houck, S.A.; Sopha, P.; Van Goor, F.; Hoffman, B.J.; Cyr, D.M. VX-809 corrects folding defects in cystic fibrosis transmembrane conductance regulator protein through action on membrane-spanning domain 1. *Mol. Biol. Cell.* **2013**, 24, (19), 3016-24. doi: 10.1091/mbc.E13-05-0240. Epub 2013 Aug 7. PMID: 23924900; PMCID: PMC3784376.

Ren, C.L.; Morgan, R.L.; Oermann, C.; Resnick, H.E.; Brady, C.; Campbell, A.; DeNagel, R.; Guill, M.; Hoag, J.; Lipton, A.; Newton, T.; Peters, S.; Willey-Courand, D.B.; Naureckas, E.T. Cystic Fibrosis Foundation Pulmonary Guidelines. Use of Cystic Fibrosis Transmembrane Conductance Regulator Modulator Therapy in Patients with Cystic Fibrosis. *Ann. Am. Thorac. Soc.* **2018**, 15, (3), 271-280. doi: 10.1513/AnnalsATS.201707-539OT. PMID: 29342367.

Rosser, M.F.; Grove, D.E.; Chen, L.; Cyr, D.M. Assembly and misassembly of cystic fibrosis transmembrane conductance regulator: folding defects caused by deletion of F508 occur before and after the calnexin-dependent association of membrane spanning domain (MSD) 1 and MSD2. *Mol. Biol. Cell.* **2008**, 19, (11), 4570-9. doi: 10.1091/mbc.e08-04-0357. Epub 2008 Aug 20. PMID: 18716059; PMCID: PMC2575159.

Rowe, S.M.; Clancy, J.P.; Wilschanski, M. Nasal potential difference measurements to assess CFTR ion channel activity. *Methods Mol. Biol.* **2011**, 741, 69-86. doi: 10.1007/978-1-61779-117-8_6. PMID: 21594779; PMCID: PMC3760477.

Rowe, S.M.; Daines, C.; Ringshausen, F.C.; Kerem, E.; Wilson, J.; Tullis, E.; Nair, N.; Simard, C.; Han, L.; Ingenito, E.P.; McKee, C.; Lekstrom-Himes, J.; Davies, J.C. Tezacaftor-Ivacaftor in Residual-Function Heterozygotes with Cystic Fibrosis. *N. Engl. J. Med.* **2017**, 77, (21), 2024-2035. doi: 10.1056/NEJMoal709847. Epub 2017 Nov 3. PMID: 29099333; PMCID: PMC6472479.

Rusnati, M.; Sala, D.; Orro, A.; Bugatti, A.; Trombetti, G.; Cichero, E.; Urbinati, C.; Di Somma, M.; Millo, E.; Galietta, L.J.V.; Milanesi, L.; Fossa, P.; D'Ursi, P. Speeding Up the Identification of Cystic Fibrosis Transmembrane Conductance Regulator-Targeted Drugs: An Approach Based on Bioinformatics Strategies and Surface Plasmon Resonance. *Molecules.* **2018**, 23, (1), 120. doi: 10.3390/molecules23010120. PMID: 29316712; PMCID: PMC6017603.

Schneider, E.K. Cytochrome P450 3A4 Induction: Lumacaftor versus Ivacaftor Potentially Resulting in Significantly Reduced Plasma Concentration of Ivacaftor. *Drug. Metab. Lett.* **2018**, 12, (1), 71-74. doi: 10.2174/1872312812666180328105259. PMID: 29595119; PMCID: PMC6350194.

Seibert, F.S.; Chang, X.B.; Aleksandrov, A.A.; Clarke, D.M.; Hanrahan, J.W.; Riordan, J.R. Influence of phosphorylation by protein kinase A on CFTR at the cell surface and endoplasmic reticulum. *Biochim. Biophys. Acta.* **1999**, 1461, (2), 275-83. doi: 10.1016/s0005-2736(99)00163-7. PMID: 10581361.

Sermet-Gaudelus, I.; Bianchi, M.L.; Garabédian, M.; Aris, R.M.; Morton, A.; Hardin, D.S.; Elkin, S.L.; Compston, J.E.; Conway, S.P.; Castanet, M.; Wolfe, S.; Haworth, C.S. European cystic fibrosis bone mineralisation guidelines. *J. Cyst. Fibros.* **2011**, 10 Suppl 2, S16-23. doi: 10.1016/S1569-1993(11)60004-0. PMID: 21658635.

Sermet-Gaudelus, I.; Girodon, E.; Roussel, D.; Deneuille, E.; Bui, S.; Huet, F.; Guillot, M.; Aboutaam, R.; Renouil, M.; Munck, A.; des Georges, M.; Iron, A.; Thauvin-Robinet, C.; Fajac, I.; Lenoir, G.; Roussey, M.; Edelman, A. Measurement of nasal potential difference in young children

with an equivocal sweat test following newborn screening for cystic fibrosis. *Thorax*. **2010**, 65, (6), 539-44. doi: 10.1136/thx.2009.123422. PMID: 20522854.

Sheppard, D.N.; Bear, C.E.; de Jonge, H.R. Editorial overview: Respiratory: Transformational therapies for cystic fibrosis. *Current Opinion in Pharmacology* **2017** doi:10.1016/j.coph.2017.11.006.

Sly, P.D.; Brennan, S.; Gangell, C.; de Klerk, N.; Murray, C.; Mott, L.; Stick, S.M.; Robinson, P.J.; Robertson, C.F.; Ranganathan, S.C.; Australian Respiratory Early Surveillance Team for Cystic Fibrosis (AREST-CF). Lung disease at diagnosis in infants with cystic fibrosis detected by newborn screening. *Am. J. Respir. Crit. Care Med.* **2009**, 180, (2), 146-52. doi: 10.1164/rccm.200901-0069OC. Epub 2009 Apr 16. PMID: 19372250.

Strub, M.D.; McCray, P.B. Jr. Transcriptomic and Proteostasis Networks of CFTR and the Development of Small Molecule Modulators for the Treatment of Cystic Fibrosis Lung Disease. *Genes (Basel)* **2020**, 11, (5), 546. doi: 10.3390/genes11050546. PMID: 32414011; PMCID: PMC7288469.

Szabo, A.; Langer, T.; Schröder, H.; Flanagan, J.; Bukau, B.; Hartl, F.U. The ATP hydrolysis-dependent reaction cycle of the Escherichia coli Hsp70 system DnaK, DnaJ, and GrpE. *Proc. Natl. Acad. Sci. U.S.A.* **1994**, 91, (22), 10345-9. doi: 10.1073/pnas.91.22.10345. PMID: 7937953; PMCID: PMC45016.

Tang, A.C.; Turvey, S.E.; Alves, M.P.; Regamey, N.; Tümmler, B.; Hartl, D. Current concepts: host-pathogen interactions in cystic fibrosis airways disease. *Eur. Respir. Rev.* **2014**, 23, (133), 320-32. doi: 10.1183/09059180.00006113. PMID: 25176968.

Tiddens, H.A. Detecting early structural lung damage in cystic fibrosis. *Pediatr Pulmonol.* **2002**, 4, (3), 228-31. doi: 10.1002/ppul.10134. PMID: 12203854.

Van Goor, F.; Hadida, S.; Grootenhuis, P.D.; Burton, B.; Cao, D.; Neuberger, T.; Turnbull, A.; Singh, A.; Joubran, J.; Hazlewood, A.; Zhou, J.; McCartney, J.; Arumugam, V.; Decker, C.; Yang, J.; Young, C.; Olson, E.R.; Wine, J.J.; Frizzell, R.A.; Ashlock, M.; Negulescu, P. Rescue of CF airway epithelial cell function in vitro by a CFTR potentiator, VX-770. *Proc. Natl. Acad. Sci. U.S.A.* **2009**, 106, (44),

18825-30. doi: 10.1073/pnas.0904709106. Epub 2009 Oct 21. PMID: 19846789; PMCID: PMC2773991.

Van Goor, F.; Hadida, S.; Grootenhuis, P.D.; Burton, B.; Stack, J.H.; Straley, K.S.; Decker, C.J.; Miller, M.; McCartney, J.; Olson, E.R.; Wine, J.J.; Frizzell, R.A.; Ashlock, M.; Negulescu, P.A. Correction of the F508del-CFTR protein processing defect in vitro by the investigational drug VX-809. *Proc. Natl. Acad. Sci. U.S.A.* **2011**, 108, (46), 18843-8. doi: 10.1073/pnas.1105787108. Epub 2011 Oct 5. PMID: 21976485; PMCID: PMC3219147.

Veit, G.; Avramescu, R.G.; Perdomo, D.; Phuan, P.W.; Bagdany, M.; Apaja, P.M.; Borot, F.; Szollosi, D.; Wu, Y.S.; Finkbeiner, W.E.; Hegedus, T.; Verkman, A.S.; Lukacs, G.L. Some gating potentiators, including VX-770, diminish Δ F508-CFTR functional expression. *Sci. Transl. Med.* **2014**, 6, (246), 246ra97. doi: 10.1126/scitranslmed.3008889. PMID: 25101887; PMCID: PMC4467693

Veit, G.; Xu, H.; Dreano, E.; Avramescu, R.G.; Bagdany, M.; Beitel, L.K.; Roldan, A.; Hancock, M.A.; Lay, C.; Li, W.; Morin, K.; Gao, S.; Mak, P.A.; Ainscow, E.; Orth, A.P.; McNamara, P.; Edelman, A.; Frenkiel, S.; Matouk, E.; Sermet-Gaudelus, I.; Barnes, W.G.; Lukacs, G.L. Structure-guided combination therapy to potently improve the function of mutant CFTRs. *Nat. Med.* **2018**, 24, (11), 1732-1742. doi: 10.1038/s41591-018-0200-x. Epub 2018 Oct 8. PMID: 30297908; PMCID: PMC6301090

Veit, G.; Roldan, A.; Hancock, M.A.; Da Fonte, D.F.; Xu, H.; Hussein, M.; Frenkiel, S.; Matouk, E.; Velkov, T.; Lukacs, G.L. Allosteric folding correction of F508del and rare CFTR mutants by elxacaftor-tezacaftor-ivacaftor (Trikafta) combination. *JCI Insight.* **2020**, 5, (18):e139983. doi: 10.1172/jci.insight.139983. PMID: 32853178; PMCID: PMC7526550.

Vergani, P.; Lockless, S.W.; Nairn, A.C.; Gadsby, D.C. CFTR channel opening by ATP-driven tight dimerization of its nucleotide-binding domains. *Nature* **2005**, 433, (7028), 876-80. doi: 10.1038/nature03313. PMID: 15729345; PMCID: PMC2756053.

Wainwright, C.E.; Vidmar, S.; Armstrong, D.S.; Byrnes, C.A.; Carlin, J.B.; Cheney, J.; Cooper, P.J.; Grimwood, K.; Moodie, M.; Robertson, C.F.; Tiddens, H.A.; ACFBAL Study Investigators. Effect of bronchoalveolar lavage-directed therapy on *Pseudomonas aeruginosa* infection and structural lung

injury in children with cystic fibrosis: a randomized trial. *JAMA* **2011**, 306, (2), 163-71. doi: 10.1001/jama.2011.954. PMID: 21750293.

Wang, F.; Zeltwanger, S.; Hu, S.; Hwang, T.C. Deletion of phenylalanine 508 causes attenuated phosphorylation-dependent activation of CFTR chloride channels. *J. Physiol.* **2000**, 524 Pt 3 (Pt 3), 637-48. doi: 10.1111/j.1469-7793.2000.00637.x. PMID: 10790148; PMCID: PMC2269903.

Wang, W.; El Hiani, Y.; Linsdell, P. Alignment of transmembrane regions in the cystic fibrosis transmembrane conductance regulator chloride channel pore. *J. Gen. Physiol.* **2011**, 138, (2), 165-78. doi: 10.1085/jgp.201110605. Epub 2011 Jul 11. PMID: 21746847; PMCID: PMC3149817.

Wang, W.; El Hiani, Y.; Rubaiy, H.N.; Linsdell, P. Relative contribution of different transmembrane segments to the CFTR chloride channel pore. *Pflugers Arch.* **2014**, 466, (3), 477-90. doi: 10.1007/s00424-013-1317-x. Epub 2013 Aug 20. PMID: 23955087.

Wang, X.; Liu, B.; Searle, X.; Yeung, C.; Bogdan, A.; Greszler, S.; Singh, A.; Fan, Y.; Swensen, A.M.; Vortherms, T.; Balut, C.; Jia, Y.; Desino, K.; Gao, W.; Yong, H.; Tse, C.; Kym, P. Discovery of 4-[(2R,4R)-4-({[1-(2,2-Difluoro-1,3-benzodioxol-5-yl) cyclopropyl]carbonyl}amino)-7-(difluoromethoxy)-3,4-dihydro-2H-chromen-2-yl]benzoic acid (ABBV/GLPG-2222), a potent cystic fibrosis transmembrane conductance regulator (CFTR) corrector for the Treatment of Cystic Fibrosis, *J. Med. Chem.* **2018**, 61, 1436 - 1449.

Wang, Y.; Cai, W.; Zhang, G.; Yang, T.; Liu, Q.; Cheng, Y.; Zhou, L.; Ma, Y.; Cheng, Z.; Lu, S.; Zhao, Y.G.; Zhang, W.; Xiang, Z.; Wang, S.; Yang, L.; Wu, Q.; Orband-Miller, L.A.; Xu, Y.; Zhang, J.; Gao R.; Huxdorf, M.; Xiang, J.N.; Zhong, Z.; Elliott, J.D.; Leung, S.; Lin, X. Discovery of novel N-(5-(arylcarbonyl)thiazol-2-yl)amides and N-(5-(arylcarbonyl)thiophen-2-yl)amides as potent ROR γ t inhibitors. *Bioorg. Med. Chem.* **2014**, 22, (2), 692-702. doi: 10.1016/j.bmc.2013.12.021. Epub 2013 Dec 21. PMID: 24388993.

Wayane, P.A.; CLSI guideline C34. Clinical and Laboratory Standards Institute; Sweat testing: specimen collection and quantitative chloride analysis. **2019**, 4th ed.

Young, J.C. Mechanisms of the Hsp70 chaperone system. *Biochem. Cell. Biol.* **2010**, 88, (2), 291-300. doi: 10.1139/o09-175. PMID: 20453930; PMCID: PMC5026485.

Young, J.C. The role of the cytosolic HSP70 chaperone system in diseases caused by misfolding and aberrant trafficking of ion channels. *Dis. Model. Mech.* **2014**, 7, (3), 319-29. doi: 10.1242/dmm.014001. PMID: 24609033; PMCID: PMC3944492.

Yoshimura, K.; Nakamura, H.; Trapnell, B.C.; Chu, C.S.; Dalemans, W.; Pavirani, A.; Lecocq, J.P.; Crystal, R.G. Expression of the cystic fibrosis transmembrane conductance regulator gene in cells of non-epithelial origin. *Nucleic. Acids Res.* **1991**, 19, (19), 5417-23. doi: 10.1093/nar/19.19.5417. PMID: 1717947; PMCID: PMC328907.

Yu, Y.C.; Sohma, Y.; Hwang, T.C. On the mechanism of gating defects caused by the R117H mutation in cystic fibrosis transmembrane conductance regulator. *J. Physiol.* **2016**, 594, (12), 3227-44. doi: 10.1113/JP271723. Epub 2016 Mar 23. PMID: 26846474; PMCID: PMC4908022

Zajac, M.; Dreano, E.; Edwards, A.; Planelles, G.; Sermet-Gaudelus, I. Airway Surface Liquid pH Regulation in Airway Epithelium Current Understandings and Gaps in Knowledge. *Int. J. Mol. Sci.* **2021**, 22, (7), 3384. doi: 10.3390/ijms22073384. PMID: 33806154; PMCID: PMC8037888.

Zeitlin, P.L. Novel pharmacologic therapies for cystic fibrosis. *J. Clin. Invest.* **1999**, 103 (4), 447-52. doi: 10.1172/JCI6346. PMID: 10021451; PMCID: PMC408112.

Zhang, J.; Hwang, T.C. The Fifth Transmembrane Segment of Cystic Fibrosis Transmembrane Conductance Regulator Contributes to Its Anion Permeation Pathway. *Biochemistry* **2015**, 54, (24), 3839-50. doi: 10.1021/acs.biochem.5b00427. Epub 2015 Jun 10. PMID: 26024338; PMCID: PMC6510985.

Zhang, Z.; Chen, J. Atomic Structure of the Cystic Fibrosis Transmembrane Conductance Regulator. *Cell.* **2016**, 167, (6), 1586-1597.e9. doi: 10.1016/j.cell.2016.11.014. PMID: 27912062.

